Table of Contents

1 Introduction

1.1 Major events in the field of magnetic fusion in 2001

During 2001, negotiations between Euratom, Japan, Russia and Canada began concerning the International Thermonuclear Experimental Reactor (ITER) project, with the goal to define the different legal instruments needed to allow the political level to decide on the construction of this device whose objective is the scientific and technological demonstration of the feasibility of fusion at a scale already close to that of future power stations. Following an earlier bid by Canada, in Europe France and Spain expressed their interest to be considered by Europe for a potential candidate site. The construction of ITER, when decided, will imply significant adaptations in the European Fusion Program, which are now under discussion and preparation by all the national partners associated to the fusion program and the European Commission.

The ITER Engineering Design Activities (EDA) phase ended in July 2001. A phase called Coordinated Technical Activities (CTA) was initiated in order to complete the test of various large components already built during the EDA. The CTA also guarantees continuity of the required expertise for the construction of ITER.

The preparation of the 6th Framework Program (6th FP) of the European Union, which covers the period 2003-2006, continued during 2001. During the discussion of the fusion program, there was unanimous agreement of all the European Member States and Switzerland on the necessity to continue the Fusion Program with an adequate community budget and to proceed without delay towards a decision on the construction of ITER. The European Parliament expressed its support of fusion as an important energy option for a long-term sustainable development. The Euratom fusion budget within the 6th FP will amount to 750 million □ and contain a substantial provision (up to 200 million □) for ITER, clearly showing the importance of ITER in the roadmap towards a fusion reactor. In this respect, the CRPP has always maintained among its priorities a substantial contribution to ITER R&D and this effort will be further strengthened in the future. Enhancing the collaboration between Associations continues in view of the large and complex tasks to be accomplished: for the CRPP, this is reflected by the large number of common activities with its European and international partners. ITER will have a major financial impact during the period of the 6th FP and beyond. Given the overall budgetary constraints for fusion, the funding level for the Associations during FP6 will be reduced and must be compensated by increased larger support by national funding in order to maintain the same scope of research. The CRPP is addressing this serious issue at the level of the Swiss Government, with the help of the Direction of the Swiss Federal Institute of Technology (EPFL).

The exploitation of JET under the European Fusion Development Agreement (EFDA) involving all European Fusion Associations achieved significant progress, demonstrating that, in the future, a successful scientific exploitation of ITER could be performed by the international partners. The CRPP made a significant contribution to the scientific programme, the development of new diagnostics as well as to the enhancement projects at JET.

1.2 The CRPP in 2001

A major event for the CRPP in 2001 was the nomination of a new Professor. Dr. Ambrogio Fasoli was nominated as Professor Assistant tenure track of the EPFL and "Professor Boursier" of the Swiss National Science Foundation. The arrival of Prof. Fasoli will open up a new research orientation at the CRPP in the field of plasma physics, as described later in this report in more detail.

The reorganisation of the whole EPFL will also have an impact on the structure of the CRPP. From 2002, the CRPP will be a Centre within the Faculty of Basic Science, with its academic members having tenure with the Institute of Physics of Energy and Particles. The preparation of this important transition was one of the major management challenges for CRPP during 2001.

Research at the CRPP has concentrated in 2001 on our fields of excellence:

- In Physics and Engineering development related to the plasma, key elements were:

    - the exploitation of the TCV tokamak, which has a unique flexibility for producing and studying strongly shaped plasmas;
    - the study of electron cyclotron heating and current drive, combining a high power and versatile additional heating scheme with the shape flexibility of TCV;
    - the theoretical and numerical simulation of the equilibrium, stability and confinement of magnetically confined plasmas, spanning the whole range from tokamak to stellarator configurations;
    - the development of high power high frequency sources for plasma heating in collaboration with other Associations and industry;
    - the research on basic plasma physics oriented towards the understanding of phenomena of importance for fusion;
    - the participation in the scientific exploitation of JET experiments and in the design of ITER;
    - the participation in experiments and numerical/theoretical work of other European Fusion Associations.

- In the field of fusion technology, the CRPP has further pursued its long standing priorities on the physics and technology of superconductors benefiting from its unique test stand SULTAN and on R&D aimed at the development of low activation materials for fusion.

- Applications of plasmas in industrial processes are a further important strand of activity of the CRPP. They play an important role in the exchange of technologies and methods between fusion and other fields and are a key element of the transfer of know-how and knowledge from a research institution such as the CRPP to industry.

The scientific and the technological achievements in these areas during 2001 are presented in the main part of this annual report.

The research activities in the field of fusion were performed within the framework of the Association Euratom-Confédération Suisse* and have benefited from collaboration with all the Associations of the European Fusion Program. These

* The activities covering applications of plasma in industrial processes are not part of the research activities of the Association Euratom-Confédération Suisse.

collaborations as well as several bilateral ones with Eastern European institutions, Japan, Korea and the US on physics and diagnostic development include the execution of joint projects, the exchange of personnel and equipment. Such scientific relationships are extremely beneficial to the CRPP and bring a very high added value to the progress of our research and its international impact.

The breadth of the research activities conducted at the CRPP, its full integration in the European Fusion Programme and its international involvement have attracted a sizeable number of young graduate students. Around 30 doctoral theses are being carried out in the different groups. Taking into consideration the long term nature of the development of fusion power and the need for a new generation of physicists and engineers, the success in our role of training young professionals is an important contribution to the overall fusion program and more generally to the fields of plasma physics, microwave engineering as well as superconductor and materials technologies.

1 Introduction

1.1 Evénements majeurs en 2001 dans le domaine de la fusion magnétique

En 2001, des négociations concernant le projet de Réacteur Thermonucléaire Expérimental International (ITER) ont été initiées entre l'Euratom, le Japon, la Russie et le Canada, avec pour but de définir les instruments légaux nécessaires à la décision politique permettant la construction de cette installation dont l'objectif est de démontrer la faisabilité scientifique et technologique de l'utilisation de la fusion à une échelle proche de celle d'une centrale électrique. Suite à une proposition du Canada, la France et l'Espagne ont exprimé leur intérêt d'être considérés comme des candidats potentiels de sites pour recevoir l'installation. La construction d'ITER, lorsqu'elle sera décidée, impliquera des adaptations significatives du programme européen de fusion, celles-ci sont en cours de discussion et de préparation auprès de tous les partenaires associés au programme fusion et de la Commission européenne

La phase des Activités de Design et d'Ingénérie (EDA) d'ITER s'est terminée en juillet 2001. Une phase d'activités de Coordination Technique (CTA) a été introduite de manière à compléter les essais sur les divers grands composants fabriqués pendant EDA. La phase CTA a aussi permis de maintenir l'expertise nécessaire à la construction d'ITER.

La préparation du 6ème programme cadre (6ème FP) de l'Union européenne qui recouvre la période 2003-2006, s'est prolongée sur 2001. Durant la discussion concernant le programme de fusion, l'accord, portant sur la nécessité de continuer le programme de fusion avec un budget communautaire adéquat et d'aboutir sans délai à une décision concernant la construction d'ITER, a été unanime entre les Etats membres européens et la Suisse. Le Parlement européen a exprimé son support à la fusion comme étant une option énergétique importante pour un développement durable à long terme. Le budget fusion de l'Euratom dans le 6ème programme cadre se monte à 750 millions d'euros et il comprend une provision substantielle (environ 200 millions d'euros) pour ITER, montrant ainsi l'importance d'ITER dans la voie aboutissant au réacteur à fusion. C'est dans cet esprit que le CRPP a maintenu, parmi ses priorités, une large contribution dans la recherche et le développement (R&D) d'ITER, et cet effort sera renforcé dans le futur. Au vu des tâches importantes et complexes à réaliser, le CRPP désire améliorer la collaboration avec les Associations, ce qui est démontré par le grand nombre d'activités effectuées avec des partenaires européens et internationaux. Pendant et après le 6ème programme cadre, ITER aura un impact financier majeur. Etant données les contraintes budgétaires concernant la fusion, le niveau de couverture financière pour les Associations va être réduit et devra être compensé par un effort financier national plus élevé, de façon à maintenir l'objectif de la recherche. Avec l'aide de la présidence de l'EPFL, le CRPP a porté ce sérieux problème devant le gouvernement suisse.

Les progrès réalisés au cours de l'exploitation expérimentale de JET, sous l'égide de l'EFDA (European Fusion Development Agreement), impliquant toutes les Associations européennes de la fusion, a démontré que, dans le futur, l'exploitation scientifique d'ITER par des partenaires internationaux, pouvait être menée avec

succès. Le CRPP a apporté une contribution significative au programme scientifique, au développement d'un nouveaux diagnostics ou encore à l'amélioration des projets à JET.

1.2 Le CRPP en 2001

Pour le CRPP, un des événements majeurs de l'année 2001 a été la nomination du Professeur Dr A. Fasoli, en tant que professeur assistant, "tenure track" de l'EPFL et "professeur boursier" du Fonds national suisse de la science. L'arrivée du professeur Fasoli va déboucher sur une nouvelle orientation de la recherche au CRPP, dans le domaine de la physique des plasmas; celle-ci est décrite dans la dernière partie du présent rapport.

La réorganisation de l'EPFL en son entier aura également un impact sur la structure du CRPP. Depuis 2002, le CRPP est un Centre intégré à la Faculté de sciences de base (FSB), dont les membres académiques à charge d'enseignement feront partie de l'Institut de physique de l'énergie et des particules (IPEP). La préparation de cette transition a été un défi majeur de gestion du CRPP en 2001.

En substance, la recherche au CRPP a été concentrée en 2001 sur nos domaines d'excellence:

- Dans le développement de la physique et de l'ingénérie du plasma:
    - L'exploitation du tokamak TCV dont l'originalité est de produire et d'étudier des plasmas de section variable et fortement allongée;
    - L'étude du chauffage électron cyclotron et la génération de courant, en combinant l'utilisation d'un système de chauffage à grande puissance avec la forme variable du plasma;
    - La simulation théorique et numérique de l'équilibre, la stabilité et le confinement des plasmas magnétisés, recouvrant la plage des configurations du type tokamak au type stéllérateur;
    - Le développement des sources haute fréquence à haute puissance pour le chauffage du plasma, en collaboration avec d'autres Associations et les industries;
    - La recherche en physique de base des plasmas orientée vers la compréhension des phénomènes pour la fusion;
    - La participation dans l'exploitation scientifique des expériences sur JET et dans le design d'ITER;
    - La participation à des travaux expérimentaux, théoriques et numériques avec d'autres Associations européennes.

- Dans le domaine de la technologie de fusion, le CRPP a poursuivi ses priorités à long terme sur la physique et la technologie des supraconducteurs, en bénéficiant de son installation d'essais SULTAN, unique dans le monde, et de son activité R&D d'étude des matériaux à faible activation pour la fusion.

- Les applications des plasmas dans les procédés industriels représentent une plage importante des activités du CRPP. Celles-ci jouent un vaste rôle dans l'échange des technologies et des méthodes entre la fusion et les autres domaines de la physique des plasmas, et c'est aussi un élément-clé dans le transfert du savoir-faire et de la connaissance d'une institution de recherche, telle que la nôtre, vers l'industrie.

Les résultats scientifiques et technologiques, obtenus en 2001, dans ces thèmes de recherche sont présentés dans la partie principale du présent rapport annuel.

Les activités de recherche en fusion ont été accomplies dans le cadre de l'Association Euratom-Confédération suisse[1] et ont bénéficié de la collaboration avec toutes les autres Associations du programme européen de fusion. Ces collaborations, tout comme celles bilatérales avec les institutions de l'Europe de l'est, du Japon, de la Corée et des Etats-Unis d'Amérique, sur la physique et le développement de diagnostics, incluent l'exécution de projets communs, les échanges de personnel et d'équipement. De telles relations scientifiques sont extrêmement bénéfiques au CRPP et apportent une haute valeur ajoutée au progrès de notre recherche et à son impact international.

Le rayonnement des activités de recherche menées au CRPP, son intégration complète au programme européen de fusion et son implication internationale ont attiré un bon nombre de jeunes diplômés. Environ 30 thèses de doctorat sont actuellement en cours dans les différents groupes du CRPP. En prenant en considération la nature à long terme du développement de l'énergie de fusion et les besoins d'une nouvelle génération de physiciens et d'ingénieurs, le succès que nous rencontrons dans notre rôle de formateurs représente une contribution importante au programme de fusion en son entier, et plus généralement en physique des plasmas, ingénérie micro-onde ou encore en technologie des supraconducteurs et en matériaux.

---

[1] Les activités recouvrant les applications des plasmas dans les procédés industriels ne font pas partie des activités de recherche de l'Association Euratom-Confédération suisse

1 Einleitung

1.1 Die wichtigsten Ereignisse auf dem Gebiet der Kernfusion in 2001

Im Jahre 2001 haben die Verhandlungen zwischen Euratom, Japan, Russland und Kanada betreffend den Internationalen Thermonuklearen Experimentellen Reaktor (ITER) begonnen. Ihr Ziel ist die Formulierung der verschiedenen rechtlichen Dokumente, die als Grundlage für die politische Entscheidung über den Bau dieser Anlage dienen können. Mit ITER soll die wissenschaftliche und technische Machbarkeit der Kernfusion in einem Umfang, der einem zukünftigen Kraftwerk nahe kommt, bewiesen werden. Nach einem ersten kanadischen Angebot haben Frankreich und Spanien ihr Interesse kundgetan, von Europa als Kandidaten für den Sitz von ITER betrachtet zu werden. Der erhoffte Entscheid, ITER zu bauen, wird zu merklichen Änderungen im europäischen Fusionsprogramm führen; die dann zu treffenden Massnahmen sind heute in Diskussion und werden von allen nationalen Partnern des Programms zusammen mit der Europäischen Kommission vorbereitet.

Die Planungsphase von ITER, genannt *Engineering Design Activities* (EDA), ist Ende Juli 2001 abgeschlossen worden. Sie wurde von einer Phase, die *Coordinated Technical Activities* (CTA) heisst, abgelöst; sie soll dazu dienen, verschiedene grosse Teilsysteme, die während der EDA gebaut wurden, zu Ende zu testen. Die CTA erlaubt auch, die für den Bau von ITER nötige Fachkenntnis aufrecht zu erhalten.

Die Vorbereitung des 6. Rahmenprogrammmes (RP 6) der Europäischen Gemeinschaft, das von 2003 bis 2006 läuft, wurde 2001 fortgesetzt. In der Diskussion über das Fusionsprogramm waren sich alle europäischen Mitgliederstaaten und die Schweiz einig darüber, dass es mit einem angemessenen gemeinsamen Budget weitergeführt und der Bauentscheid für ITER unverzüglich vorangetrieben werden soll. Das europäische Parlament hat sich klar für die Fusion als ein wichtiger Weg zur Energiegewinnung in einer zukünftigen nachhaltigen Entwicklung ausgesprochen. Im RP 6 wird das Euratom Fusionsbudget 750 Millionen □ betragen, wovon bis zu 200 Millionen □ für ITER vorgesehen sind, was klar die Wichtigkeit von ITER auf dem Weg zum Fusionsreaktor aufzeigt. Seit je davon überzeugt, hat es das CRPP immer als wichtig erachtet, einen wesentlichen Beitrag zur ITER F&E zu liefern und wird auch in Zukunft in dieser Anstrengung nicht nachlassen, im Gegenteil. Die Zusammenarbeit zwischen den einzelnen Assoziationen wird im Hinblick auf die grossen schwierigen Aufgaben, die auf uns zukommen, weiterhin verstärkt: Fürs CRPP widerspiegelt sich das in einer grossen Zahl von gemeinsamen Projekten mit europäischen und internationalen Partnern. ITER wird einen starken Einfluss auf unsere Finanzen während der Periode des RP 6 und darüber hinaus ausüben. Da das Gesamtbudget für die Fusion beschränkt ist, wird der finanzielle Beitrag der Euratom an die einzelnen Assoziationen während dem RP 6 reduziert und von nationalen Geldern ersetzt werden müssen, um die Reichweite der Forschung aufrecht zu erhalten. Das CRPP geht dieses ernsthafte Problem mit Hilfe der Eidgenössischen Technischen Hochschule (EPFL) auf schweizerischer Regierungsebene an.

Der wissenschaftliche Betrieb von JET, der von der europäischen Fusionsentwicklungs-Vereinbarung (EFDA) geregelt ist und unter Einbezug von

allen europäischen Fusionsassoziationen abläuft, ist deutlich vorwärts gekommen und hat damit gezeigt, dass die internationalen Partner ITER in der Zukunft erfolgreich werden betreiben können. Das CRPP hat merkliche Beiträge zum wissenschaftlichen Programm, zur Entwicklung von Messgeräten und zu den Leistungssteigerungs-Projekten von JET geliefert.

1.2 Das CRPP in 2001

Ein Grossereignis fürs CRPP war im Jahr 2001 die Ernennung eines neuen Professors: Dr. Ambrogio Fasoli wurde zum Assistenzprofessor *tenure track* der EPFL und Stipendiatsprofessor des Schweizerischen Nationalfonds ernannt. Mit Professor Fasoli wird am CRPP eine neue Forschungsrichtung in Plasmaphysik geschaffen; diesbezügliche Einzelheiten werden später in diesem Bericht vorgestellt.

Die Reorganisation der gesamten EPFL wird sich auch aufs CRPP auswirken. Vom Jahr 2002 an wird das CRPP ein Forschungszentrum der *Faculté des Sciences de Base* (Fakultät der Grundlagenwissenschaften) sein. Seine akademischen Mitglieder bekleiden ihr Amt im *Institut de Physique de l'Energie et des Particules* (IPEP). Die Vorbereitung dieser Änderungen war für das CRPP eine der grossen Management-Herausforderungen in 2001.

Die Forschung am CRPP hat sich in 2001 im wesentlichen auf jene Gebiete konzentriert, wo wir im internationalen Wettstreit stark sind.

- In der aufs Plasma bezogenen Physik und technologischen Entwicklung sind die folgenden Punkte zu nennen:

  - Betrieb des Tokamaks TCV mit seiner einmaligen Anpassungsfähigkeit bezüglich Produktion und Ausmessbarkeit stark verformter Plasmen;
  - Untersuchung von Elektronzyklotron-Heizung und –Stromtrieb, in der ein vielseitiges Heizsystem mit der Verformbarkeit des TCV Plasmas kombiniert wird;
  - Theorie und numerische Simulation von Gleichgewicht, Stabilität und Transport von magnetisch eingeschlossenen Plasmen aller Konfigurationen vom Tokamak bis zum Stellarator;
  - Entwicklung von Hochleistungs-Hochfrequenzquellen für die Plasmaheizung zusammen mit anderen Assoziationen und der Industrie;
  - Forschung in fundamentaler Plasmaphysik mit dem Ziel, für die Fusion wichtige Phänomene besser zu verstehen;
  - Teilnahme sowohl an den Experimenten an JET und ihrer wissenschaftlichen Auswertung als auch am Planen von ITER;
  - Teilnahme an Experimenten und theoretischen/numerischen Arbeit von andern europäischen Fusions-Assoziationen.

- Auf dem Gebiet der Fusionstechnologie hat das CRPP seine angestammten Prioritäten weiter verfolgt, nämlich, von seiner einzigartigen Testanlage SULTAN profitierend, die Physik und Technologie von Supraleitern und das F&E Programm, das zu niedrig-aktiven Materialien für die Fusion führen soll.

- Eine weitere wichtige Forschungsrichtung besteht in der Anwendung von Plasmen in industriellen Prozessen. Sie spielt eine wichtige Rolle im Austausch von Technologien und Methoden zwischen der Fusion und anderen Gebieten

und ist ein Schlüssel-Element im Technologie- und Wissenstransfer zwischen einem Forschungsinstitut wie das CRPP und der Industrie.

Die wissenschaftlichen und technologischen Leistungen in den oben genannten Gebieten aus dem Jahr 2001 werden im Hauptteil dieses Jahresberichtes vorgestellt.

Alle Forschungsarbeit auf dem Gebiet der Fusion wurde im Rahmen der Assoziation Euratom-Schweizerische Eidgenossenschaft* ausgeführt und hat stark von der Zusammenarbeit mit allen andern Assoziationen des europäischen Fusionsprogramms profitiert. Sowohl diese wie auch bilaterale Zusammenarbeit mit Institutionen in Osteuropa, Japan, Korea und den USA auf dem Gebiete der Physik und der Entwicklung von Messmethoden schliessen die Ausführung von gemeinsamen Projekten und Austausch von Personal und Geräten ein. Derartige wissenschaftliche Verbindungen sind für das CRPP äusserst vorteilhaft, indem sie zum Fortschritt und zur internationalen Ausstrahlung unserer Forschung wesentlich beitragen.

Die Breite der am CRPP betriebenen Forschung, seine volle Integration im europäischen Fusionsprogramm und seine internationale Vernetzung hat eine ansehnliche Anzahl junger Doktoranden angezogen. Im Moment sind etwa 30 Dissertationen in verschiedenen Gruppen in Arbeit. Im Hinblick auf die langfristige Natur der Entwicklung der Fusionsenergie und den Bedarf an einer neuen Generation von Physikern und Ingenieuren ist der Erfolg in unserer Ausbildnerrolle ein wichtiger Beitrag zum gesamten Fusionsprogramm und auch zur Plasmaphysik und den Mikrowellen-, Supraleiter- und Materialtechnologien im allgemeinen.

* Die Anwendungen von Plasmen auf industrielle Prozesse sind nicht Teil der Forschungsarbeit der Assoziation Euratom-Schweizerische Eidgenossenschaft.

1 Introduzione

1.1 Avvenimenti principali nel campo della fusione magnetica durante 2001

Le negoziazioni sul progetto ITER (International Thermonuclear Experimental Reactor) sono iniziate nel 2001 fra Euratom, Giappone, Russia e Canada. Lo scopo è di definire la struttura giuridica di base necessaria per la decisione politica di intraprendere la costruzione del progetto. L'obiettivo di ITER è la dimostrazione scientifica e tecnologica della fattibilità della fusione su scala simile a quella dei futuri reattori per la generazione di energia elettrica. In seguito ad una prima offerta da parte del Canada, Francia e Spagna hanno espresso la volontà di essere considerate come sito potenziale per ITER. La decisione di costruire ITER implicherà importanti cambiamenti nel programma europeo per la fusione. Tali cambiamenti sono in questo momento oggeto di discussioni e negoziazioni fra tutti i partners nazionali associati al programma fusione e la Commissione Europea.

La fase di attività di design ingegneristico (EDA) si è terminata nel luglio 2001. Una fase denominata di attività tecniche coordinate (CTA) è stata lanciata per completare le prove dei maggiori componenti già costruiti durante la fase EDA. La fase CTA permetterà inoltre di mantenire il know-how necessario alla costruzione di ITER.

La preparazione del 6^0 Programma Quadro dell'Unione Europea, che copre il periodo 2003-2006, ha continuato nel 2001. Durante la discussione sul Progrmma Fusione, tutti gli Stati Membri e la Svizzera hanno trovato unanime accordo sulla necessità di continuare le ricerche sulla fusione con un finanziamento comunitario adeguato, e di proseguire senza ulteriori ritardi verso una decisione sulla costruzione di ITER. Il Parlamento Europeo ha espresso il suo supporto per la fusione come importante opzione energetica per uno sviluppo sostenibile a lungo termine. Il finanziamento dell'Euratom per la fusione nel 6^0 Programma Quadro sarà di 750 milioni di euro, e conterrà una sostanziale provvigione (fino a 200 milioni di euro) per ITER, il che evidenzia l'importanza di ITER nella strategia comunitaria verso lo sviluppo di un reattore a fusione. In questo ambito, il CRPP ha sempre considerato prioritario un contributo sostanziale allo sviluppo e ricerca per ITER, sforzo che sarà intensificato ulteriormente in futuro. L'ampiezza e la complessità dell'impresa motivano un aumento nelle collaborazioni fra Associazioni. Per il CRPP, questo si riflette in un gran numero di attività comuni con i partners europei ed internazionali. ITER avrà un impatto finanziario significativo durante ed oltre il periodo del 6^0 Programma Quadro. Date le limitazioni complessive del budget pr la fusione, il livello di finanziamento per le Associazioni durante il 6^0 Programma Quadro sarà necessariamente ridotto, e dovrà essere compensato da un maggior supporto finanziario nazionale in modo da mantenere gli stessi obiettivi di ricerca. Il CRPP riconosce la serietà della situazione e si rivolge per risolverla al Governo Svizzero, in collaborazione con la Direzione del Politecnico Federale di Losanna (EPFL).

La sperimentazione su JET da parte di tutte le Associazioni Europee, sotto l'egida dell'Accordo Europeo per lo Sviluppo della Fusione (EFDA), ha compiuto progressi significativi, dimostrando che, in futuro, l'operazione e la sperimentazione scientifica su ITER potranno essere condotte da un gruppo di partners

internazionali. Il CRPP ha fornito contributi importanti al programma scientifico, allo sviluppo di nuove diagnostiche ed ai progetti di potenziamento del JET.

1.2 Il CRPP nel 2001

Un avvenimento importante al CRPP nel 2001 è stata la nomina di un nuovo professore: Ambrogio Fasoli è stato nominato Professore Assistente 'Tenure Track' dell'EPFL e "Professor Boursier" del Fondo Nazionale Svizzero per la Ricerca Scientifica. L'arrivo del Prof. Fasoli aprirà una nuova direzione di ricerca al CRPP nel campo della fisica dei plasmi, come illustrato in dettaglio nel seguito di questo rapporto.

La riorganizzazione di tutta l'EPFL avrà un impatto sulla struttura del CRPP. A partire dal 2002, il CRPP sarà un Centro all'interno della Facoltà delle Scienze di Base, ed i suoi membri accademici avranno cattedre presso l'Istituto di Fisica dell'Energie e delle Particelle. La preparazione di questa transizione ha rappresentato uno sforzo particolare per il management del CRPP nel 2001.

Dal punto di vista della ricerca, il CRPP ha continuato a concentrarsi sui suoi domini di eccellenza

- Nell'ambito della fisica e dell'ingegneria dei plasmi, gli elementi chiave sono stati:
  - L'operazione del tokamak TCV, caratterizzato da una flessibilità unica in termini di forme di plasma che possone essere create e studiate
  - Lo studio del riscaldamento e della generazione di corrente tramite onde ciclotroniche elettroniche, basato sulla combinazione della flessibilità del plasma con l'alta concentrazione di potenza e versatilità di configurazione del sistema di riscaldamento
  - La simulazione teorica e numerica di equilibrio, stabilità e confinamento del plasma, coprendo tutto il campo di ricerca dagli stellaratori ai tokamaks.
  - Lo sviluppo di sorgenti ad alta frequenza ed alta potenza per il riscaldamento del plasma in colaborazione con altre Associazioni e l'industria
  - La ricerca sulla fisica dei plasmi orientata ad una comprensione di base di fenomeni importanti per la fusione
  - La partecipazione alle ricerche su JET e alle attività legate al design di ITER
  - La partecipazione ad esperimenti ed a lavori teorici e numerici in altre Associazioni

- Nel campo della tecnologia per la fusione, il CRPP ha proseguito nello studio della fisica e tecnologia dei magneti superconduttori, utilizzando l'installazione di test SULTAN, unica al mondo, e nello sviluppo di materiali a bassa attivazione.

- Le applicazioni industriali dei plasmi costituiscono un altro importante aspetto delle attività di ricerca del CRPP, in particolare in termini degli scambi di tecnologie e metodi fra la fusione ed altri campi, e fra istituti di ricerca, come il CRPP, e l'industria.

I maggiori risultati scientifici e tecnologici ottenuti nei campi sopra citati durante il 2001 sono presentati nella sezione principale di questo rapporto annuale.

Le attività di ricerca nel campo della fusione sono state condotte nell'ambito dell'Associazione Euratom-Confederazione Elvetica[2] ed hanno beneficiato di collaborazioni con tutte le Associazioni del Programma Fusione Europeo. Tali collaborazioni, unitamente a quelle bilaterali con istituti dell'Est europeo, Giappone, Corea e Stati Uniti sulla fisica e lo sviluppo di diagnostiche, includono l'esecuzione di progetti comuni e lo scambio di equipaggiamenti e di personale. Questi interscambi sono estremamente importanti per il CRPP e portano un grande valore aggiunto al progresso della nostra ricerca ed al suo impatto in ambito internazionale.

L'ampiezza dello spettro delle attività di ricerca svolte al CRPP, la completa integrazione nel programma fusione europeo, ed il suo aspetto internazionale, hanno attirato un buon numero di giovani studenti di dottorato. Circa 30 tesi di dottorato sono in corso nei diversi gruppi all'interno del CRPP. Considerando la naturale lunga scadenza dello sviluppo dell'energia di fusione, ed il bisogno di nuove generazioni di fisici ed ingegneri, condurre con successo questo ruolo di formazione constituisce un importante contributo al programma fusione e, piu' in generale, al campo della fisica dei plasmi, all'ingegneria delle microonde, dei superconduttori e dei nuovi materiali.

[2] Le ricerche legate alle applicazioni industriali dei plasmi non fanno parte delle attività dell' Associazione Euratom – Confederazione Elvetica.

2 Research achievements of the CRPP in 2001

2.1 The TCV tokamak

2.1.1 Recent advances

The *Tokamak à Configuration Variable*, TCV, continues to concentrate the efforts of the CRPP in the field of magnetic confinement controlled fusion physics. TCV has a major radius R=0.88m, a minor radius a<0.255m, a toroidal magnetic field B_T<1.54T, and a vacuum vessel elongation of three. The flexibility of its configuration and control systems makes it a unique tool to investigate the effects of plasma shape on a tokamak plasmas, including stability and confinement.

This versatility is matched by that of the TCV main heating system, Electron Cyclotron Heating (ECH). The ECH power capability was upgraded during 2001 to a total of 4.5MW, of which up to 3.5MW have already been injected into the TCV plasma. This system encompasses three 0.5MW gyrotrons operating at 118GHz, and complements the existing six 0.5MW gyrotrons operating at the second harmonic extraordinary mode (X2), 82.7GHz, referred to in the report as X2. The installation of the third harmonic extraordinary mode (X3) ECH system will extend the range of densities on TCV, improving the electron-ion collisional coupling and increasing the value of plasma β, and increasing the reactor relevance of the TCV plasmas. In addition to providing a tool to improve the TCV performance and explore tokamak β limits, these systems are being used to drive plasma current non-inductively to investigate a number of questions related to current and pressure profile modifications, advanced tokamak scenarios, and the physics of suprathermal electrons.

Technical upgrades of the heating and tokamak ancillary systems consumed a large fraction of 2001, which can be considered as a year of transition between the first extensive exploitation of X2 ECH and future investigations using the new ECH power capabilities. Nevertheless, a number of important discoveries were made in 2001, both from continuing analysis of previously collected data, and from new experiments. Investigations followed the four avenues that constitute the backbone of the TCV experimental programme, namely the effects of plasma shape on operational and stability limits, H-modes and edge physics, ECH and Electron Cyclotron Current Drive (ECCD) physics, and on the use of ECH and ECCD as tools for tokamak physics of relevance for next step developments.

The TCV operational domain has been extended by applying off-axis ECH. This leads to a broadening of the current profile, which generates highly elongated discharges even at relatively low plasma currents. This technique is particularly promising to heat overdense plasmas in the core using X3 ECH and off-axis using X2 ECH.

The confinement properties of extreme plasma shapes have been assessed. These studies, a particularity of TCV, show that the electron energy confinement improves with plasma elongation, but only up to values of the order of two, above which a saturation occurs. The dependence of the lifetime of impurities on plasma shape and parameters has also been investigated by injecting traces of Silicon. While for triangularity and plasma current there seems to be little dependence, the impurity

lifetime is observed to decrease with increasing toroidal field and elongation, even if the energy confinement time remains essentially unchanged.

The role of the plasma shape in limiting the deleterious effects of MHD activity during the current ramp-up phase had previously been investigated and modest plasma shaping was shown to avoid locked modes that lead to disruptions. A reduction of sawtooth activity was also found for sufficiently large values of the plasma elongation. The possibility of controlling sawtooth stability by using a combination of injection angles for the X2 ECH has been demonstrated.

The ELMy H-mode regime, the reference scenario for ITER operation, has been studied in TCV Ohmic plasmas in terms of LH transition and ELM physics. The domain of accessibility to the H-mode has been further characterised, and an improvement to the determination of the power threshold for the LH transition has been achieved using novel statistical methods. In addition, synchronisation between sawteeth and ELMs was observed. The statistical properties and the dynamics of ELMs were investigated and experiments aimed at controlling the ELM frequency by synchronising it to externally applied perturbations gave promising results. Fast probe measurements also indicate that ELMs drive substantial inner/outer target temperature differences, hence large thermoelectric currents.

In the highly elongated TCV plasmas neither Hugill nor Greenwald expressions for the maximum achievable density seem to apply, as the density limit depends on the divertor geometry and the power flux through the separatrix. In terms of edge physics, attention was given to the problem of the probe measured electron temperature, which in general appears higher than the values predicted by the codes. A common explanation that the parallel gradient of the temperature causes this effect seems to be ruled out by TCV findings.

Preliminary assessments of the X3 ECH system continued in 2001. Initial results were obtained using vertical injection (previous third harmonic experiments had lateral launch). A sensitive dependence of the absorbed power on the poloidal injection angle has been observed. This is consistent with the need for maximising the fraction of the ray path in the resonance layer.

The behaviour of suprathermal electrons created by ECH has been studied using a hard X-ray camera and electron cyclotron emission diagnostics. Both methods reveal a substantial production of suprathermal electrons when the ECH system is used in current drive mode, i.e. when waves are launched with a finite toroidal component of the wave vector. These measurements also suggest that the X3 absorption can be enhanced by a strongly non thermal population of fast electrons produced by X2 pre-heating. The absorption of the ECH power at the X3 is in this case significantly better than that predicted by the ray tracing code TORAY.

A strong effect on the power absorption of the radial transport of fast electrons is also suggested by the data. The crucial problem concerning the absorption of the ECH power, both in terms of the overall amount absorbed and of the radial profile, is addressed using measurements of diamagnetic loops and electron cyclotron emission during modulated ECH injection.

The investigation of the optimum conditions to obtain an improvement in core energy confinement has continued. The role of the modifications of the current profile by Electron Cyclotron Current Drive (ECCD) was confirmed. ECCD is routinely used on TCV to drive fully non-inductive discharges. In 2001 the length of such discharges was extended to 4.3s by firing the two X2 gyrotron clusters in

succession. Strong central EC current drive leads to significant modifications of the current profile. This in turn allows the study of the evolution of tearing modes from conventional (driven by the current profile), to neo-classical (driven by a perturbation of the bootstrap current). The TCV results confirm for the first time that these two driving terms act in a similar way on the same mode.

2.1.2 Extension of the TCV operating space towards high elongation and higher normalised plasma current

Variation of triangularity and squareness

It is well known that both the n=1 external kink stability and the n=0 axisymmetric stability, at a given elongation, depend on triangularity (δ) and squareness (λ). In order to find the best combination of δ and λ, at a fixed elongation, we have performed stability calculations using the DPM and KINX codes. The n=0 growth rate is computed for plasmas close to the n=1 stability limit, as a function of δ and λ. We note that the n=0 growth rate has a minimum for $\delta \sim 0.6$ and $\lambda \sim 0.25$, corresponding to the optimum choice of the shape parameters. These theoretical results have been confirmed experimentally. Virtually all experiments at high elongation, $\kappa > 2.5$, were performed with triangularities in the range $0.50 < \delta < 0.63$ and squareness in the range, $0.22 < \lambda < 0.26$. Experimental variations of δ and λ outside these ranges have not produced any significant improvement in the n=0 stability. It should be noted that the optimum plasma shape depends on the shape of the conducting shell which serves as a passive stabilizer. For the TCV rectangular vacuum vessel, relatively large values of λ and low values of δ are necessary for good n=0 stability.

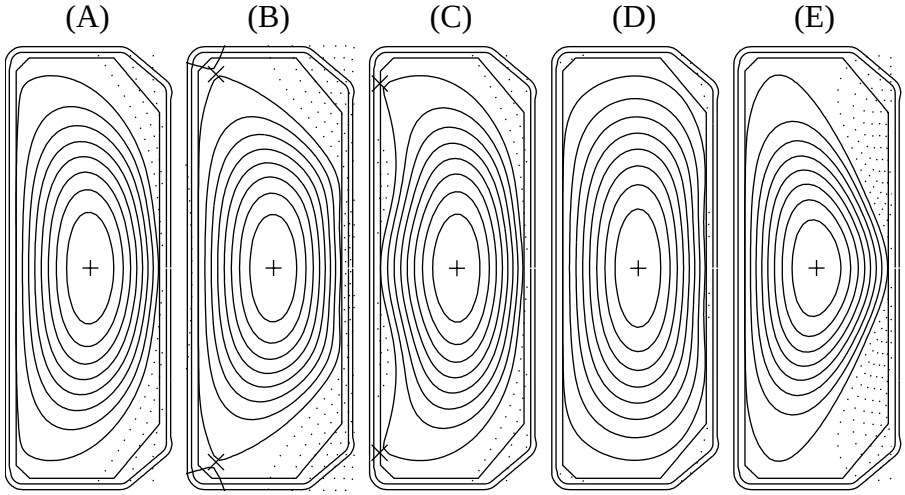

Fig. 2.1.1 *Theoretical TCV equilibria of various shapes: (A): classical D-shape, (B): trapezoid, (C): peapod, (D): racetrack, (E): triangle. Current and pressure profiles are taken from an experimental discharge with κ=2.7 (# 19034).*

New plasma shapes

The possibilities for shape variations in TCV go beyond what can be quantified by the parameters κ, δ and λ. Several alternative shapes, some of which are shown in Fig. 2.1.1, are theoretically possible. We have calculated n=0 and n=1 stability properties of these equilibria and we find that, at fixed elongation, κ=2.7, and for a fixed value of q_{95}, the trapezoid (Fig. 2.1.1(B)) is the only shape which has a lower

n=0 growth rate than the classical D-shape. In addition, it was found that the current limit of the trapezoid increases with decreasing internal inductance. This property is important since the internal inductance can be varied by current profile tailoring using ECH. The trapezoidal shape was investigated experimentally. In Fig. 2.1.2, we compare a trapezoidal plasma with a D-shaped plasma at the same values of elongation and β (κ=2.6 and β=1.1%). The D-shaped plasma has a normalised current of I_N=3.35MA/mT, which is close to the limit. In the trapezoidal scenario, we also pushed the current as high as possible, up to I_N=2.77 MA/mT. The open loop growth rates computed on the basis of the reconstructed experimental equilibria shown in Fig. 2.1.2 are γ=2730 s^{-1} and γ=2118 s^{-1}, for the D-shaped and trapezoidal plasmas, respectively. These findings are consistent with the theoretical results, indicating that the trapezoid has a lower current limit and a lower n=0 growth rate than the D-shape at the same elongation. So far, our attempts at extending the trapezoid scenario to higher elongations were unsuccessful, due to the appearance of locked modes and subsequent disruptions.

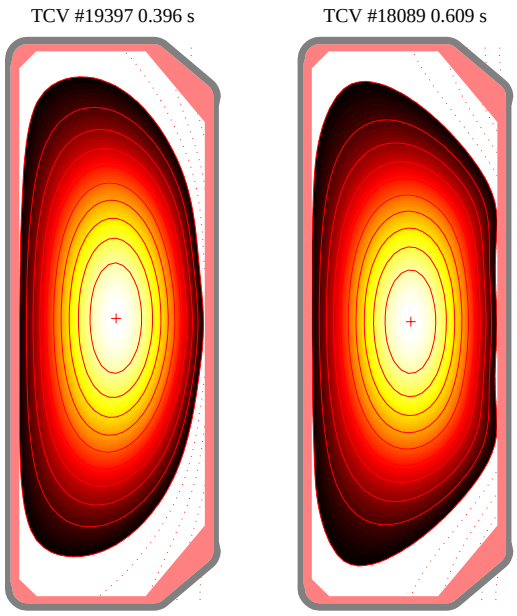

Fig. 2.1.2 *Comparison of D-shaped and trapezoidal plasmas in TCV. (A) D-shape, κ=2.60, I_N=3.35 MA/mT, β_{tor}=1.1%, $\gamma_{n=0}$=2730 s^{-1} (B) trapezoid, κ=2.61, I_N=2.77 MA/mT, β_{tor}=1.1%, $\gamma_{n=0}$=2118 s^{-1}.*

Limits to the operating space

Figure 2.1.3 shows the normalised current, $I_N=I_P/(a\,B)$, as a function of elongation for a large number of TCV discharges. The upper limit of I_N increases dramatically with κ: at the highest elongation, κ=2.8, the maximum normalised current is 4.5 times larger than at κ=1. For κ<2.3, the current limit is approximately given by q_{95}=2. For κ>2.3, however, operation at q_{95}=2 is not possible and the minimum q-value achieved increases with κ. This increase is consistent with ideal MHD stability calculations. There is also a lower limit on the normalised current, imposed by the axisymmetric mode. In Ohmic plasmas, both the internal inductance and the n=0 growth rate increase with decreasing current, and the minimum current is reached when the n=0 stability margin approaches zero. This lower limit depends on the current profile. Hence the operating space can be extended by modifying the current profile using ECCD. Note that no attempt has yet been made to reach high elongation with ECH at normalised currents I_N>1.

The ideal MHD β limit due to the n=1 external kink is shown in Fig. 2.1.4 for a D-shaped plasma with an Ohmic current profile and κ=2.5 as a function of the normalised current. The typical uncertainty of the theoretical stability limit that results from small errors in the pressure and current profiles is shown by the two blue lines. On the same figure, we plot experimental results representing virtually all TCV discharges with κ<2.5. We note that the experiments are consistent with the theoretical predictions, in particular for the current limits. The β limit has been reached at very low and very high values of the normalised current. At intermediate values of I_N, however, where the β limit is highest, the experimental data points are still far from the theoretical limit, for two reasons. First, Ohmic plasmas with κ=2.5 and I_N~2 cannot be created in TCV since they are ideally unstable with respect to the axisymmetric mode. Such plasmas can only be stabilized by broadening the current profile, using off-axis ECH, but up to now this technique has only been tried at low current, I_N<0.8MA/mT. Second, the main heating system on TCV, X2 ECH, only applies to low density plasmas, which cannot reach high β values. It should be pointed out that the results presented here do not represent the ultimate capabilities of TCV. The third harmonic ECH system should allow us to heat plasmas at higher density and to reach higher β values.

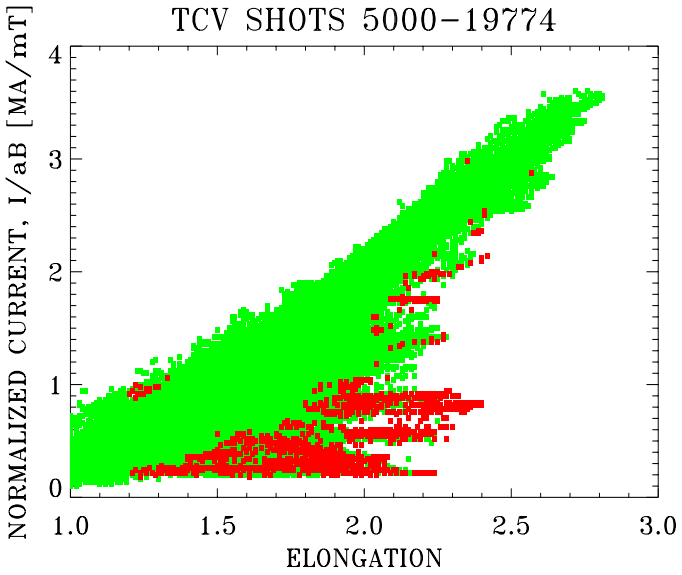

Fig. 2.1.3 *Normalised current, $I_P/(a\ B)$ [MA/mT], vs. elongation for all TCV discharges between March 1994 and May 2001. Ohmic and ECH experiments are shown in green and red, respectively.*

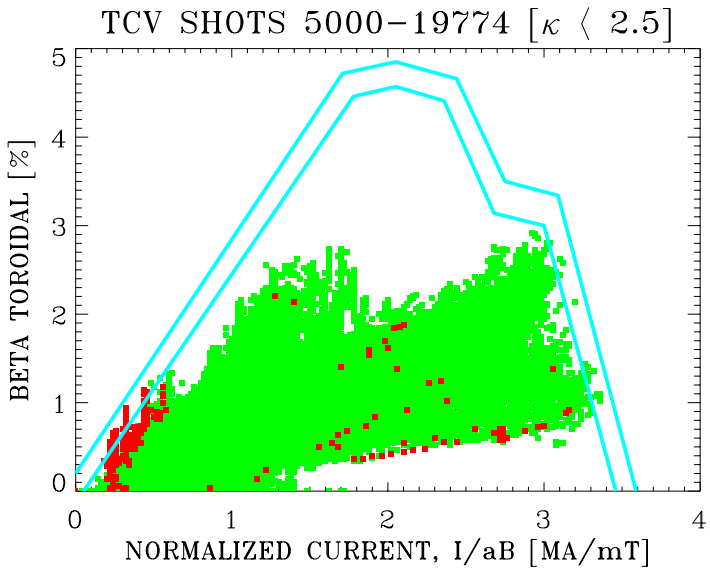

Fig. 2.1.4 *Toroidal β, as obtained from LIUQE equlibrium reconstructions, vs. normalised current, for all TCV discharges between March 1994 and May 2001 with κ<2.5. Ideal MHD stability limits for a D-shaped Ohmic plasma with κ=2.5 are shown in blue. Ohmic and ECH experiments are shown in green and red, respectively.*

2.1.3 Extensions of TCV operational domain by off-axis ECH current profile tailoring at high elongation

The study of the energy confinement time of extremely elongated plasmas and the approach to the Troyon β-limit at optimal values of the normalised current, $I_N=I_p/aB\sim2$ MA/mT, have motivated the development of TCV scenarios with high elongation and low current, using ECH. At very high elongation, low current operation in Ohmically heated discharges is limited by vertical stability, and a broad current profile is needed to extend the range of stable equilibria. Using far off-axis ECH in second harmonic X-mode to broaden the current profile, highly elongated discharges (κ ~2.4) with low current (I_p~300kA) and a high safety factor (q_{edge}~12) have already been created and stabilised in TCV. The operation has been extended to higher current (higher I_N). One of the difficulties faced when increasing the plasma current is the increased out-gassing of the wall, which leads to an increase of the density, hence reducing EC wave accessibility. However, discharges with overdense central plasma still allow far off-axis second harmonic heat deposition, thus indicating a way to produce a high density high elongation target plasma for third harmonic heating.

Both the broadening of the current profile and the associated plasma elongation depend strongly on the location of the ECH power deposition. The maximum effect is seen for deposition at the normalised radius ρ_{dep}~0.7 at the beginning of the EC heating. This results in a balance between absorption and induced current change in the edge, in qualitative agreement with PRETOR transport code simulations. To keep the normalised deposition radius constant during an elongation scan the launchers are progressively moved outward. Higher values of plasma elongation and slightly faster elongation ramp-rates than with a fixed mirror scenario can thus

be reached. However, the rate of increase of plasma elongation is intrinsically limited by current diffusion.

2.1.4 Confinement properties of highly elongated plasmas

The electron energy confinement of a set of highly elongated, limited discharges ($2.19<\kappa<2.73$) in narrow ranges of plasma current ($550<I_p<770$kA) and triangularity ($0.32<\delta< 0.43$), has been studied as a function of elongation, density, and Ohmic power flux. For constant density and power flux the confinement time is found to have only a weak, slightly positive, dependence on the already high elongation. Multi-linear regression confirms that κ is essentially an irrelevant parameter, while τ_{Ee} obeys an approximate power law $n_e^{0.88} q_{OH}^{-0.93}$, where n_e is the line-averaged density and q_{oh} the power flux through the plasma boundary (Fig. 2.1.5). Note that q_{OH} is a strong function of elongation.

Previous work on TCV Ohmic plasmas had shown a strong dependence of the electron energy confinement time on the plasma shape. Analysis of an extensive database of discharges with $1.06<\kappa<1.86$ and $-0.41<\delta<0.72$ revealed that, for constant plasma density and edge safety factor, the confinement time increases with elongation and decreases with triangularity. This variation is not caused by changes in the diffusivity, which was found to be independent of shape; rather, the dependence of the global confinement on the plasma shape is explained solely by the changes in the temperature gradients induced by the geometrical effects of flux expansion and compression, combined with degradation of the thermal conductivity with increasing energy flux.

The new results are in fact in agreement with this interpretation, since the geometrical enhancement is an increasing function of κ but tends to an asymptotic value of 2, beginning to saturate for $\kappa>2.2$; as κ goes from 2.19 to 2.73, only a 6% enhancement in confinement is predicted. This result puts into question global scaling laws with an unrestricted favourable dependence on elongation, such as the ITER 1996 L-mode scaling, which, with a $\kappa^{0.64}$ dependence, gives confinement times well in excess of our experimental values. On the other hand, the confinement time remains in good agreement with the Rebut-Lallia-Watkins scaling, as was the case in lower elongation Ohmic and most ECH heated TCV L-mode discharges.

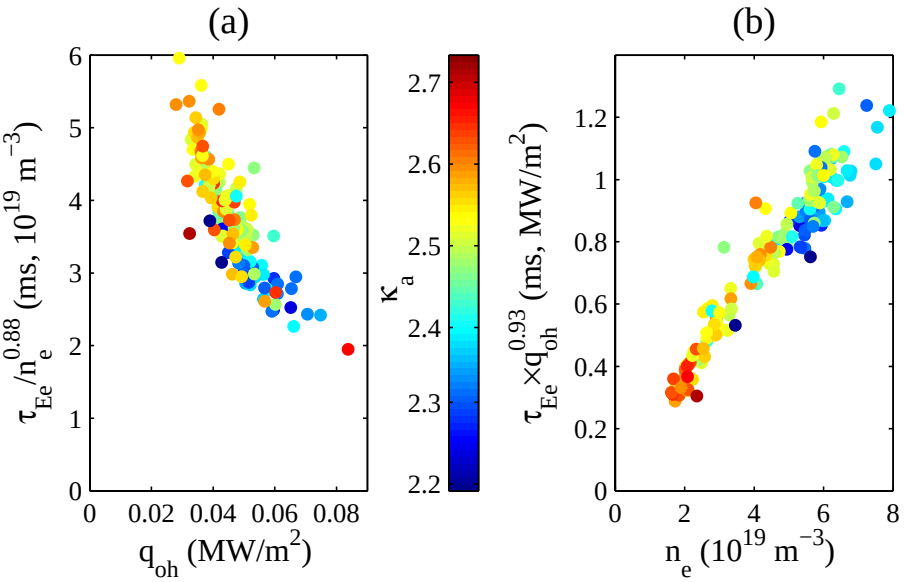

Fig. 2.1.5 *(a): Electron energy confinement time divided by $n_e^{0.88}$, plotted as a function of the power flux q_{OH}; (b): Electron energy confinement time multiplied by $q_{OH}^{0.93}$, plotted as a function of the line-averaged electron density n_e. The colour coding refers to the edge elongation κ_a.*

2.1.5 Investigation of impurity transport in TCV by means of laser ablation

The effect of plasma parameters on impurity transport has been systematically investigated by injecting Silicium trace impurities into a wide range of TCV discharges. The presence of these impurities leads to a strong increase of soft X-ray emission, which is measured using the 200 channel X-ray tomography system on TCV. X-ray signals from all viewing lines show a sharp pulse following ablation, with rise times in the range of 8-10ms. This reflects the penetration time, and is followed by a longer exponential decay phase, which is taken as the impurity lifetime in the plasma.

The lifetime of the impurities in different Ohmic L-mode plasmas has been studied as a function of the elongation ($1.6<\kappa<2.3$), triangularity ($-0.16<\delta<+0.65$), plasma current (I_P=160kA to 520kA), electron density ($n_e=1.9\times10^{19}m^{-3}$ to $6.5\times10^{19}m^{-3}$, line averaged) and toroidal magnetic field ($0.9T<B_T<1.5T$). For each scan all the other parameters were kept as constant as possible, with the exception of the elongation scan, where the normalised inversion radius was kept constant by adjusting the plasma current.

Some parameters, δ and I_P in particular, have little or no effect on the impurity lifetime for values lying above a threshold (δ =-0.16 and I_P=230kA respectively), while for lower values such parameters lead to longer lifetimes. Other parameters, such as κ (Fig. 2.1.6 (a)) and B_T (Fig. 2.1.6 (b)), show a surprising effect on the impurity lifetime, since an increase in either gives rise to shorter lifetimes, while the electron energy confinement time stays almost constant (15-17ms).

In Fig. 2.1.7 the effect of the line averaged electron density on the impurity confinement time is shown. Remarkably there is little or no influence for the case of limiter plasmas, for which the lifetime of the impurities is almost constant in the range 21-25ms. However, this is not true for higher density plasmas, for which the lifetime slightly increases up to about 28ms. In contrast, the effect of the density is clear for the case of diverted plasmas, in which the same density span almost doubles the lifetime.

The 1-D code STRAHL has been used to simulate the X-ray emission from the impurities. The code predicts the time evolution of the X-ray signals for any type and radial dependence of transport parameters (expressed as pinch velocity and diffusion coefficient). It can also simulate the effect of sawteeth with mixing radius and sawtooth period as free parameters. An acceptable set of transport parameters has to correctly reproduce the intensity and the duration of the measured signals. While the effect of sawteeth on the lifetime has been found to be less than 10%, the duration of the influx phase can be reduced significantly. STRAHL calculations also show that only the He-like and H-like Si ions contribute to the signals detected by the Beryllium-filtered Silicon detector diodes.

The simulations show that the impurity diffusivity is strongly influenced by discharge conditions, correlating inversely with lifetime. Unfortunately the dominance of sawteeth in the core prevents an estimate of the central diffusivity. The pinch velocity is found to be positive (towards the edge) and fairly independent of plasma conditions. A profile that increases linearly from zero in the centre to near 4m/s at the plasma boundary is required.

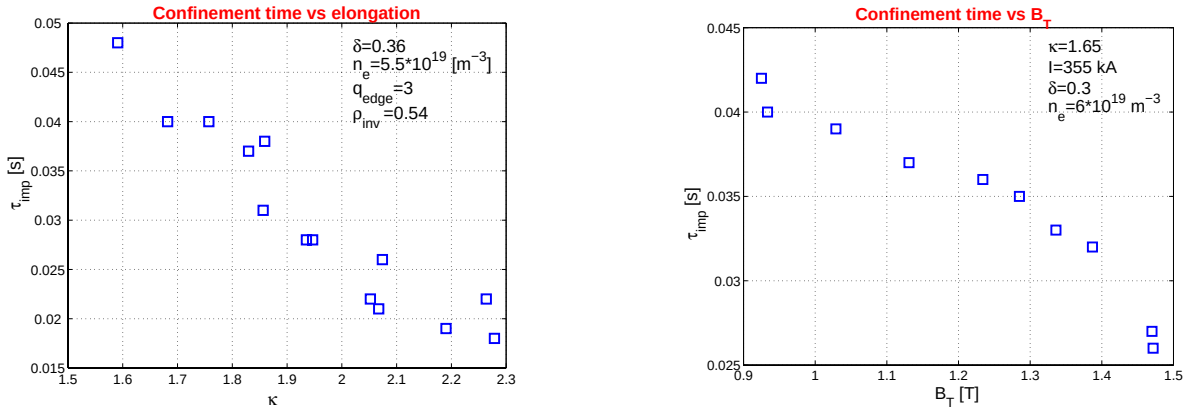

Fig. 2.1.6 *(a) Impurity lifetime vs elongation. The sawtooth inversion radius is kept constant (ρ_{inv}~0.54); (b) Impurity lifetime vs toroidal magnetic field.*

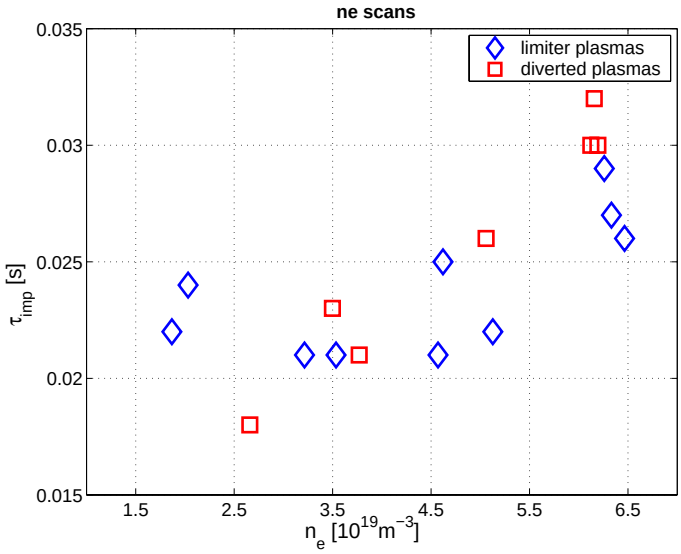

Fig. 2.1.7 *Impurity lifetime plotted as a function of electron density*

2.1.6 Characterization of MHD activity in shaped plasmas

The beneficial effect of plasma shaping during the initial current ramp up in reducing or suppressing MHD activity or disruptions was noticed early in TCV operation. A statistical analysis was undertaken to quantify this and determine the region of the parameter space (q, n_e, κ, δ) in which the crossing of q=3 is associated with the generation of locked modes and subsequent disruptions. We are now investigating the detailed evolution of the mode structure and of the coupling between modes arising on different rational surfaces, as a function of plasma shape. With reduced plasma shaping, bursts of low (m/n) MHD modes are observed when crossing flux surfaces with integer q values (q=3, 4 and 5) at the plasma

boundary as originally seen in circular cross-section tokamaks. While the modes excited when crossing q=4 and 5 remain at low amplitude and quickly vanish with no harm, crossing the q=3 surface can terminate the plasma. In the region $q_{95\%} < 3 < q_{edge}$ a mode with a dominant 3/1 component usually starts and grows in amplitude while it slows down in frequency and eventually locks to the wall. Before locking to the wall its dominant component becomes a 2/1 mode. The simultaneous presence of a 3/1 external kink mode and a 2/1 tearing mode leads, after a few milliseconds, to the destabilisation of an additional mode, the 3/2 mode and then to a disruption. Plasma shaping during the current ramp up in TCV discharges avoids the development of these modes at q=3. Both elongation and triangularity lower the global n=1 mode amplitude to a level that is insufficient to trigger the 3/2 mode. Even a small amount of plasma shaping (κ>1.3, δ>0.2) makes it is possible to avoid disruptions. This is shown in Fig. 2.1.8, where the n=1 amplitude of the dominant (n/m) mode is shown as a function of plasma triangularity and elongation. These results are consistent with the recent theoretical suggestion that plasma shaping strongly influences the coupling between different resonant surfaces thus improving the global stability of the 2/1 tearing mode.

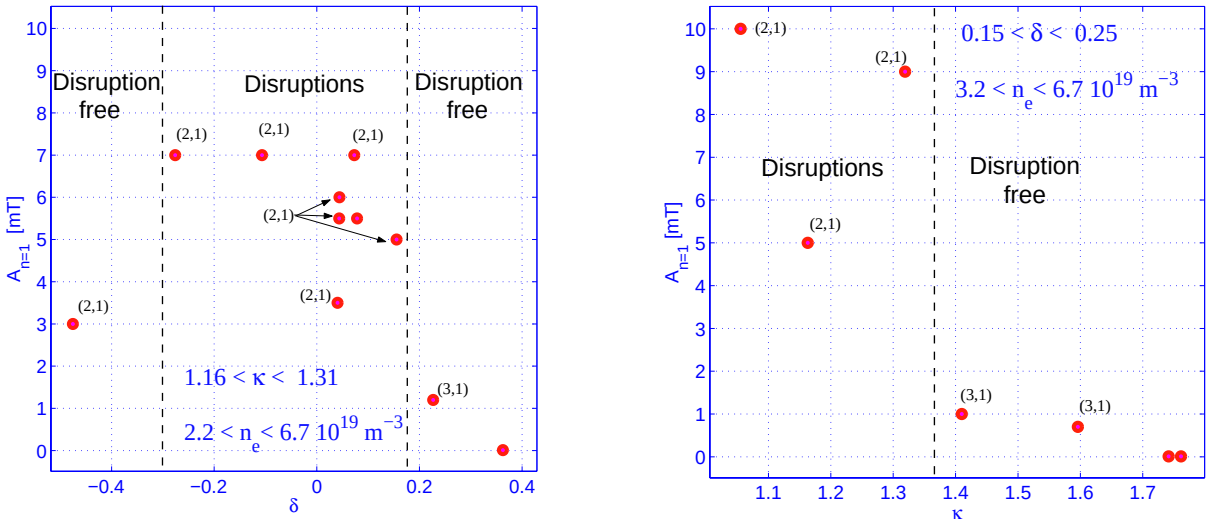

Fig. 2.1.8 *Disruption domains and dominant n=1 mode amplitude versus (a) plasma triangularity and (b) elongation.*

2.1.7 Residual mode activity replacing the disappearance of sawteeth at high elongation

Sawtooth behaviour can severely degrade plasma performance, since sawtooth crashes provide the seed islands which trigger neoclassical tearing modes. A systematic shape scan up to an elongation of 2.1 revealed a continuous decrease of the sawtooth period and amplitude with elongation. This effect is caused by a reduction of the pressure limit for the ideal internal kink mode in the plasma core. During 2001, the previously observed decrease of the sawtooth period and amplitude with increasing elongation (despite a constant inversion radius) has been confirmed for elongation values up to κ=2.6.

The flexibility of TCV has allowed us to study the stability of sawteeth in extremely elongated plasmas. The axisymmetric mode and the ideal kink mode impose well known lower and upper current limits, respectively. Occasionally, the m/n=3/2 island, rotating in the direction of the electron diamagnetic drift, is observed. For sufficiently large values of the elongation, in the range κ=2.2-2.6, sawteeth are observed to disappear abruptly. This disappearance of sawteeth is observed to take

place at a fixed internal inductance of l_i=0.69. The temperature profiles in the plasma centre, however, remain essentially flat, in spite of the disappearance of sawteeth, although a sharp rollover is exhibited close to inversion radius. The analysis of magnetic fluctuations and the soft X-ray tomography measurements shows that the sawteeth and the correlated 1/1 mode are replaced by continuous 2/2 and 3/3 modes. Contrary to usual observation these modes rotate in the direction of the ion diamagnetic drift. These new modes, which appear to have an ideal MHD character, prevent the peaking of the profiles, as do sawteeth at lower elongation.

2.1.8 H-modes and ELMs

The different studies performed on the Ohmic H-mode plasmas mostly deal with the LH transition and ELM physics.

ELMy H-mode operational limits
The operational limits of the ELMy regime have been determined for single null diverted plasmas with unfavourable ion gradB drift. The multidimensional region where transitions from the L-mode to the ELMy H-mode occur is called the gateway. This gateway is described by a multidimensional boundary involving the plasma current, density, elongation, triangularity and plasma-wall distance. Values for the boundary are shown in Table 2.1.1. The gateway is found to be narrow but reproducible even after reconditioning of the vacuum vessel. The plasma conditions at the transition to the ELMy regime have been studied in terms of edge temperature and density. However, the operational domain of the ELMy regime is found to be wider than the gateway since, once started, the ELMy discharges tolerate significant changes in plasma parameters. The influence of the main plasma parameters (plasma current, density, magnetic field, plasma and divertor shape) on the ELM characteristics such as frequency, amplitude and shape, has been studied as well as the evolution of edge density and temperature during the ELMy phase.

	I_p [kA]	n_e [10^{19} m^{-3}]	κ	δ	Plasma wall distance [m]
Gateway to the ELMy H-mode	380 : 420	4.5 : 7.5	1.6 : 1.7	0.5 : 0.6	>0.015
ELMy H-mode boundaries	360 : 480	4.0 : 10.0	1.5 : 2.1	0.45 : 0.75	>0.0005

Boundaries of the gateway to the ELMy regime and of the ELMy regime in terms of operational parameters.

Table 2.1.1 *The Elmy H-mode gateway boundary*

Ohmic power at the LH transition
The accessibility to the H-mode regime in additionally heated plasmas is generally described by a threshold power. In TCV, the LH threshold power is found to be a function of magnetic field, plasma density and plasma size. In Ohmic plasmas, the power is not a free parameter. Therefore, rather than by a simple threshold value, the accessibility to the ELM free and ELMy H-mode is described by the operational

domain in which LH transitions occur. In order to compare TCV results to those from other tokamaks, the input power is measured at the time of the LH transition. The measured values exhibit a large scatter when plotted against the scaling of the threshold power, perhaps because different scenarios were employed to obtain LH transitions.

Statistical analysis of LH transitions

In order to address the reliability of the characterization of the LH transition in terms of operational domain, a statistical method, the 'mobile centres method', has been used. This method groups neighboring data points in clusters around a center, in a multidimensional space. The ratio of the number of data points taken close to the transition, over the number of data points taken far from the transition, is the measure of the purity of the L and H phases. By this technique we find that the LH transitions occur in a well defined region of the operational domain.

Chaotic nature of the ELM time series

The study of unstable periodic orbits (UPO) in the ELM time series has continued. Statistical analysis of the UPO occurrences has led us to the conclusion that a deterministic, chaotic process governs the apparently random distribution of delay between ELMs. The influence of the plasma parameters on the characteristics and number of occurrences of these UPO has been studied. Most UPOs are found when q_{95} is around 2.8. Highly elongated plasmas (κ>1.8) show fewer UPO than at the nominal value (κ=1.7).

Synchronisation between ELMs and sawteeth

ELMy H-mode plasmas are obtained over a large range of plasma parameters. The synchronisation of ELMs with sawteeth has been studied and it appears that the ELM frequency is often either half, equal, double or even triple the sawtooth frequency. In most cases the phase relationship between the ELMs and sawteeth is constant indicating a link between the ELM dynamics and the sawtooth dynamics, Fig. 2.1.9.

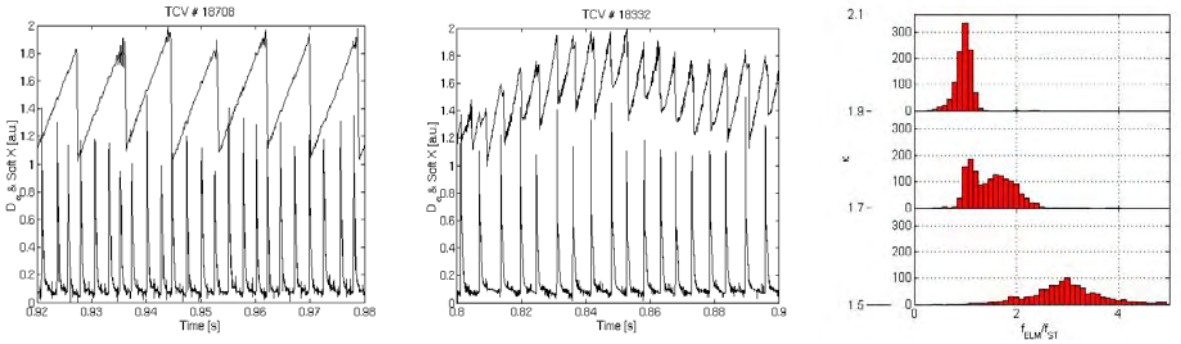

Fig. 2.1.9 *Left and middle: evolution of D_α and soft-X signals for low (1.5) and high (2.0) elongation ELMy plasmas, respectively. Right: Ratio of the ELM frequency over the sawtooth frequency for different plasma elongation ranges.*

ELM control

A first attempt at controlling the ELM frequency has been performed. The vertical position of an ELMy plasma is slightly perturbed by a modulation of the current in the inner, fast coil of TCV. The perturbation consists of a series of current spikes of about 1kA, each of 1ms duration, with a delay between spikes varying from 3 to 7 ms. The resulting deviation of the plasma position reaches 2cm.

Phase synchronisation is found between the ELM cycle and the external perturbation, lasting for multiple ELM cycles, when the amplitude of the perturbation is sufficient. These experiments indicate that the ELM frequency can be modified from its natural value of 180Hz, to values between 150 and 250Hz. This suggests a possible way of controlling the ELM frequency and therefore the ELM amplitude.

2.1.9 Density limit

In highly elongated plasmas, the Hugill and Greenwald expressions for the density limit give different values. Data from high density disruptions in TCV, both from the existing database and from new dedicated discharges, have been analysed to determine the most suitable expression for the density limit in shaped plasmas. As shown in Fig. 2.1.10, the density limit is lower than the value predicted by the Hugill expression for low elongation cases. Conversely, highly elongated plasmas show a density limit larger than the prediction. The density limit depends on the divertor geometry: plasmas with a longer separatrix leg have a higher density limit. Hence, none of the usual expressions for the density limit is in full agreement with the results of Ohmically heated TCV discharges.

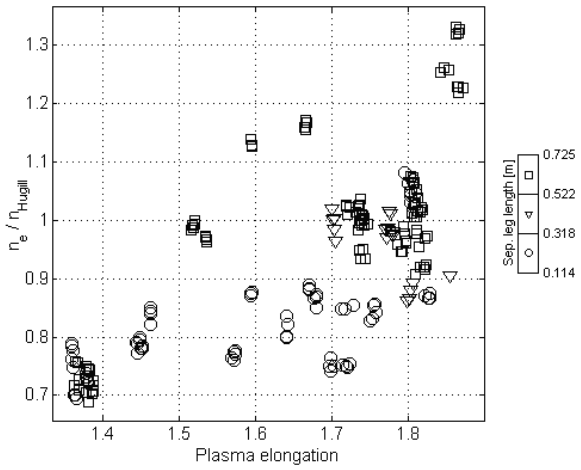

Fig. 2.1.10 *Normalised density just prior to the density limit disruption as a function of the plasma elongation for different ranges of separatrix leg length.*

2.1.10 Edge and divertor physics

Following the preliminary modelling of high recycling and detached diverted discharges using the SOLPS4.0 (B2-Eirene) code package developed during 2000 considerable effort

has been devoted during 2001 to installing both SOLPS4.0 and SOLPS5.0 (B2.5-Eirene) at CRPP. Both codes are now running routinely and, while some initial simulations including the molecular reactions thought to be important in producing the detached state in TCV have been made, the majority of code work has been devoted to modelling JET pure helium discharges (cf. Section 4.1)

An important aspect of the detached divertor work has been the difficulty in reconciling the relatively high (~5eV) values of divertor target electron temperature that are measured using arrays of embedded Langmuir probes in high recycling conditions with low predicted code values (~1eV). One possible origin of this discrepancy is the strong T_e gradient parallel to the total magnetic field that arises in the scrape-off layer (SOL) at high plasma. Since Langmuir probes are sensitive only to the high energy tail of the electron velocity distribution, a small percentage of fast electrons reaching the probe collisionlessly, from regions upstream where T_e is higher, can strongly influence the measured T_e. A simplified numerical approach, benchmarked against a full kinetic code, and using as input the B2-Eirene predicted parallel field profiles of n_e and T_e, has been used to predict the expected temperature, T_{eff} at the TCV targets. A selection of results is shown in Fig. 2.1.11, where, except at low to medium densities, the predicted and code temperatures are identical. This study would therefore indicate strongly that, for TCV at least, the high measured values of target T_e at high divertor density cannot be ascribed to strong parallel temperature gradients.

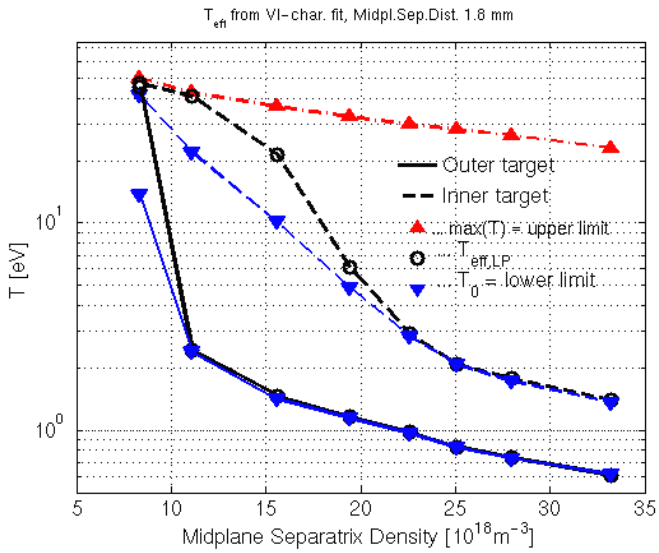

Fig. 2.1.11 *Upstream edge density dependence of B2-Eirene predicted T_e at the inner and outer targets in TCV (blue triangles) compared with the expectations of a kinetic model accounting for parallel SOL T_e gradients (black circles). For much of the density range, both values are almost identical, differing only at lower densities. The red triangles give, for each density, the maximum value of T_e in the B2-Eirene parallel profile. Simulations are appropriate to a single-null lower, Ohmic diverted discharge.*

ELMs are a serious problem for next step tokamaks. Although only Ohmic H-modes and Type III ELMs have thus far been obtained on TCV, a contribution can be made to models of ELM particle and power transport in the SOL by using Langmuir probes to study the fast time response of target currents to the ELM. An example is given in

Fig. 2.1.12, where the floating potential V_f, and current at V=0 (target potential) I_0, are plotted for probes nearest the inner and outer strike points of a single null lower discharge with Ip=400kA. The plots represent "coherent averages" of the ELM signals for long periods (several 100ms) over which ELM characteristics are constant. The average is taken with respect to the averaged peak amplitude of a vertical viewing D_α chord.

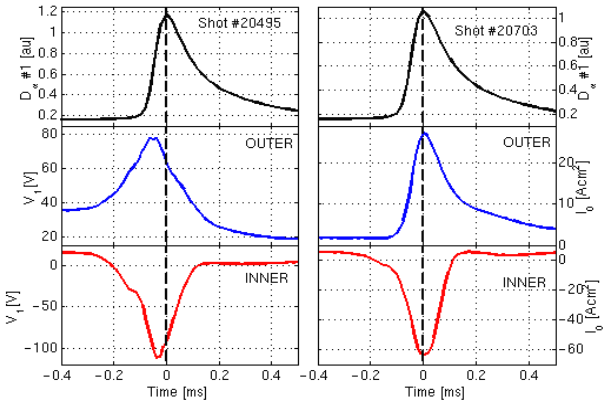

Fig. 2.1.12 *Coherently averaged floating potentials (left) and currents at V=0 (right) to Langmuir probes at the inner and outer target strike points of an ELMing Ohmic H-mode in TCV.*

At the inner target strike point, the floating potential and electron current are negative, and both are positive at the outer target. Clear ELM precursors are observed on the V_f signals and also on the inner target I_0. These precursors correlate with the start of Mirnov ELM precursor activity at the outside midplane, upstream of the divertor. The good parallel current balance obtained when integrating the inner and outer target electron currents indicate strongly that the ELMs drive substantial inner/outer target T_e differences and hence large parallel thermoelectric currents. This data will be used as input to Particle in Cell simulations of the ELM impact on the TCV SOL, which are to be performed in the future.

2.1.11 ECH second harmonic launcher alignment and sawtooth control

Experiments were performed to realign the launchers after reassembly. The target plasmas were optimised to obtain the sawtooth inversion radius from X-ray tomography with the highest possible accuracy, and to address the question of the optimum heating location, relative to the q=1 surface, for sawtooth stabilisation. The scans show that the optimum heating location is clearly outside both the sawtooth inversion radius and the q=1 radius, as determined by equilibrium reconstruction of the magnetic signals. PRETOR simulations are in agreement with this observation. Compared to Ohmic discharges, the sawtooth period could be lengthened by a factor of four with 1.3MW of ECH outside the q=1 surface. Conversely, by adding 0.47MW at an optimum destabilisation location just inside the q=1 surface, the sawtooth period could be reduced by a factor of two. This means that the stabilising effect of three gyrotrons can be negated with only 1 gyrotron. This means of sawtooth destabilisation is therefore proposed for the prevention of NTM triggering by the sawtooth instability, similarly to the ICRH scheme shown to be effective on JET.

2.1.12 *Preliminary results with vertically injected ECH power at the X3 in X-mode*

In order to extend the density range of ECH heated plasmas up to electron densities of $1.2 \cdot 10^{20}$ m^{-3}, three 0.5MW gyrotrons at a frequency of 118GHz are available. The launcher consists of a single mirror placed at the top of the vacuum vessel, which can be moved radially and poloidally. The poloidal movement can be controlled on a fast time scale whereas the radial movement is adjusted from discharge to discharge. The top launch scheme has been chosen to optimise the heating of high density plasmas while maximising single-pass absorption. In this launching configuration, the single pass absorption is strongly affected by refraction as is shown in the insert of Fig. 2.1.13, where the ray tracing calculations from the TORAY code are shown on a poloidal cross-section for three different poloidal launching angles. As the resonance layer is a vertical surface on the high field side of the cold resonance layer, the maximum absorption is obtained when the path of the ray within the resonance layer is maximised. This is the case for the 46.6° launching angle. Such strong sensitivity is confirmed experimentally, as shown in Fig. 2.1.3, where the electron energy is plotted against the poloidal launching angle for an injected X3 power of 450kW. On the right axis the peak position of the calculated single-pass absorption curve shows a good agreement with the experimental results. The level of single-pass absorption will be significantly increased when the full X3 power of 1.5MW will be injected. This is due to the strong dependence of the absorption on the electron temperature, giving rise to a positive feedback loop in the electron temperature.

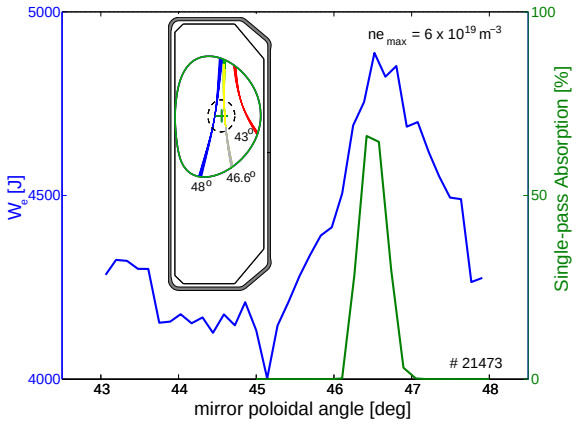

Fig. 2.1.13 *Dependence of the measured electron energy W_e (left axis, blue curve) and peak position for the calculated single-pass absorption curve (right axis, green curve) on the poloidal launching angle for an injected X3 RF power of 450kW.*

2.1.13 *Suprathermal X-ray emissivity with X2 and X3 ECH*

A multi-chord CdTe hard X-ray (HXR) camera, on loan from DRFC-Cadarache, has been used in support of the first set of experiments with combined second and X3 ECH. This instrument is sensitive to photons in the 10-200keV range and is used to diagnose the suprathermal electron population. The TCV data show that a substantial suprathermal component is generated by electron cyclotron waves launched with a finite toroidal wave vector component, thus capable of driving a non-inductive current in the plasma. Perpendicular X3 heating is applied to plasmas pre-heated with X2 ECH with varying toroidal injection angles. The absorbed X3 power, measured with a diamagnetic loop, is found to be in excess of the value predicted by linear calculations based on a Maxwellian distribution function. The absorption peaks at two angles, one positive and one negative, of approximately equal absolute value, and the larger of the two peaks (at the positive, or co-ECCD, angle) reaches approximately 100% absorption. The suprathermal X-

ray emissivity shifts to progressively larger energies as the X2 toroidal angle is increased. Conversely, the estimated total emissivity, during both the X2 and combined X2/X3 phases, peaks at the angles for which the X3 absorption is maximum, and displays a similar co/counter asymmetry (see Fig. 2.1.14). These measurements support the hypothesis that the X3 absorption is enhanced by the presence of a non-Maxwellian tail of high-energy electrons generated by X2 preheating. In addition, the most significant factor influencing the X3 absorption appears to be the total density of fast electrons rather than their energy distribution.

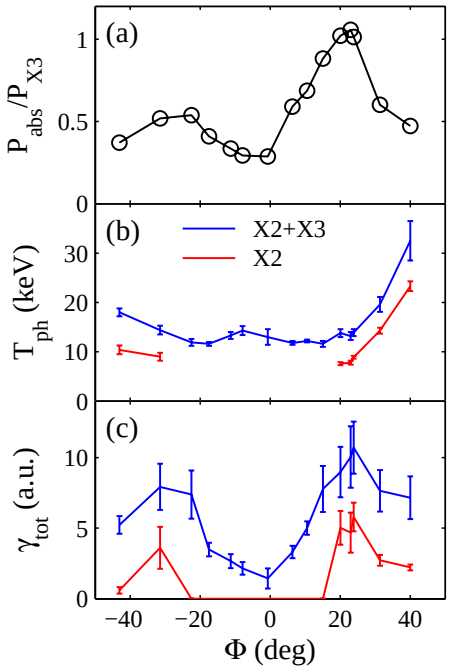

Fig. 2.1.14 *(a) X3 absorbed power fraction, (b) HXR suprathermal photon temperature (calculated from an exponential fit to the spectrum), (c) integrated HXR emissivity, vs. ϕ (complementary to the angle between X2 wave vector and magnetic field). The suppressed points correspond to cases in which only the thermal spectrum is measurable.*

In spite of the strong variation of the absolute emissivity across the plasma cross-section, the form of the spectrum is essentially uniform in space, as seen in Fig. 2.1.15. This is true in a wide variety of conditions, suggesting that the radial diffusion rate of suprathermal electrons does not depend significantly on energy.

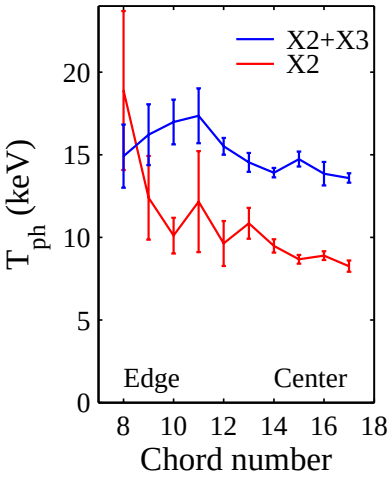

Fig. 2.1.15 *Suprathermal photon temperature from line-integrated HXR emission vs. chord number, in the X2 and X2/X3 phases of a discharge with ϕ=+24°.*

2.1.14 Electron cyclotron emission from non-Maxwellian electron distributions with ECH and ECCD

An independent experimental demonstration of the creation of a substantial energetic electron population by X2-ECCD and X3 ECH was obtained using X-mode Electron Cyclotron Emission (ECE) measurements with 24-channel radiometer in the frequency range 87-115GHz. The ECE radiation is collected from antennas on the high field side (HFS) of the vacuum chamber. This arrangement avoids re-absorption of relativistically down-shifted ECE from suprathermal electrons by thermal electrons near the 'cold' resonance layer. The emission seen from the HFS is the sum of the ECE from downshifted suprathermals and a partly reabsorbed component emitted by thermal electrons.

The apparent ECE temperature $T_{ece}=8\pi^3c^2I_\omega/\omega^2$, where I_ω is the intensity of the ECE radiation and ω the frequency, is equal to the bulk electron temperature measured using Thomson scattering (TS) only in the case of a Maxwellian electron energy distribution. The creation of suprathermals by X2 ECCD and X3 ECH was investigated in a series of experiments where the toroidal launch angle ϕ_{X2} of the X2 beam was scanned from discharge to discharge between –29° and +33°. The X3 launch angle was always fixed at $\phi_{X3}=0$. All the plasmas have an Ohmic phase of about 0.3s followed by a X2 'preheating' phase with constant power ($P_{X2}=0.47$MW) from 0.3s to 1.35s, whereas the X3 power is applied from 0.4s to 1.15s. The X3 power ($P_{X3}=0.47$MW) is kept constant except for a period of power modulation from 0.5s to 0.7s for measuring the absorbed fraction of the X3 power by a diamagnetic loop.

Figure 2.1.16 shows the central ECE temperature evolution together with the temperature from TS for a discharge with both X2 and X3 heating ($\phi_{X2}=0$). No suprathermal ECE is observed with X2 ECH only. However, as seen from the threefold increase of T_{ece} over T_{TS}, the application of X3 ECH produces suprathermals. The diamagnetic loop measurement during the modulated phase of this discharge shows that 30% of the X3 power is absorbed by the plasma. A poloidal scan of the X3 launching angle is then performed from 0.8s to 1.15s, with the first pass deposition region moving from the centre to r/a=0.7. Temperatures from all ECE channels, including those corresponding to flux surfaces crossing the X3 cold resonance deposition region, drop as the X3 power is deposited more off-axis. The ECE emission is maximum at 0.8s when X2 and X3 power are deposited on the same, near central, flux surfaces and then decreases until the X3 deposition is near r/a=0.3. At the same time the hard X-ray emission is strongly reduced and T_{TS} diminishes by 30%, also demonstrating reduced X3 absorption. Due to the particular geometry, the X3 EC beam is reflected from the inner wall tiles and returns to the plasma core when the first pass resonance is beyond r/a=0.3. This explains why T_{ece} and T_{TS} increase again for t>0.9s.

The dependence of the ECE on the toroidal launching angle of the X2 power injection, varied discharge by discharge, is shown in Fig. 2.1.17. Typical bulk temperatures are 2keV with X2 only and 2.5keV with combined central X2/X3 heating. The ECE temperature reaches its highest value for X2 injection angles of +/-20° with X2 heating only, demonstrating the creation of a suprathermal electron population. During the combined heating phase the T_{ece} increases with the injection angle up to at least 33°. These observations are consistent with the hard X- ray measurements described in the previous Section, which show that the highest values of the hard X intensity are reached for X2 ECCD or counter ECCD with $|\phi|=20°$.

The experimental results clearly show non-thermal EC radiation over a frequency range which is larger than expected from deposition at the cold X2 and X3 resonance locations. With electron energies up to a few tens of keV, as inferred both from modelling of the ECE emission and the above X-ray measurements, the relativistic downshift allows heating of electrons more than 10cm away from the cold resonance. The presence of such electrons far away from the cold resonance would suggest that transport of suprathermal electrons may be important and may have to be taken into account in Fokker-Planck ECH simulation codes.

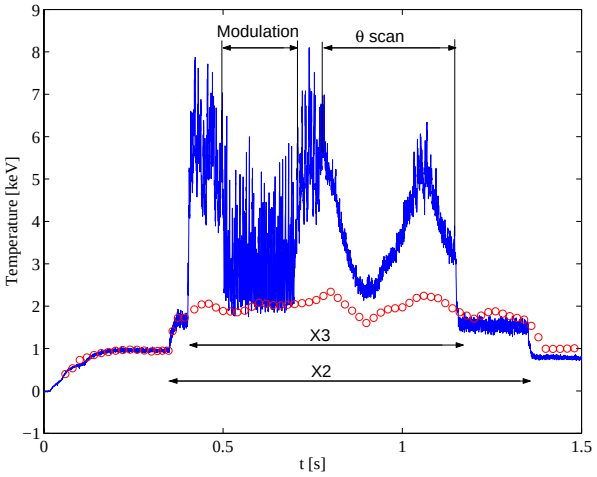

Fig. 2.1.16 *Temporal evolution of the central channel of the ECE (full line) with X2 ECH preheating followed by X3 central ECH. Between 0.8s and 1.15s a poloidal scan of the X3 launcher is performed. The circles show the central temperature from Thomson Scattering. The target plasmas in the experiments and in Fig. 2.1.17 have the following parameters:* I_p*=200kA,* q_{95}*=3.8,* κ*=1.31,* δ*=0.16,* B_T*=1.42T,* $n_e(0)=2.5x10^{19}m^{-3}$.

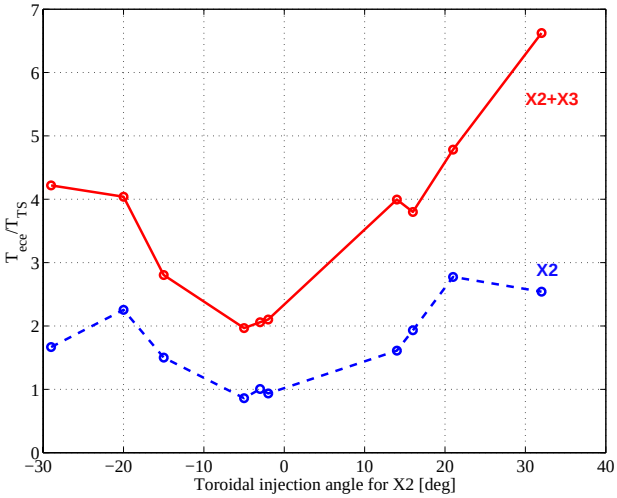

Fig. 2.1.17 *Central temperature comparison for a toroidal injection angle scan. The dashed line is the ratio of the ECE temperature at r/a=0.1 and the central Thomson temperature during the X2 phase of the discharge. The full line is the same ratio during the X2+X3 phase.*

2.1.15 Interpretation of plasma dynamic response to additional heating in ASDEX Upgrade and TCV

During 2001 investigations were conducted in collaboration with the ASDEX Upgrade team to verify the diagnostic possibilities of the plasma dynamic response to intense Modulated ECH (MECH). Attention was given to the possibility of using line integrated soft X-ray (SXR) data in order to determine the location of the power deposition. Figure 2.1.18 shows the main results of this study: amplitude and phase profiles of SXR measurements are coherent with electron cyclotron emission (ECE) data and clearly determine the deposition location.

The limitations of the previously developed method, based on the generalised singular value decomposition technique (GSVD), were also assessed. In particular, it has been demonstrated that the GSVD is incapable of removing the coupling between the sawtooth instability and the MECH, leading to potential misinterpretations of the profiles. The analysis of the ECE data on ASDEX Upgrade at the ECH shut off has shown that a new method based on system identification using the singular value decomposition technique (SVD) can be used instead. The SVD has the strong advantage of being able to determine the phase space region in which the dynamics of both the sawteeth and the shut off (and consequently the MECH) are contained but are still mixed. Treating this reduced problem with a system identification method should allow us to fully separate the different dynamics.

Finally, experiments have been performed in TCV in order to analyse SXR diagnostics in parallel with the recently installed low field side ECE system. Preliminary results confirm previous ASDEX Upgrade observations and point out the importance of a new SXR diagnostic based on a multiwire proportional X-ray detector chamber. This diagnostic ensures a very good spatial resolution, and is not affected by neutrons, a very important feature for future fusion devices.

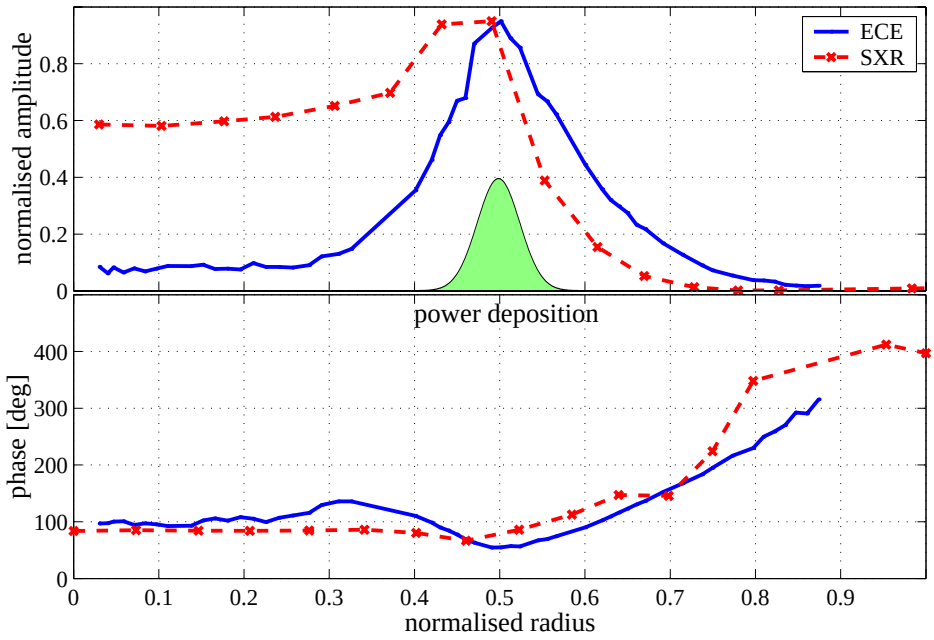

Fig. 2.1.18 *Determination of the ECH power deposition profile from the plasma response to MECH.*

2.1.16 *Modulated ECH power absorption measurements using a diamagnetic loop*

During 2001, a special effort has been made to develop a robust method of experimentally assessing the global ECH power absorption. The additional heating power absorbed by the plasma can be determined from the time derivative of the total plasma energy, which can be estimated from the diamagnetic flux of the plasma using a DiaMagnetic Loop (DML) diagnostic. The DML system consists of two loops, the first one (1-turn) wound around the vacuum vessel and the second one serving as a compensation loop. The main difficulty in using diamagnetic measurements to estimate the kinetic energy is the compensation of the flux measurement sensitivity to poloidal magnetic fields. A method based on the temporal variations of the diamagnetic flux of the plasma during Modulated ECH (MECH) has been successfully developed and applied.

The analysis of the DML data has allowed us to determine the absorbed MECH power for third harmonic X-mode heating in TCV for the first time. In particular, a MECH frequency scan has identified an optimum modulation frequency, situated within the range 200-250Hz, as well as the value of the energy confinement time for these discharges (see Fig. 2.1.19). The frequency scan is particularly important to verify that the MECH period is much shorter than the energy confinement time, so that energy losses are avoided.

The measurements of the X3 MECH discharges show that full single pass absorption is achieved for the 470kW of injected X3 with as little as 350kW of X2 preheating in a counter current drive configuration. This high absorption exceeds the predictions of the ray tracing code TORAY by more than a factor of 2 and, again, is consistent with the creation of suprathermal electrons by X2 ECH.

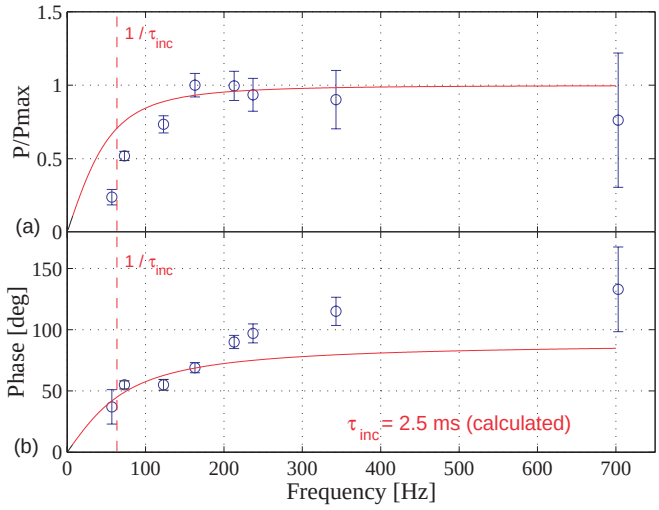

Fig. 2.1.19 *Power absorption frequency scan: (a) Averaged power absorption; (b) MECH phase response. The lines correspond to the fitted amplitude and phase. The fitting has been performed on the real and imaginary parts of the complex response.*

2.1.17 *Optimum conditions for improved core energy confinement (ICEC)*

Current profile modifications and in particular the creation of a region of reversed magnetic shear appear to be the key ingredients to obtain the improved core energy

confinement (ICEC) regime on TCV. This conjecture, supported by simulations using the PRETOR transport code, is confirmed by a series of experiments during which the orientation of the gyrotron beams was varied from discharge to discharge, thus changing the exact location of the counter current drive component near the plasma centre. A small de-centering of the beams has a pronounced effect on the central electron temperature and energy content. A comparison of two discharges is shown in Fig. 2.1.20 for discharge #19425 the counter current drive component was exactly centred, whereas for discharge #19428 the beams were moved off-centre by three degrees.

The scenario to obtain the ICEC-regime in TCV includes a pre-heating phase, with off-axis ECH near $\rho = 0.3$, followed by a phase with additional power deposition in the plasma centre combined with counter current drive. During the first phase the temperature profiles maintain a fixed shape (described as "stiff"), but become more peaked and develop much larger gradients during the ICEC phase (see Figs 2.1.21 and 2.1.22).

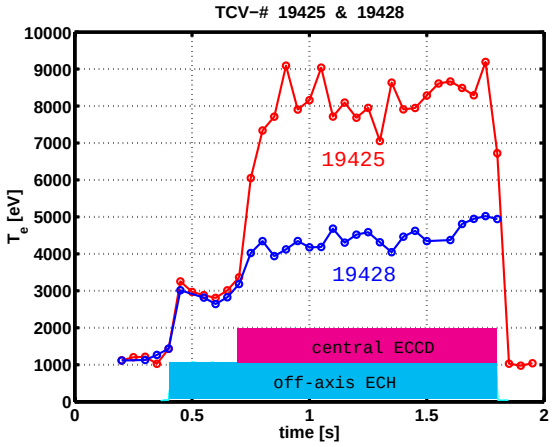

Fig. 2.1.20 *Central electron temperature from Thomson scattering for 2 discharges: a) # 19425 : well centred counter CD; b) # 19428 : slightly de-centred counter CD.*

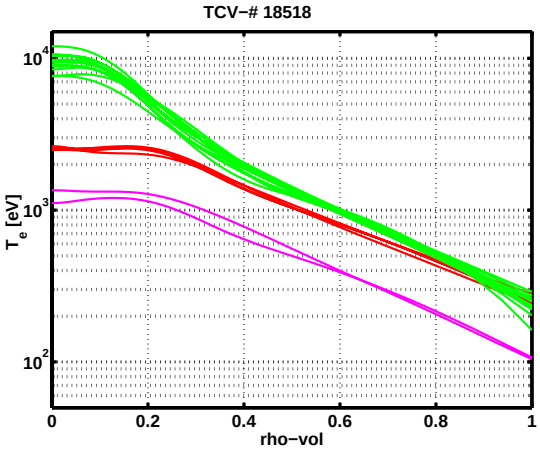

Fig. 2.1.21 *Evolution of the electron temperature profile. Ohmic phase: magenta; Pre-heating phase: red; ICEC-phase: green. Profile remains "stiff" only in the region $\rho > 0.4$.*

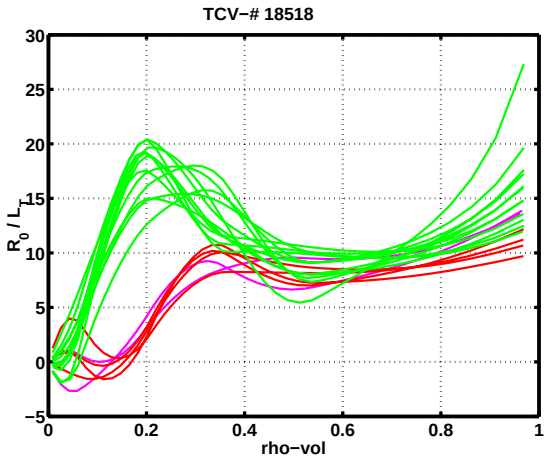

Fig. 2.1.22 *Spatial variation of the normalised electron temperature gradient. Ohmic phase: magenta; Pre-heating phase: red; ICEC-phase: green. Central region delimited by transport barrier near* $\rho = 0.2$.

2.1.18 Fully non-inductive discharges

Fully non-inductive discharges with the plasma current driven by X2 ECH are now routinely achieved in TCV. In this mode of operation the current in the Ohmic transformer primary is kept constant by feedback action. We have extended the TCV discharge length to 4.3s, well beyond the maximum length achievable in Ohmic conditions, by sustaining the current with one X2 cluster at a time and firing the two clusters in succession for their maximum pulse lengths (2s each), as shown in Fig. 2.1.23.

The versatile ECH launcher system of TCV permits careful matching of the power and deposition locations of the two clusters, resulting in minimal perturbation of the plasma conditions at the switch-over. This high degree of external control was further demonstrated by an interlaced square-wave modulation of the two clusters (180° out of phase), which yielded no visible modulation of the plasma parameters.

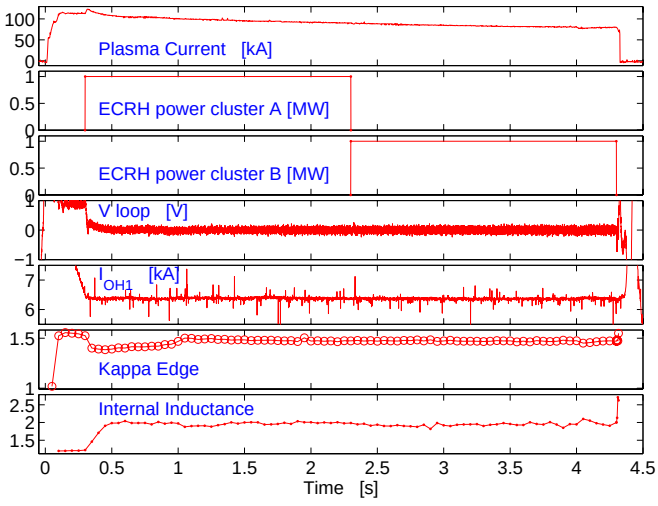

Fig. 2.1.23 *TCV record length discharge (4.3s).*

2.1.19 From current driven to neoclassical driven tearing modes

The use of strong central electron cyclotron current drive in TCV leads to significant current profile modifications compared to standard Ohmic discharges. In low density discharges m/n=2/1 islands have been observed. The growth of the width (w) of these tearing modes has two distinct phases. The first one is typical of a conventional tearing mode driven unstable by the current profile, while the second one is linked to a neoclassical tearing mode driven by a perturbation of the bootstrap current. These results provide the first clear observation of such destabilisation mechanism and reconcile the theory of conventional and neoclassical tearing modes, which only differ in their dominant driving term. The dependence of Δ' on w generally assumed by theory, $\Delta' \sim \Delta'_0 - \alpha w$, is confirmed, meaning that at large w, Δ' is negative while the bootstrap drive is always strong.

Figure 2.1.24 illustrates the time evolution of the island width. In particular, Fig. 2.1.24(a) shows the ECCD power waveform and the 2/1 island width. The mode appears 200-300ms after the ECCD is turned on. Such delay is consistent with the time needed to modify the current profile, as the current redistribution time is about 200ms. When the ECCD power is turned off, the mode decays in two distinct phases, shown in Fig. 2.1.24(b). The first rapid phase, on the energy confinement time scale, is linked to the decrease in β and of the bootstrap drive. The second phase evolves on the current redistribution time scale. During this phase the growth rate follows the time evolution of Δ' with a decreasing island w (Fig. 2.1.24(c)). Looking at the onset phase, time intervals 1-2 and 2-3, we also see two different growth rates: interval 1-2 has a constant or slightly decreasing dw/dt, while interval 2-3 exhibits the dw/dt(w) dependence typical of a strong bootstrap drive. As shown by the red curve in Fig. 2.1.24(d), this time evolution of the growth rate can be understood by considering the modified Rutherford equation, when an empirical modification of the polarisation current at small island width is included. The different contributions to dw/dt are also shown in Fig. 2.1.24(d). The latter phase of the island decay, interval 4-5 with w<5cm, is similar to the Δ' term discussed above, which is the only important term remaining once β has become very small.

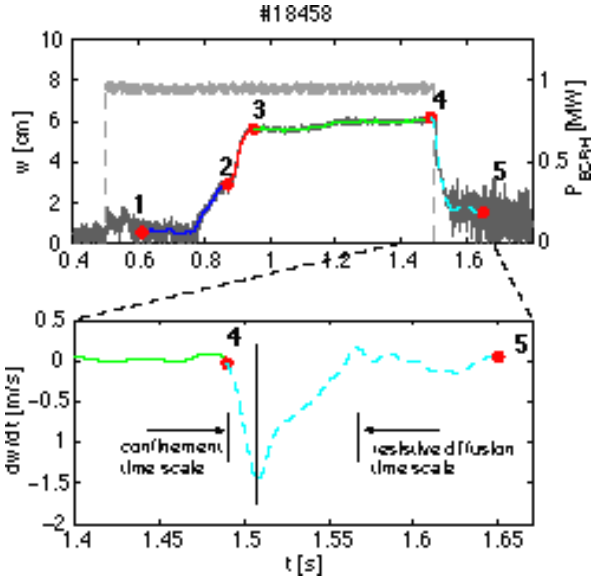

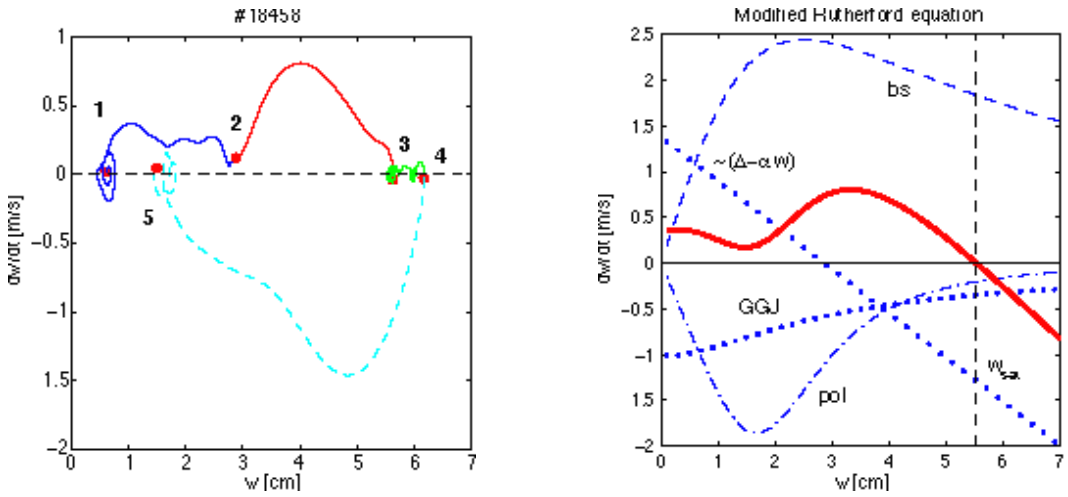

Fig. 2.1.24 *(a): A current driven tearing mode grows on a slow time scale and approaches saturation (1->2). Once w exceeds w_{crit}, the mode grows on a faster time scale to its full width (2->3). (b): After the ECH is switched off (4) the neoclassical driving term decays on a fast confinement time scale, whereas the conventional tearing mode stability evolves on a slower current diffusion time scale. (c): The experimental island growth dw/dt is shown as a function of w. (d): Different contributions to the modified Rutherford equation.*

2.1.20 Evidence for turbulent equipartition in TCV L-modes

Electron temperature and pressure profiles in L-mode tokamak discharges are known to scale with $1/q_a$ in circular plasmas, and more generally with $\langle j\rangle/(q_0 j_0)$ in shaped plasmas. A similar scaling is observed for the electron density, both in Ohmic and ECH plasmas in TCV, implying the existence of an inward particle pinch. Figure 2.1.25 shows the width $\langle n_e\rangle/n_{e0}$ (inverse peaking factors) of the electron density profile form a wide variety of discharge conditions in TCV: $1<\kappa_a<2.6$, $0.5<\delta_a<0.7$, $2<q_{95}<7$, $1.2\times10^{19}m^{-3}<n_e<1.2\times10^{20}m^{-3}$, $0.1<\nu^*_{75}<10$, where κ_a and δ_a are the elongation and the triangularity at the last closed flux surface (LCFS), and ν^*_{75} is the normalised electron collisionality at 75% of the poloidal flux. Although the example shown is for Ohmic plasmas, very similar results are obtained for ECH plasmas in L-mode. This result can be understood from Turbulent Equipartition (TEP) theories, which assume conservation of the particle magnetic moment μ and the longitudinal invariant J.

The essential prediction of these theories is that particles with given values of μ and J tend to spread evenly over the accessible poloidal flux, i.e. $\partial N/\partial\Psi\approx$const, where N is the total number of particles within a given flux surface. Figure 2.1.26 shows a superposition of more than 200 total particle number profiles as a function of poloidal flux, establishing that N increases nearly linearly with Ψ. TEP leads to density profiles roughly proportional to $(1/q)^\eta$ with $0.3\leq\eta\leq1$, where the exact value of η depends on the relative contributions of trapped and passing particles to transport. Ohmic L-modes are consistent with $\eta\approx1$, while ECH L-modes have $\eta\approx0.8$, suggesting nearly equal transport of passing and trapped particles. TEP therefore implies a scaling of inverse peaking factors with $1/q_a$ for circular discharges, and $\langle j\rangle/(q_0 j_0)$ in shaped plasmas, in agreement with observations (lines in Fig. 2.1.25).

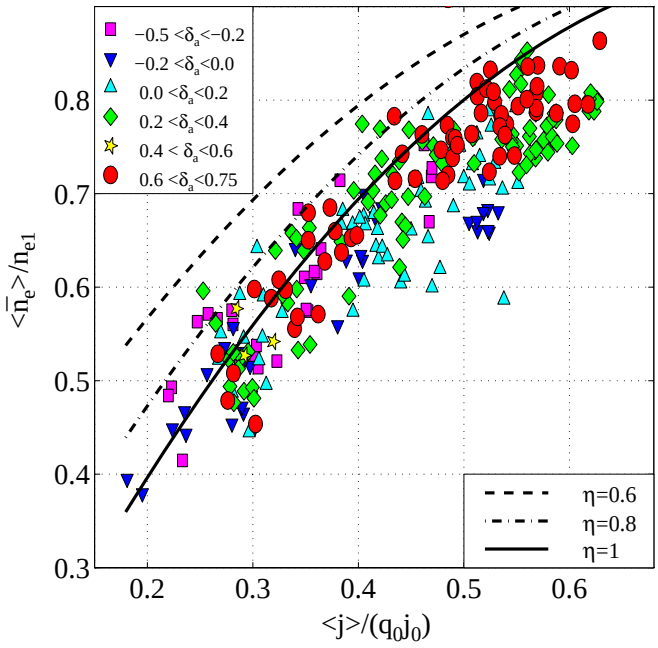

Fig. 2.1.25 *Widths of electron density profiles from experiment and widths expected for density profiles of the form $n_e \propto 1/(qd\Phi/dV)^{\eta}$. Symbols refer to classes of triangularity.*

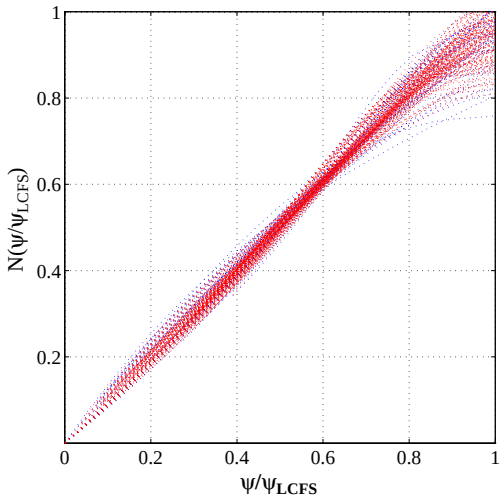

Fig. 2.1.26 *Integrated, normalised particle content versus normalised poloidal flux in OH dataset. Each line corresponds to one of 226 density profiles. Only the portion corresponding to the confinement zone is shown.*

2.2 Theory and numerical simulation

The role of theoretical activities in the CRPP is to provide a basic understanding of the physical mechanisms involved in various aspects of magnetic confinement, so that both predictions and interpretations of experiments can be made. The CRPP theory group has been active in the following topics. (1) The physics of the so-called "anomalous transport", which is a widely observed high level of energy and particle transport across magnetic field lines. (2) The exploration and optimisation of new configurations. (3) The determination of operational limits of tokamaks. (4) The

application of RF waves for heating and current drive purposes. In all these activities substantial numerical simulation efforts have been made, including new developments or improvements of the computational performance. Several of these activities are carried out in close cooperation with other Euratom (IPP-Greifswald, IPP-Garching, CEA-Cadarache, KTH) or non-Euratom laboratories (PPPL, NIFS, Keldysh, Kurtchatov).

2.2.1 Physics underlying anomalous transport

Anomalous transport is a phenomenon that affects virtually all magnetic confinement experiments. It is due to collective effects that create turbulence in the plasma and result in much larger energy and particle fluxes across the magnetic field lines than due to particle collisions alone. When equilibrium gradients (of temperature, density or magnetic field) exceed certain threshold values particular instabilities can develop, such as the Ion Temperature Gradient (ITG) mode or the Trapped Electron Mode (TEM). These unstable modes, through nonlinear coupling, may then develop a broad turbulent spectrum, leading to cross-field particle and heat fluxes and hence a degradation of the quality of the magnetic confinement. The understanding and theoretical modelling of these phenomena is one of the big challenges of fusion plasma physics.

Part of our activity has been devoted to the study of the linear stability of various eigenmodes, examining the effect of different equilibrium parameters. We have focused on the effects of radial electric fields, the dynamics of electrons and finite plasma beta (ratio of plasma pressure to magnetic pressure). Another subject is the nonlinear evolution towards a saturated turbulent state, and in particular the understanding of the behaviour and role of radial electric fields self-generated by the turbulence (called "zonal flows"). The physical model used for these studies is called "gyrokinetic". It assumes that the frequencies under consideration are much smaller than the ion cyclotron frequency, and results in perturbations that tend to align with the magnetic field.

Effect of applied radial electric fields on stability

Applied electric fields are believed to play an important role in the formation of transport barriers through their stabilising influence on microinstabilities, such as ITG modes, which underly anomalous transport. A transport barrier is a region of the plasma in which the usually high level of anomalous heat transport is substantially reduced, sometimes down to levels as low as predicted by neoclassical collisional transport theory.

The global linear gyrokinetic code LORB5 has been used for simulating experimental discharges using measured profiles and reconstructed MHD equilibria. The Asdex-UpGrade (AUG) tokamak provides a measurement of the plasma toroidal rotation using Charge Exchange Recombination Spectroscopy. We focused our analyses on the AUG pulse 13149, an L-Mode discharge with a reversed shear configuration and a relatively strong radial electric field, in which an ion Internal Transport Barrier (ITB) has been identified. A first set of simulations was performed without taking into account the poloidal rotation, in order to reconstruct the spectrum of electrostatic microinstabilities. The main instability appeared to be an ITG further destabilised by trapped electron dynamics (Fig. 2.2.1). When the radial electric field measured in the experiment was included, we found that the ExB flow was sufficient to completely stabilise these global modes, even when taking into account trapped electrons dynamics (Fig. 2.2.2).

Further investigations of this pulse are now under way in order to understand the role that other physical parameters (e.g. the q profile) play in the formation of ITBs.

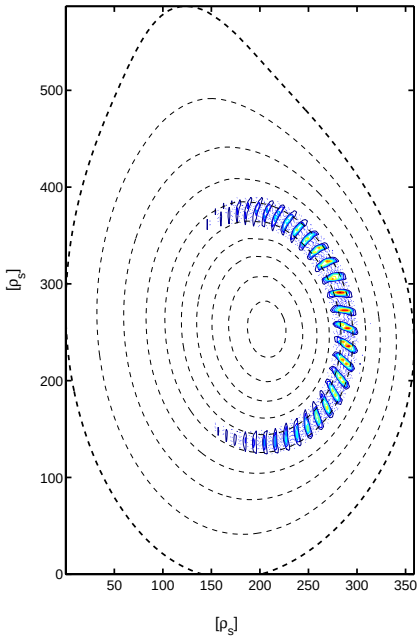

Fig. 2.2.1 *Perturbed potential contours of the most unstable toroidal-ITG mode in an Asdex-Upgrade plasma discharge with an internal transport barrier, computed here with trapped electrons and Mach=-0.01.*

We have studied the effect of applied ExB flows on ITG modes in toroidal, helical and cylindrical configurations and various types of flow profiles. Our results, obtained with global linear gyrokinetic simulations, show that the ITG growth rates depend quadratically on the shearing rate of the ExB velocity. We have also found that with a localised flow profile the ITG instability is pushed towards regions of minimum shearing rate. For a given shearing rate, the ITG growth rate increases linearly with the ion temperature gradient. The critical gradient for marginal stability is upshifted as compared to the case without ExB flows. The upshift of the critical gradient depends approximately on the square of the shearing rate.

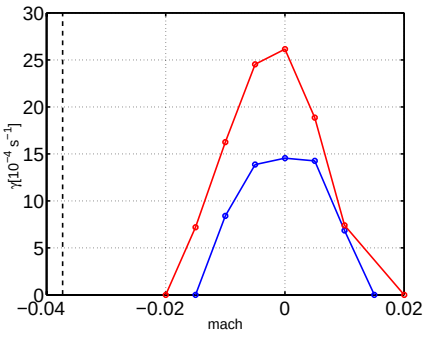

Fig. 2.2.2 *Growth rate of the most unstable mode versus Mach number for adiabatic (red) and trapped (blue) electrons (n=30). The black dashed line corresponds to the experimental value, Mach=-0.0373.*

The application of radial electric fields in situations where the dominant instability is a Trapped Ion Mode (TIM) has been found to lead to very different results from those found where the ITG mode was dominant. With an outward electric field there appears no clear stabilisation. However, with increasing strength of an inward electric field the TIM is at first stabilised but then a Trapped Electron Mode (TEM) is destabilised to even higher growth rates than the mode without radial electric field.

Self-generated radial electric fields (zonal flows)
Purely radial electric fields, called "zonal flows", can be generated by the nonlinear coupling of ITG modes. The zonal flows exert a stabilising influence on ITG modes, and thus a nonlinear feedback loop links the ITG and zonal flow amplitudes. This coupling is then a key factor in determining level of ITG turbulence in a saturated state.

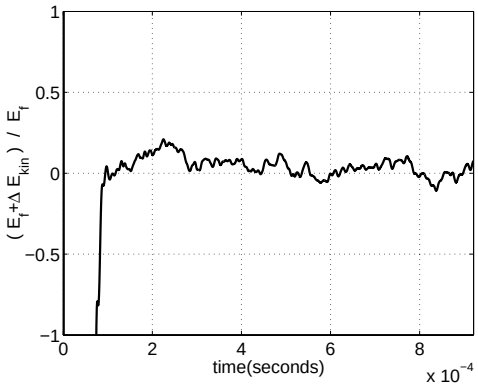

Fig. 2.2.3 *Check of the energy conservation property in a nonlinear global gyrokinetic simulation in a cylindrical plasma.*

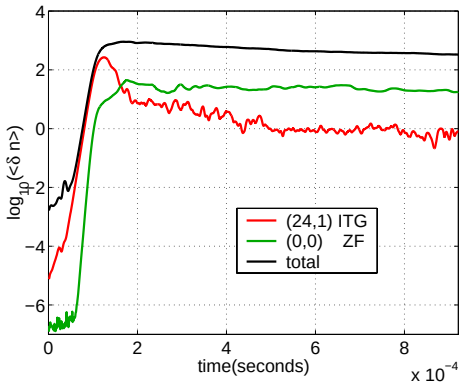

Fig. 2.2.4 *Evolution of the perturbed density (black) in the same nonlinear global gyrokinetic simulation as in Fig. 2.2.3. Zonal flow (green) and linearly most unstable ITG mode (red) amplitudes are also shown.*

We have investigated this dynamical behaviour with a global nonlinear gyrokinetic code, developed in close collaboration with IPP-Greifswald, neglecting for the moment magnetic curvature and shear. Our model does not include any collisional damping. The numerical results show that the energy is conserved to within 20% of the perturbed field energy for the whole duration of the simulation (Fig. 2.2.3). There appears also no evidence of numerical noise accumulation which is a potential problem in such schemes. Thus there appears no sign of spurious damping or drive of numerical origin. The dynamical evolution (Fig. 2.2.4) is characterised by the exponential growth of the most unstable ITG mode, immediately followed by an even faster growth of the zonal flow, until those reach a high enough amplitude to have a visible stabilising effect on the ITG modes. The system then reaches a quasi steady-state with finite levels of both ITG and zonal flows.

While the above numerical results were obtained with a Particle-In-Cell method we have pursued the development of an alternative approach, namely a semi-Lagrangian numerical scheme, in collaboration with the Euratom-CEA Association. The potential advantage of this approach is the absence of statistical numerical noise that is sometimes a limitation of PIC codes. The ion polarisation density and the zonal flow term have been introduced in the code. Comparisons with other codes are underway and improvements to the accuracy of this scheme are still to be developed.

Electromagnetic effects

Since the fusion power is roughly proportional to the square of the plasma beta for a given magnetic field, high values of beta are obviously desirable. However, increasing beta changes the character of microinstabilities from electrostatic to electromagnetic, potentially affecting anomalous transport. The aim of this work is to study the behaviour of microinstabilities including finite beta effects.

Electromagnetic microinstabilities in tokamak plasmas have been studied by means of a linear global eigenvalue code. This code is the electromagnetic extension of an electrostatic code previously developed at CRPP. Results from this code are shown in Fig. 2.2.5. While the toroidal ITG mode is stabilised with increasing beta, another instability appears at a value approximately equal to half the ideal MHD ballooning limit. The growth rate of this mode increases rapidly with beta. For the first time, the particular radial structure of this eigenmode has been obtained (Fig. 2.2.6). The remarkable feature is the very sharp field behaviour in the vicinity of rational surfaces. This is due to the non-adiabatic electron response, with a ratio of phase velocity to the electron thermal velocity changing very rapidly from very small values far from the rational surfaces to larger than unity in a narrow region in the vicinity of the rational surfaces.

We have included the effect of shifting the magnetic surfaces when plasma beta (ratio of plasma pressure to magnetic pressure) is increased (Shfranov shift). The Shafranov shift, together with electromagnetic effects, has been found to strongly stabilise toroidal-ITG modes.

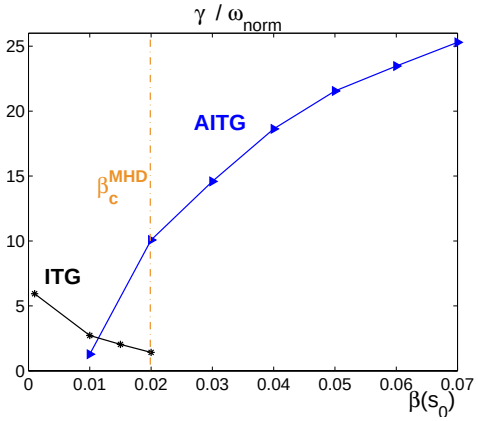

Fig. 2.2.5 *Growth rates of a toroidal-ITG mode and an Alfvenic-ITG mode as a function of plasma beta, computed from a global linear electromagnetic gyrokinetic simulation. The vertical dashed line indicates the ideal MHD ballooning stability limit.*

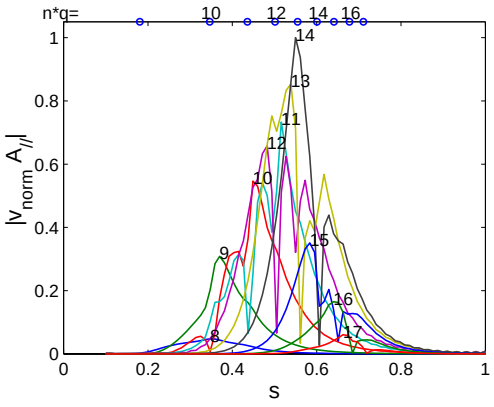

Fig. 2.2.6 *Radial structure of the electromagnetic AITG mode for beta=6%. The small circles on the top axis show the position of rational surfaces.*

2.2.2 Modeling of electron transport and of sawtooth activity in tokamak

Advances in modelling the behaviour of the main plasma parameters in tokamaks have been obtained by the extension and application of a transport code PRETOR to the simulation of electron transport in TCV and of the sawtooth period in TCV and JET.

The simulation of the electron temperature and density profiles in TCV Ohmic sawtoothing plasmas has shown that the proper description of the current density profile and of the sawtooth activity plays the dominant role in recovering the experimental profile width, and not the detailed physics involved in the transport model applied, provided that a single parameter in the model is adjusted to match the global plasma performance.

In the presence of intense ECH the heating power density profile and the current denity profile are decoupled, as compared with the situation with Ohmic heating alone. This allows one to investigate the main characterisitics of the electron transport in more detail.

Towards understanding electron transport in TCV
In several tokamaks with central heating, the electron temperature profile is stiff outside the power deposition region, that is the temperature length scale is independent of the heating power and essentially constant along the minor radius. With off-axis heating a power balance analysis shows that transport is strongly reduced in the central region of the plasma, whereas a steep increase of the heat conductivity is observed at the power deposition location. Moreover, the profile appears flexible, that is strong local gradient modifications can be induced in the confinement region.

The present TCV experimental behaviour has been satisfactorily reproduced in transport simulations by the application of the Rebut-Lallia-Watkins (RLW) local transport model. The experimental temperature gradient with ECH exceeds by far the critical electron temperature gradient involved in the model. Nevertheless, the parametric dependence of the RLW heat conductivity is such that the numerical simulations agree with the experimentally observed stiff behaviour. In general it can be stated that the RLW transport model is adequate to reproduce the electron transport for plasma parameters in the operation domain of TCV. This has enabled us to use this model to prepare and predict experimental response to changes in heating location and current drive for example.

Towards a predictive model for sawtooth periods in tokamaks
A model first proposed to predict the sawtooth period in burning plasmas has been extended and applied in very different plasma and heating conditions. In particular, effects of localised heating and current drive on sawteeth have been explored simulating experimental results obtained in TCV, whereas fast particle effects have been investigated considering recent JET experiments with neutral beam injection (NBI). The model is suited for implementation in a transport code, provided that the transport package is consistently coupled with an equilibrium solver and that geometrical effects are included in the flux surface averaged expression of the diffusion equations. Indeed the proper description of the poloidal magnetic field and therefore of the current profile is crucial for a correct application of the sawtooth period model.

Localised Electron Cyclotron Heating (ECH) and Electron Cyclotron Current Drive (ECCD) have very strong effects on the sawtooth period. The model is able to recover specific effects, such as the stabilisation obtained with localised heating and co-current ECCD when applied just outside the q=1 surface, and the destabilisaton provided by counter-current ECCD at the same location. The model allows us to single out the effects due to current drive from the effects due to localised heating. The results of a simulation, Fig. 2.2.7, show that co- and counter-current drive have comparable effects at symmetrical positions about the q=1 surface: the stabilising effect of co-ECCD just outside the q=1 surface is similar to that of counter-ECCD just inside the q=1 surface, and the destabilising effect of co-ECCD just inside the q=1 surface is similar to that of counter-ECCD just outside the q=1 surface. The experimental behaviour with ECH in TCV is found consistent with the linear stability threshold of the internal kink in the resisitive regime, and in particular is mainly determined by the modification of the dynamics of the magnetic shear at the q=1 surface incuced by ECH/ECCD.

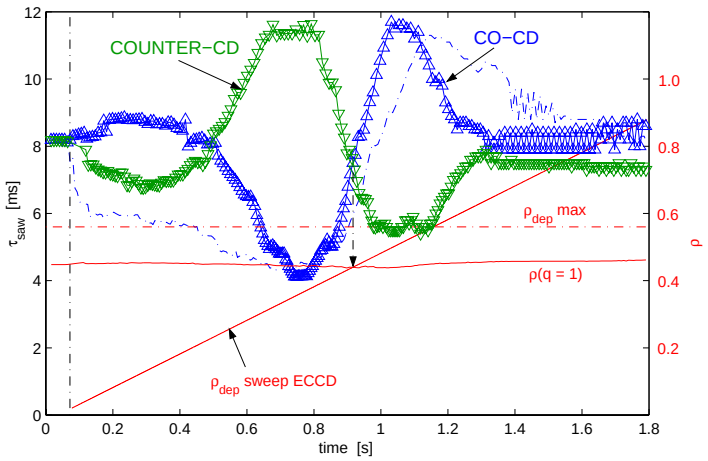

Fig. 2.2.7 *Time traces of the sawtooth period resulting from a radial sweep of localised current drive in the co direction (triangles pointing up) and in the counter direction (triangles pointing down). 1.35MW of localised heating are applied during the full sweep at the heating location* rho_{dep}^{max} *which most efficiently stabilises the sawtooth period. The sawtooth period time trace resulting from a radial sweep of the heating power density is added for reference with a dash-dotted line. With this set-up both stabilisation and destabilisation effects are emphasised.*

Recent discharges at JET have provided an experimental assessment of the role of beam ions in stabilising sawteeth. In order to investigate these experimental results, an analytical expression for the fast ion contribution to the internal kink potential energy has been checked against the results of the hybrid kinetic/MHD code NOVA-K and has been included in the sawtooth period model. The simulated sawtooth periods have been found in quantitative agreement with the actual periods. The relevant stability threshold for the resistive internal kink at play was predicted to be the sawtooth crash trigger relevant for ITER operation, with the role of beam ions in JET similar to the predicted role of alpha-particles in ITER.

2.2.3 Optimisation of 3D magnetic configurations

When the magnetic field strength varies along the field line it gives rise to trapped particles in the lower field region. When a pressure gradient is present the combined effect is to give rise to a plasma current called the bootstrap current. While in tokamaks the bootstrap current may be desirable, in 3D systems it can have an adverse effect on the magnetic configuration, in particular on the rotational transform of the magnetic field lines. Thus the importance of having a consistent equilibrium calculation that takes into account this current. An algorithm to compute the bootstrap current in the collisionless $1/\nu$ regime in 3D magnetic confinement configurations has been developed and implemented as a module in the TERPSICHORE code. This module has been applied to compute the selfconsistent bootstrap current in a 2 field period quasiaxisymmetric stellarator reactor using a nearly parabolic pressure profile at different values of β^*. An iterative computation of 3D equilibria with the VMEC code and the bootstrap current is undertaken until a converged solution is obtained. The bootstrap current increases the rotational transform above the critical value $l_c=1/2$ which can destabilise the m/n=2/1 external kink mode. At $\beta^*=5\%$, a 20% suppression of the bootstrap current, which corresponds to about 1MA in a reactor with volume ~1000m^3, can stabilise this mode.

In a sphellamak reactor system, the bootstrap current contributes only about 10% of the plasma current required to converge an equilibrium solution with the VMEC code at $\beta^*=8\%$ under conditions of peaked toroidal current associated with maximum-B properties. Alpha particles born at midradius in a region where the mod-B contours close poloidally are very well confined, while a large fraction of the trapped alpha population born at midvolume experience the full 3D structure of the magnetic field and escape the plasma.

2.2.4 Macroscopic stability of tokamaks

Studies of the dependence of the poloidal beta limit of the ideal internal kink mode on some plasma parameters like elongation, triangularity and aspect ratio have been carried out. It was shown that by changing the plasma aspect ratio from high (cylindrical approximation) to TCV values the dependence of the ideal internal kink mode growth rate on the poloidal beta inside the q=1 surface changes from quadratic at high aspect ratio to linear at real and low aspect ratio. This differs from the theoretically predicted behaviour, most probably because the simplifying assumptions which were used to produce the analytical approximations are not satisfied in cases far from cylindrical geometry. It was also shown that the critical poloidal beta inside the q=1 surface linearly decreases with increasing plasma elongation. It was also found that the stabilising influence of positive and negative triangularity depends on the peaking of the plasma current profile.

Studies of the stability of the ideal external kink mode for TCV plasmas with high edge elongation (above 2.7) have been carried out. A number of equilibria with high elongation, some reconstruction of TCV shots, were analysed. The dependence of the stability limit on plasma elongation and on q profile corresponds well with the TCV experimental results.

Global ideal MHD instabilities are affected by the presence of a conducting wall. When the resistivity of the wall is taken into account, a resistive wall mode (RWM) appears. We have included in the KINX-WR code a double wall and a simplified model for the feedback control of the instability. An analysis of an ITER steady-state scenario has shown the possibility of feedback stabilisation (with a single wall) for a plasma pressure up to twice the ideal MHD limit in the absence of wall.

The inclusion of a fast poloidal phase extraction into the KINX code has enabled us to study edge localised instabilities with very high mode numbers. This has been done in configurations with and without a magnetic separatrix at the plasma edge. The influence of the separatrix leads to a stabilisation of peeling - ballooning modes and lower growth rates of external kink - ballooning modes. Peeling modes are edge localised instabilities that appear when there is a rational magnetic surface in the vacuum near the plasma boundary. External kink modes are more global instabilities. Ballooning means the mode tends to localise in the unfavourable magnetic curvature region.

2.2.5 Radiofrequency waves

Quasi-linear effects on the electron cyclotron current-drive (ECCD) efficiency with high power density

The TCV experiment can have very high EC power densities and can drive significant currents. Therefore large high energy electron tails can be sustained which can in turn lead to increased current drive efficiencies.

The CQL3D Fokker-Planck code has been used to model ECCD/ECH experiments in the TCV. The code has a module for including radial particle transport. It has been shown that in TCV radial diffusion is an important factor in understanding the ECCD physics. Without transport the code overestimates the ECCD efficiency by a factor of five or more, due to overestimating quasi-linear effects. However, inclusion of the transport leads to a good agreement with experiments. In addition, this transport leads to a diffusion of current, resulting in a smooth, non-local current density profile. The strong effect of particle diffusion on the ECCD efficiency is due to comparable transport and slowing down times of non-thermal electrons: fast particles, which carry most of the current generated by EC waves, diffuse radially before they slow down. This leads to a reduction of the ECCD efficiency since it prevents build-up of a supra-thermal tail.

Alfvén frequencies and ICRF in 3D

The subject of the present study is low frequency electromagnetic wave heating in 3D plasma configurations in the ion-cyclotron and Alfvén frequency range. The code developed implements the full cold plasma model to describe the plasma and uses equilibria from the VMEC 3D code for the geometry. The equilibria are treated with the TERPSICHORE code in order to calculate the metric in appropriate (Boozer) magnetic coordinates. We have further developed the 1D and 2D versions of the

code and implemented a subroutine to calculate power flows in the plasma, which allows for energy conservation to be checked and for the plasma response to be calculated. The results of the 2D code in a tokamak geometry have been compared with the LION code calculations. The Alfvén resonances and the Alfvén continuum boundary positions in a tokamak configuration are in a good agreement with the LION results. Purely toroidal effects such as the gap in the continuum and the Toroidicity Induced Alfvén Eigenmode (TAE) have been tested, showing once again good agreement between the codes. The finite elements applied for the radial discretisation have been modified in order to improve the convergence.

2.3 Basic Plasma Physics Activities

As part of the initiatives related to the appointment of a Assistant Professor Tenure Track of the EPFL Physics Faculty supported by a fellowship of the Swiss National Science Foundation*, a basic experimental plasma physics group is being restarted at CRPP. The goal of the group is to isolate and investigate fundamental plasma physics problems of interest for magnetic fusion in a well-diagnosed laboratory plasma device, as well as to train students.

The group will investigate linear and non-linear wave-particle interaction phenomena, transport processes and phenomena related to magnetic reconnection in a magnetized toroidal plasma device. Design work of the related experimental infrastructure has started in the past six months. The search for the personnel to form the group, including a number of graduate students, is also under way.

2.4 Materials for fusion

The main objective of the Fusion Technology Materials group is to investigate the effects of the damage produced by radiation in metals and alloys, especially in candidate materials for structural components of the future fusion reactors. This group uses the high energy (590MeV) proton beam of the PSI accelerator, through the Proton Irradiation Experiment (PIREX) facility, to simulate experimentally the effects of the 14MeV neutrons that are the product of the fusion reactions between deuterium and tritium nuclei.

Like 14MeV neutrons, 590MeV protons produce atomic displacement cascades and transmutation nuclear reactions inside the irradiated material. From the point of view of materials science, atomic displacement cascades induce the formation of point defects, such as vacancies and interstitial atoms, while nuclear transmutation reactions produce radioactive impurities, such as helium and hydrogen atoms. The final microstructure of the irradiated material results from reactions between these different defects. It includes dislocation loops, dislocation networks, stacking fault tetrahedra, gas bubbles and/or voids resulting from the accumulation of point defects. This microstructure has an important effect on the physical and mechanical properties of any material. It can lead to significant hardening, loss of ductility and fracture toughness, as well as macroscopic swelling of the material. These effects are the main factors limiting the candidate materials. The residual radioactivity of a large amount of exposed material is also of concern and will govern the handling methods, dictate the storage periods and the overall waste

* Prof. A. Fasoli is supported by a grant from the Swiss national Science Foundation, as “Professeur Assistant Boursier du Fonds National”. His research is supported in part by this grant.

management and recycling scenarios. The development strategy that takes into account these limitations has led to the development of so-called low activation materials.

The design of materials with properties adequate for use in an irradiation environment requires an understanding of the effects of irradiation on their physical and mechanical properties. The FTM group has been active in that field for several years within the framework of the European Fusion Development Agreement and collaborates with many research institutes and industries in Switzerland as well as abroad. For some specific experiments, neutron irradiations are carried out in reactors in Denmark, Hungary, Sweden and the Netherlands and a number of materials have also been irradiated with protons in the Swiss Spallation Neutron Source (SINQ) at the Swiss Paul Scherrer Instititute (PSI). The research activities of the group include basic research on radiation damage in pure metals and alloys (see section 2.4.1), development of low activation materials for fusion applications (see sections 2.4.2 and 2.4.3), characterisation of materials for ITER (see section 2.4.3 and 2.4.4) and development of new techniques for the investigation of the structure/mechanics relationships in radioactive materials (see paragraphs 2.4.5). The main experimental tools include macroscopic mechanical testing, scanning and transmission electron microscopy (SEM, TEM) and small angle neutron scattering (SANS). The main numerical tools include molecular dynamics simulations, dislocation dynamics calculations and finite element analysis.

2.4.1 Basic research on radiation damage

The microstructure and tensile properties of irradiated pure Ni single crystals
Ni, Cu, Au and Pd are recognized as typical fcc (face centered cubic) metals for radiation effect research, with convenient variations of relevant parameters such as the stacking fault energy. Previous observations of Ni after irradiation with neutrons or energetic ions up to 503K have shown that the defect density accumulates at a lower rate in this metal as compared with either Cu or Pd in an equivalent temperature range. In addition, Zinkle and Snead have also reported a transition from a microstructure dominated by stacking fault tetrahedra (SFT's) at low doses to a microstructure dominated by interstitial dislocation loops at higher doses at 503K. Both the defect and deformation structures of Cu and Pd are now well established. In particular, dislocation channelling has been shown to be one of the main initial deformation modes in fcc materials, with a characteristic channel width and separation. The transition from the initial channel-dominated deformation to the formation of dislocation cells generally observed at the end of the tensile curves is not yet fully understood. Ni is being studied further in order to learn more about defect type and accumulation, together with tensile properties associated with each microstructure.

Tensile specimens prepared from single crystal rods of pure (99.999%) nickel have been irradiated in the PIREX facility. They were subsequently deformed in tensile tests at room temperature, in air, by using a micro-tensile machine and a shear strain rate of about $5x10^{-5}s^{-1}$. In parallel, TEM samples were prepared from the deformed unirradiated specimens and from the irradiated and deformed specimens. The microstructure was characterised in TEM by using the weak beam technique and g(5g) (with g=(200)) diffraction conditions. This diffraction vector (g) makes the SFT's clearly visible. It appears that for TEM observation using the weak beam technique the use of a beam convergence angle of 5mrad or larger improves the visibility of partial dislocations. Up to now, the microstructure of pure nickel following irradiation to 0.001dpa at 523K and to 0.13dpa at 320K in undeformed

regions of tested specimens has been examined. Both in the 0.001dpa and in the 0.13dpa specimens a high density of dislocation loops and SFT's was shown up. Table 2.4.1 summarises the defect measurements in both specimens.

	Defect density [m^{-3}]	SFT mean size [nm]	Loop mean size [nm]	Ratio of SFT's to loops [%]
0.001 dpa, 523 K	7. 8x10^{21}	3.8	5.4	13
0.13 dpa, 320 K	2.1x10^{23}	1.6	2.5	39

Table 2.4.1 *Characteristics of irradiation-induced defects in pure Ni.*

The total defect cluster density found in the 0.13dpa specimen at 320K is higher than the one found after neutron irradiation to 0.25dpa at 503K. This indicates a saturation value of about 2.1x$10^{23}m^{-3}$, as already suggested. Comparing of neutron and proton irradiations also indicates that the higher defect density in the 0.13dpa specimen relative to the 0.001dpa one can be attributed to both the higher dose and the lower irradiation temperature as well. The research in neutron-irradiated Ni revealed that more than 90% of total defect clusters at low doses are SFT's. At the same irradiation temperature, the present observations show a proportion of SFT's in the 0.001dpa specimen of 13%, much lower than in the neutron-irradiation case. The lower proportion of SFT's formed in Ni relatively to those formed in Cu can be explained by the higher stacking fault energy (130mJ.m^{-2}, compared with 73mJ.m^{-2} in Cu), which means that their formation is more difficult.

The visible defect density in single crystal Ni at 320K is almost five times lower than in Cu, as well as in Pd and Au, at the same two damage levels. This means that when the defect density in Cu reaches a saturation value of about 1x$10^{24}m^{-3}$, the defect density in Ni is still 2.1x$10^{23}m^{-3}$ for a similar damage level. This lower defect density however cannot be related to the stacking fault energy since Pd, which has a comparable high stacking fault energy (180mJ.m^{-2}), shows a similar defect density than Cu.

The results of tensile testing of unirradiated and irradiated Ni single crystals are summarised in Table 2.4.2. As expected, the proton irradiation induces hardening. The critical resolved shear stress (CRSS) at 0.001dpa is more than 3 times higher than the CRSS of the unirradiated material and, at 0.13dpa, it is 15 times higher. The elongation at failure of irradiated specimens is similar to that of the unirradiated Ni. In that respect, Ni exhibits a different behaviour from Cu, Pd and Au single crystals. These three fcc crystals present less elongation after irradiation, even at low doses.

	Critical resolved shear stress [MPa]	Work hardening rate measured at 50% plastic strain [MPa]	Mean length of deformation cells [mm]	Mean width of deformation cells [nm]
Unirradiated	8	136.3	1-4	700
0.001dpa	28	109.4	0.6-2	500
0.13dpa	123	92.5	0.6-2	400

Table 2.4.2 *Results of tensile testing of unirradiated and irradiated pure Ni.*

At the highest dose of 0.13dpa in Ni, the tensile curve exhibits a yield region with serrations and softening appearing after a marked yield point. The amplitude of the stress serrations in the yield region increases from a maximum of 0.7MPa to 3.5MPa following an increase in dose from 0.001dpa to 0.13dpa. The tensile curves at the highest dose exhibit a wide serrated yield region. In addition, the work hardening rate tends to decrease with increasing dose. Unirradiated Ni presents three stages of plastic deformation. Up to a shear strain of about 70% in the unirradiated and 0.001dpa cases, deformation transits from stage II to stage III at a stress level of about 100MPa, where dynamical recovery starts to reduce the hardening rate. For 0.13dpa, the yield point is 123MPa, which is beyond the recovery stress level. The deformation starts then already at a level of stress higher than that of stage III in the unirradiated condition. This results in the formation of smaller deformation cells (Table 2.4.2). The deformation mode of the irradiated and unirradiated samples was analysed by TEM. Both the 0.001dpa and 0.13dpa specimens show dislocation channelling at the beginning of the deformation. The dislocation channels are straight, and sometimes, present localised nodes of dislocations. Dislocations in the channels can be divided into two groups: normally moving dislocations and dislocations pinned by defects at the edge of the channels. The crowded nodes observed in the present study can be looked at as dislocations strongly pinned at the edge of the channels. Further deformation leads to the development of a deformation cell structure with rectangular shapes that start from a high-density of blocked dislocations in the channels.

Multiscale modeling of the effects of radiation

Radiation damage is an inherently multiscale phenomenon. While the displacement cascade evolves within atomic distances and picoseconds, the non-equilibrium defect concentration produced by the cascade quenching migrates over macroscopic lengths and timescales to produce substantial changes in the chemistry, phases and mechanical properties of the irradiated material. In the so-called multiscale simulations, a hierarchical system of simulation codes, extending from molecular dynamics (MD) to kinetic Monte Carlo (kMC) methods, is used to study the evolution of the damage. More recently, 3-D dislocation dynamics (DD) methods have been used to explain the characteristics of dislocation channelling. The characteristics of channelling and the basic mechanism of formation of such a slip singularities are well established. The first dislocation produced by a source in its slip plane destroys the defect clusters that represent an obstacle to its movement by cutting through them. Successive dislocations coming from the source in the same slip plane will see their movement enhanced because of the reduced density of obstacles. Although such reasoning explains how the flow localization is nucleated, there is no explanation for the scaling of the channelling: a width of 100-200nm and a distance between channels of about 1mm. Previous results using MD and kMC methods in Al, Ni, Cu and Fe have modelled the accumulation of single defects and clusters in good agreement with experimental results. Recently, an increase in the length scale has been added by describing the interaction between these defects and dislocations using DD. The DD simulation box is a cube of Cu or Pd, with a 5mm edge, that contains a density of Frank-Read dislocation sources comparable to that found in well annealed fcc crystals, distributed at random in {111} planes. In the DD simulation, plastic deformation of the single crystal is described by the explicit description of the dislocation evolution history, as a stress is applied to the crystal. For this purpose, dislocations are discretized into segments of mixed screw–edge character and the Peach-Koehler force F acting on them is calculated from stress fields caused by neighbouring dislocation segments, all other dislocation segments, all defect clusters and the applied stress. A linear mobility

model, $v_{gi} = M_{gi}F_{gi}$ is used to move the dislocation, where v_{gi} is the glide velocity of the dislocation segment, M_{gi} is the dislocation mobility and F_{gi} is the glide component of the Peach-Koehler force minus the Peierls friction. Dislocation segments that are about to experience a short range interaction are identified and a set of physical rules are used to describe the interaction that results in the formation of junctions, jogs, dipoles, etc. Cross-slip of dislocations is described as a thermally activated process with probability P given by:

$$P = \alpha \, \Omega_l \, \delta t \exp [-(\Delta W - \tau A)/kT]$$

where $\Omega_l = C_t\pi/L$ is the fundamental frequency of a vibrating dislocation segment of length L, C_t is the transverse sound velocity, δt is the time increment, ΔW the activation energy for cross slip, τ the resolved shear stress and A the area swept by the dislocation. The irradiation-induced microstructure is simulated by mapping a density of defect clusters (SFT's or loops) comparable to that measured experimentally after an irradiation under well defined conditions of temperature, dose and particle energy. The interaction between defect clusters and dislocations is simulated by using MD or computed analytically in the case of sessile dislocation loops. The initial region (up to 0.1%) of the tensile curve of an irradiated crystal has been calculated with this method, showing excellent agreement with the experimental results for different defect cluster densities and initial decoration of the dislocation structure by the irradiation-produced clusters. Furthermore, the DD simulation has shown that the cross-slip mechanism is responsible for the extent (width) of the channel. As dislocations propagate from a source, a screw segment may be pinned by the interaction with defect clusters and eventually cross-slip under the increased stress. This is followed by double cross-slip into a plane parallel to the initial one, where the cross-slipped segment becomes a new source. The process continues to propagate by the same mechanisms to other slip planes, producing a band of parallel planes with active dislocations. The spreading of the band is finally limited by the segments of opposite sign that are formed (dipoles) which exert a back stress on the segments attempting to cross-slip. According to the DD simulation this process leads to the formation of slip bands (channels) of a thickness of about 100nm, in very good agreement with the values found experimentally.

A molecular dynamics simulation of primary damage in Mo

Most of the bcc (body centered cubic) potentials used in present MD simulations of damage are of the embedded (EAM) type, that do not reproduce the bond directionality typical of the structure. A comparison has been made of the results from cascades using an EAM type of potential with those simulated with a so-called 'embedded defect' (ED) potential. A distinctive feature of the ED model is the inclusion of a global angle-dependent term in the energy expansion, which attempts to mimic some covalent aspects of the bonding thought to arise in bcc (body centered cubic) transition metals from their unfilled atomic d-shells. Previous studies of the phonon spectra and self-interstitial properties in Mo demonstrated better agreement with experiments using ED, compared with the EAM scheme. The MD simulation of the displacement threshold shows that both the Mo ED and the Mo EAM underestimate the threshold values around <100> directions and overestimate them around <111> directions. But Mo ED is in better agreement with the experimental results in the region around <100> directions. In the cascade simulations, Mo ED predicts larger vacancy clusters as well as a larger fraction of clustered vacancies, again in better agreement with experimental findings. The effect of the inelastic losses (IL) has also been studied. It was found that cascades simulated with no IL produce fewer defects than cascades at the same energy that

include IL. Probably more importantly, it also shows that although the mean square displacement of atoms is larger with no IL, the number of Frenkel pairs is the same for simulations performed with the same primary knock-out atom (PKA) energy, showing an important interplay between IL and the thermal spike duration, pointing further to the importance of the role of the electron-phonon interaction.

Computer simulations of displacement cascades in nanocrystalline Ni

In nanocrystalline materials, grain boundaries play a predominant role in determining the properties of the material. For grain sizes attainable experimentally at present, up to 30% of the atoms in the crystal belong to, or are affected by, the grain boundaries. In the case of irradiated nanomaterials, these boundaries will provide strong sinks for the defects produced by the irradiation. In ion-irradiated nano-Pd, a four-fold reduction in defect production has been observed. MD samples of nano-Ni of 5 and 12nm average grain size have been created using the methods developed by H. van Swygenhoven et al. and PKA's with energies ranging from 5 to 30keV were induced in one of the grains. From a detailed analysis of the atomic movements it was found that during the thermal spike phase there is a significant atomic movement, in the form of linear collision sequences, towards the surrounding grain boundary structure. At the end of the cascade evolution, the excess volume within the grains condenses to form vacancy clusters and SFT's, with a complex partial dislocation structure forming at the higher energies. The grain boundary structure acts then as an interstitial sink, with no significant grain boundary migration resulting.

2.4.2 The low activation ferritic/martensitic steels

The F82H steel

The F82H ferritic/martensitic steel was developed in Japan. It is investigated as part of the IEA (International Energy Agency) Fusion Materials Internationally Coordinated Program on ferritic/martensitic steels. The F82H steel is based on a Fe-8Cr-2W-V-Ta composition. It was heat treated by normalising at 1313K for 0.5 hours and tempering at 1013K for 2 hours.

Four specimens of F82H have been in-beam fatigue tested in the PIREX facility. The accumulated dose was about 0.1-0.2dpa. For comparison, another specimen has been irradiated in the same deformation device, but without deformation, up to about 0.15dpa. This specimen was then fatigue tested in a standard deformation machine. A number of unirradiated specimens of F82H have also been fatigue tested in a standard deformation machine. All fatigue tests were performed at 300°C under strain control up to failure. Two waveforms have been used: continuous triangle ramps and triangle ramps with 2min holds in tension. Hold times have been introduced to simulate the burning phase of the plasma, when the first wall is irradiated statically.

It was found that all specimens exhibit a continuous stress softening with the increasing number of fatigue cycles. In particular, no irradiation hardening occurs during in beam fatigue testing. The softening rate is however affected by irradiation. The post irradiation tested specimen exhibits the strongest softening rate. The longest fatigue life is obtained for the unirradiated specimens. The in-beam testing condition strongly reduces the fatigue life of the specimens, even more as the post-irradiation testing condition. The hold times were found to affect strongly the fatigue life of the in beam tested specimens but they have little effect on the unirradiated ones.

On the other hand, the microstructure induced by irradiation was investigated in TEM in order to identify the key elements of the deformation mechanisms. The focus was on F82H irradiated with protons or neutrons between 0.5 and 9.2dpa at temperatures between 250 and 310°C. At 1dpa the microstructure exhibits irradiation-induced 'black spots' that are heterogeneously distributed and have a mean size of 2.4nm. At 8.8dpa the microstructure presents irradiation-induced dislocation loops that are homogeneously distributed and have a mean size of 5.4nm. TEM analyses have been conducted to identify the Burgers vector of the 'black spot' damage and of the loops. The evolution of the dislocation loop structure induced by irradiation in F82H has been rationalised by the formation of small glissile 1/2 a_o <111> loops that, with increasing dose, form sessile a_o <100> loops that decorate dislocation lines and eventually fill the whole matrix. In addition, at 1dpa there are black spots homogeneously distributed and visible only with a specific diffraction vector, that could be irradiation-induced precipitates.

A quite high density of small helium bubbles (about 1nm) has been observed in specimens of the F82H steel that were proton-irradiated in SINQ at about 300°C to a dose of 10dpa. The impact of such a distribution of helium bubbles on the fracture properties of the F82H steel will be investigated in 2002.

The OPTIMAX steels

The low activation ferritic-martensitic steels known as OPTIMAX steels were developed by the group as candidate structural materials for the first wall of future fusion reactors. They contain about 9wt.%Cr and their detailed composition is based on that of MANET steels where Ni, Mo and Nb have been replaced by the W, V and Ta low activation elements. A series of casts with different contents of W, Mn and N have been produced from high purity components under clean processing conditions. The main difference between the different casts is that the steel designated as OPTIMAX A contains 0.56wt.% Mn and 0.0007wt.% N, while the conditions are reversed in alloy B which contains 0.037wt.% Mn and 0.003wt.% N. In OPTIMAX C and D, the W content was raised to 2wt.%, with a higher N content in the alloy D. A fine carbide structure has been obtained in all cases by normalising the steels at 1370K before austenization for 30 minutes at 1230-1250K (depending on the steel composition) for obtaining a final preaustenite grain size of 16-20μm. After tempering at 1020K (which was used as tempering temperature for all steel compositions) for 2 hours, the carbide volume fraction in both OPTIMAX A and B steels is about 4%. The main difference between the two steels is due to the presence of a higher density of small carbides (< 40nm) in the higher nitrogen containing steel B.

As previously found for the F82H steel, high-energy proton-irradiations at ambient temperature or 523K of the OPTIMAX materials to doses ranging between 0.3 and 1dpa lead to hardening and loss of ductility (related to the formation of small defect clusters and to carbide amorphization). Both phenomena were found to be dependent on the irradiation dose. Proton-irradiation at ambient temperature to a dose of about 1dpa clearly yields a hardening that is minimum for OPTIMAX C and a loss of ductility that is minimum for OPTIMAX A (see Fig. 2.4.1). The irradiation-induced hardening measured at ambient temperature was found to behave the same way as a function of dose for the F82H and OPTIMAX A steels; it increases with the cube root of the dose.

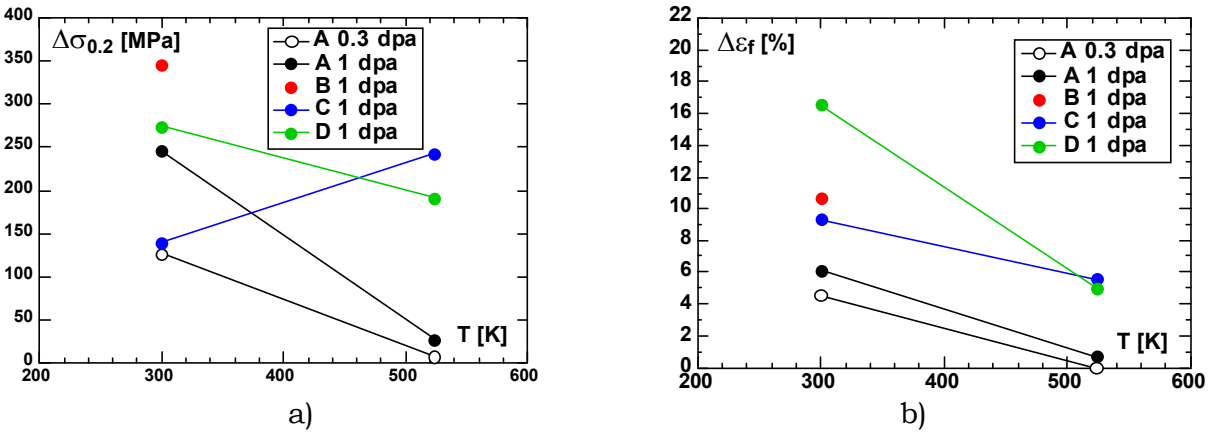

Fig. 2.4.1 *a) Irradiation-induced hardening, OPTIMAX steels; and b) Irradiation-induced loss of ductility, OPTIMAX steels.*

The EUROFER 97 steel

The EUROFER 97 ferritic/martensitic steel was developed within the EFDA Program. Its basic chemical composition is the following: 8.9wt.% Cr, 1.1wt.% W, 0.47wt.% Mn, 0.2wt.% V, 0.14wt.% Ta, 0.11wt.% C, and Fe for the balance.

The tensile and constitutive behaviors of the EUROFER 97 steel in the unirradiated condition were investigated at temperatures ranging between 77 and 723K. The

results were obtained with round DIN specimens (3mm in diameter, 18mm in gauge length) that were cut from a plate of EUROFER 97 (Heat E83697). The tensile testing was carried out at a constant piston velocity corresponding to a nominal strain rate of $5x10^{-4}$ s^{-1}. The temperature dependence of the critical stress measured at 0.2% plastic strain (or yield stress), $\sigma_{0.2}$, the ultimate tensile strength (UTS), the uniform strain (US) and total strain (TS) were determined. The yield stress and ultimate tensile stress as well as the uniform strain and total strain are reported in Figs 2.4.2a and 2.4.2b, respectively.

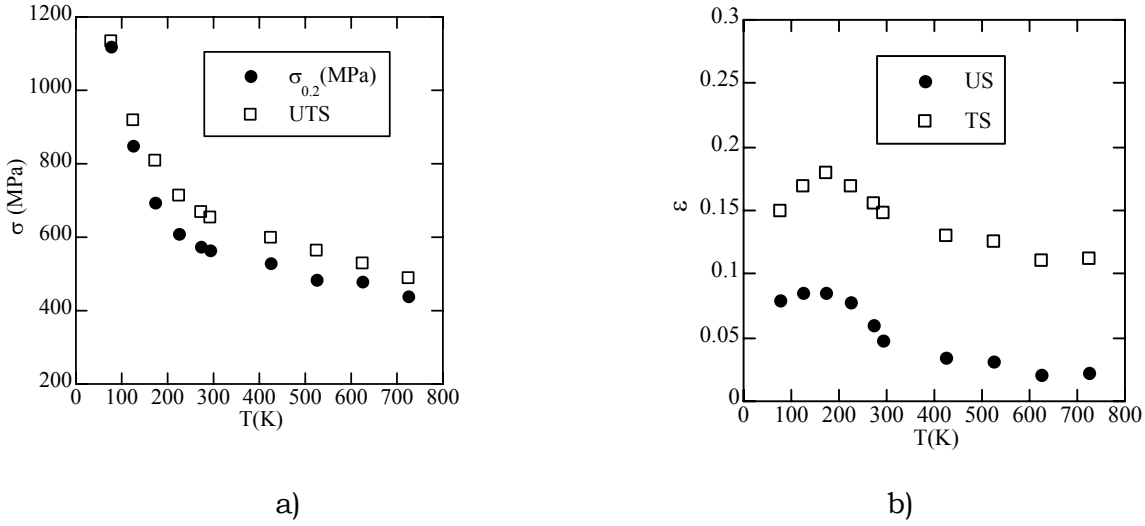

Fig. 2.4.2 *a) $\sigma_{0.2}$ and UTS versus temperature, EUROFER 97; and b) US and TS versus temperature, EUROFER 97.*

Both the yield stress and the ultimate tensile stress exhibit a similar behaviour with temperature, namely a strong decrease with increasing temperature from 77K up to about 200K, followed by a weaker and linear decrease up to 723K. The uniform strain and total strain also vary as a function of temperature in a similar manner. Starting from 77K, a modest increase of the US and TS occurs up to 173K, followed by a monotonous decrease up to 723K.

An effort to understand better the overall constitutive behaviour of this material has been made. The strain-hardening θ_p, defined as $\theta_p = d\sigma/d\varepsilon_p$ (where ε_p is the plastic strain), was systematically calculated. The curves $\theta_p(\sigma)$ were then analysed in the frame of a model based on the mechanics of dislocations which accounts for their storage and annihilation. The model used to describe the strain hardening is based on the original Kocks description of the dislocation density evolution with plastic strain, but the cellular (i.e. heterogeneous) dislocation structure constituted by the lath boundaries and prior austenite grain boundaries was accounted for. It was shown that the strain-hardening law can be written as:

$$\theta_p(\sigma_{pl}) = \frac{P_1}{\sigma_{pl}} - P_2\sigma_{pl}$$

where σ_{pl} is defined as the flow stress minus the yield stress, $\sigma_{pl} = \sigma - \sigma_{0.2}$, and describes the post-yield behaviour. Note that P_1 is related to the dislocation storage while P_2 characterises the annihilation mechanisms. Of primary interest is the mean free path of dislocations associated with the cell size, whose value can be

deduced from the fitted curves $\theta_p(\sigma)$. The deduced values are in reasonable agreement with the size of the laths measured from TEM observations. The above strain-hardening equation can be integrated to get an analytical relationship between the plastic component of the flow stress, σ_{pl}, and the plastic strain, ε_p, allowing the construction of the whole tensile curve from the yield point up to the necking. This integration yields the following equation.

$$\sigma_{pl} = \sqrt{\frac{P_1 - \left(P_1 - P_2\sigma_{pl,i}^2\right)\exp(-2P_2(\varepsilon_p - \varepsilon_{p,i})}{P_2}}$$

The origin of σ_{pl} was chosen at $\varepsilon_{p,i} = 0.001$, at which $\sigma_{pl} = \sigma_{pl,i}$. It is worth noting that a saturation stress is predicted by this analytical constitutive relation, which could not be reached during the tensile testing because of the necking instability, and which is equal to $(P_1/P_2)^{1/2}$. An example of fit is given in Fig. 2.4.3 for a test performed at 423K. This analysis constitutes the basis of a comparison between the overall constitutive behaviour of the unirradiated and irradiated materials and, furthermore, aims at better understanding the physical nature of irradiation hardening.

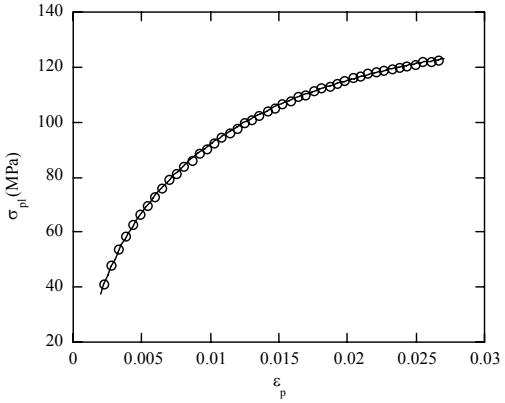

Fig. 2.4.3 *σ_{pl}-ε_p data at 423K fitted according to equation (3).*

Charpy impact tests have also been performed on unirradiated EUROFER 97 with KLST specimens, 3x4x27 mm³ - 1 mm deep notch, and the results are summarised in Fig. 2.4.4. A ductile-to-brittle transition was found around 185±3K for the half upper-shelf energy.

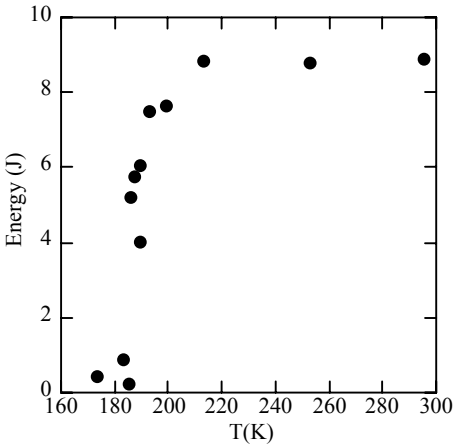

Fig. 2.4.4 *KLST impact energy – temperature curve.*

To complement irradiations performed in 2000, three tensile flat specimens (0.3mm x 2.5mm x 8mm in gauge length) of EUROFER 97 have been irradiated in the PIREX facility at about 350°C to a dose of 0.3dpa.

The ODS steels

Oxide dispersion strengthened (ODS) steels with the EUROFER 97 as matrix material and Y_2O_3 particles as reinforcement particles have been prepared by the Plansee company (Austria) by mechanical alloying and hot isostatic pressing (HIP). As EUROFER ODS has been received from Forschungszentrum Karlsruhe (FZK) in December 2000. It consists of two rods of EUROFER 97 reinforced with Y_2O_3 particles. Each rod had a diameter of about 65mm, a length of 100mm, and a weight of 2.7kg. One rod contained 0.3wt.% of Y_2O_3 particles (Heat HXN 954/4), and the other contained 0.5wt.% of Y_2O_3 particles (Heat HXN 958/2).

The microstructure of both as-received ODS steels is shown in Fig. 2.4.5. In SEM the surface appears smooth in the case of the ODS steel reinforced with 0.3wt.% Y_2O_3 (see Fig. 2.4.5a), while the ODS steel reinforced with 0.5wt.% Y_2O_3 reveals pores about 10µm in size (see Fig. 2.4.5b). This important porosity certainly results from a bad HIPping process. In TEM, both ODS steels exhibit interlocked ferrite grains whose boundaries are decorated with Cr carbides of the $Cr_{23}C_6$ type. In the case of the 0.5wt.% Y_2O_3 (see Fig. 2.4.5d), the carbides at the grain boundaries with sizes up to about 1µm are larger than in the case of the 0.3wt.% Y_2O_3 (see Fig. 2.4.5c), where they attain about 0.2µm maximum. The grain size of about 5µm in both ODS steels is smaller than in the case of the base tempered martensite EUROFER 97, which presents grains of about 15µm in size that are decomposed in a martensite lath structure with a typical lath width of 100 to 500nm. No clear microstructural difference could be identified between specimens cut in transverse and longitudinal directions.

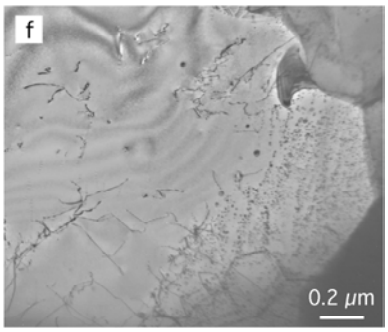

Fig. 2.4.5 *SEM micrographs of TEM specimens of the as received ODS steels with (a) 0.3wt.% and (b) 0.5wt.% Y_2O_3. TEM micrographs showing the interlocked ferrite grains decorated at the grain boundaries with carbides for (c) 0.3wt.% and (d) 0.5wt.% Y_2O_3, and showing the yttria particle distribution for (e) 0.3wt.% and (f) 0.5wt.% Y_2O_3.*

At higher magnification, TEM reveals the Y_2O_3 particles (see Fig. 2.4.5e and Fig. 2.4.5f). Energy dispersive spectrometry with a probe size of 10nm identified them as round, smaller than 50nm particles, containing yttrium and no increase in Cr relatively to the matrix. Conversely, larger, irregularly shaped particles were systematically identified as carbides. The yttria particles appear heterogeneously distributed, with regions free of them within a single grain. This is illustrated in Fig. 2.4.5e for the case of the 0.3wt.% Y_2O_3, where only the bottom left quadrant reveals oxide particles, below a region exhibiting inclined dislocations. This is also apparent in the case of the 0.5wt.% Y_2O_3 in Fig. 2.4.5f, where only the right part of the central grain exhibits yttria dispersion. The yttria particles appear in the material in either groups of round particles of about 20 to 40nm or groups of 1 to 5nm round particles. The two populations rarely mix. In both steels, the yttria particles follow a normal skewed Gaussian size distribution with a mean size of 3.8nm. While the 20 to 40nm yttria particle distribution resembles nearly parallel bead strings (Fig. 2.4.5e and Fig. 2.4.5f), no specific crystallographic directions

could be attributed to the string directions and they do not relate to dislocation lines.

The tensile mechanical behaviour of both as-received ODS steels have been investigated in detail. Typical stress-strain curves are shown in Fig. 2.4.6. It can be seen that the ODS steel reinforced with 0.3wt.% Y_2O_3 particles exhibits better mechanical properties than the ODS steel reinforced with 0.5wt.% Y_2O_3 particles. More importantly, the ODS steel with 0.3wt.% Y_2O_3 presents better tensile properties than the base material, that is the EUROFER 97 (see Table 2.4.3). At room temperature it shows an increase of the critical stress measured at 0.2% plastic strain (or yield stress), $\sigma_{0.2}$,of more than 100MPa, an increase of the ultimate tensile stress, σ_u, with more than 900MPa, of 260MPa and a uniform elongation, ε_u, that is double relatively to the base material. Above 500°C differences diminish drastically, however. At 700°C the yield stress of the ODS steel reinforced with 0.3wt.% Y_2O_3 particles is 210MPa, while the uniform elongation is still of about 5%. The ODS steel reinforced with 0.5wt.% Y_2O_3 particles presents weak mechanical properties. It exhibits a microstructure (significant porosity) that cannot sustain stresses even to the level of the base material. Note that no significant difference has been found between tensile mechanical behaviours of longitudinal and transverse specimens.

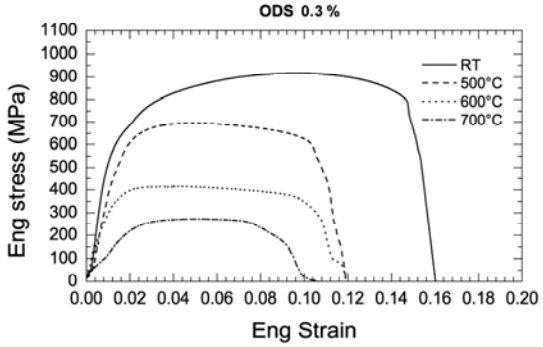

a) b)

Fig. 2.4.6 *a) Typical engineering stress-strain curves for the ODS steel containing 0.3wt.% Y_2O_3 particles; and b) Typical engineering stress-strain curves for the ODS steel containing 0.5wt.% Y_2O_3 particles.*

	ODS 0.3wt.% yttria				ODS 0.5wt.% yttria				EUROFER 97			
	$\sigma_{0.2}$	σ_u	ε_u	ε_f	$\sigma_{0.2}$	σ_u	ε_u	ε_f	$\sigma_{0.2}$	σ_u	ε_u	ε_f
20°C	698	915	9.7	14.8	633	745	3.0	3.3	565	655	4.8	14.8
150°C									532	600	3.4	13.0
200°C	643	832	13.5	17.2	456	640	4.1	4.2				
250°C									485	564	3.1	12.7
300°C	671	821	12.8	13.9	472	594	2.8	2.8				
350°C									480	528	2.2	11.1
400°C	600	800	10.6	14.5	454	570	3.3	3.4				
450°C									440	490	2.2	11.2
500°C	516	694	4.9	10.5	344	464	2.9	3.0	400	440	2.0	23
600°C	326	415	4.0	10.7	242	296	4.3	4.6	300	320	1.5	33
700°C	210	272	5.1	9.3	146	146	2.0	2.3				

Table 2.4.3 *Critical stress [MPa], $\sigma_{0.2}$, ultimate tensile stress [MPa], σ_u, uniform elongation [%], ε_u, and elongation at fracture [%], ε_f, of ODS steels reinforced with Y_2O_3 particles. Comparison with EUROFER 97.*

Charpy impact tests have been performed between room temperature and 350°C on the ODS steel reinforced with 0.3wt.% Y_2O_3 particles. No ductile regime has been shown up in this temperature range. For comparison, a ductile-to-brittle transition has been found at about 185K, respectively 373K, for the EUROFER 97 (mentioned above), respectively the ODS steel reinforced with 0.3wt.% Y_2O_3 particles (measurements performed at FZK).

2.4.3 The Titanium-base alloys

Titanium alloys exhibit a number of properties that make them attractive candidates as structural materials for fusion reactors, including: high strength-to-weight ratio, plasticity, good fatigue and creep rupture properties, small modulus of elasticity, high electrical resistivity, heat capacity, small coefficient of thermal expansion, low long-term (> 10 years after shutdown) residual radioactivity (after V and Cr, Ti exhibits the fastest decay rate), compatibility with coolants such as lithium, helium and water, corrosion resistance, high workability and good weldability, commercial availability with established mine and mill capacity, together with good resistance to void swelling under a wide variety of irradiation conditions. On the down side, titanium alloys are basically low temperature alloys, having a maximum use temperature in the neighbourhood of 500°C. In addition, titanium and its alloys have a high chemical affinity with hydrogen which, in a fusion environment, leads to hydrogen embrittlement and a significant tritium inventory. In order to make practical use of titanium alloys in fusion applications, hydrogen barrier coatings are required to prevent hydrogen intake and subsequent hydrogen isotope induced deterioration of the material.

Titanium alloys can be divided into three major classes determined by their phase constituency, referred to as α, β and α/β, where the α phase is hcp (hexagonal compact) and the β phase is bcc (body centered cubic). The alloying elements used in the titanium system can be divided into two classes based on which phase the element stabilises. The α stabilizers are Al, Zr and Sn, while the β stabilizers are V, Cr, Mn, Fe, Co, Ni and Mo.

Titanium-base alloys for ITER

An assessment of the tensile, fatigue and fracture toughness performance under irradiation of two titanium alloys for the ITER-FEAT modules is progress. The two candidate alloys are: a classical α/β alloy, Ti-6Al-4V, and an α alloy, Ti-5Al-2.5Sn. In 2000, tensile and low cycle fatigue mechanical tests showed that resistance to radiation damage at 300°C is superior for the α alloy compared with the more complex α/β alloy.

In order to comply with the working conditions of ITER, it was decided to extend the initial program and to test both titanium alloys at 150°C. Mechanical testing will include tensile tests and measurements of fracture toughness properties in the unirradiated and irradiated conditions. Charpy specimens have been pre-cracked and irradiated with protons in the PIREX facility at 150°C, to a dose of about 0.3dpa. Irradiation of tensile specimens is in progress.

Development of new titanium-base alloys
Our efforts have been concentrated in the development of new α titanium alloys. Having chosen the promising alloy Ti-5Al-2.5Sn as a reference, a series of 5 alloys was prepared in 2000, in which first the substitution of Al and Sn has been tested and also where an attempt was made to vary the associated impurities (O, N, Fe) to detect their influence on the properties. Al has been substituted with Zr, to create a Ti-5Zr-2.5Sn alloy, then Sn was removed and two binary alloys were developed, containing 5wt.%Zr and 22wt.%Zr, respectively.

Tensile specimens of Ti-22Zr have been irradiated with protons in PIREX at 220°C to a dose of about 1dpa. In parallel with this investigation, tensile and Charpy specimens of Ti-5Al-2.5Sn, Ti-5Zr and Ti-22Zr have been irradiated with neutrons in the reactor of the KFKI Atomic Energy Research Institute (Budapest, Hungary) at 250°C to about 0.5dpa. A transport back to Switzerland has just been organised. All the specimens are now stored in a hot cell at the PSI, ready to be mechanically tested in 2002.

Coatings for Titanium-base alloys
A duplex coating has been plasma sprayed in 2000 at Sulzer Innotec AG in Winterthur onto a set of specimens of an α titanium alloy, namely Ti-5Al-2.5Sn. The selected duplex coating system consisted of a 0.1-0.2mm thick bond layer of pure tantalum and a chromium oxide top layer doped with 3wt.% titanium oxide to increase the coating ductility. The achieved thickness of the top layer was about 0.6mm. The coated specimens have been subsequently tested for structural integrity, via bond strength and hardness measurements and microstructure observations, and for hydrogen permeation, via experiments performed in a Sievert's apparatus. The results were encouraging for the barrier efficiency of plasma sprayed deposits against hydrogen intake. However, bond strength measurements revealed that the adhesion of the ceramic overlay to the substrate is insufficient to guarantee the coating performance in a fusion environment.

In order to improve the adherence of the selected coating, the surface of the substrate, namely Ti-5Al-2.5Sn, has been prepared by water jet blasting, a technique developed at Sulzer Innotec AG. Furthermore, thick (in the millimeter range) layers of Cr_2O_3, respectively Al_2O_3/TiO_2, were then successfully deposited by thermal spraying onto the surface structured substrate. The coated specimens were subsequently tested for structural integrity, via bond strength and hardness measurements and microstructure observations. The adherence of the coating to the substrate was greatly improved by the use of that special preparation technique.

2.4.4 Other materials

The object of this research is to investigate the mechanical behaviour of the CuCrZr alloy in the condition of in-beam fatigue. The fatigue behaviour of this alloy had been previously extensively studied within the framework of the ITER technology program. The fatigue properties of CuCrZr are already known in the unirradiated and irradiated conditions. Since this alloy will be placed in the first wall of ITER, it will be subjected to in situ fatigue, due to the pulsed operation of ITER. It is therefore necessary to investigate the behaviour of CuCrZr when fatigue deformation is imposed simultaneously with irradiation. Fatigue specimens have been manufactured and extensometers have been prepared. A reference fatigue test

has been performed, using the in situ machine without proton beam. The in-beam fatigue testing of CuCrZr in the PIREX facility is planned for 2002.

2.4.5 New investigation techniques

Small angle neutron scattering
The resistance of a material to radiation damage can be modelled and quantified from a set of parameters that include the structure of the material, the as-cast microstructure (such as the type and size distribution of carbides in the case of steels), the type and size distribution of the irradiation-induced defects and their accumulation rate as a function of the irradiation dose. To date, attempts at characterising the latter three have been made by TEM, that allows the direct observation of defects whose size is larger than about 1nm. However, it is thought that a number of irradiation-induced defects have a size below 1nm, and contribute to the hardening behaviour of materials under irradiation. Small Angle Neutron Scattering (SANS) measurements are expected to complement TEM observations, in the sense that the resolution provided by this new technique allows the detection of object well below 1nm in diameter. In addition, it was already demonstrated, in the case of stainless steels, that the irradiation-induced defects can be clearly distinguished in SANS experiments, and that SANS results correlate well with TEM results in the case of defects larger than 1nm.

Two campaigns of SANS measurements were made in 2001 using the SANS facility at SINQ. First, in June 2001, SANS measurements have been performed on unirradiated specimens and proton-irradiated specimens (at 50°C to about 0.3dpa) of the OPTIMAX A steel. The aim of that first campaign was to test the capability, from the point of view of radiological safety, of the SANS facility at the PSI for measuring radioactive specimens. Accurate dose rate measurements were conducted by the Nuclear Security Board of the PSI. It was established that the shielding of the SANS facility allows the measurement of radioactive specimens with a maximum dose rate at the surface of 20mSv/h.

The following specimens were selected for a second campaign of measurements: unirradiated and proton-irradiated specimens (at 50°C to 0.3 and 1dpa) of F82H, unirradiated and proton-irradiated specimens (at 50°C to 0.3 and 1dpa) of EUROFER 97, unrradiated and proton-irradiated specimens (at 50°C to 1dpa) of OPTIMAX A (to complement the first series of measurements), unirradiated and proton-irradiated specimens (at 50°C to 1dpa) of pure Fe. This second campaign of measurements was carried out in November 2001.

The first series of measurements has been already analysed. It was found that the scattering intensity versus scattering vectors behaves very differently for the irradiated specimens as compared with the unirradiated one (see Fig. 2.4.7a). The size distribution of scattering objects in the irradiated specimen was observed to peak at about 0.55nm (see Fig. 2.4.7b), which means that a large number of scattering objects have a size well below the TEM resolution limit. As expected, a large number of small irradiation-induced defects were successfully shown up using SANS, which had not be seen in TEM but actually contribute to the irradiation hardening of OPTIMAX A.

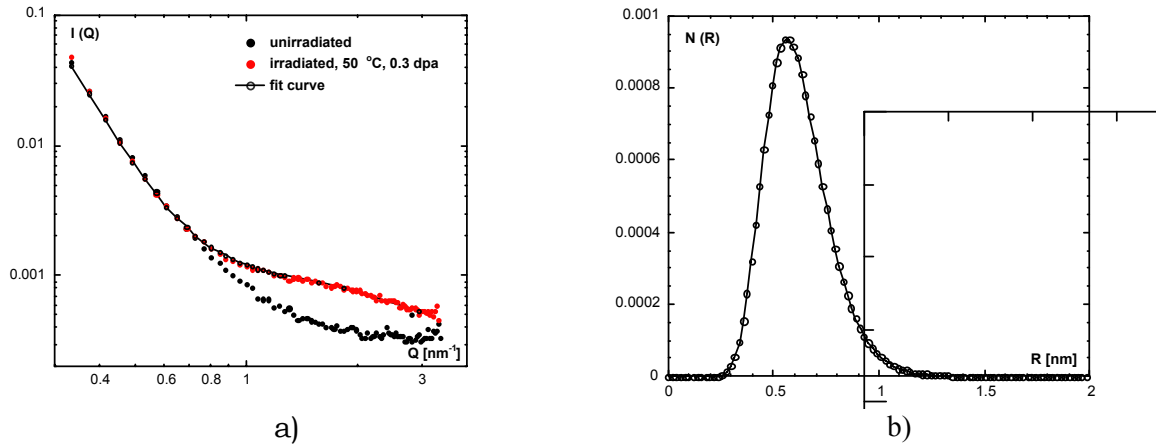

Fig. 2.4.7 *a) Scattering intensity versus scattering vectors for unirradiated and irradiated specimens (50°C, 0.3 dpa) of OPTIMAX A; and b) Size distribution of scattering objects in irradiated specimens (50°C, 0.3 dpa) of OPTIMAX A.*

Due to the small volume of the PIREX tensile flat specimens (0.3mm x 2.5 mm x 8mm in gauge length) used for SANS measurements, each specimen had to be measured for a period of about four hours in the front position of the detector (maximum neutron beam intensity). Usually, only 10 minutes are necessary for bigger specimens.

Analysis of the second series of measurements is in progress. It should be finished by February 2002. A third campaign of SANS measurements is planned for the second semester of 2002. The specimen matrix should include unirradiated and proton-irradiated specimens of Fe and model alloys (Fe-Cr, Fe-Cr-C). Results will be compared to those obtained for RAFM steels.

Small specimen technology

In 2000, a test irradiation was performed in PIREX to assess the possibility of irradiating ultra-small bend bars (1mm x 1mm x 12mm) of tempered martensitic steels. It was found that the cooling capability of the helium loop is sufficient for specimens of these dimensions and that it is possible to properly control the irradiation temperature of each specimen.

It was decided to prepare a specimen matrix of pre-cracked and side-grooved ultra-small bend bars for irradiation, with the ultimate goal of performing static fracture toughness measurements in 3-point bending tests to evaluate the irradiation-induced shift of the fracture toughness-temperature curve, K(T). A special pre-cracking procedure had to be developed to successfully introduce a crack with a/w=0.45 in specimens with a thickness, t, and a width, w, of 1mm (a is the crack length). A total of 162 specimens of EUROFER 97 were prepared, together with the corresponding specimen holders.

One set was sent to KFKI Atomic Energy Research Institute (Budapest, Hungary) for irradiation at 350°C and 0.5dpa. The corresponding specimen matrix includes the following geometries:

6 x 0.4T compact tension with a/w=0.5
24 x 0.2T compact tension with a/w=0.5

16 x 0.1T bend bars a/w=0.45 and a/w=0.1
20 KLST Charpy with a/w=0.45
20 mini tensile

The remaining specimens will be used firstly for characterising the fracture toughness baseline of EUROFER 97 and another neutron-irradiation to be done in 2002 in Budapest at 150°C and to 0.5dpa, and secondly for performing proton-irradiations in PIREX in similar conditions of dose and temperature. This will allow us to make a comparison with neutron-irradiated specimens and perhaps show up helium effects on the fracture properties, if any. One of the main characteristics of PIREX is to produce a large appm/dpa He ratio (about 130 in steel specimens).

Small punch testing

A series of ball punch tests was performed on 0.25mm thick TEM disks of unirradiated EUROFER 97 from 293K down to 80K. In order to control the temperature below room temperature, a bath of ethanol or methyl-butane was used in which the punch die was set. The testing was carried out with a machine piston velocity of 1 mm/min. Over the whole temperature range, the load-deflection curves look similar, with a first stage of elastic bending (I) followed successively by a plastic bending stage (II) and a membrane stretching stage (III), which eventually leads to instability and failure (IV) of the specimens (Fig. 2.4.8). The total deflection at failure was found to be very weakly temperature dependent down to 133K, while at 80K an unambiguous decrease of total deflection was observed. However, even at 80K, a fair amount of plasticity was obtained. The maximum load increases monotonously with decreasing temperature down to about 110±20K and clearly drops at 80K. Some SEM investigations of the fracture surfaces were performed, and it was found that quasi-cleavage prevails at 80K while at higher temperatures shear dimple patterns are observed.

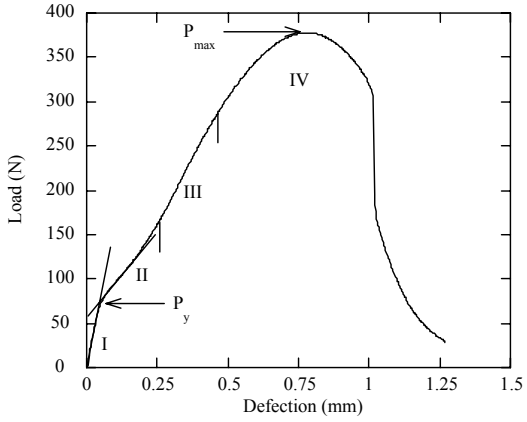

Fig. 2.4.8 *Load-deflection curve at room temperature, EUROFER 97.*

An evaluation of the tensile and impact properties of the EUROFER 97 tempered martensitic steel in the unirradiated condition by means of ball punch tests was done. The tensile testing used to compare the punch results to the usual tensile data was done over the same temperature domain at a nominal strain rate of $5 \times 10^{-4} s^{-1}$. The characteristic loads of the punch tests associated with the initiation of the plastic bending domain, P_y, and the maximum load, P_{max}, were recorded as a function of temperature and compared with the temperature dependence of the yield stress, $\sigma_{0.2}$ and of the ultimate tensile stress, UTS, obtained from plain tensile tests. The specific fracture energy of the punch tests, defined as the integral under the load-displacement curve divided by the thickness of the specimen, was also determined and recorded as a function of temperature. It was observed to increase

with decreasing temperature until a sharp decrease occurs below 133K. The ductile-to-brittle transition temperature (DBTT) obtained from the punch tests, defined as the temperature at which the energy is half the maximum value, was compared to the DBTT determined from Charpy impact tests performed on KLST specimens. Reasonable agreement was found.

2.5 Superconductivity

The effort in 2001 was mainly concentrated on the scientific exploitation of the SULTAN test facility. The full characterisation of Japanese conductors is part of the European commitment in the ITER technology tasks. Experimental results useful for the development of cable in conduit conductor (CICC) for the program was also gained through the test of Chinese CICC. In the frame of the conductor optimisation R&D for ITER, the test of two Nb_3Sn subsize samples prepared at the CRPP led to dramatic results for the DC and AC loss performance under electromagnetic cyclic load, triggering further investigations on the fatigue behaviour of large size Nb_3Sn cable-in-conduit conductor. Five more samples based on NbTi technology have been prepared with parametric variations in the layout and are ready for testing in early 2002.

The R&D on large current leads included in 2001 the design, development and manufacture of a pair of conventional, 80kA current leads, using the CRPP technology applied in the SULTAN test facility. The current leads are tested for thermal load at the CRPP and will be operated at full current in the Toska facility at FZK. The first phase of a collaboration with FZK on HTS Current Leads was completed in 2001 with the test of a 10kA twin lead assembly.

2.5.1 Conductor Optimisation

Test results on two Nb_3Sn subsize samples

The SeCRETS experiment addressed the issue of the stabiliser segregation in Nb_3Sn cable-in-conduit conductors one year ago. In the discussion of the SeCRETS results at a workshop at Morschach (Switzerland) in September 2000, a strong interest was generated to continue the investigations in the areas of AC losses over an extended frequency range, DC with cyclic load and stability with direct calibration of the deposited energy.

The remaining sections of the SeCRETS conductors were an attractive candidate for the above tests, due to the broad data base already available. For each of the SeCRETS conductors, a 7m section was bent into a hairpin shape to be tested as a “short sample” in the SULTAN facility with vertical access. The U-bend at the bottom replaced the “bottom joint” and eliminated the criticism frequently raised about the short current re-distribution length between the joint and the high field section, Fig. 2.5.1. The two Nb_3Sn cable-in-conduit short samples, named SecA (without segregated copper) and SecB (with partly segregated copper) became part of the CONDuctor OPTimization program (CONDOPT).

Fig. 2.5.1 *SecA sample during assembly, with the U-bend replacing the bottom joint*

The instrumentation included new features compared with the former short samples. For current distribution monitoring, four annular arrays, each with 8 miniature Hall sensors, were placed around the conductor, all oriented along the background field, to enhance the accuracy of the self field measurements. A new cryogenic pressure sensor was also installed to monitor any transient pressure changes at the high field section. Demountable temperature sensors, bolted onto welded fittings on the jacket penetrations, were used with the advantage of a separate calibration and the possibility of recycling. A miniature heater was installed to create strong thermal gradients over the conductor cross section. Voltage taps were attached to sense both the longitudinal field along the conductor and the voltage drop across the conductor.

The tests of the critical current, I_c, and the current sharing temperature, T_{cs}, were carried out at a 8, 9, 10 and 11T background field and over a temperature range from 4.5 to 8K. To apply a cyclic load on the conductor, the current in the sample was raised, in a background field of 10T, from 0 to 15kA and back to 0 at a rate of about 500A/s. The triangular continuous sweep, with about 2s hold time at 0 and 15kA, was controlled by the superconducting transformer. Every 200 cycles, an I_c test at 4.6K and slow current rate (<100A/s) was carried out up to the conductor quench. Under optimum conditions, up to 400 cycles per day could be carried out on an extended shift.

The Lorenz force acting on the hairpin sample pushes the two conductor sections apart. Strong clamps keep the CICC in position. The cable is pushed against one wall of the jacket with a peak force of 150kN/m, over the 0.5m conductor section exposed to the high field, see Fig. 2.5.2. The transverse load, σ_t, is measured by the Lorenz force divided by the cable space diameter, d_{cs}=12.5mm, $\sigma_t = B \cdot I / d_{cs}$=12MPa. This compares well with the operating conditions of the Insert model coil, but is smaller than in the actual ITER CICCs, where σ_t(TF)≈20MPa and σ_t(CS)≈18MPa.

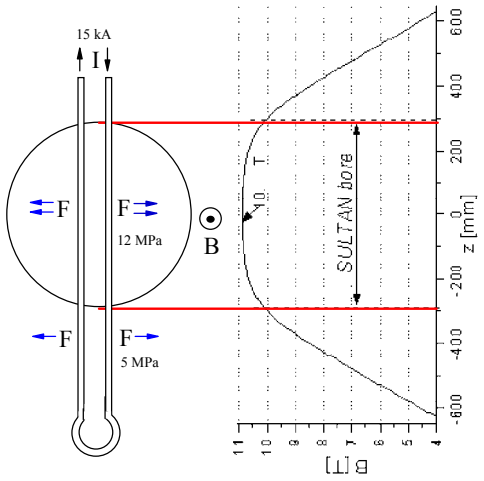

Fig. 2.5.2 *Transversal load on the hairpin sample lowered in the SULTAN test well*

The results before cycling are in good agreement with those of the SeCRETS experiment, where a criterion of 1μV/cm was applied in the DC tests. The transversal load in the SeCRETS winding was in the range of 6 to 10MPa. The

smoothness of the superconducting transition at I_c is measured by fitting the voltage-current curve with an exponential curve of exponent "n". The n factor for the Nb_3Sn cable-in-conduit results is always much smaller than in the individual strands: for SecA and SecB, the n factor drops from ≈32 in the strands to ≈13 in the cable-in-conduit.

After the initial DC tests, the samples were subjected to 3400 (SecA) and 3000 (SecB) full load cycles as described above. From the I_c tests carried out every 200 cycles, a large drop of the n factor and of the I_c at low electrical field criterion was observed, Figs 2.5.2 and 2.5.3.

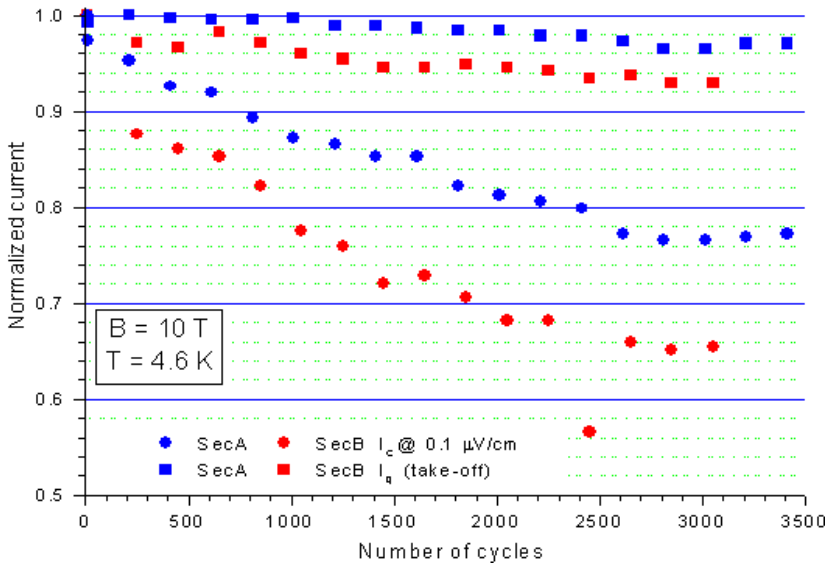

Fig. 2.5.3 *Normalised critical current, I_c, and quench current, I_q, as a function of the number of load cycles for SecA and SecB samples*

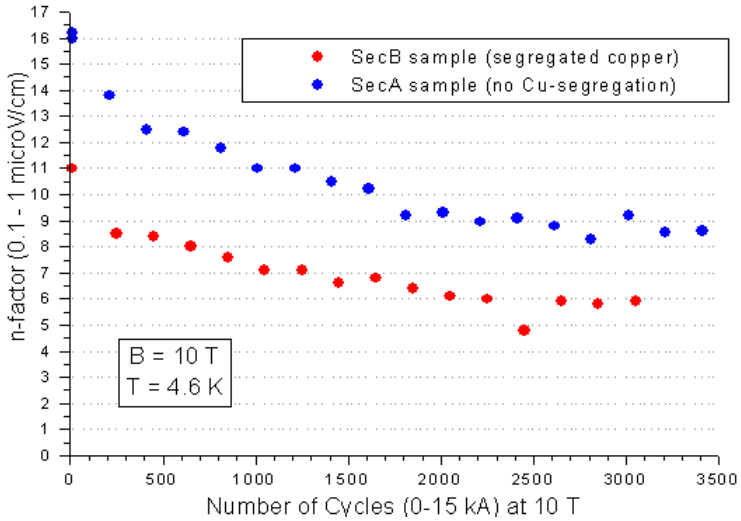

Fig. 2.5.4 *Evolution of n factor for SecA and SecB vs. number of load cycles*

After completing the cyclic load, an I_c test was carried out on the SecA sample after warming up at room temperature. The results are summarised in Fig. 2.5.5. No recovery of the performance loss was observed after warm-up. In addition to the

standard test, the sample is lifted in the SULTAN facility, exposing a section of the sample which was in low field during the cycling to high field, see also Fig. 2.5.2, so it was loaded with ≈5MPa instead of 12MPa.

The sample sections exposed to lower load did not show any fatigue effect. The performance drop occured only above a load threshold and did not recover after a thermal cycle to room temperature. Additionally, recoverable drop of I_c and n was observed at the first run after a cool-down and after reversal charge, as happened to the SecB sample after 2400 cycles, Figs 2.5.3 and 2.5.4.

In agreement with earlier results, the load threshold for fatigue effects linked to the local void fraction and possibly to other parameters of the cable layout. An effect of cyclic load cannot be ruled out for the ITER coils, designed to operate at load levels as high as 20 MPa and void fraction in the range of 36% (the actual void fraction in the model coil conductors is lower than designed).

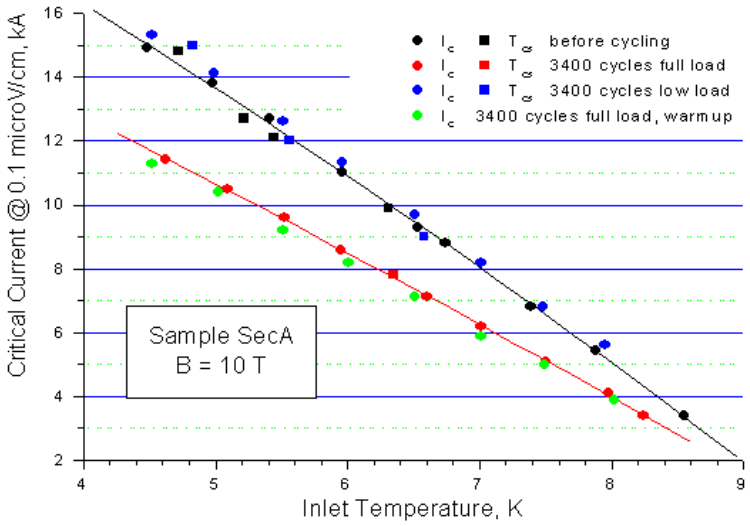

Fig. 2.5.5 *Critical current @ 0.1μV/cm vs. temperature for SecA in different conditions: before cycling, after cycling at 12MPa (before and after warm-up), after cycling at 4 to 5MPa*

The very smooth transition (low n factor), with a broad resistive range, is evidence of an early current sharing process among strands. However, the voltage associated with the current sharing is too large to be sustained by a resistance unbalance at the nearby (solder filled) joints. Even with very high interstrand resistance at high field, low voltage current re-distribution would take place at the joint. The ability to locally re-distribute the current among strands was verified, both before and after the cyclic load. The high field voltage did not decrease when a quench (i.e. homogeneous current distribution) was artificially induced at a lower field section. A current unbalance among the strands in the cable cannot explain the low n factor. The hypothesis (as yet unverified) of a microscopic, permanent damage of the Nb_3Sn filament structure upon transverse (cyclic) load may explain both the early current sharing and the high voltage at the high field section. Post mortem investigations on strands extracted from the cable are under way.

For low frequency AC loss measurements, a magnetisation apparatus was set up, consisting of two pick-up coils (one attached to the conductor, the other, with similar linked flux, on the other side of the pulsed field coil), a resistance bridge to balance the pick-up coil voltages and an analogue integrator. The balanced and

integrated voltage of the pick-up coil was plotted against the sinusoidal pulsed field to build a magnetisation loop with area proportional to the AC loss. The energy loss is calibrated by comparison with the calorimetric results for the same runs, taken at higher frequency. The loss results of the SecB sample (with segregated copper) are shown in Fig. 2.5.6. The full symbols are from calorimetry, the open symbols are from the magnetisation curve. At higher frequency, the effect of the cyclic load is marginal and the coupling loss from the slope of the loss curve is the same as measured in the SeCRETS experiment. The low frequency loss after cyclic load converges to the expected value of hysteresis loss. Before cyclic load, the loss behaviour deviates (for f<0.4Hz) from the higher frequency trend. The lowest frequency test point is at 0.07Hz.

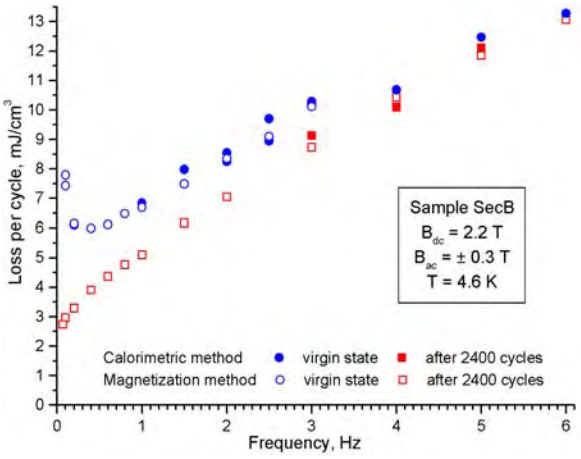

Fig. 2.5.6 *Loss curves of the SecB sample before and after cyclic load*

The large loss at low frequency before cycling is evidence of large, long lasting induced current loops with time constants in excess of 5 seconds, due to the low interstrand resistance after the Nb_3Sn heat treatment. The low resistance loops may have a spatial periodicity much longer than the cable pitch, their size depending on the location of very low resistance strand crossovers. Although only a 390mm conductor section is exposed to the AC field, the induced currents may close over a longer length. In agreement with former results, the cyclic transverse load on the cable disengages the low resistance contacts and the large time constant loops disappear. However, the loss curve after cyclic load is not perfectly linear at low frequency, suggesting that a small number of interstrand current loops are still present.

The losses of the SecA sample, Fig. 2.5.7, have been measured after cyclic load on conductor sections loaded with different transverse loads. In the low frequency range, it is clear that the amplitude of the cyclic load plays an important role to break the low resistance current loops: at 12MPa load, the low frequency loss peak vanishes, but it is still present for 4.5MPa average load. The estimated amplitude of the peak of the low frequency loss, much smaller than the expected peak of the standard coupling loss curve, suggests that the large loss loops only affect a small volume of the cable. In other words, a small geometry factor (n), likely <0.1, must be associated with the very large time constant (τ>5s) to obtain the correct $n\tau$ to be used at low frequency, in agreement with the loss constant observed in the CSMC winding (30 to 250ms).

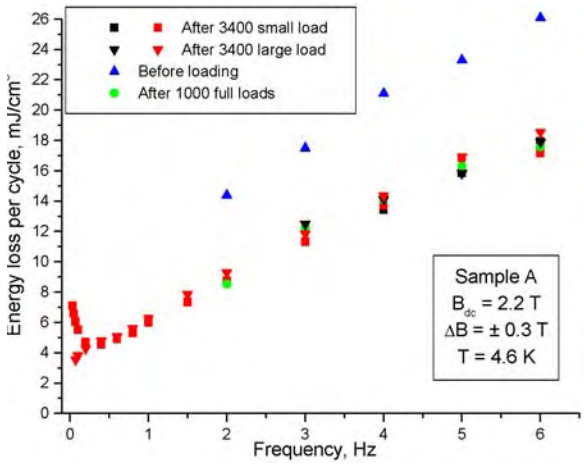

Fig. 2.5.7 *Loss curves of the SecB sample before and after cyclic load at different levels*

The coupling currents loss in Cr plated Nb_3Sn CICC has a complex behaviour, with a minor loss peak at very low frequency (f<0.03Hz). The current loops with large time constant are restricted to a limited cable volume, i.e. they are associated with a very small n factor. The low frequency loss only vanishes upon cyclic load at high load level. In a large coil, with a broad distribution of Lorenz forces, the overall heat load from the coupling loss may not be dramatically affected by the cyclic load. Above 0.2 Hz, the coupling loss does not depend on the cyclic load and is very small, probably restricted to the interfilment loss. The conductor design must use different loss parameters, $n\tau$: a large constant for a slow time-varying field (e.g. coil charge) and a small one for transient events (plasma initiation and disruption).

The stability under pulsed transverse field was measured over a broad range of pulse duration and amplitude. The deposited energy was measured calorimetrically applying the pulse field at zero transport current. The stability was very high, due to the very low coupling currents loss, with an equivalent time constant, $n\tau$, smaller than 1ms. The duration of the disturbance, between 32 and 146ms, has no significant impact on the conductor stability for a given deposited energy. The smooth I_c transition of the samples, allows the local temperature to exceed the current sharing temperature, defined at 0.1μV/cm for short time, without a thermal runaway. As a consequence, the conductor withstands very large field transients, in excess of $100T^2/s$, even when the temperature margin is zero.

To explore the stability, a range of transient fields has been applied (several hundreds of T^2/s) beyond any realistic application. Practical transient field disturbances, e.g. plasma disruption in fusion magnets, are one to two orders of magnitude smaller and can be withstood without any dedicated temperature margin in the design criteria. However, a design margin must be maintained for other issues. Conventional models for transient stability, with abrupt voltage increases and power generation above T_{cs}, are not adequate for CICC with a low n-factor. A refinement of the models is of little practical interest since the transient stability is not an issue for this kind of conductor.

The question arises whether current re-distribution among the strands is possible locally. To address this issue, a small heater (resistive foil) was attached in the high field region, next to the array of eight Hall sensors, which monitor the current distribution in the cable, see Fig. 2.5.8. The heater is designed to provide non-homogeneous, pulsed heat loads to the conductor. As the transverse heat transfer by helium convection inside the cable is poor, only the strands underneath the heater are affected by the heat and a strong temperature gradient builds up over

the cable cross section. If the conductor operates close to I_c, a voltage develops at the heated strands. According to the interstrand resistance, current re-distribution may take place either locally, at the high field region (in case of good interstrand current sharing), or at the sample termination, about 2m downstream, where the cable is solder filled and the interstrand resistance is at least 50 times lower than in the cable-in-conduit.

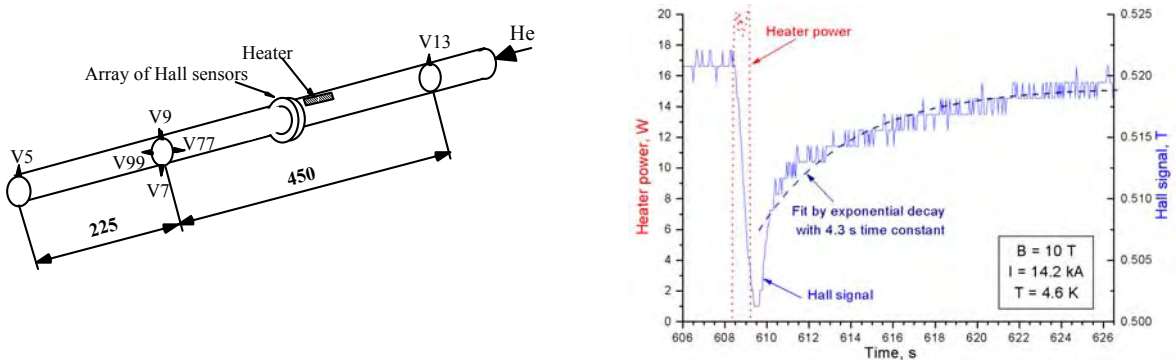

Fig. 2.5.8 *Current displacement and relaxation at the Hall sensor after a local, pulsed heat load*

At 10T, the operating current is raised to 14.2kA (in the current sharing region, with electric field >0.2μV/cm) and the heater is switched for a duration of ≈0.7s at increasing level of power, in excess of 20W, until a quench eventually occurs. During the heat pulse, a clear current displacement is observed at the Hall sensors, see Fig. 2.5.8. The self-field signals change linearly (either positive or negative, depending on the sensor location) and then decays with a time constant of about 4s. The current displacement, i.e. the amplitude of the Hall voltage change, is proportional to the heater power.

The changes of the Hall voltage are also observed, with a smaller amplitude, at the other Hall arrays, far away from the high field. Comparing the signal of a high field sensor with one placed 1.92m downstream, the longitudinal diffusion speed of the current displacement can be assessed, see Fig. 2.5.9 in the range 4±0.5m/s. The delay observed between the two Hall sensor signals is evidence that the current re-distribution occurs locally, at high field. Further evidence of current displacement is obtained from the voltage taps, placed along the conductor and over the cable cross section. The longitudinal voltage at high field (V13V9) is large, up to 280μV and the peak electric field is likely above 20μV/cm. The transverse voltage is large for taps V77V99 and is zero for V7V9, clearly showing the direction of the transverse current.

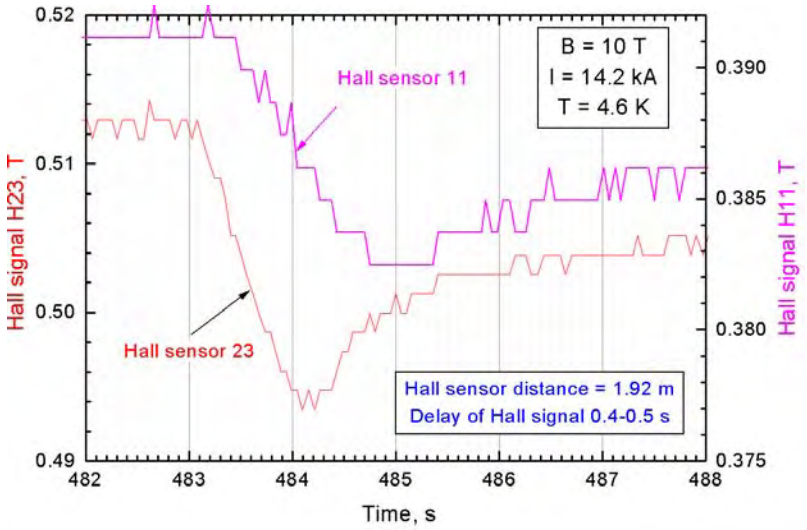

Fig. 2.5.9 *Diffusion of current re-distribution observed by Hall sensors placed at high field (H23) and 1.92m downstream (H11)*

Despite the very low coupling loss, local current re-distribution among strands occurs whenever thermal gradients are applied over the cable cross section. Relaxation time constant in the range of few seconds and diffusion speed of few m/s have been observed in the Nb_3Sn CICC sample.

Preparation of five NbTi samples

Little R&D work has been carried out in the last ten years on the NbTi cable-in-conduit conductors for the PF coils of ITER, as the NbTi technology is considered less critical than the Nb_3Sn. In the scope of the Conductor Optimisation, we have now prepared five, medium size, NbTi cable-in-conduit samples with parametric variations, to investigate the role of strand coating, cable pattern, subcable wraps and copper segregation on the overall performance. The test program will be similar to the one applied for the Nb_3Sn samples, with DC, AC loss, transient field stability and cyclic load.

Three types of NbTi strand have been procured from Alsthom. The strand characteristics are:

Strand Identification	*Strand Diameter*	*Cu:non-Cu*	*Twist pitch*	*Total Length*
ZR500191	0.87 mm	≈ 1.12	7 mm	≈ 2 180 m
ZR500192	0.70 mm	≈ 1.05	7 mm	≈ 19 150 m
ZR500193	0.70 mm	≈ 7.5	7 mm	≈ 9 100 m

Five cable-in-conduit conductor sections, each about 18m long, have been cabled and jacketed at VNIIKP (Moscow) to our specification. The strand coating (either SnAg solder or Ni electroplating) has also been applied at VNIIKP. The conductor characteristics are:

CICC	*Strand Type*	*Strand Coating*	*Cable pattern**	*Cable space ø*	*Outer diameter*
# 1	ZR500191	Ni	(1+**7**) x 3 x 4 x 4	16.5 mm	18.5 ± 0.1 mm
# 2	ZR500192	Sn base	(**1**+6) x 3 x 4 x 4	16.5 mm	18.5 ± 0.1 mm
# 3	ZR500192	Ni	(**1**+6) x 3 x 4 x 4	16.5 mm	18.5 ± 0.1 mm
# 4	ZR500192	Ni+subcable wraps	(**1**+6) x 3 x 4 x 4	16.5 mm	18.5 ± 0.1 mm
# 5	ZR500193	Ni	(**1**+6) x 3 x 4 x 4	16.5 mm	18.5 ± 0.1 mm

*** Bold** figures are segregated copper wires. For conductor #1, the copper wires have ø=0.62mm. For conductors #2-5 the copper cores have ø=0.70mm

From the five conductor sections, five hairpin samples, with U-bend replacing the bottom joint, have been prepared and instrumented in a similar way to the Nb_3Sn samples. Testing of the NbTi samples will start in SULTAN after the January 2002 shutdown.

Cyclic load on a full size Nb_3Sn sample

After the dramatic performance degradation under cyclic load of the Nb_3Sn samples SecA and SecB, an older, full size Nb_3Sn sample was installed in SULTAN for fatigue test. The sample, SS-FSFJ, consists of a section of TF Model Coil cable in a circle-in-square jacket. The sample was first measured in 1999. Now the sample has been loaded about 2100 times up to 70kA in a background field of 11T, with a peak transverse load $\sigma_t = B \cdot I / d_{cs} \approx 19$MPa. Every 150 cycles, an I_c test was carried with tight control of the operating temperature (6.2K) and mass flow rate (5.5g/s).

The results for critical current, Fig. 2.5.10, show a much smaller, yet still visible, performance loss (of the order of 5%), compared with the subsize samples. The quench, which started in the right leg for the first 1000 cycles and then shifted to the left leg, suggests that the performance degradation is larger in the left leg. After 2100 cycles, one cycle was carried out at –70kA, i.e. reversing the load direction. Afterwards, three consecutive I_c tests were carried out, with substantial performance loss, which was only marginally recovered.

A drop of the n value after cyclic load was observed, Fig. 2.5.11. The variation after fatigue loading small compared with the large drop from strand to cable. The reverse loading also caused a drop of the n factor.

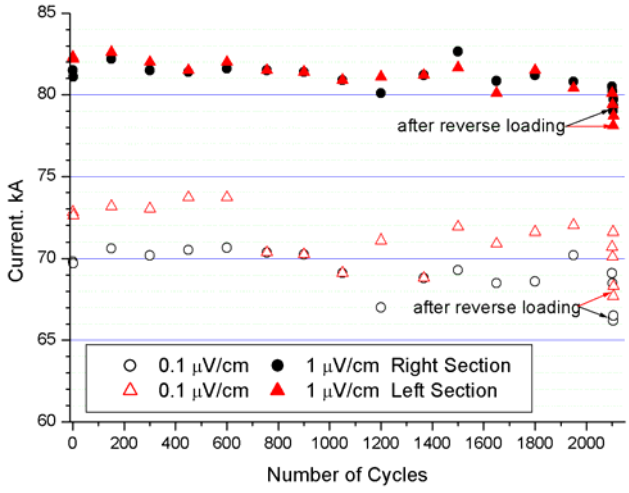

Fig. 2.5.10 *Critical current vs. cycle number at 0.1 and 1μV/cm criteria for both legs of SS-FSJS*

The full size sample SS-FSJS was much less sensitive with fatigue load compared to the subsize samples SecA and SecB. Whatever the reasons (lower local void fraction, strand layout, cable pattern), the result is good news for the ITER magnets. However, the drop of the n value and the critical current under transverse load in Nb_3Sn CICC must be further investigated and understood to have confidence in the conductor design.

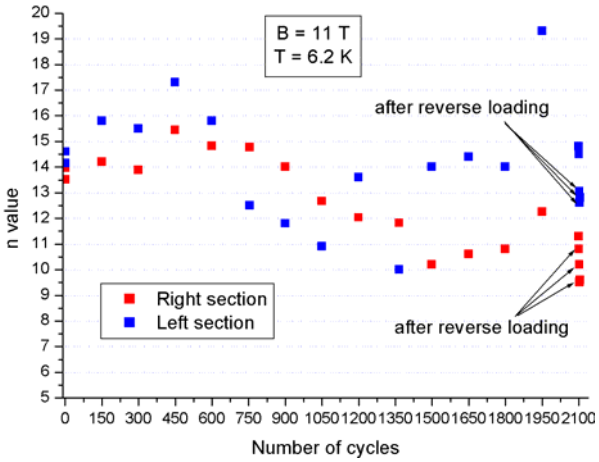

Fig. 2.5.11 *Evolution of n factor vs. cycle number for right and left legs of SS-FSJS*

2.5.2 Conductor Test in SULTAN

Nb_3Al from JAERI

A sample consisting of two identical legs with a hairpin joint was delivered by JAERI at the end of February 2001. The sample is built from Nb_3Al conductor sections left from the winding of the Insert coil, which will be tested in the CSMC facility at Naka in 2002. The hairpin joint, prepared by Hitachi, was not relevant to any coil design and JAERI did not request a dedicated joint test. The only test carried out on the joint was the resistance test.

The sample was out of dimensional tolerance, due to a slight bend between the conductor and the termination. Machining the termination and filling the gap between the termination were necessary to restore the required straightness.

After the measurement system check, the main testing steps were

- I_c and joint resistance in background field of 9,10,11T and temperature 8, 7.5, 7, 6.5, 6 and 5.5K
- Current distribution check by holding time during the current ramp
- Pulse field test (AC loss measurement by calorimetric method)

NbTi from China

Fusion technology in China is making a major step with the construction of a superconducting tokamak, HT-7U. For both toroidal and poloidal field coils, the chosen conductor is a square, 20x20mm cable-in-conduit based on NbTi strands, operating at about 15kA. A critical boundary condition for the design is the use of Russian NbTi strand, developed and produced in large amount few years ago for an accelerator project, which was terminated before the magnets were built. The Cu:non-Cu ratio in the strand is smaller than that required by the design criteria of the HT-7U conductor. Therefore, segregated copper wires have to be added to provide the overall Cu cross section for protection and stability. The verification of the conductor performance at operating conditions and beyond is on the critical path of the Chinese project. The key issues are the selection of the strand coating that controls the interstrand resistance, and the cable pattern.

Four conductor sections with either solder or Ni strand coating and with or without subcable wraps were prepared and assembled into two SULTAN samples. The hairpin joint was made according to a CRPP design developed in 1998. The test results of the Chinese conductors will add valuable information in crucial areas, including interstrand current transfer, current-voltage characteristic in cables, transient stability.

The test program was drafted from the experience with the short samples SecA, SecB. It included a DC test, $I_c(T, B)$ and $T_{cs}(I, B)$ for the four conductors at five fields and five temperatures. The AC loss was measured by both calorimetric and magnetisation methods over a broad range of frequency, with $\Delta B=\pm 0.1$ and ± 0.2T in a sinusoidal sweep. Transient stability was measured with a transverse field transient 140ms long. The results were judged satisfactory by ASIIP. From the DC runs, a high n was observed, with a short range for current sharing. The quench occurred at electric field levels as small as 0.3-0.5μV/cm, independent of the strand coating.

The AC loss was much higher in the solder coated strands compared with the Ni coated ones. The effect of the subcable wraps was observable only in the lossy, solder coated cable. After normalising to the overall cable cross section, the loss constants of the solder coated conductors are 40-50ms (no wraps) and 25-30ms (with wraps). As the Ni coating reduces the loss in the range of the interfilament one (≈8ms), the subcable wraps had no effect in the Ni coated cable. The loss constant for Ni coated conductors (normalised to the overall cross section) is 2-3ms both with and without wraps.

The stability results were consistent with the loss results. In the Ni coated cables, the wraps had some detrimental effect on stability. The resistance of the small hairpin joints is 2-3nΩ. As both samples have not been lifted in the test facility to expose the joint to the pulsed field, no ac loss and stability results are available for the joints.

2.5.3 80 kA Current Leads for Toska

For the test of the Toroidal Field Model Coil in the TOSKA facility, Karlsruhe, two normal-conducting 80kA current leads were urgently needed as a back-up solution in case the repair of the nominal superconducting current leads was not successful. A pair of 80kA gas cooled current leads has been developed at the CRPP and manufactured according to the same concept design used in the past for smaller size leads in SULTAN (5-10-16-20kA). The design relies on the silver coated copper filament concept, fitting the space limitation of the TOSKA facility and the existing

joint design. The leads are thermally tested in the standby (no current) configuration at the CRPP. A full current test is planned at a later time in TOSKA.

The two current leads are designed to fit exactly into the available space of the TOSKA, see Fig. 2.5.12. The current leads were equipped with the same contact pieces as the Toroidal Field Model Coil, namely a half-circular termination on the cold side and a water-cooled stepped cylinder on the warm side. The available cooling input is supercritical helium at 4.5K, with a mass flow of maximum 5g/s per lead. The zero mass flow stability was defined to be larger than 120s. In case of over pressure during a quench of the Toroidal Field Model Coil, the current leads are designed to withstand pressures up to 15bar. An overall He^4 leak-tightness of 10^{-8}mbar litre/sec is requested for the work in the vacuum and cryogenic environment of the facility.

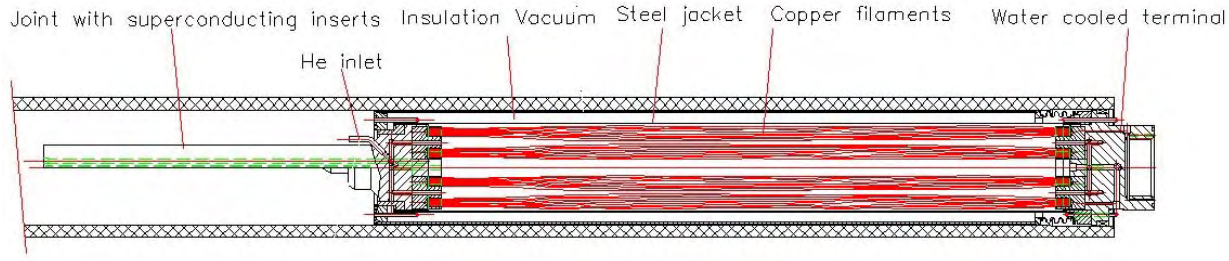

Fig. 2.5.12 *A longitudinal cross section through the 80kA current lead for TOSKA*

The current carrying elements are 436000Ag plated copper filaments (RRR=90) embedded in a stainless steel jacket. At the two ends, the filaments are pressed in copper blocks. The upper block is externally cooled with water at room temperature. The lower block has a 560mm semicircular extension with a flat face in which four superconducting cables are embedded. The current is transferred to or from the copper to the superconductor such that a large part of the extension, which forms the joint, is practically non-resistive. Supercritical He^4 at 4.5K and a pressure of 3.5bar circulates in four channels drilled in the semicircular extension and then in the free space between the filaments providing the necessary cooling. The main functional parameters of the current leads are:

Operating current	*80kA*	*Copper cross-section*	*3424mm²*
Length of heat exchanger	*1.23m*	*Diameter*	*175mm*
Copper current density	*23.36A/mm²*	*Nominal mass flow*	*4.15g/s*
Heat load at cold end	*34W*	*Heat load at warm end*	*2kW*

The current leads at the end of the manufacturing process and the functional test performed in a dedicated cryogenic facility are shown in Fig. 2.5.13. After performing a pressure test at 15bar and a He^4 leak test, each current lead was tested in cold conditions and the results of the measurements were compared to the numerical simulation for the same cooling conditions. The results were more than satisfactory with a deviation between measured and calculated temperature profiles of a few percent.

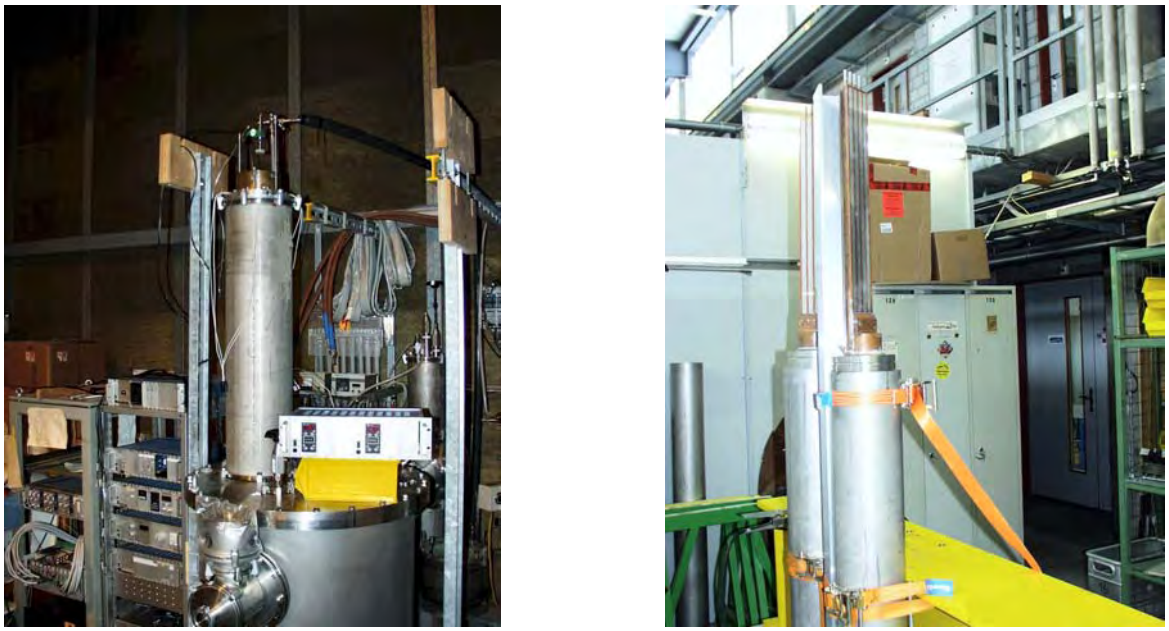

Fig. 2.5.13 *The two current leads(left) and 0-current, thermal load test (right).*

2.5.4 High Temperature Superconducting Current Leads

In the frame of the European Fusion Technology Programme, the CRPP and the Forschungszentrum Karlsruhe (FZK) are developing a 70kA current lead for the toroidal field coils of ITER using high temperature superconductors (HTS). The advantages provided by HTS are the elimination of Joule heating and the extremely small thermal conductivity of these materials. The use of binary current leads with a conduction cooled HTS and a wire bundle type heat exchanger part actively cooled by 60K helium gas, would therefore reduce the heat load at 4.5K by a factor of 10. The electrical input power required to cool the HTS current lead including the copper heat exchanger part is 1/3 of the power needed to cool metallic current leads. This improved performance was previously demonstrated for two 10kA current leads constructed of Ag/Au stabilised Bi-2223 [$(Bi,Pb)_2Sr_2Ca_2Cu_3O_{10}$] tapes. In principle, Bi-2212 ($Bi_2Sr_2CaCu_2O_8$) bulk material is a low-cost alternative to the Ag/Au stabilised Bi-2223 tapes. To study the possibility to use this material for the 70kA current leads of the toroidal field coils of ITER-FEAT a 10kA current lead formed of two 5kA Bi-2212 tubes in parallel was constructed and tested.

The 5kA Bi-2212 modules supplied by NEXANS are coated with a 0.2mm thick layer of Ag/Au to lengthen the time available for quench detection and discharge of the powered magnet. The heat exchanger part and the copper interconnection of the 10kA current lead are actively cooled by helium gas of typically 60K inlet temperature. The two Bi-2212 modules in parallel are cooled only by heat conduction. The cold end of the current lead is immersed in a small volume of liquid helium separated from the main volume. The heat load at the cold end can be deduced from the measured boil-off rate of liquid helium, which is calibrated using a small heater. The positions of the temperature sensors and the voltage taps in the low temperature part of the current lead are shown in Fig. 2.5.14.

The critical currents (1μV/cm criterion) measured at 77K and the self field are 3648 and 2943A for Tubes A and B, respectively. The quench current of the current lead is approximately 10kA for a temperature of 74K at the warm end of Tube A. The temperature at the cold end of the heat exchanger depends on the current, the inlet

temperature and the mass flow rate of the helium gas. To reach temperatures of 65K or less, a mass flow rate of 0.84g/s is required for a current of 10kA. The heat load exclusively due to heat conduction has been found to be 1.13W for a temperature of 62K at the warm ends of the Bi-2212 tubes. From the differences in the mass flow rates with and without current for unchanged temperatures at the warm ends of the HTS tubes the total resistance of the lower contact region can be determined. The calorimetric measurements provide a total contact resistance of 6.9nΩ including 4.5nΩ from the lower copper connection to a NbTi superconductor attached to the conventional return lead. Thus, the total contact resistance at the cold end of the current lead is 2.4nΩ. Because of the uneven current distribution between the two HTS tubes it was not possible to measure the contact resistances at the warm ends of Tubes A and B.

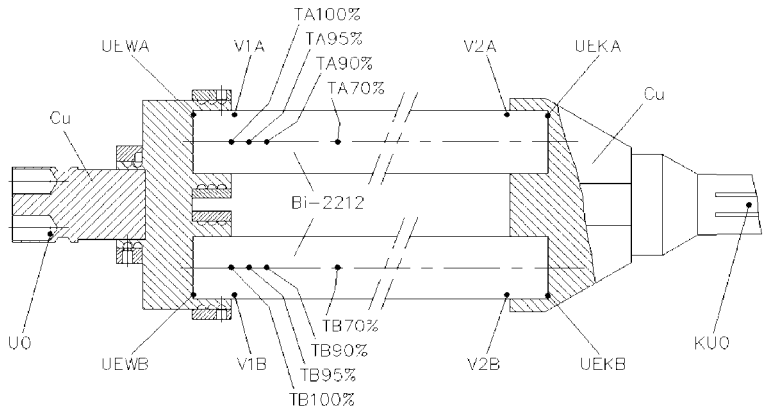

Fig. 2.5.14 *Positions of the voltage taps and the temperature sensors. The cold end is on the right.*

To determine the distribution of the currents between the HTS Tubes A and B, the azimuthal magnetic fields were measured by small Hall probes attached to the surfaces of the two tubes (see sketch of Fig. 2.5.15). The higher fields at Tube A and the opposite signs of the fields measured by the Hall probes Bi and Bo indicate that a much larger fraction of the current flows in Tube A. To explain the large negative value found for Bi an uneven current distribution within the tubes is required in addition to the current imbalance between Tubes A and B. A reasonably good agreement between measured and calculated field values can be obtained when each tube is subdivided into six segments carrying different currents. The simulation suggests that the current in Tube B is only 730A, while a current of 9270A flows in Tube A. The small current in Tube B flows preferentially in a single segment on the side opposite to Tube A, whereas 75% of the current in Tube A is carried by the 3 segments on the side facing Tube B. In the present measurements currents along the circumference of the tubes are not detected. Considering only current flow in axial direction may overestimate the current imbalance between the two HTS tubes. Further evidence that most of the current flows in Tube A is the voltage V1AV2A (Fig. 2.5.15) which increases considerably as soon as the current approaches a value of 10kA (t≈125s). The expected critical current of Tube A is around 9kA for a temperature of 60K at the warm end. Figure 2.5.16 shows the temperature evolution in both tubes during a quench. The considerably higher maximum temperature in Tube A again suggests that the current flows mainly in this tube.

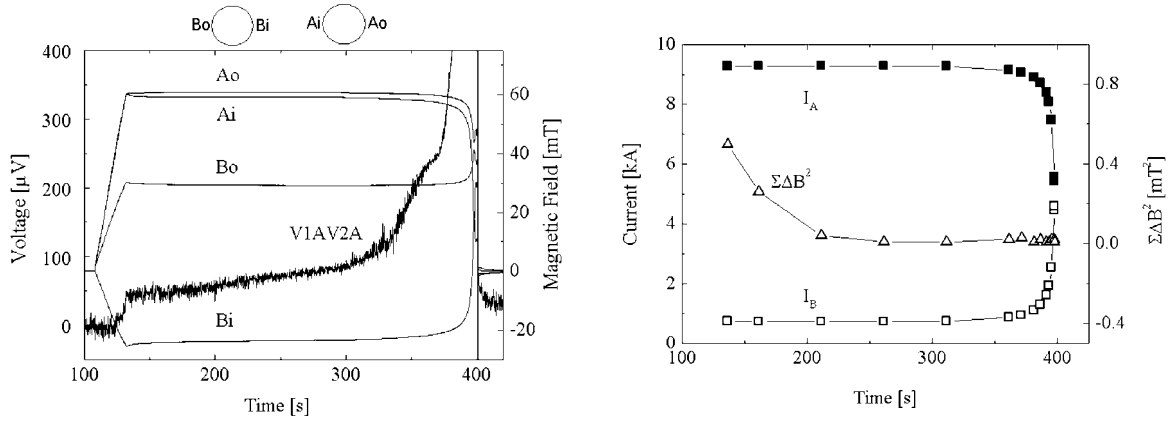

Fig. 2.5.15 *Azimuthal magnetic fields measured by Hall probes close to the surfaces of Tubes A and B, indicating that the current flows mainly in Tube A. The voltage V1AV2A across Tube A suggests that the current in this tube is close to the critical value (left). The simulation of the current distribution generating the measured field is show in the plot (right)*

Reasons for the strongly uneven current distribution could be different contact resistances which may even vary along the circumference of each tube. Due to the considerably different ways through the common copper contact (Fig. 2.5.14) we would expect that the current preferentially enters the tubes on the sides facing each other. This behaviour is indeed observed for Tube A.

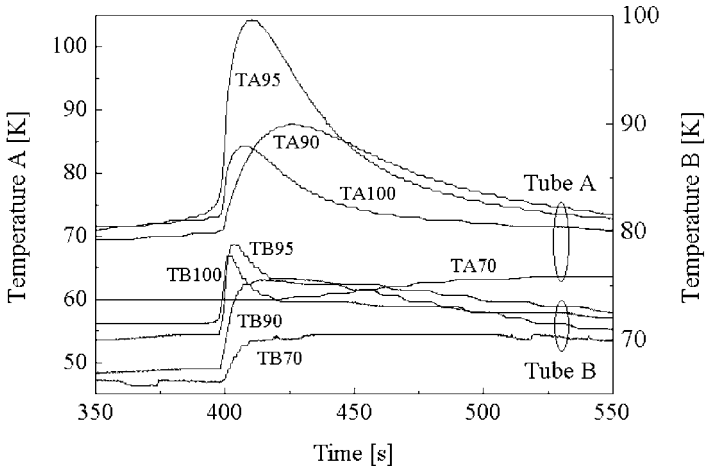

Fig. 2.5.16 *Temperatures in Tubes A and B for a quench at I=10kA. The temperature at the warm end of Tube A is as high as 104K, while the maximum temperature of Tube B reaches only 79K.*

In spite of a large current imbalance, the current lead could be safely operated under steady state conditions at the nominal current of 10kA. The results suggest that a design based on two Bi-2212 modules in parallel is unfavourable because of the reduced effective critical current and the deteriorated quench behaviour in the case of a large current imbalance. On the other hand, the existing technology is not adequate to manufacture a single 70kA Bi-2212 module. Considerable more development work is therefore indispensable before Bi-2212 bulk material can be used in current leads for such high nominal currents.

2.5.5 Superconductivity Studies

Analysis of the TFMC current sharing temperature with ramp heating

To heat the ITER Torodial Field Model Coil (TFMC) up to the current sharing temperature, T_{cs}, ramp heating was proposed by CRPP in 1999 as a compromise between two heating procedures: (1) heat slug injection (the experiment has confirmed the result of the analysis: helium choking leads to a systematic quench at the inner joint) and (2) the steady state heating (although expected to exceed the cryoplant capability, quasi steady state conditions could be reached in the experiment). The analysis of the ramp heating was completed by combining simulations, superconducting strand data and the experimental run (at FZK) which ended with a quench: 80kA in TFMC, 60s ramp heating, 320W final power in pancake DP12, 180W in DP11. The boundary conditions used for the analysis of DP12 are: measured data of helium temperature, pressure and massflow, current sharing model, joint heat generation, and heat exchange at the joint as a function of the temperature difference between DP12 and DP11.

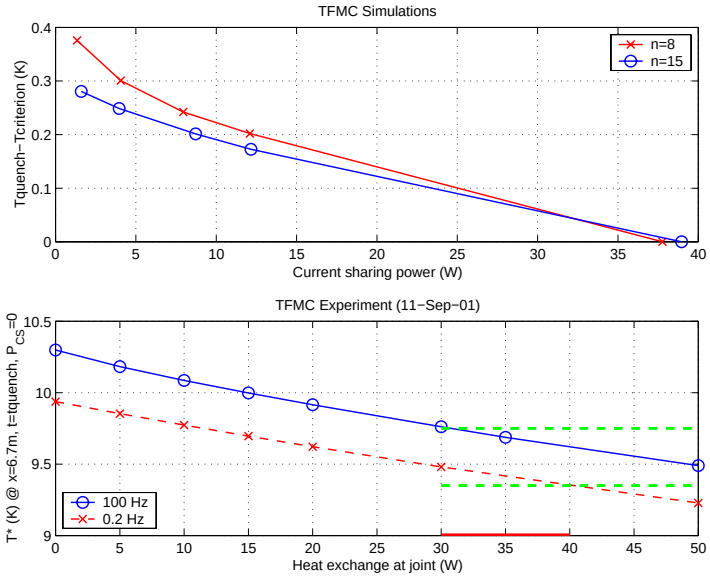

Fig. 2.5.17 *Results of TFMC simulations (top) and analysis (bottom) of the run with 60 s ramp heating. The factor n is the exponent of the voltage-current power law (top). 100Hz and 0.2Hz are the Data Acquisition rates (bottom).*

In the run with ramp heating the inlet temperature is not a reliable figure for the temperature downstream, where the quench is predicted at the maximum field (B_{max}). The run analysis was mainly devoted to the estimate of the temperature at the location of B_{max} at the time of the quench event (t_{quench}). However, the strand temperature at quench is affected by the current sharing power leading to the runaway. The goal of the simulation was to assess the difference ΔT between the temperature at the selected quench criterion of 500μV, and the maximum temperature at other V-criteria, i.e. ΔT depends only on the ramp slope and the characteristics of the cable (the factor n). At the ITER criterion of 50μV/m, the current sharing power in the short length exposed to Bmax is ~2W and can be neglected. The Gandalf (CryoSoft) thermal hydraulic code was finally used to

extrapolate the temperature T* at B_{max} and t_{quench} from the experimental inlet temperature, assuming no current sharing power. The estimated range of T* in the expected range of heat exchange at the joint is 9.4-9.8K. The expected T_{cs} is 8.8K, i.e. using Summers law, strand data and assuming a longitudinal strain of -0.61%. In conclusion, (1) the ramp heating leads to a quench in the winding (and not in the joint) of the TFMC, as predicted by the analysis; (2) a quantitative assessment of the Tcs from the test results of the 60s ramp run (dT/dt~6K/min) tends to overestimate the performance due to the slow runaway and slow thermal hydraulic dynamics; (3) as far as the cryoplant allows, a very slow ramp would be suitable to assess the conductor limits, avoiding the small transients of the multi step heating.

Electric and thermal analysis of the CONDOPT experiment

Current sharing and current distribution in large superconducting cables for high field magnets are a concern which is difficult to address owing to the complex nature of the interaction between the electric and the thermal behaviour of the cable. Experimental results of large magnets indicate that premature current sharing and resistive voltage development can be a limiting factor for operation. The same result was reproduced in a SULTAN experiment, see section 2.5.1. In support of the interpretation of the experimental results, the analysis of the current distribution and its effects on cable performance was performed with the THEA code (Thermal Hydraulic and Electric Analysis) (CryoSoft). The model consists of the last-but-one cable stage as 4 twisted superstrands with uniform properties. The non-linear voltage-current characteristic was used, with the exponent of the power law n=15, as measured in the cable in virgin state. The superstrands are independently cooled by a single helium flow, and are coupled electrically through mutual inductances and interstrand conductance. The electrical joints have been included using simple approximations of ideal conditions, i.e. perfect contact among the superstrands (zero joint impedance) and prescribed current at each superstrand (infinite joint impedance). Critical current runs and current sharing temperature runs were simulated, both in the virgin state and after cycling. One interesting feature that was observed experimentally, and was reproduced by the simulation, is that the highest transverse electric field is measured in the direction of the background field (i.e. smallest field gradient) and not in the direction perpendicular to this (i.e. largest field gradient). Another main result of the experiment, reproduced by the simulations, was the observation of a change in the voltage-current characteristic of the sample with the increase of the interstrand resistance. The analysis has confirmed that the exponent n is a good measure of the collective behaviour of the cabled strands.

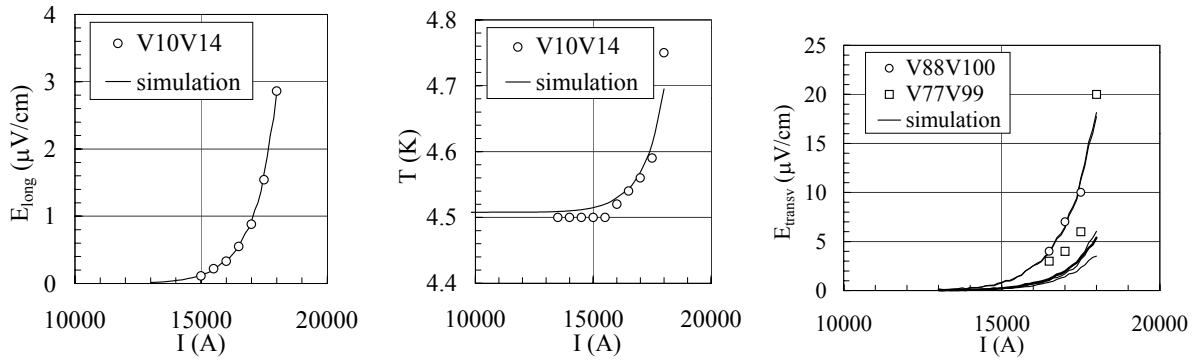

Fig. 2.5.18 *Results for the sample in the virgin state during a critical current run. Measured and simulated results are in good agreement, i.e. longitudinal electric field at the location of the voltage taps V10V14*

(left), temperature at the outlet of the high field region (center) and transverse voltage as differences among the four superstrands at the two locations of the voltage taps V77V99/V88V100 (right).

High-T_c Superconductors: a critical comparison between magnet conductor candidates

The use of high-T_c superconductors (HTS) has the potential to make next generation fusion reactors more attractive. A design incorporating HTS offers an advanced tokamak concept and in the longer term substantial cost saving.

So far, Bi-2212 and Bi-2223 are the most advanced high-T_c superconductors. From both materials long multi-filamentary wires or tapes have been successfully fabricated. In the case of Bi-2212 ($T_c \approx 90K$) round wires as well as textured tapes can be manufactured. Bi-2223 superconductors ($T_c \approx 110K$) are presently available only as tapes. Better in-field current densities are available with biaxially–aligned YBCO coated conductors. In fact, this second generation HTS is the most promising high-T_c superconductor but the fabrication of long biaxially textured conductors at a reasonable cost level has not yet been demonstrated. Consequently, planned design studies will focus on Bi-2212 and Bi-2223 but will keep an eye on the second generation of HTS as a possible option for fusion magnets.

High current superconductors, required for fusion magnets, are built up from many individual basic elements by a cabling or braiding process. The shape of the basic elements determines not only the handling and cabling procedures that can be used but also their AC properties. Furthermore, due to the anisotropy of the critical current density of Bi-based tapes regarding the magnetic field direction, the geometry of the basic element will play an important role in the design of the magnet. While round wires are the easiest to handle, rectangular conductors are quite difficult to handle, being more flexible in one direction than in the other. Although much of present HTS demonstrators at 77K use Bi-2223 tapes, Bi-2212 wire is easier to fabricate and has a better J_c in high magnetic fields and temperatures close to 4.2K. On the other hand, Bi-2223 tape conductor, which is the preferred candidate for 20K operation, is a special rectangular conductor with high aspect ratio. This geometry requires special cabling procedures thereby limiting the number of methods to construct a cable.

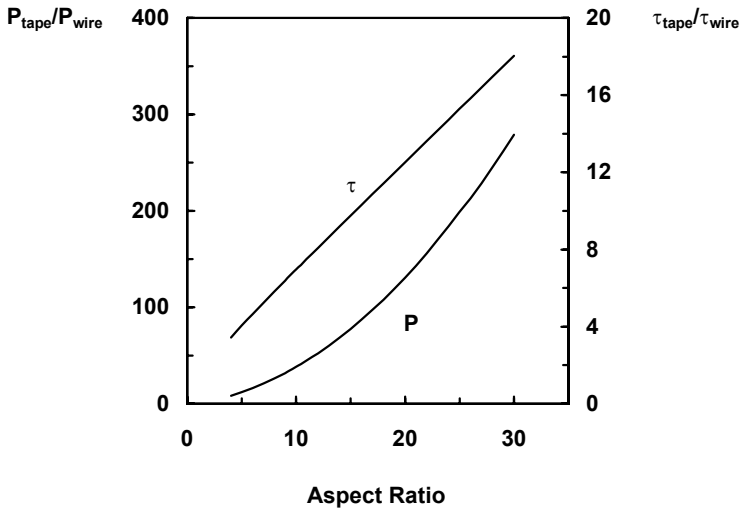

Fig. 2.5.19 *Relative coupling losses P_{tape}/P_{wire} and relative decay time constant τ_{tape}/τ_{wire} as a function of tape aspect ratio, (c/d); c is the tape width and d its thickness.*

A further important issue is the AC loss behaviour. Due to the large aspect ratio of the tape configuration, AC magnetic field components perpendicular to the plane of the tape are unfavourable as they cause filament coupling and consequently large losses. As shown in Fig. 2.5.19, the coupling losses of round wires have to be multiplied by a factor close to 1/3 of the square of the aspect ratio in order to derive the losses for tapes. However, producing HTS AC-optimised tapes is in progress. Twisting the filaments and resistive matrix materials is already being done in developmental conductors. Further steps like filament decoupling using non-metallic barriers and less bridging between filaments are highly desirable in order to reduce substantially the AC losses of tape superconductors.

In the design of solenoidal magnets (like the ITER CS coil), the anisotropy of the critical current density has to be considered. Approaching the ends of a solenoid the radial magnetic field component (the field perpendicular to the tape surface) begins to dominate. Because the field dependence of J_c is less pronounced for fields parallel to the tape surface than for those perpendicular, the peak field that can be reached in a solenoid made of tapes is determined by the radial field intensity within the winding. The CS coil of ITER-FEAT consists of six electrically independent modules. Consequently, the six modules can be operated with different currents. At some intermediate equilibrium plasma conditions, the end modules carry currents opposite to those in the central modules. To estimate the maximum radial magnetic field, operation with the same current density and direction in all six modules of the CS coil is assumed.

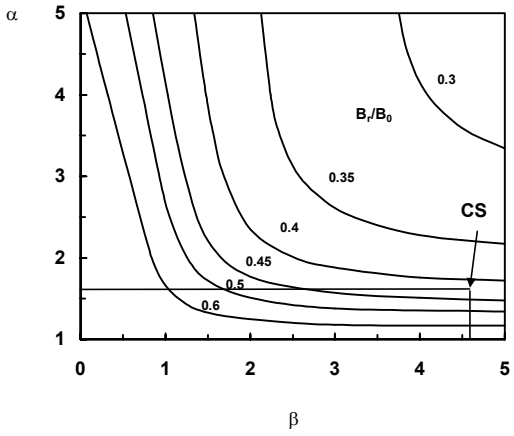

Fig. 2.5.20 *Ratio of the maximum radial magnetic field B_r and the central field B_0 as a function of the shape factors α and β in a solenoidal magnet. For the CS coil the maximum radial field exceeds 40% of the central field.*

Figure 2.5.20 shows the ratio of the maximum radial field B_r and the central field B_0 as a function of the shape factors α and β. The shape factor α is the ratio of the outer and the inner radius of the solenoidal winding, while β is the ratio of the length to the inner diameter of the winding. The figure shows that the ratio B_r/B_0 decreases with increasing winding thickness and length. However even in long solenoids with $\alpha < 2$, the maximum radial field reaches more than 35% of the central field. The figure indicates that for shape factors of $\alpha \approx 1.6$ and $\beta \approx 4.6$ corresponding to the ITER-FEAT CS coil the maximum radial magnetic field exceeds 40% of the central field. The magnetic field at the conductor of the CS coil is limited to 13.5T which leads to a maximum radial field of slightly less than 6T. The maximum field of 13.5T at the conductor in the central plane is parallel to the axis, and hence along the tape surface.

Figure 2.5.21 shows the critical current of Ag/Bi-2223 tapes normalised to the value at 77K and zero applied field as a function of temperature for an axial magnetic field of 13.5T parallel to the tape surface and a radial magnetic field,

perpendicular to the tape surface. Considering only the axial magnetic field the critical current would reach 2.45 I_c(77K, B=0) at 20K. Operation at 80% of the critical current would provide a temperature margin of 7.7K as indicated in the figure. On the other hand, the critical current is limited to 1.45I_c(77K, B=0) for the unfavourable field direction and a field as low as 6T. Moreover, the temperature margin is reduced to 3.6K.

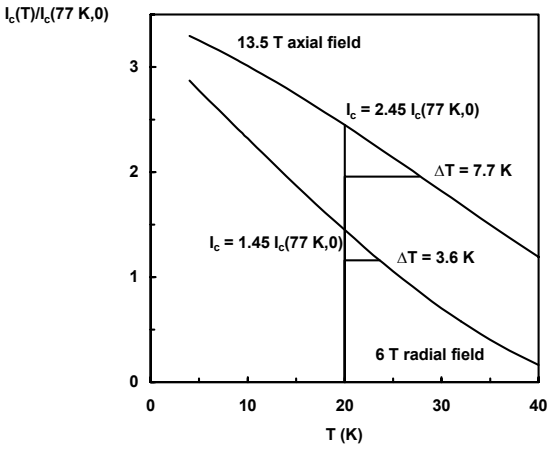

Fig. 2.5.21 *Temperature dependence of the critical current for Ag/Bi-2223 tapes exposed to an axial magnetic field of 13.5T and to a 6T radial field. The critical current has been normalised by its value at 77K and zero applied field.*

*2.6 Gyrotron development**

The Association has continued in 2001 its long standing collaboration with other European Associations and industry for the development of gyrotrons to be used in different devices such as the stellerator W7-X or the tokamak Tore Supra.

2.6.1 140GHz gyrotron development for W7-X

Long pulse test of the gyrotron was performed at FZK in the frame of a collaboration with the Association FZK, IPP-Garching, CEA and the European industry Thalès. The first tube of this development has achieved world record value as far as output energy is concerned (Table 2.6.1) At power level of 0.5MW the pulse duration (180s) was limited not by the tube behaviour but by the available power supply. 10MJ pulse was achieved during the test at an efficiency of 50% using a depressed collector.

Pulse length [s]	Power [MW]	Efficiency*
180	0.47	(23%)**
140	0.64	
100	0.74	(32%)**
40	0.86	39%
10	0.98	50%
5	1.05	47%

* Efficiency measured with depressed collector

* This work was performed in collaboration with the Associations FZK (D), CEA and the industry Thalès (F).

** Efficiency without depressed collector

Table 2.6.1 *140GHz gyrotron performance*

2.6.2 Test of the 118GHz gyrotron

During the long pulse test of the 118GHz-0.5MW gyrotron at CEA-Cadarache, anomalous behaviour of the tube was noticed. The test was repeated at shorter pulse length (up to 2s) at the CRPP premises. The excitation of parasitic modes in the internal launcher part of the tube was identified. These parasitic modes may cause excessive heating and deformation of the tube. Corrective measures have been designed and will be implemented in the final version of the tube for the tokamak Tore Supra at CEA.

*2.7 Industrial process plasmas**

2.7.1 The physics of plasma enhanced CVD for large area coating

The aim of this CTI project was to develop a large area, high throughput coating system for mass production of silicon thin film solar cells. The project was carried out in a collaboration between the CRPP Lausanne, IMT Neuchatel, and Unaxis Truebbach. The CRPP investigated the reactor and plasma parameters, the deposition of the intrinsic layer (the i-layer), and contributed to investigations of the boron contamination between the p- and i-layers. The IMT concentrated on layer properties and interface optimisation, boron contamination, and cell fabrication and evaluation. Unaxis developed an industrial reactor system. In collaboration with Unaxis, a load lock chamber for the CRPP was designed and installed in April 2001, allowing several deposition runs per day, and also to test novel scenarios for reducing boron contamination between the p- and i-layers.

Reactor design and plasma parameters
The main process parameters investigated were the electrode gap and the plasma excitation frequency. Topics concerning the reactor technology have also been investigated, including modelling of segmented electrodes, reactor impedance, matching design, power transfer efficiency, plasma edge uniformity and various scaling up issues.

The increase of the excitation frequency from 13.56MHz to 27.12MHz and the decrease of the electrode gap both lead to a significant increase in the deposition rate. The deposition rates obtained approach discharge conditions of maximum utilisation of the silane source gas. At small electrode gap, characteristic inhomogeneities in the form of a turtle shell structure could appear. The intense edge plasma, due to electric fringing fields at the RF electrode perimeter, causes non-uniform deposition and requires that the substrate edge be 5cm away from the reactor walls. Numerical plasma modelling showed that the fringing fields could be reduced by using dielectric inserts at the reactor walls. Other sources of non-uniformity are the gas flow rate due to showerhead design, and the propagation of

* The work described under this section was not performed within the frame of the Association Euratom – Confédération Suisse.

perturbations to the RF voltage due to the edges of the reactor and dielectric substrate.

In addition it could be shown that segmentation of the RF electrode along the lines of symmetry does not give any improvement, whereas segmentation into rings can reduce the overall non-uniformity, but with discontinuities across the ring boundaries.

Deposition and quality of the intrinsic layer

PDS spectroscopy performed at the IMT in Neuchâtel demonstrated that the initial defect density of the obtained films meets the device quality. As a complementary quality check, the porosity of these i-layers was evaluated using two methods: spectral ellipsometry and infrared absorption spectroscopy. Ellipsometry performed at the CRPP was shown to be more sensitive to the residual porosity in the high density range appropriate for solar cells, and it was used for quality control of films produced at CRPP and IMT. The i-layers deposited at high rates (> 5Å/s at 200°C) were generally found to be more than 10% porous. This porosity appears to be linked to excessive degradation of the final solar cell.

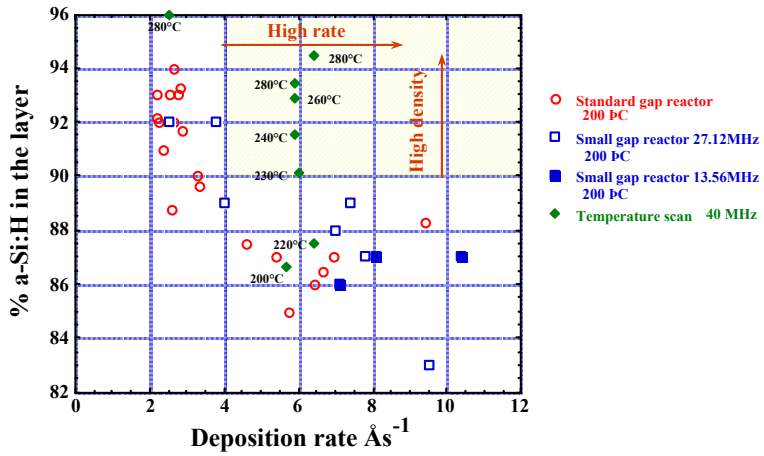

Fig 2.7.1 *Film density versus deposition rate as obtained in the Unaxis KAI reactor*

A significant observation is that the i-layer density is principally determined by only two parameters: the substrate temperature and the deposition rate. The film density improves at higher temperatures, but deteriorates with higher deposition rates. Phenomenologically this is because the radicals must be capable of diffusing to thermodynamically preferable sites before depositing: high temperature increases radical mobility, whereas high deposition rate reduces the time available. Exhaustive studies showed that the plasma parameters are only of secondary importance in influencing the layer density, although higher RF frequency and smaller electrode gap do help. A possible reason for the plasma effect, according to modelling, is that an excess of strongly reactive radicals such as SiH_2 is produced in high power plasmas, which in turn could lead to columnar growth and a porous film.

Substrate temperatures above 250°C yielded very dense films even at deposition rates >5Å/s. However, industrial experience generally dictates that the substrate temperature should not exceed 200°C, otherwise the open circuit voltage of the final

cell deteriorates. To obtain dense films, this fixes an upper limit for the allowable deposition rate to approximately 3Å/s, which is well within the capability of the plasma processes studied in the KAI reactor. It was found that 3Å/s still represents a significantly useful improvement in state-of-the-art solar cell manufacture.

Boron contamination reduction for single chamber operation
A critical issue for the single reactor system used is the question of boron contamination of the i-layer following deposition of the boron-doped p-layer in the same reactor chamber. A pre-study showed that boron cross contamination of p-i-n solar cells produced in single reactor chamber is less severe if trimethylboron (TMB) is used because of its thermal stability compared with the commonly-used diborane, which decomposes at the hot reactor walls. Even when using TMB, boron contamination of the i-layer remains a major problem for a single-chamber reactor. Therefore, many different scenarios were evaluated for their effectiveness in inhibiting boron contamination without damaging the final solar cell. Sandwich structures of p- and i-layers were deposited using various interface treatments, and the depth profile of the boron concentration was analysed by secondary ion mass spectrometry (SIMS). At the IMT, the contamination of the i-layer by boron from the p-layer was also monitored by current-voltage and spectral response measurements of completed cells. Both the fill factor and spectral response are very sensitive to boron contamination of the i-layer through the reduction of Rp.

It was found that a simple flushing of the reactor with gases such as argon, hydrogen, and oxygen is not effective to reduce the contamination. Various plasma treatments of the reactor chamber are effective provided that the substrate is removed to the loadlock during this time, otherwise the final cell is deteriorated. The best results in this case were obtained using a O_2 or CO_2 plasma, or plasma etch cleaning of the p-layer, or amorphous silicon coating to bury the boron. However, from the point of view of throughput for industrial processing, it is preferable to keep the substrate in the reactor during any interface treatment. An in situ oxidation process has been developed at IMT which strongly reduces the boron contamination from the p- to i-layer compared to a single short pumping. Buffer layer without oxidation could be an other solution. The buffer layer is a thin layer (100 to 150Å) located between the p- and i-layers which aims to adjust the gaps of these two layers. This layer is also used to trap the boron contamination from the p-layer, in order to avoid a contamination tail in the i-layer. To summarise, the work done up to now has demonstrated that the boron contamination problem for single-chamber reactors can be solved, although the final industrially usable method for doing so has yet to be defined.

2.7.2 Plasma spraying

Diagnostics of a supersonic DC plasma jet expanding at low pressure
Low Pressure Plasma Spraying (LPPS) or Vacuum Plasma Spraying (VPS) make use of plasma torches operated inside a vessel under reduced pressure. In contrast to Atmospheric Plasma Spraying (APS) these processes offer the advantage of a controlled atmosphere to avoid oxidation or contamination of the powders and sprayed deposit. This also allows an extension of the specific operation parameter space by controlling the chamber pressure.

Even though these LPPS processes are extensively used in a wide range of applications, only a few studies aiming to determine their plasma jet properties,

either experimentally or numerically, have been reported. This is probably due to the great complexity of these high enthalpy, supersonic plasma jets, and to the inherent difficulties to setup and interpret measurements when the jet is not in aerodynamic equilibrium. Most of the previous experimental investigations were limited to a range of pressures down to 100mbar.

At lower chamber pressure (below 10mbar) the plasma jet exhibits unconventional behavior related to very weak collisionality and large dimensions. In this regime a new process (LPPS Thin Film) has been shown to rapidly deposit thin dense layers of metals or ceramics over large areas.

The plasma gun investigated is a Sulzer Metco F4-VB gun with different conical nozzles (Fig 2.7.2). It is mounted inside a $2m^3$ vacuum vessel and the vessel pressure is regulated in the range 2–100mbar by means of a 3-stage pumping system. A modified enthalpy probe system is used to measure the stagnation pressure and enthalpy in low pressure plasma jets. A fast, 12 bit CCD camera is used to visualize the total plasma jet emission. The camera exposure time is 100μs. The gun anode has been modified to allow static pressure measurements inside and at the exit of the nozzle. This is used to determine whether the jet exhibits over-expanded or under-expanded flow. The operating parameter range investigated is 400-600A current, 40–60SLPM Ar flow and 2–100mbar chamber pressure.

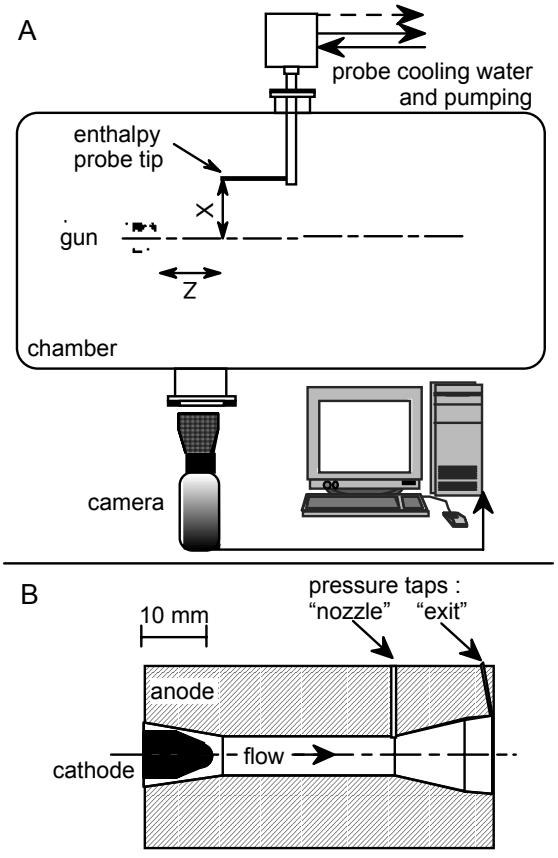

Fig. 2.7.2 *Schematic top view of the experimental arrangement (A), and cross-section of the torch nozzle showing the pressure taps (B).*

Supersonic jets differ in their behaviour from subsonic jets. The major difference is that the former can exit a nozzle at a pressure that is different from the ambient pressure. When the fluid at the exit plane of the nozzle reaches the speed of sound or higher speed, the pressure waves carrying the chamber pressure information are

unable to reach the flow inside the nozzle. Therefore, the chamber pressure is not felt by the flow and the geometry of the nozzle governs the pressure distribution inside the nozzle along with the torch operating conditions, namely the power. In that case, the jet exit pressure can differ from the chamber pressure.

Figure 2.7.3 shows the structure of a supersonic over-expanded where the exit pressure of the jet is lower than the chamber pressure. It is shown that oblique shock waves originating from the edge of the nozzle are formed. This mechanism increases the jet static pressure to the level of the pressure of the chamber by turning the flow (from zone a to b). However, these shock waves are reflected on the jet axis. This leads to a second compression of the flow that brings the fluid to a pressure higher than the chamber pressure (from zone b to c) while turning the flow so it is parallel to the axis. The increase of pressure and temperature after the oblique shock waves can be observed by the increased luminosity of the plasma, if the shock is strong enough.

The shock waves meet the jet boundary and are reflected in the shear layer in the form of a series of expansion waves. They decrease the flow pressure back to the chamber pressure (from zone c to d). These expansion waves are also reflected on the jet axis so that the flow will then go through another series of successive expansion/compression waves (from zone d to g). The pressure change through each cell is attenuated from cell to cell by the viscous effects, which also thickens the shear layer. Eventually the pressure is brought back to the chamber pressure.

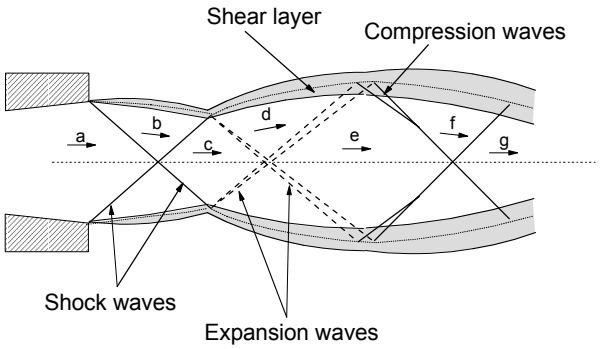

Fig. 2.7.3 *Compression/expansion mechanisms in an over-expanded jet*

Chamber pressure effect on the jet topology

Figure 2.7.4 shows images of the plasma jet as a function of the chamber pressure in the range 20–100mbar. At 100mbar for example, the flow is over-expanded, as indicated by the oblique shocks which converge from the nozzle exit edges towards the jet axis. This is confirmed by a measured nozzle exit pressure smaller than the back pressure. This over-expansion leads to a radial compression of the jet by the oblique shock wave originating from the nozzle exit edge. This builds up a compression zone around the jet axis, extending between 4.5 and 12mm from the nozzle exit, visible as a bright emission patch. This compression leads to a local static pressure which exceeds the surrounding pressure and consequently the jet expands as it flows downstream. This is evidenced by an increased jet radius with weaker emission around z=18mm. This process of successive compression/expansion repeats further, until the local jet static pressure is in equilibrium with the surrounding pressure, due to viscous effects (around z=60mm in Fig. 2.7.4).

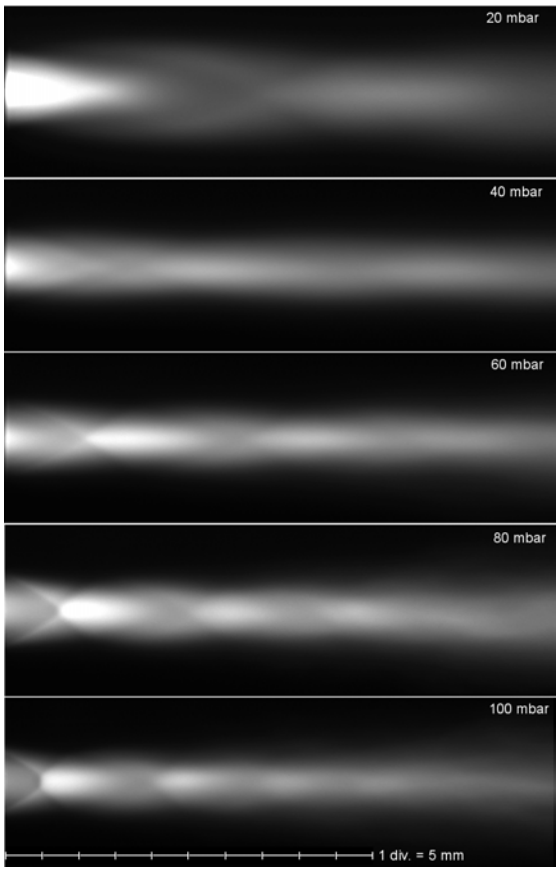

Fig. 2.7.4 *Images of the plasma jet at different chamber pressures. Torch parameters: 600A, 60SLPM Ar.*

As the chamber pressure is reduced, these successive compressions/expansions are stretched, and build up farther from the nozzle exit. This is mainly because of the absolute pressure reduction: the jet needs more distance to equilibrate pressure as evidenced in Fig. 2.7.4 for 80 and 60mbar. Around 45mbar chamber pressure (for the conditions of Fig. 2.7.4), both exit and chamber pressures are equal which corresponds to the so-called "design pressure" (indicated by arrows on Fig. 2.7.5). The jet static pressure is in equilibrium with the surrounding pressure and no longer exhibits successive compressions/expansions. In Fig. 2.7.4, the jet at 40mbar is close to this situation and very weak shock structure is visible. Since the jet properties are the most homogeneous at the "design pressure", it might be worth tuning the chamber pressure to approach this regime as close as possible for best spraying conditions. However, it should be noted that the "design pressure" strongly depends on the torch parameters, as shown in Fig. 2.7.5 for two plasma conditions.

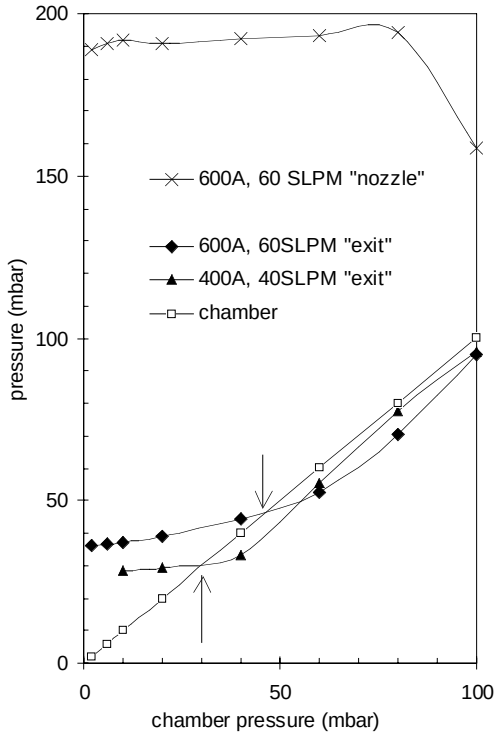

Fig. 2.7.5 *Dependence on the chamber pressure of "nozzle" and "exit" pressures for two torch parameters. (Arrows indicate the "design pressure").*

Figure 2.7.5 also shows that the pressure measured at the beginning of the conical section of the nozzle is almost independent of the chamber pressure below 80mbar. Therefore, here, the sonic transition (M=1) of the flow takes place at the end of the cylindrical section of the nozzle, whereas for chamber pressures above 80mbar it occurs in the conical part. This means that the geometry of the nozzle, for given torch operating conditions, also influences the value of the "design pressure". If the chamber pressure is further reduced below 45mbar, the jet progressively switches to an under-expanded flow.

Figure 2.7.6 shows images of the plasma jet for pressures below 20mbar. These under-expanded jets are characterized by a hot and dense plume exiting the nozzle, whose length increases as the chamber pressure decreases. This plume is followed by an expansion with a significant drop in temperature and pressure close to the jet axis. The edges of this first expansion zone are brighter because barrel shocks are formed by reflection of the expanding flow from the cold, dense surrounding gas. This leads to a compression and converts part of the kinetic energy into thermal energy. There is a local increase of the temperature and density, and hence of the light emission. Subsequent expansions / compressions occur until the local jet pressure equilibrates with the chamber pressure, as shown in Fig. 2.7.6 for the 20 and 10mbar cases. For lower chamber pressures, the flow structure, as evidenced by the plasma emission, looks different and can no longer be described by classical gas dynamics.

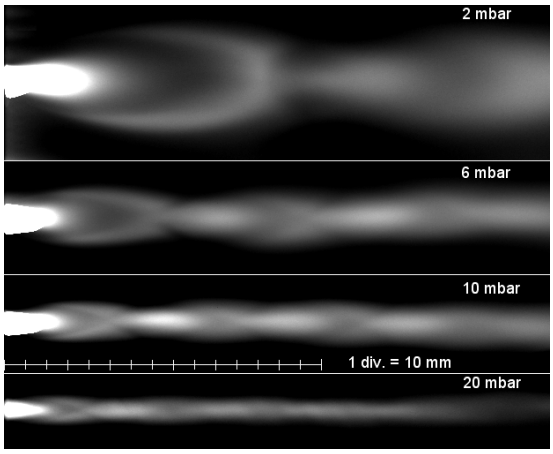

Fig. 2.7.6 *Images of the plasma jet for pressures below 20mbar. Torch parameters : 50SLPM Ar, 500A current.*

Enthalpy probe measurements

A modified enthalpy probe system is used to measure the specific enthalpy and the stagnation pressure profiles throughout the jet. Determination of the local free-stream jet parameters, such as the temperature and velocity, for the case of supersonic flow is made assuming an isentropic frozen stagnation process at the probe tip.

Figure 2.7.7 shows radial profiles of the measured stagnation pressure and total enthalpy at axial positions corresponding to successive expansion and compression zones in the 100mbar jet. In Fig. 2.7.7A, the stagnation pressure profiles are maximum on axis in the compression zones (z=26 and 40mm) whereas they are hollow and broader in the expansion zones. At z=18 mm the pressure profile drops

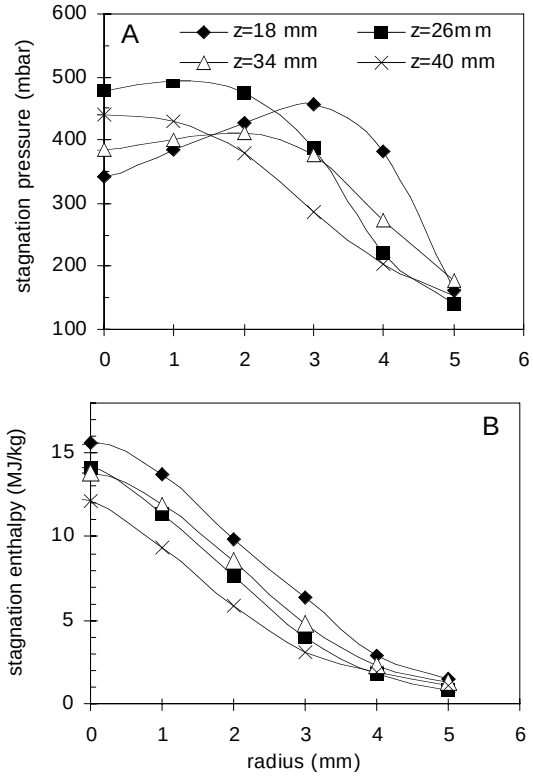

Fig. 2.7.7 *Measured radial profiles of the stagnation pressure (A) and total enthalpy (B) at different axial positions at 100mbar.*

significantly on axis. This is probably because the flow crosses a Mach reflection at z=4.5 mm around the axis. This is a strong, non-isentropic normal shock which reduces the dynamic pressure. The stagnation enthalpy profiles are always maximum on axis because this is the region of maximum temperature and velocity, but they are also broader in the expansion regions.

Figure 2.7.8 shows the calculated temperature and velocity radial profiles using a iterative procedure assuming isentropic stagnation process at the probe tip and LTE thermodynamic properties.

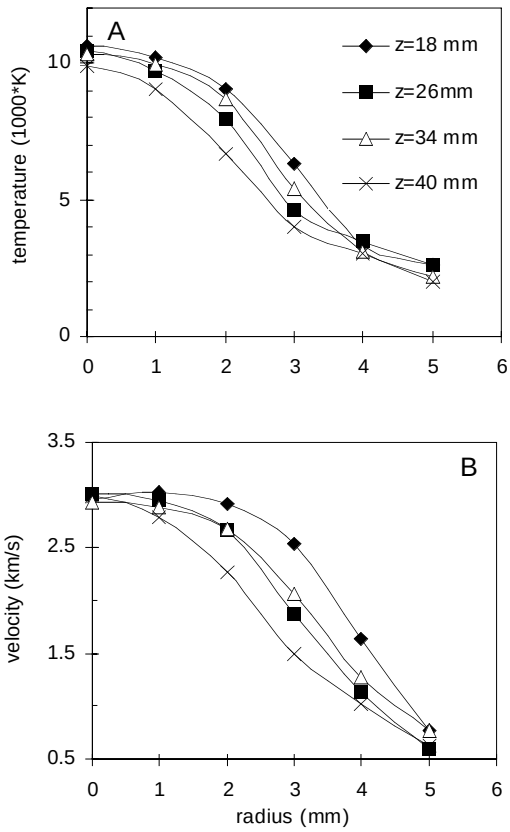

Fig. 2.7.8 *Temperature (A) and velocity (B) radial profiles at different axial positions determined from the measured data of Fig. 2.7.7.*

Both the temperature and velocity profiles of Fig. 2.7.8 are broader in the expansion regions in agreement with the jet topology. But their values on axis do not drop substantially downstream, over the axial region investigated here. This reveals an efficient isolation of the jet core from the surroundings, as regards heat and momentum losses. However, the area-integrated heat flux throughout the jet cross section decreases from 8kW at 18mm down to 5kW, at 40mm for a net torch power of 10.5kW. This drop of the integrated heat flux and the shapes of the radial profiles of Fig. 2.7.8 show that the jet is cooled and slowed down from the mixing zone at the edges, outside the barrel shocks. This differs from subsonic plasma jets which experience turbulent surrounding gas engulfment and cooling straight through the core. Here the core jet flow is supersonic and non-turbulent over the whole region investigated, with Mach numbers approaching 2 on axis and falling down to around 0.7 at the edges of the measured profiles.

We have been able to perform total enthalpy and stagnation pressure measurements at chamber pressures down to 20mbar with the present arrangement. However, the actual iterative procedure used to calculate the free stream jet properties using the measured total enthalpy and stagnation pressure

failed for positions off jet axis at pressures below 80mbar. At these positions, the calculated kinetic component of the total enthalpy, given by half of the calculated squared velocity, exceeds the measured total enthalpy already at the first iteration. This is attributed to non-LTE effects and jet deflection by the probe tip.

2.7.3 Design of a new large area high density plasma source (HDS)

High density plasmas at low pressure can be obtained in the well-known inductively-coupled plasma (ICP) source often driven at an excitation frequency of 13.56MHz. But also microwave discharges working at an excitation frequency of 2.45GHz are well suited as high density plasma sources. The typical electron densities achieved by these techniques can be as high as 10^{12} electrons per cm^3 which is about 2 orders of magnitude higher than the densities reached in conventional capacitively-coupled RF plasma reactors driven at 13.56MHz.

There is an alternative way to achieve high density plasmas which consists of using very high excitation frequencies while keeping the design similar to parallel plate reactor design. It has been clearly shown in the past that the sheath voltage decreases rapidly with increasing excitation frequency. This gives the possibility to couple much higher RF power into the plasma while keeping a moderate sheath voltage thus preventing substrate damage. Electron densities higher than $10^{11}cm^{-3}$ have already been obtained in Ar plasmas at higher gas pressures. However little is known about plasma operation at low gas pressures as typically applied in dry etch applications.

One of the major difficulties of high frequency plasma is the scaling up, which becomes more difficult as the frequency increases since the typical dimensions of the reactor become non-negligible compared to the excitation wavelength. An appropriate design of the high frequency coupling is necessary to overcome this problem: this represents the main topic of a new CTI project started during the year. In the fore-field of the project it has been theoretically shown that with convenient shaping of the RF electrode, uniform RF voltages can be achieved, a necessary ingredient for uniform deposition or etching. We demonstrated that an analytical solution of Maxwell's equations for this design has the property of suppressing the radial standing wave non-uniformity even when the lateral dimension of the reactor becomes comparable or larger than a quarter of the wavelength. The innovative design of the new plasma source substitutes one of the conventional flat RF electrodes by an appropriately-shaped electrode. The main aim of the present work is to experimentally verify these theories and simulations and to finish up with a new industrial high density plasma source for deposition and in particular also for etching purposes.

2.7.4 Plasma diagnostics for the electrical discharge machining (EDM)

In recent years the advances of Electrical Discharge Machining (EDM) has been mainly dictated by improvements in the accuracy and automation of the machining tool part of the equipment and in the design of sophisticated power supplies to produce and control the electrical discharge between the electrode and the work piece. The present EDM equipment on the market is able to machine most of the required forms and materials with sufficient performance (accuracy, high cutting speed, small surface roughness...). Currently EDM allows machining of work pieces with details of a few micrometers and for the accuracy the limits are about one micrometer. However in order to still improve the performances of EDM, the

electrical discharge and its interaction with the material must be better controlled. This implies that the interaction of the spark with the substrate and its dependence on the discharge parameters have to be better understood.

However despite the wide industrial application of EDM, the physical basics of the electrical discharge and its interaction with the material are completely unknown. Only a few restricted or confidential reports and only very few publications and works have tried to enlighten the complex process of electrical discharge machining.

One of the difficulties in the investigation of the EDM processes lies in the diagnostics of the plasma. Plasma diagnostics is considerably more complex for the transient arc or spark than for continuously running plasma sources such as RF and microwave sources. Nevertheless, recent advances in plasma diagnostics and its technology now allow deeper investigations of the arc and spark discharges. Work on this interesting Topnano 21 project started at the end of the year.

Modelling for the industrial plasmas

Modelling of the various industrial plasmas is a necessity in order to improve the process performances and to increase understanding of the underlying basics of plasma physics and plasma chemistry. For the various applications and processes developing specific codes simulating and modelling the plasma and plasma reactors is a key issue. Since the industrial plasmas are related to several technologies modelling of other topics such as mechanics and electronics is also absolutely necessary. For these reasons the group of industrial plasma processing made a big effort in advanced modelling of the plasmas and the plasma reactors. One example emerging in the last year is the modelling of the deposition rate profile in a KAI reactor of Unaxis.

Large area plasma enhanced chemical vapour deposition (PECVD) of thin films such as silicon nitride or amorphous silicon is widely used for thin film transistor fabrication in the flat panel display industry. During the last decade, for economical reasons and because of the increase of the individual display size, the rectangular substrate size followed a steady growth starting with a diagonal length of about 0.5 m one decade ago, to more than 1 m in actual reactors and with projection of more than 2 m in future. At the same time, the uniformity requirement of the film properties over the substrate area was maintained or even bettered.

This strong increase in the substrate size implies that the different sources of non-uniformity have to be understood in order to design larger plasma reactors. Among them, we can cite: the voltage uniformity distribution, the powder contamination, the perturbations due to the reactor edge and the gas flow and chemistry distribution in the reactor.

In this investigations the gas flow and a chemistry model for silicon nitride PECVD in a large area rectangular reactor have been studied. Until now only few models of silicon nitride PECVD have been done. In all these models, the geometry was limited to two dimensions, one dimension being the electrode gap. This is sufficient to predict the uniformity in cylindrical geometry, but not in rectangular geometry. In the developed model, we also limited the geometry to two dimensions by averaging the transport equations over the electrode gap. This allowed to predict the deposition uniformity throughout the full electrode area. In the chemistry of the process only the most important processes have been retained in order to reduce the complexity of the calculations. With these simplifications, without losing reality, the computation time is reasonably small on a desktop computer.

Plasma induced surface modifications
Together with laboratories of the former Material department of the EPFL in particular with the Laboratoire de Métallurgie Chimique (LMC; Prof. H.J. Mathieu) various investigations on the surface modifications of polymer films by plasma have been performed.

Plasma treatment has been found to be an extremely attractive way to modify the surface chemistry and morphology of polymeric materials. The industrial applications of these investigations are mainly for biological or medical applications. There are a number of polymeric materials that have very good physical properties but do not have an active surface for immobilisation of biomolecules for instance. Such polymers need selective modifications so that specific functional groups may be imparted to the surface for the binding of biomolecules and culturing cells.

One of the applications studies in the frame of the collaboration the Laboratoire de Métallurgie Chimique is the plasma treatment of PET films by an RF argon plasma followed by exposure to an oxygen atmosphere. The films underwent considerable changes in surface composition and morphology, as was demonstrated by contact angle measurements, FTIR-ATR, AFM, and XPS. It was found that the surface acquired oxygen containing polar functional groups such as -C=O, -OH, and -OOH, which increased in number as the plasma treatment time increased. During storage, the treated films underwent significant surface reorganization, and both the time and temperature contributed to the increase in the contact angle. As revealed by AFM measurements, these changes were accompanied by an increase in roughness in the form of ridges. The ridges were observed to grow in height with increasing treatment time, although their spacing showed little evolution. A correlation among the observations obtained from various techniques was established, giving a comprehensive picture of the structure and dynamics of plasma-treated PET surfaces.

An additional application of plasma treatment is the surface modification of polyvinylchloride intubation tubes to control bacterial adhesion. As well in collaboration with the Materials and the Rural Engineering Department of the EPFL first works on the surface modification of polyvinylchloride intubation tubes have been made. The motivation for this work is that bacterial colonization of intubation tubes is responsible for 30% of all nosocomial pneumonia cases, 40 % of which lead to death, despite aggressive antibiotic therapy. Therefore, a strategy to reduce bacterial adhesion is desirable. We are developing an approach based on the surface modification of the polymer used for this application, medical grade poly(vinyl chloride) (PVC). The strategy is to mask the PVC substrate with a chemically inert teflon-like fluoropolymer layer, which serves as an ideal platform for further surface modification due to its low surface energy. Protein and bacterial repellant molecules, e.g. amphiphilic Pluronics, are bound to the fluoropolymer films using hydrophobic-hydrophobic interactions.

We investigated fluoropolymer films created on PVC substrates through plasma-enhanced chemical vapour deposition. The films are deposited in an RF-plasma reactor, using C_2F_6 as a precursor and H_2 as a carrier gas. XPS data suggest that the films completely mask the substrate, as no remaining signatures of PVC are detectable. Moreover, alpha step measurements show a uniform film, with a thickness of approx. 200nm. The fluoropolymer films were found to be highly hydrophobic, with a water contact angle >100°.

Preliminary contact angle measurements of the Pluronic surfaces show a significant decrease in contact angle, (approx. 20°) indicating adhesion to the fluoropolymer layer. Feedback from imaging XPS is then used to optimize Pluronic monolayer formation on the fluoropolymer film. Protein adsorption and in vitro bacterial adhesion studies will also be reported.

Other collaborations and industrial mandates

Several industrial mandates have been carried out during 2001. These mandates involved essentially basic research and development of new processes or improvement and control of existing plasma processes. Numerous industries consulted us during the last year and this resulted in many small experiments and tests which have been performed on the existing plasma reactors at the CRPP .

Two mandates from Swiss and international companies have been carried out. Furthermore plasma processing of SiO_x coatings as a permeation barrier in packaging was investigated for TetraPak R&D Plasma Technology in Romont. During the year it was agreed to continue to collaborate on the establishment of the basic understanding of the plasma chemistry and physics. A new project proposal is under discussion.

Besides these industrial activities, the industrial plasma group contributed to the organisation of courses (collaboration in the French-spoken Swiss Vacuum courses) and workshop (collaboration in the first Swiss Plasma Processing meeting in Zürich)

It should be added that the collaboration with industry and the confidence of industry is excellent and very stimulating for a small group like the plasma processing group of the CRPP.

3 Technical achievements of the CRPP in 2001

3.1 TCV tokamak operation

TCV was operated for 6 months in 2001 with a total of 1594 technical and physics discharges following a lengthy shutdown. Operational statistics as a function of time of day for the discharges considered as "useful for physics exploitation" are shown in figure 3.1.1. Operation started late in May 2001 and was again retarded until the end of June 2001 for alignment of the Thomson and FIR-interferometer sub systems as well as final commissioning of the X2 and X3 gyrotron launchers.

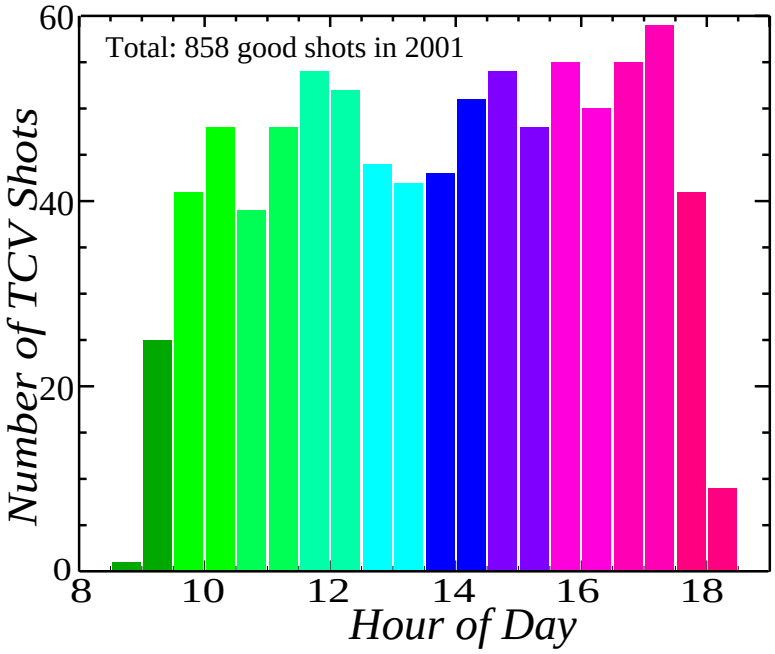

Fig. 3.1.1 *TCV physics discharges for 2001 as a function of hour of day. The operational procedure in which one team operates the machine until 13:00 and another until the end of the working day allows a continuous operation throughout the day.*

3.2 TCV Diagnostics

Thomson Scattering

In order to improve the spatial resolution of the Thomson electron temperature diagnostic on TCV, 10 scattering spectrometers are being installed on load from RFX, Padova, Italy. These will use the existing Thomson optics on unpopulated chords to observe the plasma edge with a resolution of ~10mm in comparison with the 35mm spatial resolution of the main Thomson diagnostic

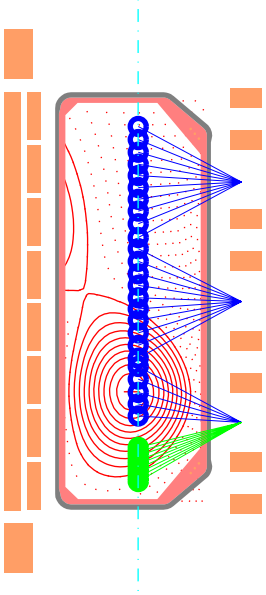

Fig. 3.2.1 *Blue lines indicate the current Thomson observation chords and the green lines the initial positions of the Padiva spectrometers. They are shown for a TCV configuration which transits into H-mode where the edge temperature profile is strongly modified.*

Fast Bolometry (AXUV)

Preliminary tests with the prototype bolometer detectors that use AXUV diode arrays have been completed. A new design featuring an array of 7 cameras equipped with 2 similar diode arrays is underway. One of the diode arrays in each camera will be used, as initially suggested, as a bolometer array which is not sensitive to neutral particles and the other will be equipped with visible light interference filters or simple absorption filters to observe the complete Deuterium light emission profile which can be related to the ionisation source distribution inside TCV. By optimising the camera lines of sight, within the constraints of the physical TCV port dimensions, the tomographic inversion of the chords to provide radiation emissivity can be greatly improved.

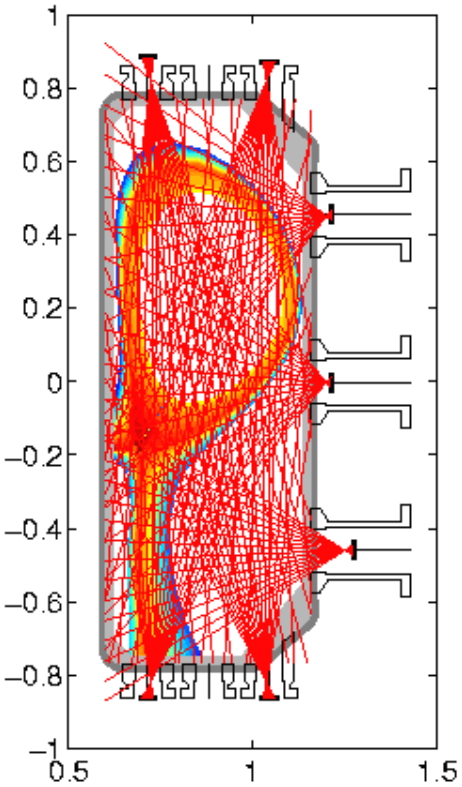

Fig. 3.2.2 *Plan of the 7 camera AXUV diode arrangement. The red lines indicate the chords of the cameras. In this example, the radiation from plasma edge emission has been modelled. When viewing this radiation, the plasma appears as a hollow radiating cell since the plasma core radiates little.*

Active Neutral Beam Spectroscopy (DNBI)
Following poor emissivity observations and an unexpectedly high passive emission from TCV, both the DNBI and the associated spectroscopic diagnostic systems were upgraded.

In the first stage of the beam upgrade, which is to be completed in 2002, the beam current from the source was increased to nearly 2.5A and the beam extraction optics was optimised to maximise the full energy component in the neutral beam. Later stages of this upgrade will include a more powerful plasma source power supply and a new extraction grid assembly. A further improvement to the beam will be discussed with the Budker Institute of Nuclear Physics (BINP) following completion of this upgrade to increase the injected neutral particle density in the region of spectroscopic observation.

The spectroscopy optics was completely re-optimised. Two fibres were assigned to each observation chord, the collection lenses were changed and the spectrometer grating diffraction efficiency was improved.

The overall result was an improvement in the Active/Passive emissivity ratio of up to 70% and an over of 5x improvement in the observed signal/noise ratio. This system now permits Ion Temperature measurements at plasma densities up to $6.10^{19}/m^3$ in the plasma core. New spectroscopic systems including a high tendue spectrometer and back illuminated CCD detectors have been purchased to further improve the statistical quality of the acquired data and increase the number of usable observation chords back from 8, which resulted from pairing up the observation fibre optic chords, to the initial design s 16 chords per spectrometer.

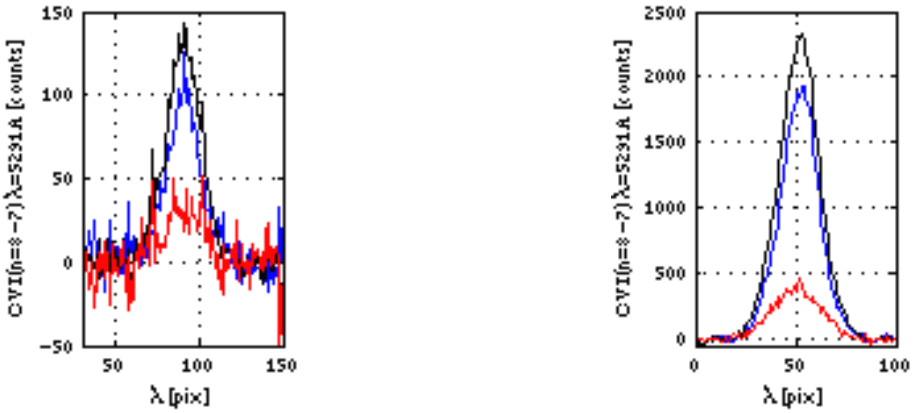

Fig. 3.2.3 *Left hand figure shows the previous situation and the Right hand figure shows the current situation for similar plasma conditions. In blue is the measured signal without DNB in black with and the difference which is used by this diagnostic in red.*

Edge profile spectroscopy
Using the method of a separate fibre optic telescopes coupled to the entrance slit of an imaging spectrometer, a multi-chord spectrum of the TCV edge plasma region has been obtained. Currently this system uses the same spectrometers as for CXRS

achieved by simply changing the spectrometer entrance slit optics. In the current arrangement, there are 16 chords observing the outer 30% of the plasma volume. This is intended for experiments where a strong change in the temperature and density edge profiles are often observed such as H-mode.

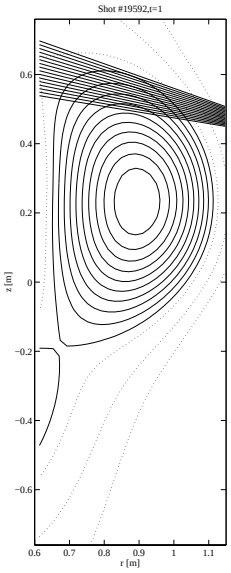

Fig. 3.2.4 *The chords for edge observation are shown for a plasma configuration where H-mode is obtained on TCV*

SPRED spectrometer

The installation of the SPRED VUV spectrometer was completed. During 2001, the SPRED has provided routine coverage of the 120nm to 10nm spectral range with a 1 to 10ms time resolution. The spectrometer uses a Reticon diode array with a read-out system built at the CRPP. This system can read out the full 2048 spectroscopic channels in 640μs. A hollow cathode spectral lamp was purchased from the Institut fuer Atom- und Molekuelphysik, Hannover to provide spectral lines with an intensity referenced to a Synchrotron source. Following some doubts on the correct focussing of the SPRED, as delivered from the manufacturer, a test rig is being constructed which allows the lamp to be scanned across the spectrometer étendue to examine the spectrometer's focussing properties.

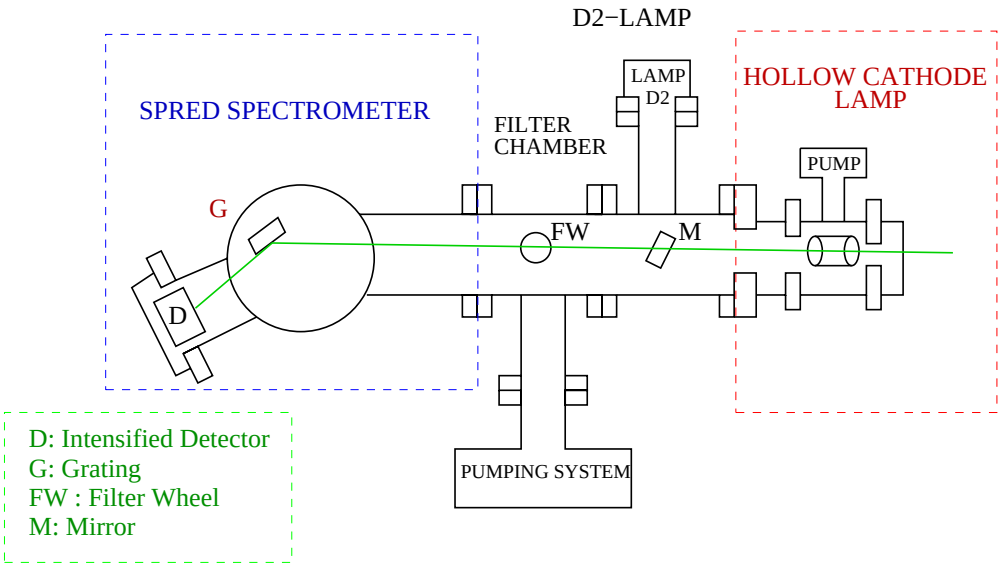

Fig. 3.2.5 *A Schematic of the calibration source and the SPRED spectrometer.*

Ultrasoft X-ray spectroscopy (USX)
The USX spectrometer, produced by the IPP Prague, has been re-configured to provide a radial impurity profile by rotating the spectrometer 90° such that each spectrometer channel observes a different poloidal region of the plasma.

Hard X-ray measurements
The hard X-ray camera, on loan from Tore Supra, France, was operational on TCV for the whole of 2001. It was used extensively to measure both the spatial and spectral distribution of Bremsstrahlung emission from fast electrons during ECH and ECCD experiments on TCV. A design project is underway to replace this system with an array of hard X-ray sensitive diodes optimised in the 10-200keV energy range with a spatial resolution of ~1cm. This array will use fast 8-bit ADC acquisition to provide energy resolution of the detected photons with a maximum count rate in excess of 5MHz.

Soft X-ray Pulse Height Analysis (PHA)
The thick Ge solid state diode, installed on TCV in collaboration with the CFN-IST, Lisbon, Portugal, has been extensively operated during 2001. The IATG module, developed by the CFN, was optimised to allow a count rate to up to 30kHz of analysed soft X-ray photons from TCV. This system measures the energy spectrum of soft X-rays from the TCV plasma which can then be used to determine the electron temperature, deviations from a Maxwellian velocity distribution as obtained with ECCD and the presence of plasma impurities which emit characteristic line radiation.

An upgraded system featuring a Roentec Xflash Silicon Drifted diode detector has been ordered to replace the bulky liquid Nitrogen cooled Ge detector. This diode features electronic cooling, (down to –10°C), the ability to be mounted vertically in the high magnetic field of TCV without further shielding and excellent photon energy resolution (<170ev). A commercial DSP pulse treatment and histogramming module, (Xia, DXP-2X, USA), is being purchased to exploit the high count rate possibilities of this detector. A practical count rate of over 300kHz should be possible with this combination with little deterioration in the energy resolution. Further extension of this system could include multi-diode arrays, to improve peak count rate, and the development of a real-time fitting algorithm in the DSP to obtain real-time electron temperature and impurity contamination signals that may be used as a feedback signal for the TCV control system.

Fig. 3.2.6 *Shows a photograph of the Roentec detector and cooler power supply*

MultiWire Proportional X-ray detector (MPX)

A Multiwire Proportional X-ray (MPX) detector has been installed on TCV as a high spatial resolution X-ray imaging diagnostic. This, vertically viewing, 64 channel X-ray system has been designed to complement the existing 10x20 chord pinhole camera system TCV which only have a spatial resolution of ~3cm. The diagnostic measures the plasma emission in the 3-30keV range with a radial resolution of about 5mm and a frequency bandwidth of a 50kHz. The multiwire proportional detector consists of 64 non-separated channels each with a sensitive area of 2x40 mm^2. The camera is separated from the vacuum vessel by a first beryllium window of thickness 250µm. The MPX detector has a second beryllium window of thickness 100µm and an additional aluminium foil of thickness 308µm can be included in the optical path. The voltage on the wires can be controlled remotely and a range of chamber gases can be used to modify the detector's energy response.

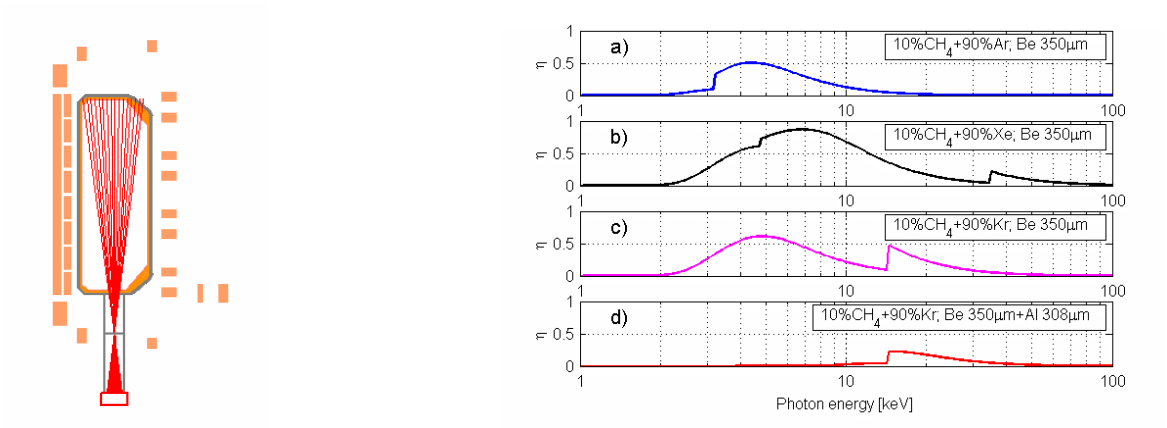

Fig. 3.2.7 *a) shows the viewing chords of the MPX detector with respect to TCV. b) shows the spectral sensitivity of the detector as a function of the gas fill.*

Rotating Crystal Spectrometer

A rotating crystal spectrometer, where the Bragg angle of a collimated X-ray beam from the plasma onto a diffracting crystal is varied, has been obtained on loan from

the Princeton Plasma Physics Laboratory (PPPL). With a range of crystals, this spectrometer can cover the 500eV to 10keV X-ray range albeit with a resolution of only ~300. This spectrometer will be sensitive to the presence of even small quantities of high-Z impurities such as Fe and Cr which can result from machine wall interactions with the plasma. It is sensitive to ionisation stages corresponding to the plasma core of TCV. By fixing the Bragg angle to diffract a particular spectral line, this spectrometer will also be used for impurity ablation experiments on TCV where trace samples of medium-Z impurities are injected into the plasma to measure the ion confinement time.

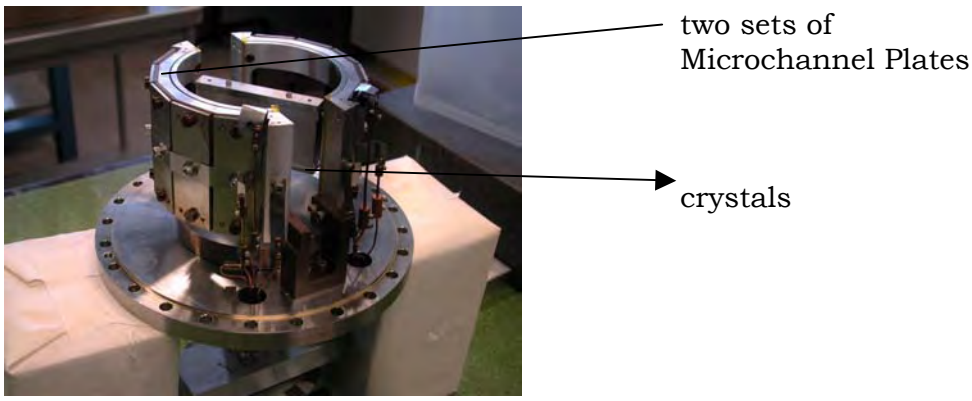

Fig. 3.2.8 *Picture of the inside components of the Bragg Rotor Spectrometer. Plasma radiation passes through the collimator onto the diffracting crystal positioned on a rotating mount and is recorded by the Microchannel plate detectors*

2mm and 1mm microwave Interferometers

Particularly for use at the low densities associated with X2 ECH experiments, the 2mm interferometer is being refurbished with the purchase of a new source and detector. To extend the operational range of this diagnostic to higher densities, the interferometer will later be upgraded to a 1mm wavelength system. This will initially use the same waveguides as the 2mm system but will feature two phase-locked oscillators in a superheterodyne arrangement which is expected to considerably reduce the effects of vibration on the measured signals.

Digital CCD cameras

4 12-bit Digital CCD cameras have been purchased to replace the analogue CCD camera observation of the TCV divertor visible radiation emission. These cameras feature a frame rate of up to 76Hz with a 320x240 pixel image and have extended UV sensitivity. As in the preliminary analogue system, a telescope images the plasma divertor leg onto a coherent fibre-optic bundle. A beam splitter arrangement at the other end of the fibre bundle splits the light into four channels that are passed through a wavelength selecting interference filter before being imaged onto the CCD detectors. The optical system and cameras, together with their real-time acquisition systems will be installed close to TCV during 2002 for divertor detachment and Helium plasma experiments.

Neutral Particle Analyser (NPA)

The TCV NPA analyser has been reworked and made operational in 2001. The system is now routinely operated both in scanning mode, where the 5 spectrometer

energy channels are repetitively scanned so as to provide complete coverage from ~300 to ~8000eV and in fixed mode where the detector channel energies are set for the TCV discharge duration. Preliminary calculations have shown that the NPA would provide more information on the TCV core conditions if mounted on a horizontal port of TCV where the neutral path absorption from the core to spectrometer is reduced, but in this arrangement the NPA would not be able to observe all TCV configurations. With the advent of CXRS ion temperature measurements of the plasma bulk, the NPA is finding a new use in the measure of fast ion populations. Modifications to increase the high energy range of the NPA are being examined. Discussions were held with the neutral particle group at Tore-Supra who are building a neutral beam test stand to absolutely calibrate the NPA response as a function of neutral particle energy.

Neutron Detector

A ^{3}He filled gas proportional detector is used on TCV to detect the neutrons resulting from fusion reactions. The analogue amplifier electronics of this system has been examined and a digital filter designed to compensate a strong over-shoot in the pre-amplifier section. The detector, which is currently operational on TCV, can be used to deduce an effective ion temperature and to detect the existence of a fast ion velocity tail which has been observed in previous ECH experiments.

Thomson Scattering

In order to improve the spatial resolution of the Thomson electron temperature diagnostic on TCV, 10 scattering spectrometers are being installed on load from RFX, Padova, Italy. These will use the existing Thomson optics on unpopulated chords to observe the plasma edge with a resolution of ~10mm in comparison with the 35mm spatial resolution of the main Thomson diagnostic

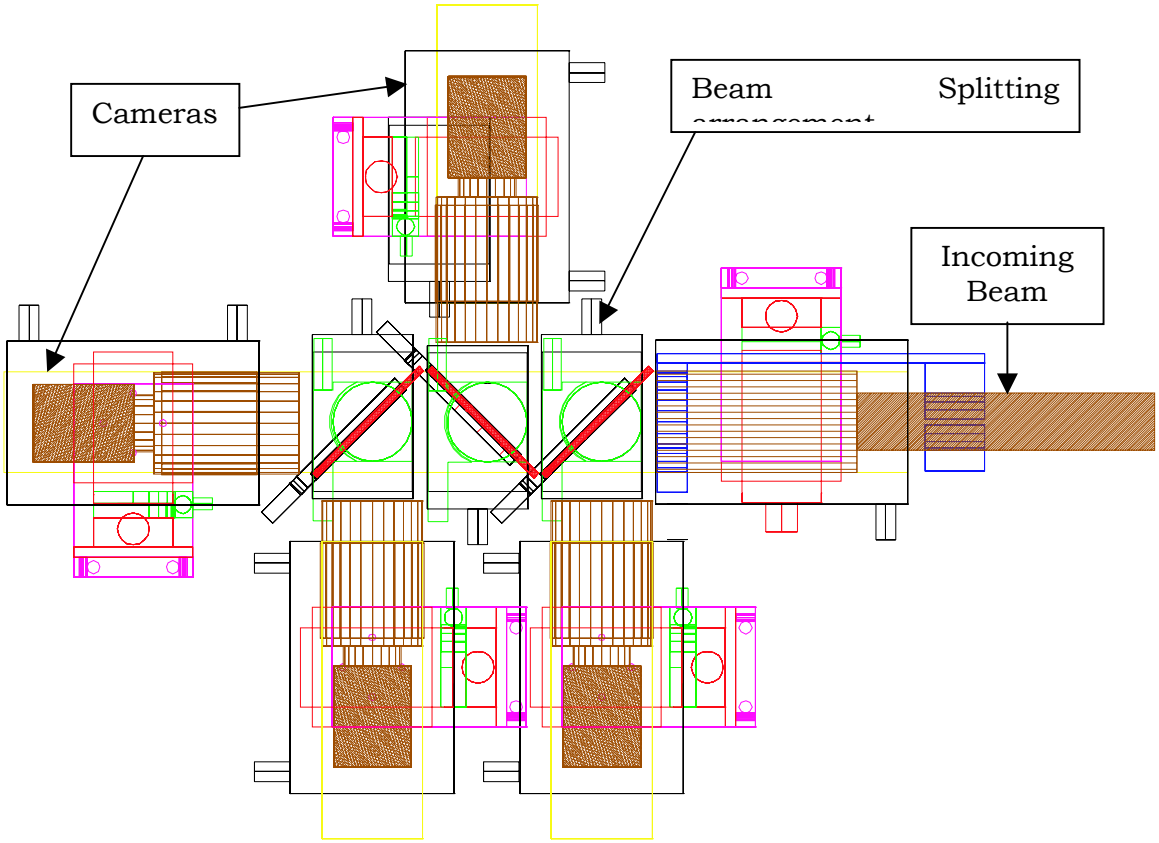

Fig. 3.2.9 *Optical plan of the 4 camera observation system*

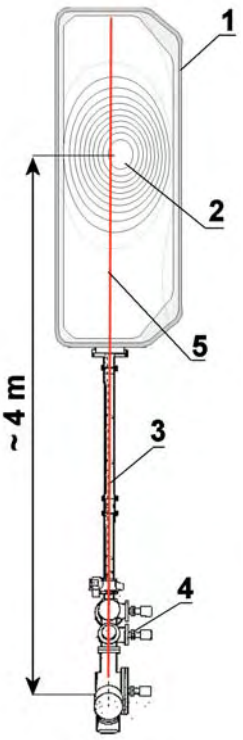

Fig. 3.2.10 *NPA layout on TCV*
1-TCV vacuum chamber
2-plasma
3-NPA duct
4-NPA
5-viewing line.

3.3 X2 and X3 system developments

3.3.1 X2 System at 83GHz

The six X2 gyrotrons (each 0.5MW and 2.0s pulse length) and the associated transmission lines and launchers continued operation on TCV during the campaign period of 2001. No modifications to the gyrotrons were made during this period, all six gyrotrons operated correctly without failures.

A vacuum compatible wave guide switch was introduced into one of the X2 transmission lines, which permitted the operation of either an X2 or an X3 gyrotron into the transmission line and X2 launcher. This option allowed preliminary operation of an X3 gyrotron into TCV before the installation of the X3 launcher. The X2 launcher was designed from the onset (1993) to be compatible with both operating X2 and X3 operating frequencies. Approximately 100 X3 shots at full power were injected into this lateral X2 launcher during 2001.

Four of the six launchers were removed from the TCV vessel during 2000. Some of the components of these launchers were made of PEEK; these pieces were replaced with a machineable ceramic. These four modified launcher were tested at full power and pulse length throughout 2001. The modifications improved both the poloidal and toroidal movements of three of the launchers, however, the fourth launcher still had problems of 'sticking' during the launcher's poloidal movement.

3.3.2 TCV X3 series gyrotrons (118GHz)

The three X3 gyrotrons are now in operation on TCV, working at full specifications (500kW, 2s).

3.3.3 Transmission lines

The assembly of the X3 transmission lines was successfully completed during summer 2001. So far, 2 transmission lines are fully operative on the X3 (top) launcher, whereas the option of injecting the power of the third tube laterally, using one of the X2 antennas is still kept.

3.3.4 Launcher

The X3 launcher was put in place during the opening period of summer 2001 and was successfully commissioned by the end of 2001.

3.3.5 Commissioning

The integration of the X3 ECH system into the TCV technical environment is presently underway. The control and acquisition systems dedicated to the X3 heating have been implemented and tested. Initial experiments dedicated to the validation of the mirror motion system and to the calibration of the incident and deposited power measurements have been carried out. Up to 1MW of microwave power has been injected from the top.

Fig. 3.3.1 *Overview of the X3 launcher on top of TCV*

3.4 Design of a New Basic Plasma Physics Device

During the second half of 2001 the design of a magnetized toroidal plasma device for basic plasma physics studies has started. This device, named TORoidal Plasma Experiment (TORPEX), is aimed at studying a variety of basic phenomena, including turbulent transport and magnetic reconnection. The design is based on the principle of maintaining a large degree of flexibility both in the achievable magnetic field configurations and in the plasma production schemes. The magnetic field coils, part of which are available from a previous linear magnetized plasma experiment at the CRPP, will produce a toroidal field (up to 0.3T), a vertical field and a quadrupole (or cusp) field with a magnetic X-point at the centre of the device. The plasma will be produced initially by ECRH at 2.45GHz, with power <50kW, for a duration of about 200ms. An Ohmic transformer for inducing a relatively large toroidal electric field both for transport studies and to force reconnection in the plasma is also foreseen. The preliminary design shown in the figure below shows the modularity of the vacuum vessel, which will guarantee easy access for installation of plasma sources and diagnostics. The design of the device will be completed in 2002. Procurement and installation of all the major systems are foreseen for the second half of 2002.

Fig. 3.4.1 *Preliminary design of the TORPEX device*

3.5 SULTAN Facility

After the yearly shut-down for maintenance in January 2001, the SULTAN facility was continuously in operation until Christmas 2001, with a single interruption between May 21st and July 16th, as the facility cryostat had to be opened to fix the current leads of the pulsed field coils. The facility was warmed up in a record time of 10 days, supplying an electric power of 2–5kW to the coils in addition to the warm gas circulation at a controlled temperature.

The pulsed coil leads broke as the mechanical restraints of the coil assembly loosened after the first four months of operation. The pulsed coils did not suffer any damage. The leads were repaired and strong wedges have been attached to the coil assembly to rigidly block it in the bore of the main SULTAN coils (the forces acting between the pulsed field and the main background field cause a mechanical torque between the two coil systems).

To load the conductor samples with a large number of cycles, the superconducting transformer was operated in a continuous triangular sweep, at the maximum achievable ramp rate. The limit for the rate of cycling is the removal of the heat generated in the primary winding by ac loss; the heat is removed by indirect cooling over a pipe attached to the winding. Up to 400 cycles/day could be obtained on an extended shift for two samples at 15kA. In the third sample, the largest loading rate to 70kA was 80 cycles/day.

3.5.1 Control System Upgrade

After the implementation of the new control system in SULTAN, successfully performed in 1999 and 2000, a considerable effort was dedicated in 2001 to complete the upgrade. The hardware and software migration from the old SatCon PLC to SatLine, the latest generation PLC system of ABB, done in the year 2000, was mainly dedicated to the cryogenic and vacuum systems. In 2001, after gathering enough operational experience with the new system, it was decided to continue the system integration and unification by implementing the remaining functionalities: control of magnetic field, mass-flow and temperature regulation of the short sample insert, pulse heaters, superconducting-transformer quench heaters, control of mass-flow in the SULTAN current leads and improvement of cool-down and warm-up sequences.

The magnetic field in the SULTAN facility is generated by three pairs of concentrically nested superconducting solenoid pairs. In order to achieve a given magnetic field in the centre of the magnet system, the currents in the three solenoid-pairs were ramped-up to the prescribed set points following a prescribed function of time. This procedure was initially implemented in three local D/A converters as part of the three DC power supplies for the SULTAN coils. At low field range the three power supplies could be ramped-up together at the same rate, at a higher field the prescribed ramping procedures were different and rather complicated resulting in rather long charging/discharging times for the coil system. After a thorough AC losses re-assessment, it was concluded that the ramp time could be cut-down to about one hour and that the three coils can be ramped to a given field in the allowed range 0-11T simultaneously i.e. using a single time-

scaling function, to be integrated it in the SatLine system together with the cryogenic and vacuum system.

The hardware part of the new magnetic field control system consists of three analog outputs (0-10V) 12bit cards as part of the SatLine system delivering the set points to the three power supplies and of three analog inputs for the process values (currents) measured by Rogowsky coils in the power supplies. The ramp function is generated in the software part and is a linear function of time. Special software routines have been also implemented allowing the change of the magnetic field from each possible start point to each possible end point in the range 0-11T. The rate for any field change of the SULTAN background field is now 0.165T/min.

The short sample insert in the SULTAN facility is composed of two full-size superconducting cables (legs) joined at the lower end by a “praying-hands” copper joint and attached to the two terminals of a superconducting DC transformer. The two cable legs are electrically connected in series forming a closed circuit with the secondary coil of the transformer. From the hydraulic point of view, the two legs are connected in parallel i.e. there are two independent He circuits for cooling such that the He mass flow in each leg can be controlled independently. Using heaters attached to each leg, the He temperature can be independently adjusted. In the old control system, the set-up of mass flow and temperature in each leg was done by hand and there was no regulation loop on either mass flow or temperature. This had the consequence that the set-up of mass flows and temperatures in the two legs was a very tedious procedure in view of the fact that in such a cryogenic circuit the mass flow is dependent on the hydraulic resistance of the cable which in turn is strongly dependent on temperature. A whole series of adjustments and readjustments used to be necessary in order to reach a given set point and besides this the stability was rather poor. Additionally, the temperature of each leg was set by increasing the power in the heaters until the desired value was reached in a trial and error procedure which was again a time consuming procedure. In view of all this facts it was decided to implement control loops on the mass flow and temperature on each leg as shown on the left panel in Fig. 3.5.1.

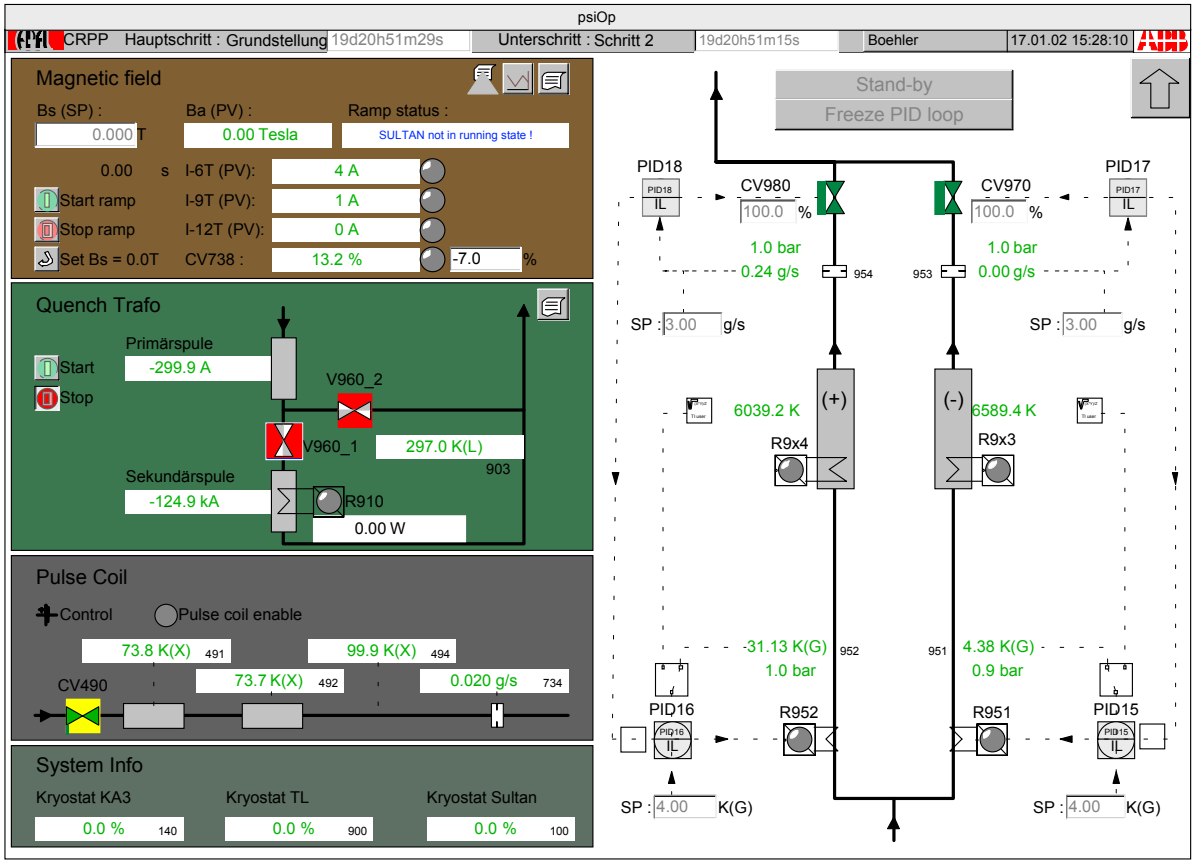

Fig. 3.5.1 *The new mass flow and temperature control system of the short sample insert*

The mass flow control loops are PID17 and PID18 with process values from the flow meters FI953 and FI954 and outputs to the regulating valves CV970 and CV980. The temperature control loops are PID15 and PID16 with process values either from cryogenic system TI951 and TI952 or from user temperature sensors depending on the position of the corresponding soft switches. The user temperature sensors are provided with a mathematical input block for the input of the calibration table. Additionally, two user pulse heaters R9x3 and R9x4 can be controlled independently by setting the desired voltage and pulse time. The control logic is provided with options for operation, stand-by and PID-freeze conditions.

The pulsed field coils are cooled by supercritical He taken from the cryogenic system through the valve CV490 and returned as warm gas to the He compressor. The temperature of the two coils and the mass flow of circulating He are critical parameters. The control and operation of the transverse pulse coils was implemented as shown in the third panel on the right side of Fig. 3.5.1. The valve can be remotely operated and the He mass flow and the temperatures in the two coils are indicated.

Before starting a current test or after such a test has been performed, it is necessary to prepare the 100kA superconducting transformer for the next current ramp. The current in the primary is ramped to a negative value (max. -300A). To avoid a negative current in the sample during this phase, it is necessary to drive the secondary in the resistive state i.e. to quench it before starting the ramp in the primary circuit. In order to quench the secondary, the cooling is stopped by closing the valve V960_1, the bypass valve V960_2 is opened and the heater R910 is

activated. When the current in the secondary has reached the set value the above sequence is repeated backwards i.e. the hater is stopped and the cooling reactivated. The state is reached with the primary at full negative current and with the secondary at zero current. In the old system the whole procedure described above was done manually. In the new control logic it was implemented as an automatic sequence, which is initiated by simply pressing the START button in the "Quench Trafo" panel, the second panel on the right of Fig. 3.5.1.

In the old version of the operation system, the SULTAN current leads were cooled with the maximum amount of He, independent of the value of the magnetic field. The He used to cool the current leads is returned by necessity as warm gas and this means an additional load on the refrigerator which is lost for the applications: for each g/s warm returned He, the refrigeration loss is about 150W. After numerical simulation it was established that the SULTAN current leads have enough design reserve to be operated in the transient mode during the charging of the coils. The following procedure was adopted. At zero magnetic field, the current leads are cooled with 20% of their specified mass flow for 11T in order to compensate for the heat conduction. When the magnetic field is ramped-up the mass flow in all current leads is increase proportional to the magnetic field using the same time-scaling function as for ramping the field. In order to reduce the cost, the six current leads valves were not changed but an additional valve was installed on the collecting line, which was hydraulically dimensioned such as to induce linear variation of mass flow in each current lead without changing the position of the old current lead valves.

3.5.2 Extended Range for Time Varying Field

The commissioning in SULTAN of the new set of pulsed field coils (designed and manufactured in 2000) was carried out in February 2001. The permanent instrumentation of the coils, now integrated in the set of facility sensors, includes two temperature sensors attached to both copper windings to monitor the self heating of the coils in operation and two Hall sensors, oriented in the direction of the pulsed field. Another temperature sensor is at the outlet of the cooling circuit. A pick-up coil is also attached to the coil assembly, far away from the location of the sample, to be used as compensation coil whenever magnetization measurements are carried out on the sample.

The inductance and resistance of the coils, measured at the feed-through of the SULTAN tank, are L=10.18mH, R≈2 mΩ. When the saddle coils are connected with the pulse battery, the resonating frequency of the LRC circuit is 7.8Hz (128ms full wave period). Decreasing the number of capacitors in the battery, the resonance period can be reduced to 40ms. The field to current ratio in the middle of the experimental space, i.e. where the sample is placed, is 8.69G/A, in agreement with the coil design and computed field profile. With the bipolar power supply (±500A), the maximum field in steady state mode is up to ±0.434T. Using the pulsed battery charged at 1050V, a peak field amplitude up to 3T could be obtained in the background field of 10T.

Due to the symmetric location of the pulsed field windings with respect to the SULTAN coils, the voltage induced by the pulsed field on the DC coils is cancelled in the voltage bridge of the quench detector. Only for fast pulses of amplitude higher than 3T, the residual unbalance of the quench detector triggers a fast discharge.

For AC loss measurements, the coils are operated with a bipolar sinusoidal current. To reliably measure the steady state regime of the losses, the duration of the field sweep must be long enough to establish a constant temperature increase downstream of the pulsed field (10 to 20s, depending on the coolant speed and the accuracy of the temperature rise). On the other hand, the accumulation of the heat dissipated in the copper windings limits the duration of the current sweep. The maximum duration is assessed through the temperature rise at the winding sensors, TI 491X and TI 492X. A conservative threshold of 60K at TI 491X and TI 492X is currently retained in the temperature control system as an upper limit for coil operation. The lower threshold temperature to enable a new pulse is 6K. The coil temperature, and hence the sweep duration, depends on the operating current, the background magnetic field (magnetoresistance) and the ability of the cooling circuit to remove heat from the coils during the sweep. The test reported in Fig. 3.5.2 shows the case of a sinusoidal sweep (ΔB=±0.15T, i.e. I=±177A, duration of 60s) at a background field of 10T. The peak temperature at the winding is 33K and the re-cool time below 6K is of the order of 4 minutes.

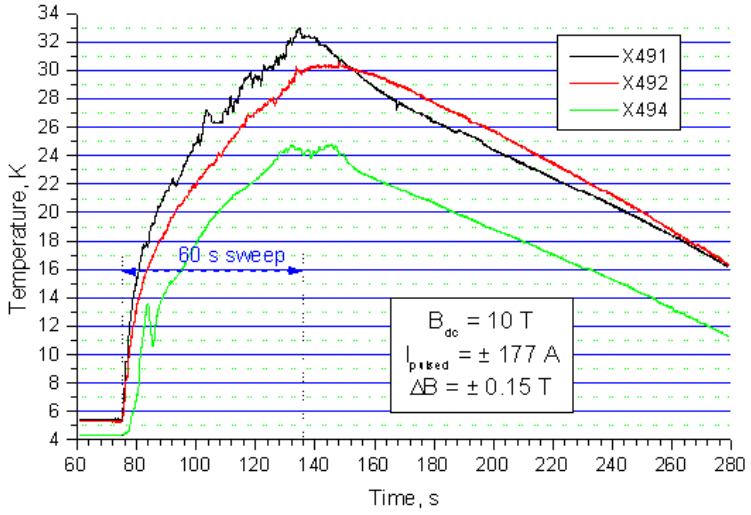

Fig. 3.5.2 *Self-heating of the saddle coils for quasi steady state operation (60s). The black and red traces are the sensors attached to the winding. The green trace is the outlet coolant temperature*

3.5.3 Standard Protocol for Conductor Tests

In the effort to standardise the test procedure for the ITER full size conductor samples, a test protocol has been drafted and submitted to the community of potential users. A minimum set of sensors has been defined and their characteristics and location on the sample are specified. A standard test program is also specified for both conductors and joints, with the aim to provide a full qualification and, whenever required, the crucial performance for acceptance:

- DC test, $I_c(T)$ from 4.5K up, at least 5 points, two field levels, ramp rate 75A/s, 4g/s
- DC test, $T_{cs}(I)$ at three current levels, two field levels, ≈4g/s
- DC test, I_c@5K, ramp rate 200A/s with and without 5 minutes hold at 75% of I_c
- AC loss. Loss curve ±0.3T at 2T background field, virgin state, 0 current
- AC loss. Loss curve ±0.3T at 2T background field, after high field dc test, 0 current

- AC loss. Loss curve ±0.3T at 10T (5T for NbTi) background field, 0 and 40kA current
- Stability. Limiting current @5K, at least five points with decreasing I_{op}/I_c,3 and 6g/s
- Stability vs. ΔT, at I_{op}=40 and 60kA, 4g/s, at least five points with increasing ΔT

4 International and national collaborations

4.1 Exploitation of the JET facilities

Collaboration with the JET-EFDA Task Force M (MHD)
CRPP collaboration to Task Force MHD for JET-EFDA experiments has been focussed on leading experiments in Spring 2001 and finalising analyses of experimental data and of simulations during the rest of the year. An important part of the work has also been related to coordinating the important contributions of TF M members to the EPS conference in Madeira.

The experiments coordinated by CRPP were mainly on sawteeth control and the effect of NBI fast particles, and on measuring the marginal beta limit of neoclassical tearing modes (NTMs). In the first set of experiments the direct relation between fast particles generated by NBI heating and the sawtooth period has been clearly demonstrated. The effect of shape on sawtooth period has also been tested and a weak effect has been found. This weak effect is actually in agreement with TCV results as these discharges had to be performed at low current due to the high triangularity. The experiments on NTMs have shown that the marginal beta limit of these modes is very low, at the level of the L-H transition. This means that JET H-modes with q_{95}~3.4 are metastable to NTMs. This actually explains why very low beta onsets have been measured with NTMs triggered after long sawtooth periods, assuming that the latter trigger larger seed islands.

The effects of NBI on sawteeth have been successfully modelled by the same model used to simulate the effects of ECCD/ECH on sawtooth periods in TCV, with the inclusion of the stabilising fast particles contribution to the MHD potential energy. In this way quantitative comparison have been successful and the simulation have explained the sharp increase in sawtooth period during the NBI power ramp as due to the transition to another trigger condition. This is important as these trigger conditions are predicted to be the relevant ones in ITER-like plasmas.

The effects of stabilisation and destabilisation of sawteeth on NTM onset have been further analysed, as well as the comparison of the low marginal beta limit with theoretical predictions. This latter confirm the different terms included in simulating the time evolution of the saturated island width. In addition the effects of density peaking and of long sawtooth periods induced in EDA experiments on NTM onsets have been analysed in more details in collaboration with Task Force S1

Collaboration with the JET-EFDA Task Force E (Exhaust)
In common with CRPP activities in 2000, CRPP participation at JET within the Exhaust Task Force (TFE) during 2001 was performed within the framework of the two separate programmes described below.

Pure Helium plasmas
From 8 – 28 March 2001, an extensive campaign of pure helium discharges with He neutral beam injection was executed on JET. This was the first such occasion on which such a lengthy series of experiments in He had been performed on a tokamak

the size of JET and was driven in part by the requirement to investigate,on a reactor relevant machine, the potential of He discharges for the low activation phase of ITER. With regard to TFE experiments during this campaign, CRPP assumed the lead roll in coordinating the campaign, including the construction of an extensive website at JET detailing the experiments. Following the campaign, this coordinating roll has continued, including the organisation of two Helium plasma workshops at JET held in March and November 2001.

A total of 13 JET sessions were allocated to TFE experiments in He, with the result being over 100 useful discharges covering a wide range of scrape-off layer and divertor experiments for which discharges were selected so as to match as closely as possible previous, well characterised D-plasmas. The possibility, at JET, for conversion of the neutral beams to He, allowed this comparison to be made in both L and ELMing H-modes. For I_p and B_T in the range 1-2.5MA and 1-2.4T respectively and P_{NBI} up to 12 MW, He concentrations near 90% were routinely achieved, with the global particle balance being dominated not by the wall, as in D, but by the plasma particle content. Although analysis is still underway at the time of writing, results point to the important conclusion that the main chamber is the dominant source of C production in both He and D, with chemical sputtering being strongly suppressed in the divertor as expected during He plasmas. With regard to the physics of divertor detachment in Helium, CRPP has assumed the lead role in B2.5-Eirene modelling of this process and has produced the first ever simulations of a JET diverted helium plasma. Figure 4.1.1, shows one example of the very reasonable agreement which is permitting the code to be used as an important tool in helping to understand the very great differences between the detachment phenomena observed when exchanging He for D and also in computing reliable photon efficiencies for the correction of spectroscopic measurements of plasma line radiation.

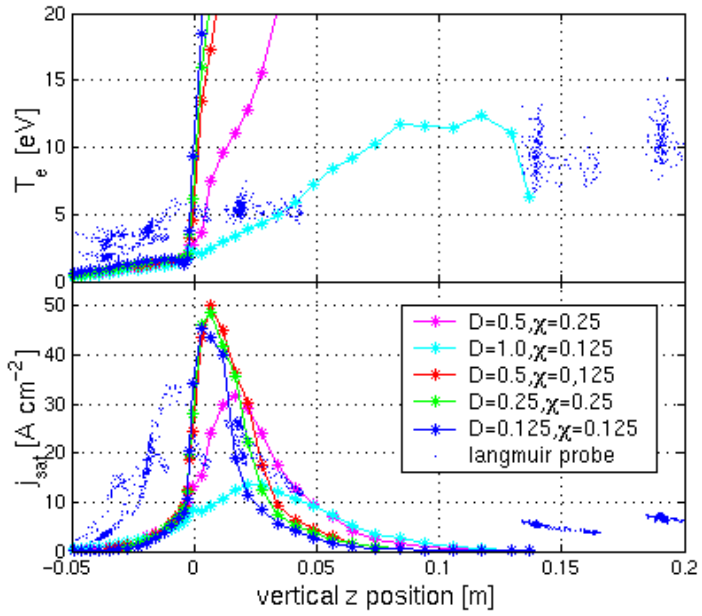

Fig. 4.1.1 *Illustrating the first B2-Eirene simulation results of divertor target T_e and n_e during a high density pure helium discharge in JET. For the correct choice of upstream density and transport coefficients, very good agreement with target parameters is obtained.*

Retarding Field Analyser enhancement project
Following a series of important hardware modifications in 2000 to the existing probe head under the recommendation and supervision of CRPP, the JET Retarding Field Analyser (RFA) probe was operated with great success during the C4 pure He campaign in March 2001. The probe was operated parasitically, primarily by reciprocation into low power and limited phases of a variety of discharges, but in all cases extremely satisfactory operation was obtained along with some of the best quality edge ion temperature data ever collected with this device on JET. Multiple reciprocations were possible without the overheating and outgassing effects that plagued the original JET design. These successful design modifications, along with further improvements resulting from operational experience during the C4 campaign, were incorporated into the components of a new probe head, manufactured at, or sub-contracted by CRPP during the summer of 2001 under the auspices of a JET Enhancement Project (Order: JW-OEH-SWIS-03). The full set of components was shipped to JET in mid-October 2001 for assembly followed by installation on the JET KY3-A reciprocating drive in November. Full commissioning in plasma is expected in early 2002 followed by dedicated physics experiments during sessions in campaigns C5 and C6. The photos in Fig. 4.1.2 illustrate the details of the RFA probe head internal components together with the robust graphite coated, boron nitride probe housing protecting the delicate electrodes from the high plasma power fluxes.

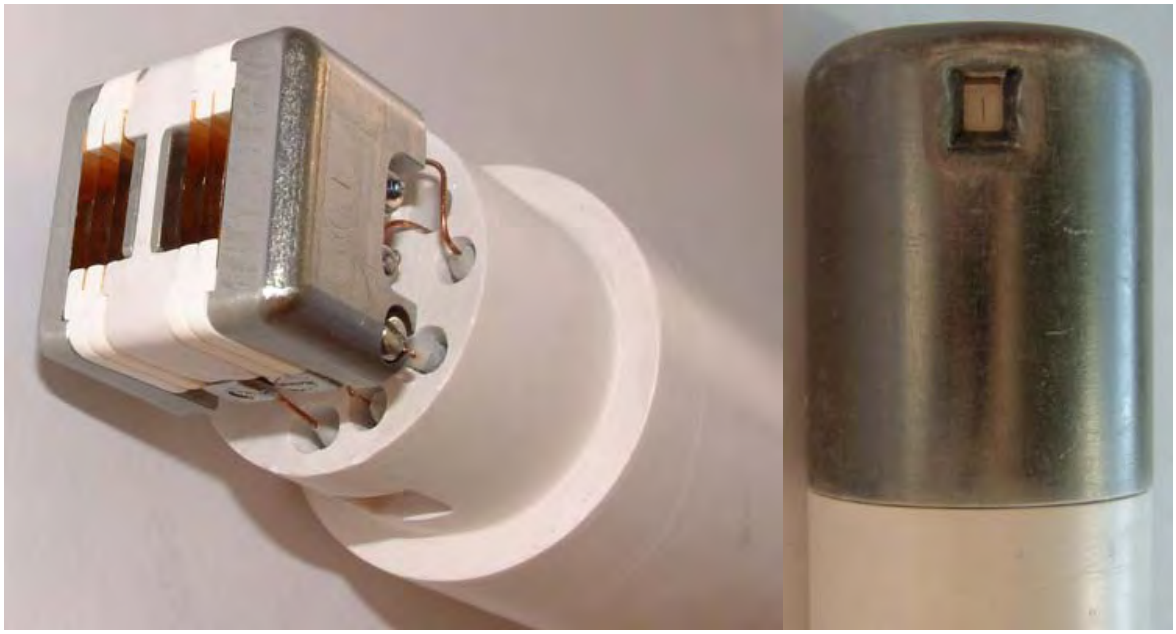

Fig. 4.1.2 *Showing the delicate internal RFA electrodes (left), including BeCu retarding grids, boron nitride ceramic spacers and thick TZM slit plates in which the tiny (30 μm wide, 4 mm long) laser cut entrance slit through which the ions enter the device can be seen. The RFA electrodes are protected during insertion into the plasma (on a fast reciprocating drive) by a graphite coated boron nitride housing (right).*

4.2 JET-EP project work

The general objective of the JET EP ECRH project is the design (and related test-activities) of an ECRH system equipped with 6 to 8 Gyrotrons (with depressed

collector and their matching optic unit, MOU), their superconducting magnet (SCM), transmission lines, diamond windows, launcher, power-supply, cooling and cryo systems, control system, auxiliaries.

The sub-system has to fulfil the following functions/specifications determined for the whole ECRH system and linked to the gyrotron emission capability: ability to control neo-classical tearing modes (NTM); Heating & Current Drive; Te/Ti control; wide range of operating toroidal magnetic fields (first harmonic at 3-4T, and 2nd harmonic at lower fields); technical compatibility with ITER-like 170GHz gyrotron(s); power modulation (up to 10KHz) and modulation depth (0.3-1MW). The tendering process for two gyrotrons was under way in 2001. The rest of procurement and installation remains to be decided.

The CRPP's main task is the design (and related test-activities) of the whole 113.3GHz gyrotrons system delivering 1MW-10s, 0.6MW-30s each, with a total power of 5 to 7MW delivered to the plasma and the design of the transmission line (63.5mm diameter corrugated waveguide) from the MOU to the launcher. The overall system composed by the gyrotrons with their magnets and the evacuated waveguide transmission line up to the JET torus is shown in Fig. 4.2.1.

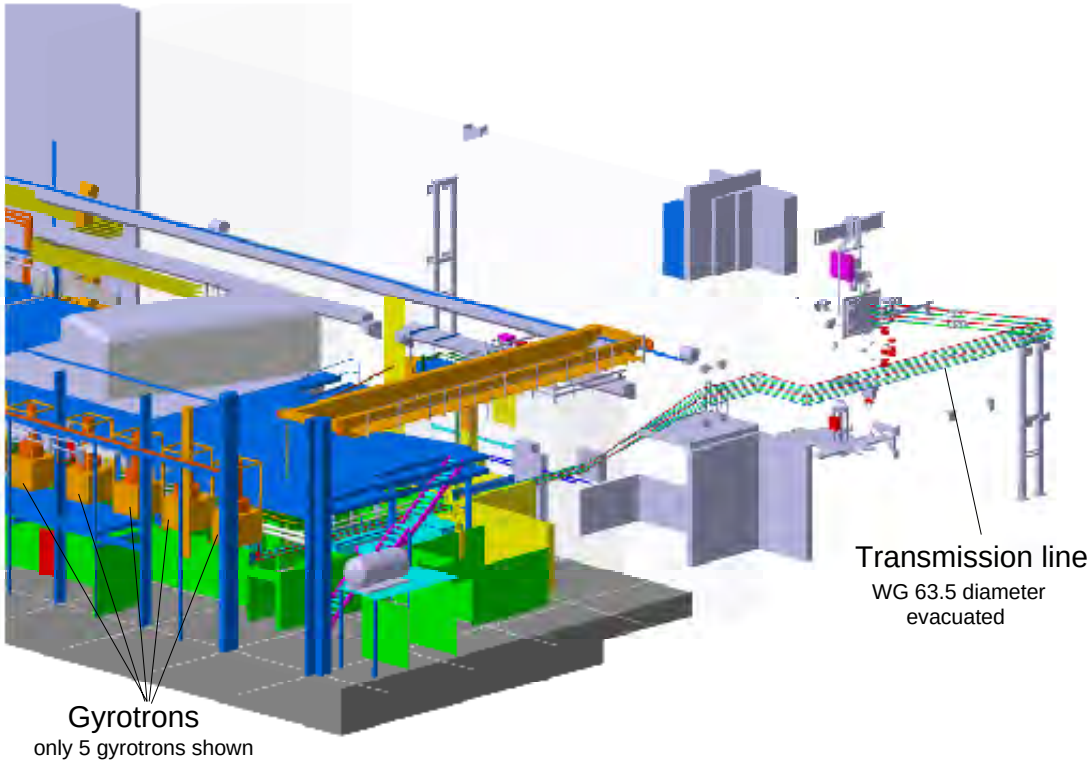

Fig. 4.2.1 *Layout sketch of the ECH transmission lines*

4.2.1 Work Performed:

The principle contribution from CRPP during 2001 for the JET-EP ECRH program concentrated on the following three categories

- Gyrotron specifications
- Pre-design of gyrotron platform in the J1D area
- Evacuated waveguide transmission line proposal

The activities for gyrotrons and magnets in 2000 and 2001 have resulted in a call for tender based on a detailed specification.

The main gyrotron parameters are listed in Table 4.2.1.

The general and specific requirements, commercial aspects, quality control, etc. were integrated in the call for tender. Analysis of the offer was performed in 2001.

The interfaces between the deliverables described in the gyrotron call for tender and the entire JET-EP/ECRH system have been identified. A significant effort has been devoted in collaboration with the ECRH team to the system integration of the entire JET-EP/ECRH system which clarifies the boundaries of responsibilities between the Associations and the UKAEA Operator.

Parameter	**Value**
Frequency	113.3 ±0.5 [GHz]
Power measured in calorimetric load	1.0 [MW]
RF pulse length	10 [s]
Reduced power operation: Power/pulse length	0.7MW/20s 0.6MW/30s
Output mode at window	TEM_{00} (Gaussian)
Mode purity at window	97%±1%
Window	Diamond
Efficiency with depressed collector	≥ 45 %
Gun type	Diode
Modulation capabilities Frequency Modulation depth	 10Hz to 10kHz (triangular) 1MW to 0.3MW

Table 4.2.1 *Gyrotron parameters*

CRPP provided a preliminary design of the platform in the J1D area where the gyrotrons will be located. The design specified the location of the control cabinets, water cooling lines, cryogenic lines, high voltage zones, etc. related to the gyrotron platform.

In 2001 the design activities have resulted into two alternative, comparable transmission lines. One transmission line consists of a wave-guide, WG 87, in the J1D hall and a Quasi Optical transmission line in the J1T hall. The other, proposed by CRPP, is made of evacuated wave-guides, WG 45 or 63.5, all along from the gyrotron to the tokamak. A choice for the evacuated wave-guide transmission line (WG63.5) has been made in November. The study concentrated on the 45mm diameter wave-guide, but also did preliminary investigation of a 63.5 diameter evacuated wave-guide. A final choice was made for the 63.5 diameter evacuated wave-guide, the main motivation of this choice was the possibility of reusing the WG63.5 wave-guide on ITER, therefore allowing a reduction in the hardware investment cost of the ITER-ECRH system.

Within the JET-EP/ECRH project, the responsibility on the transmission line was transferred to CRPP near the end of 2001 and preliminary design work and interface has started towards the end of 2001.

4.3 *Heating and current drive for sawtooth control in JET*

In order to avoid seeding NTMs with large sawteeth, methods capable of reducing sawtooth amplitude are developed. We have determined the JET ECRH system power and launcher angles requirements for sawtooth control.

Sawtooth stability is highly sensitive to the localisation of the EC power deposition in the q=1 surface region. In TCV, a deposition close to q~1 destabilises sawteeth (short periods) and a deposition slightly further out (+Δq~0.05) stabilises sawteeth. It was shown that the (de)stabilisation depends on the local current and not on the total I_{CD}. In JET, ICCD localised deposition has recently been used successfully to produce large sawteeth to seed NTMs in a regime where the present available additional heating power in JET is generally considered insufficient to generate NTMs. The effect of EC deposition on sawtooth stability has been modelled in time dependent transport simulations of TCV discharges. The effect of NBI fast particles on sawtooth stability has also been modelled in time dependent transport simulations of JET pulses using the same sawtooth model.

Ray-tracing calculations have been undertaken for TCV experimental cases and for the JET ECRH launcher geometry and JET equilibria using TORAY, see Fig. 4.3.1(a). TCV results show that the maximum driven current density is reached at a relatively small toroidal injection angle, Fig. 4.3.1(b), leading to a requirement in injection angles that is reduced from the case of maximising the total driven current.

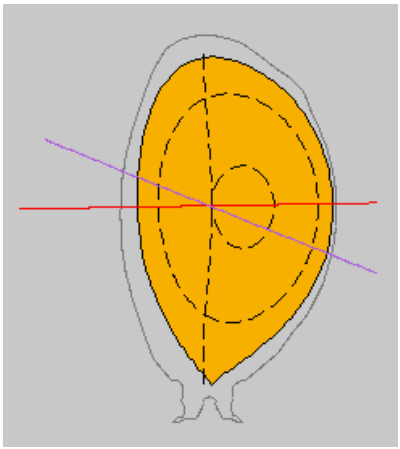

a)

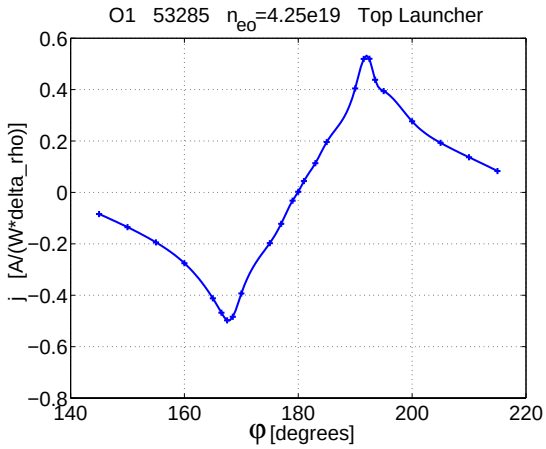

b)

Fig. 4.3.1 *a) Fundamental O1 ECCD launch on the high field side q=1 region for the (de)stabilisation of sawteeth, from the top or bottom launcher of the 4 mirror array (8 beams).*
b) The driven current density, the quantity relevant for sawtooth (de)stabilisation, reaches a maximum at a small toroidal angle of less than 10° off normal, a condition easy to fulfil with the planned launchers.

First harmonic ordinary-mode schemes at full field and second-harmonic schemes at reduced field have been calculated for different densities and temperatures. In

the case of second harmonic, high field side – the usual scheme at first harmonic – and low field side q=1 deposition are assessed. The current drive reduction due to third harmonic absorption is addressed in the 2nd harmonic HFS case. Among all these cases, the largest toroidal angles (φ_{max}~12-16°) are required in the full field scheme, essentially due to the higher electron temperatures. This range of angles is easily covered by the present JET launcher design. Typical total driven currents of I_{CD}=0.1-0.15MA can be obtained at φ_{max} for 5MW EC power, representing 2.5-5% of the plasma current, a value sufficient to obtain a significant sawtooth stabilisation/destabilisation effect on TCV.

4.4 ITER Tasks and Research & Development

4.4.1 Plasma Control Design Task FU05-CT2001-00018 EFDA/00-551

The effect of the feedback controller on superconducting tokamak AC losses are investigated. Superconducting coils in a Tokamak are subject to AC losses when the field transverse to the coil current varies. A simple model to evaluate the AC losses has been derived and benchmarked against a complete model used in the ITER design procedure. The influence of the feedback control strategy on the AC losses is examined using this model. An improved controller is proposed, based on this study.

4.4.2 H-Mode database

The International Confinement Database and Modelling Expert Group addressed the question of the scattering in the data used for the determination of the H-mode threshold power. The TCV data contained in the international database were analysed. The plasma shape, the sawteeth and the ion grad B drift were found to have some influence on the power at the LH transition, but the scattering remains important

4.4.3 ITER R&D: Benchmarking of the DINA code

A collaboration between Kurchatov and Triniti institutes has brought the DINA simulation code to TCV, for benchmarking the code before using it for TCV. During the past year, the work on simulating the Vertical Displacement Events in TCV, provoked by cutting the feedback loop which stabilises the vertical position, has been completed. The agreement between DINA and the experimental results was satisfactory and the non-linear evolution of the plasma position as the plasma current "fell" through spatially varying vertical field decay index proved that this non-linear effect was well modelled.

4.4.4 Conceptual design of the ITER ECRH upper launcher

The task is related to the conceptual design of the ITER ECRH upper launcher, which will be used to stabilized neo classical tearing modes (NTM). The European Party has decided to focus its effort on this launcher, the design of the equatorial one for heating and current drive being addressed by the Japanese Party. The work was aimed towards the assessment of the use of front steering mirrors, taking into

account engineering constraints such as the size of the shielding structure, the cooling of the whole system. The study will be completed in 2002.

4.4.5 Superconductivity

Most of the activities in the SULTAN test facility are carried out under EFDA contract in fulfilment of ITER Task Agreement between the ITER Joint Central Team (which became the International Team (IT) during the Coordinated Technical Activities phase) and the European Participating Team. A specific ITER Task covers the "Test of Full Size Conductor and Joint Samples" provided by European and non-European partners. Another Task is about the "Development and Test of High Temperature Current Leads", carried out in collaboration with FZK. Many items of the CRPP Conductor Optimisation program are specified as ITER task (stability for segregated copper, ac loss with different strand coating, cyclic loading for full size and subsize conductors).

Another Task, about "Development and Test of a Low Cost NbTi Joint" is ready to start as soon as the required conductor sections are supplied by the Russian Home Team.

4.5 Collaborations with other EURATOM Associations

P. Amorim, *Dept di Física i Centro de Física Atómica da Faculdade de Ciências da Universidade de Lisboa, Portugal*, **T.I. Madeira**, *Centro de Fusão Nuclear, IST, Lisboa, Portugal*, "X-ray spectroscopic diagnostics on TCV"

ASDEX Team, *IPP Garching*, Germany, "Analyses of modulated ECH studies on the tokamak ASDEX Upgrade"

J. Bakos, *KFKI, Budapest*, *Hungary,* "Impurity transport using Laser ablation on TCV"

T. Hender, D.C. Robinson, T.N. Todd, *UKAEA Fusion*, *UK,* "ST/Sphellamak Hybrid configuration"

A. Jaun, *KTH, Sweden,* "TAE study"

MAST Team, *UKAEA Fusion, UK*, "Neoclassical Tearing Modes"

MAST Team, *UKAEA Fusion, UK*, "Comparing tight aspect ratio and conventional tokamak equilibrium and control"

E. Minardi, *Assoc. Euratom CNR, Milano, Italy*, "Comparison of predictions of stationary magnetic entropy based theory with TCV data"

J. Nuehrenberg, *MPIPP Teilinstitut Greifswald, Germany*, **V.D. Shafranov**, *Kurchatov Institute, Moscow, Russia* **S. Medvedev**, *Keldysh Insitute of Applied Mathematics, Moscow, Russia* **V. Nemov**, *Kharkov Institute of Physics and and Technology, Ukraine,* "Novel Approaches to Improve Confinement in 3D Systems"

Y. Peysson, L. Delpech, *DRFC, Association EURATOM-CEA, France*, "Temporary installation of an imaging hard-X-ray camera"

V. Piffl, *IPP Prague, Czech Republic*, "Collaboration on ultrasoft X-ray spectroscopy"

B.N. Singh, *Riso National Laboratory, Denmark,* "He effects in Fusion Materials and modelling"

W. Treutterer, *IPP-Garching, Germany*, "Modelling the plasma response of ASDEX-UG"

J. Vomvoridis, J. Pagonakis *National Technical University of Athens, Greece*, "Physics of electron beam physics used in gyrotron"

4.6 Other International Collaborations

T. Diaz de la Rubia, B. Wirth, M.J. Caturla, *Lawrence Livermore National Laboratory, USA*, "Multiscale computer simulations"

R.W. Harvey, *CompX, San Diego, USA*, "The effect of radial diffusion of fast electrons on the electron cyclotron current drive efficiency"

K. Yamazaki, K.Y. Watanabe, Y. Narushima, S. Okamura, C. Suzuki, *National Institute for Fusion Science, Toki-shi, Japan,* "MHD Stability in Heliotron and Quasiaxisymmetric Systems"

J. Egedal, J. Nazemi, J. Dorris, M. Porkolab, *MIT-PSFC, USA*, Collaboration on Collisionless Magnetic Reconnection. The experimental group based on the Versatile Toroidal Facility (VTF) was developed by A. Fasoli at MIT to investigate the physics of magnetic reconnection. Such experiment is still active and continues to provide results revealing aspects of the plasma dynamics during forced reconnection in a collisionless plasma regime, of interest for tokamak plasmas as well as for space plasmas.

V.E. Lukash, *RRC Kurchatov, Institute of Nuclear Fusion, Moscow, Russia and* **R.R. Khayrutdinov**, *TRINITI, Troitsk, Russia*, "Simulation of TCV plasma control experiments using the non-linear DINA code"

S. Medvedev, A. Martynov, Y. Poshekhonov, *Keldysh Institute, Moscow, Russia,* **M. Isaev, A. Subbotin, M. Mikhailov, V. Shafranov** *Kurchatov Institute, Moscow, Russia*, "Equilibrium and Stability of 2D and 3D Plasma Configurations"

A. Melnikov, *Kurchatov Institute, Moscow, Russia*, "Heavy Ion Beam probe diagnostic system on the T-10 tokamak"

D. Monticello, G.Y. Fu, M. Redi, G. Rewoldt, A. Reiman, L.P. Ku, M. Zarnstorff, *PPPL, USA*, "Design of the NCSX quasi-axisymmetric stellarator"

R. Odette, G. Lucas, *University of California, Santa Barbara, USA,* "Small specimen technology and fracture mechanics"

K.A. Razumova, V. Andreev, A. Sushkov, *Russian Research Centre Kurchatov, Moscow, Russia,* "Simulation of ECRH and ECCD in TCV plasmas", "Heat deposition location in ECH by EC shut-off method"

J.Snipes, D.Schmittiel, R.Parker, *MIT-PSFC, USA*, "Collaboration on MHD spectroscopy on C-Mod"

A. Sushkov, *Russian Research Centre Kurchatov, Moscow, Russia,* "Implementation of a multiwire proportional X-ray detector for high sensitivity, high speed, high time resolution in TCV"

K. Yamazaki, K.Y. Watanabe, Y. Narushima, H. Yamada, S. Okamura, *NIFS, Japan*, "LHD and CHS-qa MHD stability analysis"

R. Yoshino, Y. Nakamura, *Naka Fusion Research Establishment, JAERI, Japan*, **D.J.N. Limebeer, J.P. Wainwright, A. Sharma**, *Imperial College of Science Technology and Medicine, U. London, UK*, "Development of a plasma response model for JT-60U"

4.7 Collaborations within Switzerland

A. Mangili (*CSCS*), **S. Haberhauer** (*NEC-ESS*), *Centro Svizzero di Calcolo Scientifico, Manno*, "Computation of Stellarator Coils, Equilibrium and Stability"

H. van Swygenhoven, *PSI***,** "The mechanical properties of nanocrystalline metals and computer damage simulations of pulsed irradiation conditions"

F. Groeschel, A. Almazouzi, *Group Hot Labo, PSI*, "Participation in the European INTERWELD program"

M. Semadeni, D. Spreng, *Centre for Energy policy and Economics CEPE, Swiss Federal Institutes of Technology*, "Fusion and the Public Opinion"

Other collaborations, in the field of plasma processing, are described in detail in Chapter 2.7

5 The Educational Role of the CRPP

The CRPP plays a role in the education of undergraduate and postgraduate students, particularly in the Faculté des Sciences de Base. Advanced education and training in fusion and plasma physics topics is carried out as part of the research activities of the Association. Section 5.1 presents the 7 courses given to physics undergraduates and to engineering undergraduates. In their fourth and final year, physics undergraduates spend time with a research group at the EPFL, typically one day per week for the whole year. During this period, they perform experimental or theoretical studies alongside research staff, discovering the differences between formal laboratory experiments and the "real" world of research. After their final examination at the end of the 4th year, physics students are required to complete a "diploma" work with a research group, typically lasting a full semester. This diploma work is written up and defended in front of external experts. The CRPP plays a role in all of these phases of an undergraduate's education, detailed in Sections 5.2 and 5.3.

As an academic institution, the CRPP supervises many Ph.D. theses, also in the frame of the Physics Department of the EPFL. 5 PhDs were awarded in 2001. At the end of 2001 we had 28 Ph.D. students supervised by members of the CRPP, mostly in Lausanne but also 3 in Villigen. Their work is summarised in Section 5.4.

5.1 Undergraduate courses

K. Appert, *Chargé de cours, and* **A. Fasoli,** *Assistant Professor – "Plasma physics II"*
Option course presented to 4th year Physics students, introducing the theory of hot plasmas via the foundations of kinetic and magnetohydrodynamic theory and using them to describe simple collective phenomena. Coulomb collisions and elementary transport theory are also treated. The students also learn to use various theoretical techniques like perturbation theory, complex analysis, integral transforms and solution to differential equations.

N. Baluc, *Chargée de cours – "Material Physics"*
Basic course on material physics, presented as an option to 4th year Physics students. The course covers the theory of diffusion, dislocation and plasticity as well as the characterisation of materials. Experimental techniques used in materials studies, as well as analysis methods are presented for super-alloys, quasi-crystals, ceramics, composites and polymers.

J.B. Lister, *Chargé de cours – "Plasma Physics III"*
An introduction to controlled fusion, presented as a one semester option to 4th year Physics students. The course covers the basics of controlled fusion energy research. Inertial confinement is summarily treated and the course concentrates on magnetic confinement from the earliest linear experiments through to tokamaks and stellarators, leading to the open questions related to future large scale fusion experiments.

M.Q. Tran, *Professor – "General Physisc I"*
Winter semester 2001-2002 (2 hours of lecture and 2 hours of exercises) for the "Communications Systems" section. The course covers kinematics and basic Newtonian mechanics of material points.

M.Q. Tran, *Professor – "Plasma Physics I"*
An introduction to basic plasma physics, presented as a one semester optional course to 3rd year Physics students. The course treats the fundamental physics of magnetised and non-magnetised plasmas.

L. Villard, *Maître d'Enseignement et Recherche (MER) – "General Physics I-II"*
An elementary introduction course in physics for engineering students at the EPFL, covering mechanics, special relativity and thermodynamics.

5.2 Undergraduate work performed at the CRPP

EPFL Students

Chong DING, *"Plasma diagnostic of a capacitively coupled RF plasma"*. The aim of this work was to get used to the most popular plasma diagnostic. The diagnostic methods have been adapted to investigate plasma surface modifications as used industry. The applied methods are Langmuir probe, mass spectrometry and ion beam probe. First correlation between plasma parameters and surface modifications such as surface energy have been established.

Nicolas FREMAUX, *"CCD Multi-Camera imaging of the TCV Divertor"*. Previous observations of impurity and bulk visible line radiation emission from the TCV divertor with analogue CCD cameras is being extended by the installation of 4 Digital CCD cameras. In this system the plasma is viewed by a single lens system focussed onto a coherent fibre-optic bundle and the image is beam-split through interference filters onto separate CCD detectors. In this TP, the complete image system from viewing telescope, fibre-optic bundle through the beam-splitting optics and filter to the detector were modelled and the lens arrangement was optimised. The student then used a test Digital CCD camera to compare with the model calculations and then optimise a complete optical arrangement for the 4 camera system. This system is now under construction for installation on the TCV Tokamak in Q3 of 2002.

Steve GIRARDIN, *"Linked mirror stellarator with circular coils"*. A magnetic field line tracing study was undertaken to examine the magnetic field properties of a 4-period linked mirror system. The configuration can be viewed as a toroidal structure that has been cut and separated into quadrants to produce quarter tori that are joined by straight sections. The toroidal coils are inclined with respect to the vertical and the resulting vertical field is compensated with currents in a set of poloidal coils. This arrangement is shown to yield configurations with closed vacuum magnetic surfaces. The enclosed volume, the rotational transform and the magnetic well were calculated as a function of the straight section lentgh and as a function of the current ratio of the middle coil at each corner to the adjacent coils.

Joël GROGNUZ, *"Electron Bernstein Waves emission in TCV"*. Electron Bernstein waves open the possibility of heating the plasma at densities above the usual cut-off density for Electron Cyclotron Waves. Before starting heating experiments using the coupling to these waves, emission measurements from the plasma edge help to determine the range of useful angles. Preliminary measurements using an ECH launcher in the reception mode started with a spectrum analyser in high-density discharges. These measurements indicate the need to use a radiometer for its

higher sensitivity. An analytical model to calculate the expected angle range for different density gradients has been implemented, which will allow a better planning of future experiments. The design of a microwave switch to change between reception and heating mode is planned.

Fabrice MERENDA, *"Base de donées des décharges standard au TCV"*. The aim of this exercise was to extend the analysis, begun in 1996 (R.A. Pitts et al., J. Nucl. Mater. 241-243 (1997) 867), of wall recycling and its effect on plasma performance in the TCV tokamak. Since this earlier work, no further attempt to categorise the long term changes in recycling had been performed, despite the rather large modifications to the first wall graphite armour made in 1998. Using the new database building and plotting routines (MDB and DBPLOT) now available at TCV, a new recycling database has been constituted during the TP comprising all TCV standard discharges from shot #10000, the last pulse in the previous database. Analysis of the new database, also performed within the context of this TP, has revealed, amongst other interesting results, a remarkable effect of the new graphite protection (extending the previous ~60% first wall coverage to 90%) in improving the pumping capacity of the vacuum vessel walls and leading to better and more reliable density control of TCV plasmas. This is particularly important in view of the now routine injection of high power electron cyclotron heating power into TCV plasmas. The database also indicates (although the reasons are still unknown), a gradual decrease of the net plasma purity over an operational period of several years.

Francesca PALAZZI, *"Hot plasma effects on ray-tracing for 2nd harmonic X-mode heating in TCV Tokamak"*. The ray-tracing/absorption code TORAY which is used for calculating the RF deposition profile with the ECH system installed on TCV does not take into account hot plasma effects in the ray-tracing part of the code. With a low-field side injection of the electron cyclotron waves, the hot-plasma effect on the refraction near the resonance layer (anomalous dispersion) can be such that the rf wave is refracted out of the plasma and is therefore not absorbed. In a simplified slab model (1D), the importance of these effects for relevant TCV parameters are studied.

Philippe PITTET, *"Electron Density Measurements using the Microwave Cavity Technique Applied to Large Area PECVD Industrial Reactors"*. The free electron number density is a fundamental parameter for defining plasmas conditions. A straightforward technique is to measure the shift in resonance frequency Δf of a microwave cavity in presence of the plasma with respect to its value in vacuum. Large area PECVD reactors are flat rectangular boxes which are strongly overmoded cuboid cavities presenting a complicated frequency spectrum of many superposed resonant modes. By selectively exciting only one mode across the RF electrode gap, the frequency product $f.\Delta f$ of all cavity modes is identical because the plasma is designed to be uniform over the planes parallel to the electrode surface. The main goal of this study was to design and test the antennas to send the microwave signal (2 – 5 GHz) and to measure the cavity response with and without a plasma.

Christian SCHLATTER, *"Modification of the TCV rapid tomography algorithm to the bolometry diagnostics and its application on TCV bolometry data"*. Plasma diagnostics on TCV includes two systems designed for tomographic analyses: soft X-ray (200 AXUV elements) and bolometry (64 golden foil elements). In early 2001 a rapid algorithm for soft X-ray tomographic reconstruction based on time averaged smoothing was successfully introduced. Important modifications of the algorithm were needed in order to adapt it to bolometric measurements. Within the scope of this TPIV, the modified code called FABCAT was edited, thoroughly tested and run

on real data. It allows post-shot tomographic inversion of bolometric data, straightforward computation of plasma radiated power as well as storage of all results into the MDS database. Detailed code manual with illustrative example of shot #21515 reconstruction were published in CRPP internal report INT 205/02 "Fast-Algorithm Bolometric Computer Aided Tomography (FABCAT)".

Daniel TAMBURRINO, "*Experimental study of a RF inductive plasma discharge by electrical characterisation and optical emission spectroscopy*". RF inductive plasma discharges can be used to produce thin-film depositions on powders by Chemical Vapour Deposition (CVD). The aim was to understand the basics of an RF inductive plasma discharge and notions like skin-depth, impedance and matching. Experimentally, one goal was to optimise the matching of the RF discharge, i.e. maximise the power delivered to the plasma at 13.6 MHz. Measurement of the circuit electrical characteristics is not straightforward because of the influence of the measurement devices themselves. Different ways to measure the voltage, current and phase allowed to study the impendence of the measurement devices and therefore to understand their influence in the circuit. A study of the electrical characteristic of the RF discharge, such as current, voltage and phase was performed as function of the delivered power, pressures and for different gas mixtures (argon and air). At the same time, optical emission spectroscopy was also performed to compare line intensity of the different species present in the plasma.

Themistoklis VASCO BOUTOS, *"Soft X-ray measurements with a multiwire proportional counter (MPX)"*, With its 64 channels, the MPX diagnostics provides the best spatial resolution in the soft X-ray range in TCV and allows unprecedented MHD activity measurements, at a sampling rate of 200kHz. Measurements with an important additional Aluminium absorber thickness yielded promising signals for the detection of the emission from suprathermal electrons. Investigations with different gases in the wire cell allowed us to increase the signal in different operational regimes, depending on whether the measurements were aimed at maximising the sensitivity to thermal or suprathermal emission.

Pierre WEBER, *"Le photomultiplicateur pour la mesure de la charge effective d'un plasma".* A diagnostic measuring the effective ion charge (Zeff) profile from Bremsstrahlung radiation in the visible region in the TCV plasma is proposed. The system uses vertical multi-chord observation combined with photomultipliers and interferential filters (with a passband around 534.0 nm) for light detection. The electronic system used to amplify and acquire the plasma signals was built at CRPP. The measurement is based on the dependence of Zeff on the intensity of the continuum radiation, electron density and temperature. This work describes the photomultiplier and its application for the Zeff measurement including an experimental evaluation of the gain and quantum efficiency.

Exchange students

Laurence CORNET from ESPEO – Université d'Orléans, France, *"Characterisation of a non-self sustained DC current arc".* The goal of this 2-month project was to characterise and better understand the role of a noble gas in a non-self sustained high DC current plasma source. To achieve this goal, electrical characteristics were obtained for He, Ne, Ar and Kr as a function of the experimental parameters of the arc discharge. Optical emission profiles were also performed. The electron density, measured in similar conditions for these noble gases, showed good agreement with the ionisation potential, i.e. a higher density for the heavier atoms with lower ionisation potential. At the same time, the power injected was also lower for the

heavier atoms, which make Kr and Ar good candidate working gases for sustaining the discharge. Comparison of the measurements by optical emission and electron density of the noble gas discharges showed similar profiles, unaffected by the presence of a magnetic field, suggesting a two-step excitation/ionisation process via metastable states. These results are important for discharges with hydrogen, nitrogen as process gases, since a high electron density is usually suitable for exciting and dissociating molecular gas. The control of the multi-step process should also lead to enhancement of other processes.

Sarah KEW, from Imperial College, UK, *"Electron cyclotron current drive"* An Erasmus student, Sarah compared the current drive efficiency in TCV using the ray-tracing code TORAY and the Fokker-Planck code CQL3D. These studies showed that the standard use of the TORAY code was inaccurate and led directly to a change in usage allowing a more accurate estimate of current drive efficiency and power deposition location. The study provides a basis for understanding important physical effects - such as incomplete absorption, strong refraction, Ohkawa currents and absorption in the trapped region of velocity space - which dominate under different aiming conditions. In particular, it was shown that there is only a moderate increase in current drive efficiency when increasing the toroidal launch angles beyond a certain, relatively small, minimum angle. Furthermore, for off-axis current drive, envisaged for stabilisation of NTM's or modification of the sawtooth period in ITER, there is a prefered launching location which minimises this minimum toroidal angle. This can have an impact on the ease of engineering ECH antennas.

Nicholas MACDONALD, from Imperial College, UK, *"Density limits in TCV"*. Another Erasmus exchange student, Nicholas was involved in density limit studies and built a database containing critical data from all TCV discharges with high density. He classified the discharges by plasma configuration and shape, in order to extract the relationship between the density limit and the plasma parameters. He also used this classification to study the influence of the plasma configuration and shape on the density limit. He participated in the first experiments dedicated to the determination of the density limit.

Alexandre ROCHAT spent only 3 weeks at the CRPP. He was involved in the characterisation of the operational domain of the LH transition. He extracted groups of data with similar plasma configuration from the LH transition database. Then, for each group, he used the 'Mobile Centre' algorithm, a statistical classification technique, to check whether this 'geometric' classification corresponds to the classification between far from/close to the LH transition. The result was quite positive.

5.3 EPFL Diplomas awarded in 2001

Gilles ARNOUX, *"Brehmstrahlung measurements of Z_{eff} on TCV"*. The CRPP has decided to implement a continuum radiation measurement system on TCV in the visible light spectral region. To improve the sensitivity, the optics must have the highest transmission with enough spectral rejection to isolate a spectral region where line radiation from the plasma impurities does not affect the measurement. Two systems were proposed and studied. One was composed of an interferometer filter and a photomultiplier and the other was composed of a transmission spectrometer with a large aperture and a CCD camera. The CCD-spectrometer system has a lower efficiency than the photomultiplier-filter, taking into account the low emissivity around 530nm wavelength of the plasma especially at the edge.

In the other hand, the CCD-spectrometer system has the advantage of better spectral resolution and it was shown that up to a central density of the plasma of $4x10^{19}m^{-3}$, the signal to noise ratio of the CCD camera is acceptable.

Yann CAMENEN, *"Current profile tailoring with far off-axis ECH power deposition in TCV elongation experiments"*. In TCV, the study of the energy confinement time for extreme plasma shapes and the approach to the Troyon beta-limit at intermediate values of the normalised current, $I_N=I_p/aB\sim2$ MA/mT, are the main motivations for the development of scenarios with high elongation and modest plasma currents, using Electron Cyclotron Heating (ECH). At very high elongation, low current operation in ohmically heated discharges is limited by vertical stability and current profile broadening is needed to extend the range of stable equilibria. Using far off-axis 2^{nd} harmonic, X-mode, ECH to broaden the current profile, highly elongated discharges ($\kappa\sim2.4$) with low current ($I_p\sim300$kA) and a high safety factor ($q_{edge}\sim12$) have been created and stabilised in TCV. A model enables us to distinguish between the effect of the current profile and that of the plasma shape on the value of the internal inductance. Knowing the plasma shape, the internal inductance then gives information about the current profile. The analysis of the discharges shows that the current profile broadening and consequently the plasma elongation depend strongly on the location of the ECH power deposition. The maximum effect is seen for $\rho_{dep}\sim0.7$ at the beginning of the ECH pulse. To keep the normalised deposition radius constant during an elongation process, the launchers are progressively moved outward. This leads to higher values of plasma elongation and at a slightly faster rate than with a fixed mirror scenario. The rate of increase of plasma elongation is still limited by current diffusion.

Antoine DESCOEUDRES, *"Time resolved mass spectrometry of powder modulated electronegative capacitively coupled RF discharges"*. Radio-frequency discharges in electronegative gases are widely used for the fabrication of microelectronic devices. In spite of their great industrial importance, these plasmas are less known than the electropositive ones because of their complexity and the difficulty to measure negative ions, which are electrically trapped by the sheath during the discharge. In this work, we studied the behaviour of negative ions in O_2, CF_4 and SF_6 power modulated plasmas with time resolved mass spectrometry, Langmuir probe, emission spectroscopy and electrical measurements. We observed lots of different negative ions in CF_4 and SF_6 that are mainly etching products of the silicium contamination in the reactor. These ions are measured only during the afterglow once the electrons have disappeared. The oxygen plasma, weakly electronegative, behaves differently: only a small flux of O^- is measured during the discharge. Our results are consistent with the attachment and detachment cross sections and show different behaviours for the negative ions. In O_2 they are lost during the afterglow by strong detachment and recombination. In CF_4 and SF_6 they are created in the plasma by high (resp. low) energy resonant attachment and lost during the afterglow by diffusion. We also observed an interesting 'attachment / ionisation instability' in O_2 and CF_4 plasmas under specific conditions of pressure and power. A theoretical criterion of instability based on attachment and ionisation cross sections was applied to demonstrate why the SF_6 discharge remains stable.

Beat SCHAERZ, *"AC-Loss Minimisation in the ITER Tokamak"*, Superconducting coils in a Tokamak are subject to AC losses when a field transverse to the coil current varies. During this diploma work a simple model to estimate the magnitude of these losses has been developed, taking into account the two most important loss sources, the hysteresis and coupling-current losses. Existing codes, using more complete descriptions of the machine and the superconductor physics have long calculation times and are therefore not suitable for frequent use, whereas the

simplified model completes within seconds, which allows us long series of tests to determine the influence of certain parameter on the AC losses. Due to the uncertainties in the calculation of AC losses, the precision of the simplified model is believed to be similar to the more complicated models. In a second part, the existing ITER control system was examined, in order to determine which of its parameters influence the AC losses and by what amount these can be reduced. An optimised control strategy has been proposed based on the work done.

5.4 Postgraduate studies

3rd cycle: "Physique des plasmas confinés magnétiquement"
Postgraduate course in the 3rd cycle *"Applied Superconductivity I"* R. Wesche and P. Bruzzone.
This 39-hour course started in the winter semester 2001/2002 and will be complemented in the summer semester of 2002 by *"Applied Superconductivity II"*. The two main subjects of the course are large low temperature superconductors for fusion magnets and the metallurgy of high temperature superconductors.
In the introductory part of the course, an overview on the different classes of superconducting materials is given, including the critical state model, Ginzburg-Landau and BCS theory. Because of their importance for superconductivity applications, the AC loss behaviour, the stability and the effects of mechanical loads on the current carrying capacity are examined in depth. Relationships between the microstructure and the transport critical current density are considered for low and high temperature superconductors. The consequences of the anisotropic physical properties of high temperature superconductors on magnet design are discussed. The reduction of the refrigeration operation and investment costs provided by the use of high temperature superconductors is estimated.
After the discussion of technological aspects (conductor and winding manufacture) an overview on magnet (fusion magnets, nuclear magnetic resonance, magnetic separation, accelerator magnets) and power applications (fault current limiter, transformer, power cables, superconducting magnetic energy storage, magnetic levitation) is given. In addition, design considerations for superconducting current leads and power cables including economic aspects are presented. The results of performance tests of superconducting power cables and current leads are discussed.

Doctorate degrees awarded during 2001

Clemente ANGIONI: *"Modelling of electron transport and of sawtooth activity in tokamaks"*, EPFL Thesis No. 2669(2001)
Within the vast framework of transport studies, three topics were tackled in this thesis. Firstly, we computed the neoclassical transport coefficients for general axisymmetric equilibria and arbitrary collisionality regimes. This work, involving both analytical developments and a numerical implementation in existing Fokker-Planck codes, finally allowed us to provide simple analytical formulae for all the transport coefficients, valid for arbitrary aspect ratio and collisionality in general realistic geometry. Secondly, we analysed the electron temperature behaviour and modelled the electron heat transport of plasma discharges in TCV. The main experimental features of the electron temperature profile in TCV are well reproduced by the semi-empirical Rebut-Lallia-Watkins local transport model. Characteristics of the model which lead to the compatibility with the experimental observations have been pointed out. The RLW model, included in the PRETOR transport code, has allowed transport simulations which were particularly useful in

the analysis and design of experiments leading to improved electron confinement regimes in TCV. Thirdly, we modelled and simulated the sawteeth in TCV discharges with different plasma heating conditions. A model for the sawtooth period has been extended and its predictions are consistent with the experimental observations in TCV discharges with ECH and in JET discharges with neutral beam injection (NBI). This work has therefore allowed the identification of the physical mechanisms cause ECH to affect the sawtooth period and demonstrated the role of beam ions in stabilising sawteeth, validating a stability threshold for the internal kink which was predicted to be the sawtooth crash trigger, relevant for ITER operation.

Olivier FISCHER: *"The behaviour of magnetic field lines and drifts in 3D configurations"*. EPFL Thesis No. 2380(2001)
To investigate the magnetic field line topology and the guiding centre particle drifts as well as neoclassical transport in 3D confinement devices, the MFLT3D and VENUS codes were developed. It was demonstrated that a transport barrier for magnetic field lines and circulating particles resulted from the activation of Dynamic Ergodic Divertor (DED) coils in simulations of the Textor tokamak with reversed shear in the region of minimum safety factor. Trapped particles are lost due to ripple effects and are unaffected by the DED coils. Saddle coil magnetic field perturbations were shown to control tearing modes in the JET tokamak. The nearly isodynamic structure in the plasma core of a Sphellamak reactor system yields a high level of alpha particle confinement and neoclassical transport properties similar to an equivalent 2D tokamak.

Ivo FURNO: *"Transient transport events in TCV"*, EPFL Thesis No. 2434(2001)
This work significantly advanced the understanding of transient heat and particle transport, essentially connected with the sawtooth cycle in Ohmic and ECH plasmas and using the TCV soft X-ray tomography system. The scientific achievements include:

1) an essential contribution on inversion radii, which allowed a scaling law for the sawtooth inversion radius in circular discharges to be extended to plasmas of arbitrary shape;
2) an understanding of the bewildering behaviour of sawteeth in the presence of localised ECH, using a fairly simple transport model accounting for the presence of a (1,1) island;
3) the observation and documentation of the phenomenon of 'density pumpout' from the plasma core in the presence of central ECH or ECCD. This phenomenon has been linked to the presence of an island in the plasma core and can lead to a local inversion of the density gradient;
4) a significant contribution to the development and the commissioning of two prototype fast bolometer cameras using AXUV diodes.

As a tribute to the exceptional quality of his work, the jury recommended him for a nomination for the 'prix de doctorats' of the EPFL.

David MAGNI: *"The chemistry in a hexamethyldisiloxane (HMDSO) plasma and consequences for the deposition of silicon oxide"*, EPFL Thesis No. 2461(2001)
The oxygen-diluted HMDSO plasmas as often used for the deposition of SiOx was studied by infrared absorption spectroscopy and mass spectrometry. It could be shown that the dominant species in gaseous phase come from the homogeneous reaction between oxygen and the radical CHx abundantly produced in the plasma. Two principal pathway were shown to occur. A first way leads to hydrocarbon formation such as methane and acetylene. A second way leads to the formation of molecules from the combustion of CHx, such as formaldehyde, formic acid, carbon monoxide, carbon dioxide and water. Moreover it was demonstrated that the CO2

results from a heterogeneous reaction between the carbon on the surface and the oxygen coming from the plasma.
Particle formation in oxygen-diluted HMDSO plasmas was studied by means of Mie scattering, infrared absorption spectroscopy as a function of radiofrequency power at high and low dilution. The composition of the particles produced was compared to thin films produced in the same conditions. It was shown that oxygen etches the carbon present in the particles and the carbon present in the film. Oxygen also propagates a polymerisation reaction leading to SiOSi structures which are found in the particles produced in oxygen-diluted HMSDO plasmas.

Holger REIMERDES: *"MHD stability limits in TCV plasmas"*, EPFL Thesis No. 2399(2001)
In the pursuit of the exploitation of nuclear fusion as a commercial energy source, one tries to maximise the pressure of magnetically confined tokamak plasmas. Magnetohydrodynamic (MHD) instabilities, however, can limit the pressure and degrade the confinement of these plasmas. In this work, the "Tokamak a Configuration Variable" (TCV), unique due to its capability to produce a variety of poloidal plasma shapes, and equipped with a flexible electron cyclotron wave heating and current drive system, has been used to study several instabilities which are relevant for the operation of a fusion reactor.
The flexibility of the TCV experiment was extensively used in an analysis of "sawteeth", which are central relaxation oscillations common to most tokamak scenarios. Systematic scans revealed a strong dependence of their behaviour on the plasma shape, which can be linked to the role of ideal or resistive MHD in triggering the relaxation. The relevance of ideal MHD was underlined in experiments at very high plasma elongation, which allowed to test and confirm a predicted deviation from the well-established linear Troyon-scaling of the global pressure limit with plasma current at these plasma shapes. New insight was gained into the dynamics of coherent magnetic oscillation, which precede edge-localised modes (ELMs). Unlike conventional MHD modes, these ELM precursor oscillations are observed to start at one toroidal location. This toroidal asymmetry coincides with a central mode, indicating a hitherto unobserved coupling between central modes and ELMs. This work provided the first clear observation of a transition of a current driven "conventional'' tearing mode to a pressure driven neoclassical tearing mode.
The results obtained reveal several previously unobserved features of commonly observed performance limiting instabilities. Since most of the new observations can be explained by theory, they confirm the predictive capabilities with respect to new experiments.
For the work contained in this thesis, Holger Reimerdes received the Swiss Physical Society Award, offered by the firm ABB, for research work of exceptional quality in any field of physics for the year 2001.

Ph.D. Theses underway at the end of 2001

Paolo ANGELINO: M. Angelino started his Ph.D. in November 2001.

Gilles ARNOUX: *"3rd harmonic electron cyclotron resonance heating in TCV tokamak plasmas"*
Third harmonic extraordinary mode heating in the TCV tokamak in top launch configuration results from a compromise between heating of high density plasmas and the optimisation of single pass absorption. The single pass absorption strongly depends on plasma refraction, hence on angle beam injection. The first results of X3 injection experiments confirm this dependence and agree with simulation by a

linear ray-tracing absorption code. To verify the predicted absorption in various launching configurations, a diamagnetic loop has been used to measure the absorbed power. During modulated ECH, the diamagnetic flux variation yields the absorbed power. A systematic comparison between the absorbed power measurement and the simulation was performed. Feedback control of the launcher will be developed to optimise the absorbed power in the plasma.

Juliette BALLUTAUD: *"Study of high deposition rate amorphous silicon in Plasma Enhanced Chemical Vapour Deposition (PECVD) reactor for silicon thin-film solar cells"*
During the last year, we have done a systematic study of the influence of process parameters (pressure, power, gas flows, RF frequency) on the deposition rate of aSi:H layer and on the layer qualities (layer density, defect absorption). This study was done in a standard inter-electrode gap reactor, 2.4cm. We obtained layers with a good deposition rate of 7Å.s^{-1} and higher. As in the small gap reactor (1.3cm gap), the layer density decreases when the deposition rate increases. Solar cells made with this porous aSi:H layer have very bad degradation. An explanation for this phenomenon is that at high deposition rate, radicals involved in the layer growth have less time to diffuse and react at the surface. It leads to a porous structure of the layer. But an increase of the temperature increases the surface diffusion and reaction rate of radicals. Previous experiments were performed at 200°C. We tested higher process temperatures up to 280°C. For the same process parameters, we measured no variation of the deposition rate (6Å.s^{-1}) but a great improvement of the layer density: from 85% of aSi:H at 200°C to 92% of aSi:H at 280°C (ellipsometric analysis). A future work is to analyse the hydrogen concentration of the layer as a function of the deposition rate and the process temperature.

Patrick BLANCHARD: *"Study of the suprathermal emission in TCV with electron cyclotron heating"*
A new Electron Cyclotron Emission (ECE) system that allow us to observe and analyse the EC emission of the plasma coming from the High Field Side (HFS) of the torus has been installed on TCV. When suprathermal electrons are created, we observe that the EC radiation from the HFS is composed of a thermal part and a suprathermal part, whose fractions depend of the corresponding optical thickness, temperatures and densities. Suprathermal electrons are produced in many experimental conditions, in particular with X2 ECCD and X3 ECH with X2 preheating. This work focuses on the understanding of this radiation from an experimental and a theoretical point of view. In Ohmic plasmas or in pure ECH plasmas, the EC emission comes from the thermal bulk and is proportional to the electron temperature. In X2 ECCD plasmas, the EC emission is no more proportional to the bulk temperature. There is a strong correlation between the EC emission and the geometry of X2 injection. Current work is aimed at modelling the radiation taking into account a velocity distribution function of the electrons either bi-Maxwellian or as a solution of the Fokker-Plank equation.

Paolo BOSSHARD: *"Charge exchange spectroscopy measurements of ion temperature and impurity ion density"*
During last year, the Diagnostic Neutral Beam Injector and the CXRS (Charge Exchange Recombination Spectroscopy) diagnostic of TCV have been upgraded to increase both the ratio between the active CX signal (due to the beam) and the background (line emissions produced by CX reactions between carbon impurities and thermal neutrals at the edge of the plasma), and the signal-to-noise ratio of the measured CX carbon emission. The current extracted from the DNBI source has been increased from 1.7 to 2.75A by changing the DNBI power supply, providing an increase of the active signal of ~50%. The modifications to the CXRS spectroscopic system have increased the signal level by an order of magnitude, resulting in signal-

to-noise improvement from 2 to 5. All these modifications allow ion temperature measurements to be performed with higher accuracy (less than 20% error) at line averaged plasma densities up to $8.10^{19}m^{-3}$. Ion temperature profile measurements have already been performed on a wide range of Ohmic and ECH plasmas, showing that the energy stored in the ions is not negligible (even in the case of TCV where ions are heated only through collision with the electrons) and can rise by up to 30% during ECH.

Alberto BOTTINO: *"Modelling of magnetically confined plasmas"*
The LORB5 global, linear Particle-In-Cell (PIC) code has been used for simulating experimental discharges using experimental profiles and reconstructed MHD equilibria. The main goal of this work was the study of the interplay between the sheared ExB flow, generated by a radial electric field, and the magnetic shear in stabilising drift-waves. The AUG tokamak provides a measure of the plasma toroidal rotation using Charge Exchange Recombination Spectroscopy and a collaboration with the AUG team (Dr. A.G. Peeters) has been established. We focused our analyses on the AUG pulse 13149, an L-Mode discharge in a reverse shear configuration and a relatively strong radial electric field, in which an Internal Transport Barrier (ITB) has been identified. A first set of simulations was performed without taking into account the poloidal rotation, in order to reconstruct the spectrum of electrostatic microinstabilities. The main instability appeared to be an ITG further destabilised by trapped electrons dynamics. When the radial electric field was included, we found that the ExB poloidal flow was sufficient to completely stabilise global modes even taking into account trapped electron dynamics.

Yann CAMENEN: *"Extension of the TCV operational range at high elongation using ECH"*
The study of the energy confinement time of extremely elongated plasmas and the approach to the Troyon β-limit at optimal values of the normalised current, $I_N=I_p/aB\sim2$ MA/mT, have motivated the development of TCV scenarios with high elongation and low current, using ECH. At very high elongation, low current operation in Ohmically heated discharges is limited by vertical stability, and a broad current profile is needed to extend the range of stable equilibria. Using far off-axis ECH in 2^{nd} harmonic X-mode (X2) to broaden the current profile, highly elongated discharges ($\kappa\sim2.4$) with low current ($I_p\sim300$kA) and a high safety factor ($q_{edge}\sim12$) have been created and stabilised in TCV during the last year. To achieve higher current and elongation, influence of the ECH deposition location has been studied. Experimental scans and the fixed boundary transport code PRETOR are in good qualitative agreement and show that a maximal broadening of the current profile - and so a maximal elongation - is obtained for a normalised deposition radius around 0.7.

Florian DALLA TORRE: *"Mechanical properties of nano-crystalline metals in relation to their microstructure"*
The microstructure of commercially available nano-crystalline electroplated Ni foils is studied by means of X-ray diffraction and transmission electron microscopy. It is shown that the microstructure is inhomogeneous and batch dependent. Tensile properties at strain rates between 10^{-5} and $10^{3}s^{-1}$ are performed and compared with results of coarse-grained Ni. Data on strength, strain rate sensitivity and work hardening are presented. At the highest strain rates, shear banding with local grain growth is observed in the nano-crystalline structure. It is also suggested that the differences found in nano-crystalline Ni for 3 and 20mm tensile specimens is a size effect related to the inhomogeneous microstructure.

Thierry DELACHAUX: *"Study of carbiding and nitriding plasmas in a high current arc reactor, with application to zirconium coating"*
The process of nitriding zirconia has been developed successfully in our research reactor during the past years. The treated surfaces have high wear resistance and an interesting yellow gold colour. This year we showed that the reactivity of the nitriding process is very sensitive to the zirconia preparation. Indeed, the plasma conditions lead to weak changes on the layer formation, whereas adequate pre-treatment of the samples allows to enhancing the nitrided layer thickness by a factor of 3. Experiments seem to indicate that this enhancement is due to modifications of the surface microstructures.
This year, an increase in scale to an industrial reactor was made. This transition highlighted problems of heat load due to the presence of a great number of samples to treat in a run. A simple simulation of the sink effect generated by a sample showed a perturbation of several centimetres on the reactive species in the plasma. A solution to the heat load was found by increasing these species as function of the load.

Christian DESCHENAUX: *"Dust growth mechanisms in reactive plasmas"*
Light polarisation measurements were conducted on small particles formed in RF capacitive plasmas containing methane as source gas. With light scattering experiments we demonstrated the non-sphericity of these particles. Particles collected and analysed on TEM grids confirmed the mainly heterogeneous origin of the particles, despite the fact that isolated spherical particles were detected among them. By contrast, abundant homogeneous spherical particles were observed in methane-argon discharges. Measurements were conducted in-situ on the spectrum of the light scattered by silicon particles illuminated by a monochromatic laser beam at 488nm. Luminescence was detected at 2.13eV, which could be explained by photoluminescence of porous silicon with typical crystalline nanostructures of 2-4nm. Measurements with another illumination wavelength at 632.8nm have to be done to confirm a possible Raman feature in the spectrum. Simultaneous infrared absorption spectroscopy showed an infrared absorption band at 2100cm^{-1}, which could be attributed to a crystalline phase, to large defects in the structure of the particles, or to a large surface/volume ratio for the vibration bands intensity.

Gloria FALCHETTO: *"Electromagnetic effects on microinstabilities in tokamak plasmas"*
The threshold for the destabilisation of an electromagnetic mode, the so-called Alfvénic Ion Temperature Gradient mode (AITG) or Kinetic Ballooning Mode (KBM), has been identified. Due to the global formulation, the radial structure of this mode has been observed for the first time. The stability of the AITG mode has been analysed as a function of plasma pressure and of the toroidal mode number. The inclusion of non-adiabatic trapped electrons has shown that they increase the growth rates of AITG modes. Comparisons with simulations from a local dispersion relation have only shown a qualitative agreement, largely overestimating the AITG mode growth rates and predicting an opposite effect for the coupling to trapped electrons. Finally, the effect of the Shafranov shift has been implemented in the model: owing to the large aspect ratio geometry considered, we could derive its expression analytically, by solving the Grad-Shafranov equation, and then deriving the modified gyrocentre trajectories. Results from simulations including the Shafranov shift have revealed an even stronger stabilisation of toroidal ITG modes than that due to the sole effect of the electromagnetic perturbation.

Jean-Yves FAVEZ: *"Application of modern control methods to a tokamak plasma"*
All present-day tokamaks routinely use PID controllers, designed on crude assumptions and tuned by experience. Thus, as a result, the control performance is

rather limited. Recently, considerable attention has focused on optimal controllers with enhanced robustness like LQG and H (infinity). Although these linear controllers have shown valid results, they usually fail to maintain control in the presence of large disturbances (ELMs). This weakness is due to the saturation of the actuators and can cause considerable damages to the plant. The future work aims at the investigation of non-linear methods, which could avoid this problem by maintaining the tokamak in a stable and safe operational domain even if large disturbances occur. A further goal in tokamak control research is to find a way to reduce the power consumption and the AC-losses while maintaining a fast response time. This work is targeted at the TCV, JET and ITER tokamaks. Work has so far concentrated on understanding the modelling of the tokamak and on studying the controllability regions of second order unstable SISO (single input, single output) systems with a saturated input. This project is carried out in collaboration with the Institut d'Automatique (IA) at the EPFL.

Sergi FERRANDO: *"Bootstrap current in 3D configurations".* A zero-dimensional analysis of the relevant TCV parameters is performed for both Ohmic and ECH scenarios. Assuming the MHD Troyon limit, other widely used approximations and limits such us the Rebut-Lallia-Watkins scaling law for the energy confinement time and the Greenwald density limit, and fixing the geometric relations of the device itself, there are only a few free parameters left. We aim to optimise these remaining parameters to have the beta as close as possible to the Troyon limit in the two scenarios. The bootstrap current has been calculated for different reactor-size stellarator configurations. A self-consistent method is used in the TERPSICHORE code. We consider plasmas in the low collisionality regime with electrons and ions having the same temperature, assumptions that are reasonable when considering reactor-like devices. Three different configurations have been studied with different expected values for the bootstrap current: a Quasi-Axisymmetric configuration, a reactor-size extrapolation of the WENDELSTEIN7-X experiment in Greifswald, and an extrapolation of the Helically-Symmetric Experiment (HSX) in Wisconsin. The effect of the bootstrap current on the iota profile and, hence, on the internal geometric properties of the configuration is observed, showing its importance in the stability and confinement.

Malko GINDRAT: *"Experimental study of the behaviour of a DC plasma spraying torch operated at low pressure"*
The Low Pressure Plasma Spraying (LPPS) processes, which use DC plasma jets expanding at low pressure, are widely used for the deposition of various kinds of layers. During the first year of the thesis the aim was to study the effect of the pressure on a DC plasma spraying torch operated at low pressure. A fast CCD camera was used to analyse the topology of the plasma jet under different plasma production conditions. Pressure measurements inside the nozzle were performed to support the observations made on the plasma jet. The imaging showed the existence of 3 types of flows: an over-expanded (or under-expanded) flow, where the pressure at the nozzle exit is lower (or higher) than the chamber pressure and a so-called "design pressure" flow where the pressure at the nozzle exit is equal to the chamber pressure. In this case the plasma jet becomes more uniform along its axis. eEnthalpy probe measurements were performed to determine temperature, velocity and mach number profiles of the plasma jet operated at pressures between 100 and 20 mbar for different currents and gas flows. At low pressure (<100 mbar) the jet becomes compressible and supersonic and is almost always composed of compression and expansion zones. Because of the presence of a shock in front of the enthalpy probe it is necessary to calculate the free-stream enthalpy of the plasma jet right before the shock-front to determine its velocity and temperature. The enthalpy measurements show that the jet properties are almost constant along

the axis. The core of the plasma jet seems to be isolated from the surrounding cold gas. Similar measurements were also performed on an installation of the industrial partner of the project (Sulzer Metco) under LPPS-Thin Film conditions to allow comparison with powder temperature and velocity measurements.

Jan HORACEK: *"Measurement of edge electron temperature and turbulence in the tokamak plasma boundary"*
The thesis will concentrate on electrostatic Langmuir probe (LP) measurements of edge electron temperature in TCV with the aim both of characterising turbulence in electron temperature (Te) and studying the general validity of LP Te measurements in the presence of strong turbulence and gradients in Te.
A collaboration has started with the University of Toronto, Canada and MIT, USA, dedicated to the numerical and analytic study of the effect of parallel field Te gradients in the tokamak edge on the overestimation of Te measured by LP. Parallel Te gradients cannot explain the experimental overestimation, at least in detachment.
Infra-red camera thermography of first wall surfaces is a useful tool for investigating the validity of Langmuir probe Te measurements. Two new divertor viewing systems have been prepared for TCV and effort has been devoted to modelling the first of them to aid the reconstruction of the observed deposited power flux and comparison with LP measurements.
First attempts, before optimisation of the system, have been made to measure fluctuations in potential and particle flux leading to some preliminary characterisation of time and space dimensions and poloidal velocities of edge plasma turbulent structures.

Igor KLIMANOV: *"Study of the electron distribution function during Electron Cyclotron Current Drive (ECCD)"*
The study requires the development of new diagnostic and numerical tools. A new 24-channel Low Field Side (LFS) radiometer is being designed and will be built in the year 2002. It will allow LFS and HFS measurements simultaneously. Vertical and Oblique ECE measurements will also be possible. In order to extract the information on the electron distribution function from the ECE measurements, a comparison with the results of numerical calculations, which may be based on a Fokker-Plank model is needed. A numerical module to simulate the ECE emission spectra for any distribution function, any mode and any angle of propagation will be developed. This technique can be applied to ECCD and X3 Electron Cyclotron Heating regimes. A second diagnostic system, the Multiwire Proportional Detector (MPX) will be upgraded to cover the energy range of interest (HFS ECE data analysis indicates 20-35 keV). The MPX results will complement those of the ECE system.

Laurent KLINGER: *"3D numerical simulation of a plasma torch using a finite volume method"*
In order to simulate DC plasma torches operated in a steady mode, we added an electrical part to a full Navier-Stokes solver. After test cross-flows in square ducts at low currents, we found numerical problems when evaluating gradients on the realistic (non-orthogonal) 3D meshes of an F4 torch. A numerical method using isoparametric transforms on tetrahedra was developed to address this problem. Moreover, typical arc core temperatures required the inclusion of the real gas equation of state, which is now given in tabulated form to the Navier-Stokes solver.

Adriano MANINI: *"Dynamic response of the plasma temperature to additional heating"*
The year 2001 began with a collaboration with ASDEX Upgrade with the aim of verifying the diagnostic possibilities for the analysis of the dynamic response of the

plasma under intense modulated ECH. The most important results obtained focus on the possibility of using line integrated soft X-ray data in order to determine the power deposition location and on the strong limitations of the method that had previously been tested in order to reduce the sawtooth coupling to the modulated ECH, the generalised singular value decomposition technique. The analysis of ECE data on ASDEX Upgrade at the ECH shut-off has shown that a new method based on time constants determination after each intermediate shut-off of the modulation phase can be implemented. This work is still in progress. During the 2001 TCV campaign, special experiments were performed to analyse the X-ray diagnostics in parallel with the recently installed low field side ECE system. Preliminary results confirm the previous ASDEX Upgrade observations and point out in particular the increasing importance of a new X-ray diagnostic based on a multiwire proportional detector chamber.

Andrei MARTYNOV: *"MHD activity of tokamak plasmas"*
Studies of the dependence of the poloidal beta limit of the stability of the internal ideal kink mode on elongation, triangularity and aspect ratio were carried out, aiming at a better understanding of the role of these factors on mode stability. It was shown that by changing the plasma inverse aspect ratio from high (cylindrical approximation) to real values the dependence of the ideal internal kink mode growth rate on the poloidal beta inside the q=1 surface is changing shape, from quadratic at high aspect ratio to linear at real lower aspect ratio. This is different from the theoretically predicted behaviour, most probably because the simplifying assumptions, which were used to produce the analytical approximations, are not satisfied in cases far from cylindrical geometry. It was shown also that the limiting poloidal beta inside the q=1 surface decreases linearly with plasma elongation. The stabilising influence of positive and negative triangularity depends on the peaking of the plasma current profile. Studies of the stability of the external ideal kink mode for TCV plasmas with high edge elongation (above 2.7) were also carried out. A number of simulated and real TCV equilibria with high elongation were analysed and the external kink mode stability limits were found. The dependence of the stability limits on the plasma elongation and on the q profile agrees well with the TCV results.

Stefan MUELLER: *"Basic investigation of turbulence and transport in toroidal plasmas".*
Local plasma modes, such as drift waves, are major candidates for the still missing explanation of anomalous transport in fusion relevant plasmas. As this phenomenon is limiting the achieved confinement times in existing machines, there has recently been much effort to understand and - if possible - to find ways to inhibit it. Due to recent progress on massively parallel supercomputers, simulations using different models (fluid, gyrokinetic) become more and more realistic. Much work is currently being done to trace back the mechanism of local plasma turbulence leading to global macroscopic particle and energy transport. However, there is currently nearly no experimental benchmark available for the mass of numerical data. This can be explained by the fact that experiments were designed to push forward fusion power - not to investigate small scale phenomena. The plasma core is not enough accessible to diagnostics, especially not for diagnostics with the required time and space resolution to trace back turbulence and local modes. The TORPEX device at CRPP/EPFL is being designed exactly to fit these needs. Aiming at low density and low temperature plasmas, it will be armed with the most modern diagnostics and with highly flexible magnetic fields to produce the needed data to benchmark the many physical and numerical models being developed at the moment - and to hopefully lead to a better understanding of turbulent transport. This work aims at contributing to this understanding via

experiments and comparisons with existing and new modeling tools. In the present initial phase the work is focussed on contributing to the development of the TORPEX experimental device, including designing magnetic field configurations, dimensioning coils and electrical circuits, and calculating dynamical force loads.

Petri NIKKOLA: *"Simulations of electron cyclotron wave propagation in TCV"*
The CQL3D Fokker-Planck code has been used to model ECCD/ECH experiments in the TCV. The code has a module for radial particle transport. It has been shown that radial diffusion is an important factor in understanding the ECCD physics in TCV. Without transport, the code overestimates the ECCD efficiency by a factor of five or more. However, inclusion of the transport leads to a good agreement with experiments and a realistic current density profile.

Pavel POPOVITCH: *"Electromagnetic wave propagation in 3D plasma configurations"*
Low-frequency electromagnetic wave heating in 3D plasma configurations is investigated, concentrating in particular on waves in the ion-cyclotron resonance and Alfvén frequency range. The code developed implements the full cold plasma model to describe the plasma and uses VMEC equilibria for the geometry. The equilibria are treated with the TERPSICHORE code in order to calculate the metric elements in Boozer magnetic coordinates. We have further developed the 1D and 2D versions of the code and calculate power flowsin the plasma which allows the verification of energy conservation and the plasma response calculation. The results of the 2D code in a tokamak geometry have been compared with LION code calculations. The Alfvén resonances and the Alfvén continuum boundary positions in a tokamak configuration are in a good agreement with the LION results. Purely toroidal effects such as the gap in the continuum and the Toroidicity Induced Alfvén Eigenmode (TAE) have been tested, showing good agreement between the results. The finite elements applied for the radial discretisation have been modified in order to improve the convergence.

Andrea SCARABOSIO: *"Studies on MHD activity as a function of plasma shape in standard TCV scenarios and MHD phenomena in advanced scenarios"*
With reduced plasma shaping, bursts of low (m,n) MHD modes have always been observed when flux surfaces with integer q_{edge} value (q=3, 4 and 5) approach and cross the plasma boundary during current ramp-up. When crossing the region $q_{95\%} < 3 < q_{edge}$ a mode with a dominant 3/1 component starts and grows in amplitude, while it slows down in frequency and eventually locks to the wall. Before locking to the wall, and at sufficient amplitude, its dominant component clearly becomes a 2/1 mode that leads to mode cascade and subsequent disruption.
Both elongation (κ) and triangularity (δ) lower the global n=1 mode amplitude below a critical value avoiding this mode cascade. Already with a small amount of plasma shaping (κ>1.3, δ>0.25) it is possible to avoid disruptions as well as with strong negative triangularity (δ<-0.4).
MHD activity, limiting the plasma performance, has been observed during the ICEC (improved central electron confinement) scenario in TCV. A 2/1 mode appears in the region of the steepest pressure profile and causes crashes in the emissivity of the soft X-ray in the core region. Often a (1,1) mode is seen to precede and then to lock to the 2/1 after slowing down in frequency.

Edgar SCAVINO: *"Impurity transport measurements using laser ablation of impurities"*
The study of impurity transport in various shapes of TCV plasmas has been continued. A fully operational laser ablation system produces short puffs of non recycling impurities and the electromagnetic emission is collected by other existing diagnostics, above all the soft X-ray tomography camera. The shape of the

characteristic peaked line integrated signals is used to determine the inflow speed, the lifetime of the impurities in the plasma core and the global confinement time, which is defined as the time constant of the exponential decay of the signal. Scans of many parameters have been performed in ohmic L-mode plasmas, namely the triangularity, elongation, plasma current, toroidal magnetic field, electronic density. The impurity confinement time (τ_{imp}) has been compared with the electron energy confinement time and some regions have been identified in which the ratio τ_E/τ_{imp} shows unfavourably low values. The STRAHL simulation code is systematically being used in order to determine the radial profiles of the diffusion coefficient and the inward pinch velocity. These parameters are adjusted to reproduce the shape and time duration of the X-ray signals obtained in actual injection experiments.

Hannes SCHMIDT: *"VHF Plasma Source for Plasma Etching and Deposition"*
The subject of this thesis is the development of a very high frequency plasma source for plasma etching and deposition.
In a first phase, a cylindrical reactor has been designed and constructed. The reactor shall be used to show the “proof of principal” of the novel electrode design. The reactor parameters are 100cm electrode diameter at an excitation frequency of 100MHz. This setup will be used to demonstrate that uniform electrode voltages can be obtained at these high excitation frequencies, a necessary condition for homogeneous etching and deposition. In addition, it will be used to show that at this high excitation frequency high electron densities can be obtained, compared with the one obtained in conventional 13.56MHz plasmas.
The cylindrical geometry of the reactor has been chosen in order to allow easier comparison with theories and simulations already performed by the CRPP and UNAXIS France SA. In addition to that demonstration, the test plasma reactor will be used to prove that with this new technology, high performance plasma etching can be carried out. For this purpose, the reactor will be operated in different etching gases in order to perform test on the etching of silicon dioxide (SiOx). These performance tests will allow a decision as to whether the novel plasma reactor is competitive and whether the construction of an industrial reactor should be started.
The second phase comprises the development of the new high density industrial plasma reactor for PECVD application in collaboration with UNAXIS France SA.

Lukas STINGELIN: *"Beam Cavity Interactions in High Power Cyclotrons"*
The MAFIA commercial computer code allowed analyses of wake potential, coupling impedance and eigenmodes for the PSI main cyclotron cavities. From the first simulations it was concluded that MAFIA will not be suited to accurately model our huge cyclotron cavity with its approximately two hundred simultaneous bunch crossings. MAFIA's structured grid can not properly handle the deformed geometry, furthermore it only supports serial computers. An international collaboration between PSI, ETHZ and SLAC has been initiated. The eigenmode (Omega3P) and time domain (Tau3P) solvers under development at SLAC use unstructured grids and MPI for large scale electromagnetic computations. Omega3P was already used for a simulation of the excitation of higher order modes by the beam. Comparison with measurements at the cavity pick-ups showed that the method still has to be refined in order to take the cavity deformation and the non homogeneous radial bunch distribution into account. It is also planned to modify Tau3P for cyclotron applications during the following year. In order to get acquainted with the C++, MPI and OpenGL programming, a small FDTD program was written for parallel computers.

Marco WISCHMEIER: *"Divertor Detachment in the TCV and JET Tokamaks"*

Both TCV ASDEX-type, in-vessel fast pressure gauges successfully installed during the early part of 2001 have been operated routinely simultaneously in diverted configurations thanks to a set of power supply and control electronics on loan from JET. Preliminary results show that the neutral pressure compression ratio during detachment is an order of magnitude lower than in tokamaks with higher divertor plasma densities. As suspected, this strongly implies that the mechanisms leading to detachment must be of a very different character than in larger machines. Efforts will continue in 2002 to understand why this is so using a fluid Monte Carlo code package, B2-Eirene, supported by IPP Garching. The code exists in two versions, SOLPS4.0 and SOLPS5.0, both of which are installed on the CRPP IBM 9000. Simulations of TCV diverted configurations have been performed with both. Benchmarking SOLPS5.0 against SOLPS4.0 for different boundary conditions has begun in preparation for the imminent withdrawal of SOLPS4.0 in favour of the more sophisticated SOLPS5.0. Simulations thus far have reproduced earlier results from code runs TCV in which the observed target profiles could not be matched by the code. Similarly, the code could not reproduce the observed degree of detachment at high plasma density. Efforts continue on the effects of molecular reactions in the Eirene simulations. Such reactions are not normally required to explain detachment in tokamaks with higher divertor densities than observed in TCV and it is thought that molecules play an important role in the ion conversion process. Considerable effort has been devoted to the simulation of JET Helium discharges. The first ever B2.5-Eirene simulations of JET helium discharges were successfully performed and good agreement was found between theory and experiment. In collaboration with UKAEA Culham, SOLPS5.0 runs for the tight aspect ratio tokamak MAST are being setup. Detachment has recently been observed on this device despite the divertor plasma density being a factor of 10 lower than on TCV. In common with TCV, it is thought that molecular processes will be required in the simulations to explain the observed detachment.

Zhongwen YAO: *"Mechanical properties and microstructure of irradiated metals"*
Single crystal Ni specimens were irradiated to 0.1dpa, 0.01dpa and 0.001dpa in PIREX at 293K and 523K. Yield shear stress appears to increase with increasing dose. The tensile curves indicate a yield drop, which is larger for the higher irradiation dose. The total elongation of the 0.1dpa specimen is degraded relative to the unirradiated specimen, while the 0.01 and 0.001dpa specimens keep a similar elongation. While the activation volume of the unirradiated specimen decreases rapidly with increasing strain to asymptotic value, that of the irradiated single crystal is smaller at a given strain than those of the unirradiated Ni. After going through a maximum they tend to the same asymptotic value measured for the unirradiated single crystal. TEM observation of the specimen irradiated to 0.1 dpa at room temperature and to 0.001 dpa at 523K was done. The defects density and their mean size were measured. In both cases most of defects were resolvable as SFT and loops. The relative densities of SFT's and loops are about $0.8\times10^{23}m^{-3}$ and $1\times10^{23}m^{-3}$ for 0.1 dpa. TEM observation shows that the deformation microstructure in two irradiated specimens presents channelling as the main deformation mode at the start of the tensile curve. With increasing deformation, the dislocation cells start to appear and eventually dominate the microstructure. When compared with the unirradiated case, the two observed irradiated specimens show smaller dislocation cells.

Alexei ZABOLOTSKY: *"Particle transport in TCV"*
The new experimental arrangement for space resolved measurements of Ultra-Soft-X-ray (USX) radiation was studied. The radiative power of the C^{V} (308eV) and C^{VI} (368eV) spectral lines was measured. A computer model based on STRAHL code was used for modelling theresults. The radial flux density was described by

diffusive and convective terms whose radial and temporal dependences were obtained by comparison of the experimental and the simulated data. It was found that this method is suitable for determination of the particle edge transport parameters in Ohmic plasmas, especially in the presence of the edge barriers, as in the case of the H-mode.
In order to establish the base for future transport analysis in the case of ECH plasmas, the replacement of the present 2mm interferometer by a 1mm superheterodyne interferometer (280GHz) was prepared. The new interferometer will allow measurement of the low densities when the FIR interferometer fails because of vibration. At the same time, new interferometer should back up the TCV density feedback control which is dependent on the FIR operation.

6 Public awareness of fusion research

6.1 3D Stereoscopic Movie "The Starmakers" was awarded a prize

This 8 minute stereoscopic movie is viewed with passive polarised glasses in order to take the spectator along a virtual visit of a controlled fusion reactor. The concept is based on the ITER project which will hopefully be operational during the first quarter of this century. This movie, totally made by computer, is a 3D real virtuality. It has been produced by the CRPP with the financial support of the European Commission, Direction de la Recherche. The images have been computerised by Digital Studio SA (Paris) based on the ITER Catia Cad integration design (Home-Team Garching).

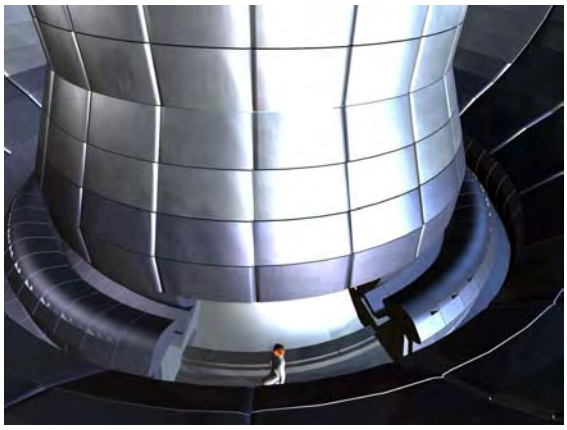

It was awarded the "Grand Prix" at the FIFEL in March 2001 (Festival International du Film sur l'Energie de Lausanne) for scientific popularisation with the following laudatio: "Un film où la technique et l'expression sont en parfaite adéquation avec le message. Un regard visionnaire sur l'énergie qu'on voit et revoit avec plaisir".

6.2 CRPP Public Relations activities 2001

We had a very large number of visitors during the spring of 2001 during the "Open days at the EPFL". About 1500 people visited the CRPP over 2 days to see the TCV

tokamak and its ancillary systems and the plasma processing facilities. The movie “The Starmakers” was also shown in 3D at this occasion. The CRPP was present for a full week in the centre of Lausanne (Science et Cité, 5-11 May, Espace Arlaud) and also at the Hotel de Ville for a public debate. Besides the poster display created by the CRPP team, some panels were provided by the “ Fusion Expo ” team and we gratefully acknowledge this collaboration.

Within the frame of the usual visit of the CRPP, about 1200 people visited in various groups or associations. The level ranged from secondary school to university, including both Swiss and foreign visitors.

During the summer of 2001: 65 high school pupils (13-17 years old) came for a half-day on four occasions (Summer Science Passport).

The Fusion Expo went to the engineering "Haute Ecole Spécialisée" in Yverdon. About 1000 persons visited the exhibit. The Fusion Expo was also presented to energy specialists, to policy makers and to some electricity utilities.

The Expo (renovated) returned to its starting place (CERN, 1993) and was visited by also about 1000 people during July and August.

Department of Physics Day at EPFL: During a one day devoted to physics research at the EPFL, M.Q. Tran presented fusion research and the involvement of the Swiss Association in the European programme

6.3 Fusion and industry

A one-day conference and discussion with Swiss firms already involved or interested in fusion engineering was held in December in Bern. The goal of the meting was to present to industry fusion technologies, specially those related to ITER which will be required during its construction. Presentations were made by R. Andreani, EFDA Associate Leader for Technology, R. Aymar, Director of ITER-CTA, J.-F. Conscience (OFES/BBW), J.-P. Rager, EU Commission- Head of Joint Development of Fusion and M.Q. Tran (CRPP). The ITER project was described, with its objectives and the required industrial involvements, as well as the perspectives in this field. About 40 firms were represented.

6.4 Publications aimed at a general audience

A brochure was prepared for the Bulletin de l'Association Suisse pour l'énergie atomique entitled "Fusion: Energie des 21 Jahrunderts", N3, Februar 2001, ISSN 1421-0436, edited by P.J. Paris

An article in the Revue des Electriciens Romands: "Comment domestiquer l'énergie des étoiles?: La fusion thermonucléaire", targeted high schools and the Expo visitors.

A description of the CRPP: "The EPFL Plasma Physics Research Centre" was produced in English, French and German), presentation of CRPP for Open Days and visits. This document also appears on the CRPP web site as pdf file.

Articles on plasma and fusion by A. Benz, H. Bruhns, P. Vandenplas, P.J. Paris, M.Q. Tran & Ch. Hollenstein were prepared for the "Les Cahiers de l'électricité" No 48, October 2001.

The CRPP web site has been regularly updated and improved, targeting specialist and non-specialist surfers.

APPENDIX A Articles Published in Scientific Reviews During 2001

Alberti S., Tran M.Q., et al., *"European high-power CW gyrotron development for ECRH systems",* Fusion Engineering and Design 53, 387 - 397 (2001), ISSN 0920-3796, Proceedings of the Joint Meeting of the IAEA Technical Committee Meeting on ECRH Physics and Technology for Fusion Devices and the 11th Joint Workshop on Electron Cyclotron Resonance Heating, Oh-arai, Ibaraki, Japan, October 4-8, 1999

Anghel A., *"Self-field effects in large superconducting cables for ITER"*, 21st Symposium on Fusion Technology, Madrid, Spain, September 2000, Fusion Engineering and Design, Part. B, **58-59**, 7 - 11 (2001) (ISSN 0920-3796)

Anghel A., Pourrahimi S., Takahashi Y., Vécsey G., *"Correlation between quench pressure and normal zone voltage observed in the QUELL experiment"*, Chats 2000, Frascati, Italy, 2000, Cryogenics **40**, 8-10, 549-553 (2000, appeared in 2001)

Belinger A., Bulkin P., Delaunay L, Elyaakoubi M., Perrin J., Schmitt J., Turlot E., Hollenstein Ch., Howling A.A., Sansonnens L., *"Electrostatic charging: mechanism of substrate charging after plasma processing"*, Panels (Business & Technical news from Unaxis Displays) 1st Edition,19-21, September 2001

Bruzzone P., *"Pressure drop and helium inlet in ITER CS1 conductor"*, 21st Symposium on Fusion Technology, Madrid, Spain, September 2000, Fusion Engineering and Design, Part. B, **58-59**, 211 - 215 (2001) (ISSN 0920-3796)

Bruzzone P., *"Superconductivity: Hysteresis and Coupling Losses"*, Engineering Superconductivity, Peter J. Lee Editor, Wiley-Interscience, ISBN 0-471-41116-7, 138-152 (2001)

Bruzzone P., *"Forced Flow Conductor Manufacturing"* in Engineering Superconductivity, Peter J. Lee Editor, Wiley-Interscience, ISBN 0-471-41116-7, 218-240 (2001)

Bruzzone P., *"Superconducting Magnets for Fusion Reactors"* in Engineering Superconductivity, Peter J. Lee Editor, Wiley-Interscience, ISBN 0-471-41116-7, 568-576 (2001)

Bruzzone P., Fuchs A.M., Vecsey G., Stepanov B., Zapretilina E., *"Test Results of SeCRETS, a Stability Experiment about Segregated Copper in CICC"*, IEEE Appl. Supercon. **11**, 2018-2021 (2001)

Bruzzone P., *"Contact Resistance Distribution at the Termination of Cable-in-Conduit Conductors",* IEEE Appl. Supercon. **11**, 1893-1895 (2001)

Bruzzone P., *"Superconductors and Joints tests and trends for future development",* Fusion Engineering and Design, **56-57**, 125-134 (2001)

Caturla M.J., Diaz de la Rubia T., Victoria M., Corzme R.K., James M.R., Greene G.A., *"Multiscale modeling of radiation damage: applications to damage production by GeV proton irradiation of Cu and W and pulsed irradiation effects in Cu and Fe"*, J. Nucl. Mater. **296**, 90 (2001)

Coda S., Porkolab M., Burrell K.H., *"Signature of turbulent zonal flows observed in the DIII-D tokamak"*, Phys. Rev. Letters **86**(21), 4835-4838 (2001)

Coda S., Porkolab M., Burrell K.H., *"Characterization of density fluctuations during ELMs in the DIII-D tokamak"*, Nucl. Fusion **41**(12), 1885-1896 (2001)

Condrea I., Haddad E., Côté C., Gregory B.C., *"Characterization of impurities in L and H modes created by divertor biasing and plasma triangularity in TdeV"*, Plasma Phys. & Contr. Fusion, **43**, 71-98 (2001)

Cooper W.A., Okamura S., Yamazaki K., *"Effect of toroidal current and profile on ballooning instability mechanisms in a quasiaxisymmetric stellarator"*, Plasma Phys. & Contr. Fusion **43**, 839 - 847 (2001)

Dai Y., Jia X., Chen J.C., Sommer W.F., Victoria M., Bauer G.S., *"Microstructure of both as-irradiated and deformed 304L stainless steel irradiated with 800 MeV protons"*, J. Nucl. Mater, **296**, 174 (2001)

Dammertz G., Alberti S., Arnold A., Giguet E., LeGoff Y., Thumm M., *"Cold test measurements on components of the 1 MW, 140 GHz, CW gyrotron for the Stellarator Wendelstein 7-X"*, Fusion Engineering and Design **53**, 561 - 569 (2001), ISSN 0920-3796, Proceedings of the Joint Meeting of the IAEA Technical Committee Meeting on ECRH Physics and Technology for Fusion Devices and the 11th Joint Workshop on Electron Cyclotron Resonance Heating, Oh-arai, Ibaraki, Japan, October 4-8, 1999

Darbos C., Magne R., Alberti S. et al., Tran M.Q., *"The 118GHz ECRH experiment on Tore Supra"*, 21st Symposium on Fusion Technology, Madrid, Spain, September 2000, Fusion Engineering and Design, Part. A, **56-57**, 605 - 609 (2001) (ISSN 0920-3796)

Degeling A.W., Martin Y.R., Bak P.E., Lister J.B., Llobet X., *"Dynamics of edge localized modes in the TCV tokamak"*, Plasma Phys. & Contr. Fusion **43**, 1671-1698 (2001)

Dorier J.-L., Gindrat M., Hollenstein Ch., Salito A., Loch M., Barbezat G., *"Time-resolved imaging of anodic arc root behavior during fluctuations of a DC plasma spraying torch"*, IEEE Trans. on Plasma Science Vol. **29**(3), 494-501 (2001)

Duchateau J.L., Fillunger H., Fink S., Heller R., Hertout P., Libeyre P., Maix R., Marinucci C., Martinez A., Meyder R., Nicollet S., Raff S., Ricci M., Savoldi L., Ulbricht A., Wuechner F., Zahn G., Zanino R., *"Test program preparations of the ITER toroidal field model coil (TFMC)"*, Fusion Engineering and Design, **58-59**, 147-151 (2001)

Duval B.P., Llobet X., Isoz P.F., Lister J.B., Marletaz B., Marmillod Ph., Moret J.-M., *"Evolution not revolution in the TCV tokamak control and acquisition system"*, 21st Symposium on Fusion Technology, Madrid, Spain, September 2000, Fusion Engineering and Design, Part. A, **56-57**, 1023 - 1028 (2001) (ISSN 0920-3796)

Fasel D., Lucia C., Ganuza D., Doyharzabal I., *"30 kV/10mA solid state anode modulator for gyrotron plasma heating, design issues and results"*, 21st Symposium on Fusion Technology, Madrid, Spain, September 2000, Fusion Engineering and Design, Part. A, **56-57**, 633 - 637 (2001) (ISSN 0920-3796)

Franz D., Grangeon F., Delachaux T, Howling A.A., Hollenstein Ch., KarnerJ., *"Rapid deposition of hydrogenated microcrystalline Silicon by a high current DC discharge"*, Thin Solid Films **383**, 11-14 (2001)

Fuchs A.M., Blau B., Bruzzone P., Vecsey G., Vogel M., *"Facility Status and Results on ITER Full-size Conductor Tests in SULTAN"*, IEEE Appl. Supercon. **11**, 2022-2025 (2001)

Furno I., Angioni C., Porcelli F., Weisen H., Behn R., Goodman T.P., Henderson M.A., Pietrzyk Z.A., Pochelon A., Reimerdes H., Rossi E., *"Understanding sawtooth activity during intense electron cyclotron heating experiments on TCV"*, Nuclear Fusion **41**(4), 403 - 420 (2001)

Gelles D., Schäublin R., "*Post-irradiation deformation of Fe-9%Cr"*, Mat. Science & Engin. **A309-310**, 82-86 (2001)

Henderson M.A. , Goodman T.P., Hogge J.-Ph., Pietrzyk Z.A., Pochelon A., Sauter O., *"Poloidally asymmetric plasma response with ECH deposition near q=1 in TCV"*, Fusion Engineering and Design **53**, 241 - 248 (2001), ISSN 0920-3796, Proceedings of the Joint Meeting of IAEA Technical Committee Meeting on ECRH Physics and Technology for Fusion Devices and the 11th Joint Workshop on Electron Cyclotron Emission and ECRH, Oh-ari, Ibaraki, Japan, October 1999

Hofmann F., Behn R., Coda S., Goodman T.P., Henderson M., Lavanchy P., Marmillod Ph., Martin Y., Martynov A., Mlynar J., Moret J.-M., Pochelon A., Reimerdes H., Sauter O., and the TCV Team, *"Stability and energy confinement of highly elongated plasmas in TCV"*, 28th EPS Conference on Controlled Fusion and Plasma Physics, Funchal, Madeira, Portugal, June 2001, Plasma Physics and Controlled Fusion **43**(12A), A161 - A173, 2001 (ISSN 0741-3335)

Jaun A., Fasoli A., Testa D., Vaclavik J., Villard L., *"Gyrokinetic modelling of macro-instabilities in high performance tokamak plasmas"*, 28th EPS Conference on Controlled Fusion and Plasma Physics, Funchal, Madeira, Portugal, June 2001, Plasma Physics and Controlled Fusion **43**(12A), A207 - A216, 2001 (ISSN 0741-3335)

Jost G., Tran T.M., Cooper W.A., Villard L., Appert K., *"Global Linear Gyrokinetic Simulations in Quasi-Symmetric Configurations"*, Physics of Plasmas **8**(7), 3321 - 3333 (2001)

Khayrutdinov R.R., Lister J.B., Lukash V.E., Wainwright J.P., *"Comparing DINA code simulations with TCV experimental plasma equilibrium responses"*, Plasma Physics & Contr. Fusion **43**, 321-342 (2001)

Koizumi N., Azuma K., Tsuchiya Y., et al., Fuchs A., Bruzzone P., Blau B., Vecsey G., Nyilas A., Okuno K., *"Evaluation of critical current performance of 13 T - 46 kA steel jacketed Nb3Al conductor"*, Fusion Engineering and Design, **58-59**, 1-5 (2001)

Kraishi T.A., Zbib H.M., Diaz de la Rubia T., Victoria M., *"Modelling of irradiation induced hardening in metals using dislocation dynamics"*, Phyl. Mag. Lett. **81**, 583 (2001)

Lister J.B., Khayrutdinov R., Limebeer D.J.N., Lukash V., Nakamura Y., Sharma A., Villone F., Wainwright J.P., Yoshino R., *"Linear and non-linear*

plasma equilibrium responses on the JT-60U and TCV tokamaks", 21st Symposium on Fusion Technology, Madrid, Spain, September 2000, Fusion Engineering and Design, Part. A, **56-57**, 755 - 759 (2001) (ISSN 0920-3796)

LoPiccolo B., Spätig P., Kruml T., Martin J.-L., Bonneville J., *"Characterising thermally activated dislocation mechanisms"*, Materials Science & Engineering **A309-310**, 251-255 (2001)

Maccio M., Vaclavik J., Villard L., *"Effect of E x B flows on global linear ion temperature gradient modes"*, Physics of Plasmas **8**(3), 895 - 906 (2001)

Marinucci C., Bottura L., Luongo C., Vécsey G., *"Proposal for a database for the validation of simulations in superconducting cables"*, Cryogenics **40**, 8-10, 677-678 (2000, appeared in 2001)

Marinucci C., Vécsey G., *"Heat slug propagation and quench initiation analysis of the ITER toroidal field model coil"*, Cryogenics **40**, 8-10, 501-510 (2000, appeared in 2001)

Marmy P., Leguey T., *"Impact of irradiation on the tensile and fatigue properties of two titanium alloys"*, J. Nucl. Mater. **296**, 155-164 (2001)

Minardi E., Weisen H., *"Stationary magnetic entropy in ohmic tokamak plasmas: experimental evidence from the TCV device"*, Nuclear Fusion **41**(No 1), 113 - 130 (2001)

Müller H., Howling A.A., Hollenstein Ch., *"Power laws for the spatial dependence of electrical parameters in the high voltage, capacitive RF sheath"*, IEEE Transactions on Plasma Science **28**, 1713 (2000)

Peysson Y., Coda S., Imbeaux F., *"Hard X-ray CdTe tomography of tokamak fusion plasmas"*, 11th Int. Workshop on Room Temperature Semiconductor X/gamma-ray detectors and Associated Electronics, IAEA, Vienna, Austria, October 1999, Nucl. Inst. and Methods in Phys. Res. A **458**, 269-274 (2001)

Pietrzyk Z.A., Angioni C., Behn R., Coda S., Goodman T.P., Henderson M.A., Hofmann F., Sauter O., *"Long-pulse improved central electron confinement in the TCV tokamak with Electron Cyclotron Heating and Current Drive"*, Phys. Rev. Letters, **86**(8), 1530 - 1533 (2001)

Pitts R.A., Duval B.P., Loarte A., Moret J.-M., Boedo J.-A., Coster D., Furno I., Horacek J., Kukushkin A.S., Reiter D., Rommers J., and TCV Team, *"Divertor geometry effects on detachment in TCV"*, 14th Int. Conference on Plasma Surface Interactions in Controlled Fusion Devices, Rosenheim, Germany, May 2000, J. Nucl. Mater., **290-293**, 940-946 (2001),

Pochelon A., Hofmann F., Reimerdes H., Angioni C., Behn R., Duquerroy R., Furno I., Goodman T.P., Gomez P.,Henderson M.A., Martynov A., Nikkola P., Sauter O., Sushkov A., *"Plasma shape effects on sawtooth/internal kink stability and plasma shaping using EC wave current profile tailoring in TCV"*, (18th IAEA Fusion Energy Conference, Sorrento, Italy, October 2000), Nucl. Fusion **41**, 1663 (2001)

Porcelli F., Airoldi A., Angioni C., Bruschi A., Buratti P., Califano F., Cirant S. Furno I., Grasso D., Lazzaro E., Martynov A.A., Ottaviani M., Pegoraro F.,

Ramponi G., Rossi E., Sauter O., Tebaldi C., Tudisco O., *"Modelling of macroscopic magnetic islands in tokamaks"*, Nucl. Fusion **41**(9), 1207-1218 (2001)

Reiman A., Ku L., Monticello D., et al., Cooper W.A., *"Recent advances in the design of quasiaxisymmetric stellarator plasma configurations"*, Physics of Plasmas **8**(5), 2083-2094 (2001)

Ryter F., Angioni C., Beurskens M., et al., *"Experimental studies of electron transport"*, Plasma Phys. & Contr. Fusion 43, A323 (2001)

Sanchez R., Isaev M.Yu, Hirshman S.P. et al., Cooper W.A., *"Ideal MHD stability calculations for compact stellarators"*, Comp. Phys. Commun. **141**, 55-65 (2001)

Sakakibara S., Yamada H., Wakanabe K.Y., Narushima Y., et al., Cooper W.A., *"MHD characteristics in the high beta regime of the large helical device"*, Nuclear Fusion, **41**(9), 1177 – 1183, (2001)

Sauter O., Goodman T.P., Coda S., Henderson M., Hofmann F., Hogge J.-P., Peysson Y., Pietrzyk Z.A., Pitts R., Reimerdes H., Weisen H., *"Sustained fully non-inductive scenarios using pressure and current profile control with ECCD"*, Fusion Engineering and Design, **53**, 289 - 299 (2001), ISSN 0920-3796, Proceedings of the Joint Meeting of IAEA Technical Committee Meeting on ECRH Physics and Technology for Fusion Devices and the 11th Joint Workshop on Electron Cyclotron Emission and ECRH, Oh-ari, Ibaraki, Japan, October 1999,

Sauter O., *"Steady-state fully non-inductive operation with ECCD and current profile control in the TCV tokamak"*, Invited paper at the 42nd Annual Meeting, APS Division of Plasma Physics, Quebec, Canada, October 2000, Physics of Plasmas **8**, 2199 (2001)

Spätig P., Baluc N., Victoria M., *"On the constitutive behavior of the F82H ferritic/martensitic steel"*, Materials Science and Engineering **A309-310**, 425-429 (2001)

Varela M., Fernandez B., Muñoz A., Leguey T., Pareja R., Ballesteros C., *"Titanium segregation mechanism in deformed vanadium-titanium alloys"*, Philosophical Magazine Letters **81**, 259-264 (2001)

Victoria M., Baluc N., Spätig P., *"Structural materials for fusion reactors"*, Nuclear Fusion **41**, 1047 - 1053 (2001)

Weisen H., Furno I. and the TCV Team, *"Particle transport in high power ECH and ECCD discharges in TCV"*, presented at 18th IAEA Fusion Energy Conference, Sorrento, Italy, October 2000, Nuclear Fusion **41**(9) 1227 - 1233, (2001)

Weisen H., for TCV Team, *"Overview of TCV results"*, 18th IAEA Fusion Energy Conference, Sorrento, Italy, October 2000, IAEA-CN-77/OV5/1, Nucl. Fusion **41**, 1459 (2001)

Weisen H., Minardi E., *"Evidence for role of magnetic entropy and turbulent equipartition in stationary ohmic tokamak discharges"*, Europhysics Letters **56**(4), 542 - 548 (2001)

Yamada H., Komoi A., Ohyabu N. Kaweko O. Kawahata K. et al., Cooper W.A., *"Configuration, flexibility and extended regimes in large helical device"*, Plasma Phys. & Contr. Fusion **43**, A55-A71 (2001)

Zarnstorff M.C., Berry L.A., Brooks A., et al., Cooper W.A., *"Physics of the compact advanced stellarator NCSX"*, Plasma Phys. & Contr. Fusion **43**, A237-A249 (2001)

APPENDIX B Conferences and Seminars

B.1 Conference proceedings published in 2001

Bottura L., Marinucci C., Bruzzone P., *"Application of the code THEA to the CONDOPT experiment in SULTAN"*, Proc. of MT 17, Geneva, September 2001

Bruzzone P., Formisano A., Martone R., *"Optimal Magnetic Probes Location for Current Reconstruction in Multistrands Superconducting Cables"*, Proc. of Compumag 2001, Evian, June 2001

Bruzzone P., Fuchs A.M., Stepanov B., Vecsey G., *"Performance Results of Nb_3Sn Cable-in-Conduit Conductors under cyclic Load"*, Proc. of MT 17, Geneva, September 2001

Bruzzone P., Fuchs A.M., Stepanov B., Vecsey G., *"Transient Stability Results for Nb_3Sn Cable-in-Conduit Conductors"*, Proc. of MT 17, Geneva, September 2001

Bruzzone P., Anghel A., Fuchs A.M., Pasztor G., Stepanov B., Vogel M., Vecsey G., *"Upgrade of Operating Range for SULTAN Test Facility"*, Proc. of MT 17, Geneva, September 2001

Bruzzone P., *"Coupling currents loss in Nb_3Sn cable-in-conduit conductors"*, Proc. of MT 17, Geneva, September 2001

DallaTorre F., VanSwygenhoven H., Victoria M., Schäublin R., Wagner W., *"Mechanical properties of nanocrystalline Ni in relation to ist microstructure"*, Mat. Res. Soc. Symp. Proc. Structure and Mechanical Properties of Nanophase Materials – Theory and Computer simulations vs Experiment, D. Farkas, H. Kung., M. Mayo, H. VanSwygenhoven and J. Weertman (Eds), 634, B.2.8.1-B2.8.6 (2001)

Dorier J.-L., Gindrat M., Hollenstein Ch., Loch M., Refke A., Salito A., Barbezat G., *"Plasma jet properties in a New spraying process at low pressure for large area thin film deposition"*, in Thermal Spray 2001, New Surface for a New Millenium (Ed) C.C. Berndt, K.A. Khor and E.F. Lugscheider, Published by ASM International, Material Park, Ohio, USA 2001

Fikar J., Bonneville J., Baluc N., Guyot P., *"High temperature plastic behaviour of icosahedral Al-Cu-Fe quasicrystals"*, Mat. Res. Soc. Symp. Proc. on Quasicrystals, 643, K7.3.1-K7.3.6 (2001)

Fikar J., Bonneville J., Rabier J., Baluc N., Proult A., Cordier P. Stretton I., *"Low temperature plastic behaviour of icosahedral Al-Cu-Fe quasicrystals"*, Mat. Res. Soc. Symp. Proc. on Quasicrystals, 643, K7.4.1-K7.4.6 (2001)

Fuchs A.M., Wesche R., Anghel A., Roth F., Heller R., Tasca M., *"Test Results of a 10 kA Current Lead using Ag/Au cladded Bi-2212 Tubes"*, Proc. of MT 17, Geneva, September 2001

Heller R., Friesinger G., Fuchs A.M., Wesche R., *"Development of High Temperature Superconductor Current Leads for 70 kA"*, Proc. of MT 17, Geneva, September 2001

Howling A., Sansonnens L., Hollenstein Ch., Belinger A., Perrin J., *"Measurement of substrate charging after plasma processing"*, Proc. Frontiers in Low Temperature Plasma Diagnostics IV, Rolduck, Netherlands, March 2001, p. 230

Ilyin Yu. A., Nijhuis A., ten Kate H.H.J., Bruzzone P., *"Self Field Measurements by Hall Sensors on the SeCRETS Long Sample CICCs in SULTAN"*, Proc. of MT 17, Geneva, September 2001

Leguey T., Bailat C., Baluc N., Victoria M., *"High energy proton irradiation of pure titanium"*, Mat. Res. Soc. Symp. Proc. on Microstructural Processes in Irradiated Materials, G.E. Lucas, L. Snead, M.A. Kirk, R.G. Elliman (Eds), 650, R3.1.1-R.3.1.6 (2001)

Marian J., Wirth B.D., Perlado J.M., et al., Schäublin R., *"Direct comparison between modelling and experiment: an alpha-Fe ion implantation study"*, Mat. Res. Soc. Symp. Proc.: Microstructural Processes in Irradiated Materials, G.E. Lucas, L. Snead, M.A. Kirk Jr., R.G. Elliman (Eds), 650, R3.2.1-R3.2.6 (2001)

Marinucci C., Bottura L., Bruzzone P., *"Transient stability analysis of the SeCRETS experiment in SULTAN"*, Proc. of MT 17, Geneva, September 2001

Mayoral et al., Sauter O., *"Sawtooth and neoclassical tearing mode seed island control by ICRF current drive on JET"*, Proc. 14th Topical Conf. On Radio Frequency Power in Plasmas, Oxnard, 7-9 May 2001

Schäublin R., Victoria M., *"Identification of defects in Ferritic/Martensitic steels induced by low dose irradiation"*, Mat. Res. Soc. Symp. Proc.: Microstructural Processes in Irradiated Materials, G.E. Lucas, L. Snead, M.A. Kirk Jr., R.G. Elliman (Eds), 650, R1.8.1.1-R.1.8.6 (2001)

Schmitt J., Belinger A., Hollenstein Ch., Howling A.A., Perrin J., Sansonnens L., Turlot E., Elyaakoubi M., *"Mechanism of substrate charging after plasma processing"*, Proc. 15th International Symposium on Plasma Chemistry, Orléans, France, July 2001, Vol. I, 33-39 (2001)

Spätig P., Schäublin R., Victoria M., *"Relation between microstructures and constitutive behavior of advanced tempered martensitic steels"*, Mat. Res. Soc. Symp. Proc. Material Instabilities and Patterning in Metals, San Francisco, USA, April 2001, H.M. Zbib, G.H. Campbell, M. Victoria, D.A. Hughes and L.E. Levine (Eds), 683 E, BB1.10.1-BB1.10.6 (2001)

Spätig P., Donahue E., Odette G.R., Lucas G.E., Victoria M., *"Transition regime fracture toughness-temperature properties of two advanced ferritic/martensitic steels"*, Mat. Res. Soc. Symp. Proc. on Multiscale Modelling of Materials, L.P. Kubin, J.L. Bassani, K. Cho, H. Gao, R.L.B. Selinger (Eds), 653, Z7.8.1-Z7.8.6

Wesche R., *"High-Temperature Superconductors: A New Class of Materials for Fusion Magnets"*, 2001 Swiss Workshop on Materials with Novel Electronic Properties, Les Diablerets, October 2001

B.2 Participation to conferences in 2001

Allfrey S., Bottino A., Hatzky R., Jost G., Villard L., *"Characterisation of ion temperature gradient driven (ITG) modes in the W VII-X stellarator configuration"*,

28th EPS Conference on Controlled Fusion and Plasma Physics, Funchal, Madeira, Portugal, June 2001, P5.042

Behn R., Pietrzyk Z.A., Angioni C., Coda S. , Goodman T.P., Henderson M.A., Hofmann F., Mlynar J., Sauter O., Scarabosio A., Weisen H., and the TCV Team, *"Improved core electron energy confinement in TCV tokamak plasmas with central EC counter current drive",* 28th EPS Conference on Controlled Fusion and Plasma Physics, Funchal, Madeira, Portugal, June 2001

Belo P., et al., Sauter O., *"On the amplitude of sawtooth pre-cursors at the onset of neo-classical tearing modes"*, 28th EPS Conference on Controlled Fusion and Plasma Physics, Funchal, Madeira, Portugal, June 2001

Blanchard P., Weisen H., Alberti S., Coda S., Gomez P., Goodman T., *"Measurements of electron cyclotron emission from non-Maxwellian electron distributions in TCV plasmas with ECH and ECCD"*, 28th EPS Conference on Controlled Fusion and Plasma Physics, Funchal, Madeira, Portugal, June 2001

Bosshard P., Duval B.P., Mlynar J., Weisen H., *"Charge exchange recombination spectroscopy optimisation with the TCV diagnostic neutral beam"*, 28th EPS Conference on Controlled Fusion and Plasma Physics, Funchal, Madeira, Portugal, June 2001

Bottino A., Villard L., Allfrey S., Sauter O., Vaclavik J., *"Effects of E x B flows on electrostatic microinstabilities"*, 9th European Fusion Theory Conference, Helsingor, Denmark, October 2001

Buttery R.J., Hender T.C., Howell D., et al., Pochelon A., and the EFDA-JET team, *"Rotation and shape dependence of neoclassical tearing mode thresholds on JET"*, 28th EPS Conference on Controlled Fusion and Plasma Physics, Funchal, Madeira, Portugal, June 2001, P5.011

Coda S., Peysson Y., Alberti S., Goodman T.P., Henderson M.A., Nikkola P., Sauter O., *"Suprathermal X-ray emissivity with 2nd and 3rd harmonic electron cyclotron heating in the TCV tokamak"*, 28th EPS Conference on Controlled Fusion and Plasma Physics, Funchal, Madeira, Portugal, June 2001

Condrea I., Haddad E., Coté C., Gregory B.C., *"Characterisation of impurities in L and H modes created by divertor biasing and plasma triangularity in TdeV"*, 28th EPS Conference on Controlled Fusion and Plasma Physics, Funchal, Madeira, Portugal, June 2001

Cooper W.A., Sanchez R., Hirshman S.P., Ku L.P., Isaev M., Fu G.Y.,Mikhailov M.I., Monticello D.A., Reiman A.H., Subbotin A.A., *"Cobra-Terpsichore benchmark for the compact stellarator NCSX"*, 28th EPS Conference on Controlled 28th EPS Conference on Controlled Fusion and Plasma Physics, Funchal, Madeira, Portugal, June 2001

Cooper W.A., Heyn M.F., Isaev M. Yu., Kalyuzhnyj V.N., Kasilov S.V., Kernblicher W., Mikhailov M.I. Nemov V.V., Nührenberg J., Samiton M.A., Shafranov V.D., Subbotin A.A., *"Topology of the magnetic field strength surfaces and particle confinement in mirror-type stellarators"*, 28th EPS Conference on Controlled 28th EPS Conference on Controlled Fusion and Plasma Physics, Funchal, Madeira, Portugal, June 2001

Cooper W.A., Isaev M. Yu., Okamura S., Yamazaki K., *"MHD stability of 3D plasma confinement systems with finite plasma current"*, Joint Conference of the 12th Int. Toki Conference on Plasma Physics and Controlled Nuclear Fusion and the 3rd General Scientific Assembly of Asia Plasma Fusion Association "Frontiers in Plasma Confinement and Related Engineering/Plasma Science, Toki, Japan, December 2001

Dalla Torre F., Schäublin R., Victoria M., Valier A., Van Swygenhoven H., *"Microstructure of nanocrystalline Ni"*, Dreiländertagung für Elektronenmikroskopie - Conference on Modern Microscopical Methods, Innsbruck, Austria, September 2001

DeCastro V., Leguey T., Monge M.A., Muñoz A., Parea R., Victoria M., *"Discontinously-reinforced titanium matrix composites for fusion applications",* 10th Int. Conference on Fusion Reactor Materials, Baden-Baden, Germany, October 2001

Degeling A.W., Martin Y.R., Bak P.E., Lister J.B., Llobet X., *"Dynamics of edge localised modes on TCV"*, 28th EPS Conference on Controlled Fusion and Plasma Physics, Funchal, Madeira, Portugal, June 2001

DeVries P., Pochelon A., Naver F., Johnson M., Howell D., Sauter O. and contributors to the EFDA-JET Workprogramme, *"Analysis of shaping effects on sawteeth in JET"*, 28th EPS Conference on Controlled Fusion and Plasma Physics, Funchal, Madeira, Portugal, June 2001, P5.002

Dorier J.-L., *"Plasma Jets at low pressure, for the development of new spraying processes for large area thin film deposition"*, International Thermal Spray Conference, May 2001, Singapore

Favez J.-Y., Khayrutdinov R.R., Lister J.B., Lukash V.E., *"Comparing DINA code simulations with TCV experimental VDE responses"*, 28th EPS Conference on Controlled Fusion and Plasma Physics, Funchal, Madeira, Portugal, June 2001

Giguet E., Alberti S., Arnold A., et al., Tran M.Q., *"High-power CW gyrotron development for ECRH systems",* IVEC 2001, 2-4 April 2001, Huis ter Duin, Noordwijk, The Netherlands

Giguet E., Alberti S., Fasel D., Hogge J.-P., Tran M.Q. et al., *"High power CW gyrotrons for ECRH experiments of fusion research"*, 26th Int. Conf. On Infrared and Millimeter Waves, September 10-14, 2001 Toulouse, France

Gindrat M., Dorier J.-L., Hollenstein Ch., Loch M., Refke A., Salito A., Barbezat G., *"Effect of specific operating conditions on the properties of LPPS plasma jets expanding at low pressure"*, submitted to the ITSC 2002 Int. Thermal Spray Conference, March 4-6, 2002, Essen, Germany

Goodman T.P., Alberti S., Blanchard P., Coda S., Gomez P., Henderson M.A., Nikkola P., Sauter O., *"The role of non-Maxwellian electron distribution functions in 2nd and 3rd harmonic electron cyclotron absorption in TCV"*, 28th EPS Conference on Controlled Fusion and Plasma Physics, Funchal, Madeira, Portugal, June 2001

Grandgirard V., Bertrand P., Depret G., Garbet X., Ghizzo A., Manfredi G., Sauter O., Tran T.M., Vaclavik J., Villard L., *"A semi-lagrangian method for the resolution of a drift-kinetic equation applied to ITG studies"*, 28th EPS Conference on Controlled Fusion and Plasma Physics, Funchal, Madeira, Portugal, June 2001

Hennequin P. Hender T.C., Alper B. et al. Pochelon A., *"MHD performance limits in JET optimised shear discharges"*, 28th EPS Conference on Controlled Fusion and Plasma Physics, Funchal, Madeira, Portugal, June 2001, P2.022

Hofmann F., Behn R., Coda S., Goodman T.P., Henderson M., Lavanchy P., Marmillod Ph., Martin Y., Martynov A., Mlynar J., Moret J.-M., Pochelon A., Reimerdes H., Sauter O., and the TCV Team, *"Stability and energy confinement of highly elongated plasmas in TCV"*, 28th EPS Conference on Controlled Fusion and Plasma Physics, Funchal, Madeira, Portugal, June 2001

Jodoin B., Gindrat M., Dorier J.-L., Hollenstein Ch., Loch M., Barbezat G., *"Modelling and diagnostics of a supersonic DC plasma jet expanding at low pressure"*, submitted to the ITSC 2002 Int. Thermal Spray Conference, March 4-6, 2002, Essen, Germany

Koslowski R. et al., Sauter O., *"MHD studies in radiating mantle plasmas on JET"*, 28th EPS Conference on Controlled Fusion and Plasma Physics, Funchal, Madeira, Portugal, June 2001

Kuntze M. , Alberti S., Dammertz G., Erckmann V., Giguet E., Illy S., Kasparek W. ,Legoff Y., Leonhardt W., Michel G., Mueller G., Piosczyk B., Schmid M., Tran M.Q., Thumm M., *"Advanced high power gyrotrons",* 29th IEEE Int. Conference on Plasma Science, Las Vegas, Nevada, U.S.A., June 2001

Lagrange T, Schäublin R., Grammon D., Gotthardt R., *"Microsctructure of Ni2+ ion irradiated binary Ti-Ti thin films"*, Dreiländertagung für Elektronenmikroskopie - Conference on Modern Microscopical Methods, Innsbruck, Austria, September 2001

Leguey T., Baluc N., Jansen F., Victoria M., *"Characterization of hydrogen barrier coatings for titanium-base allyos"*, 10th Int. Conference on Fusion Reactor Materials, Baden-Baden, Germany, October 2001

Leguey T., Baluc N., Schäublin R., Victoria M., *"Structure/mechanics relationships in proton irradiated pure titanium"*, 10th Int. Conference on Fusion Reactor Materials, Baden-Baden, Germany, October 2001

Llobet X., Duval B.P., *"128 channel PCI-based acquisition for MDSplus"*, IAEA Technical Committee Meeting on Control, Data Acquisition and Remote Participation for Fusion Research, Padova, Italy, July 2001

Maddison G. et al., Sauter O., *"ELM moderation in high density H-modes on JET and Alcator C-Mod"*, 28th EPS Conference on Controlled Fusion and Plasma Physics, Funchal, Madeira, Portugal, June 2001

Mantsinen M.J. et al., Sauter O., *"Analysis of ion cyclotron current drive at w~2wch for sawtooth control in JET plasmas"*, 28th EPS Conference on Controlled Fusion and Plasma Physics, Funchal, Madeira, Portugal, June 2001

Maraschek M.E. et al., Sauter O., *"Density dependence of the onset of neoclassical tearing modes in H-mode and pellet refueled discharges in JET and ASDEX Upgrade"*, 28th EPS Conference on Controlled Fusion and Plasma Physics, Funchal, Madeira, Portugal, June 2001

Martin Y., Equipe TCV, *"La recherche en physique des plasmas en Suisse - Résultats récents obtenus avec le tokamak TCV"*, SFP01, VIIème Congrès "Plasmas", Piriac, France, Mars 2001

Martynov An., Sauter O., *"Shape effects on stability of internal kink mode",* 9th European Fusion Theory Conference, Helsingor, Denmark, October 2001

Medvedev S.Y., Hender T.C., Sauter O., Villard L., *"Theoretical MHD limits in tokamaks with a separatrix"*, 28th EPS Conference on Controlled Fusion and Plasma Physics, Funchal, Madeira, Portugal, June 2001, Or.07

Mikhailov M.I., Isaev M.Yu., Nührenberg J., Subbotin A.A., Cooper W.A., Heyn M.F., Kalyuzhnyi V.M., Kasilov S.V., Kernbichler W., Nemov V.V., Samitov M.A., Shafranov V.D., *"Topology of magnetic field strength surfaces and particle confinement in mirror-type stellarators"*, 28th EPS Conference on Controlled Fusion and Plasma Physics, Funchal, Madeira, Portugal, June 2001

Mlynar J., Bosshard P., Duval B., Weisen H., *"Diagnostics neutral beam injector at Tokamak TCV"*, 10th Annual Conference of Doctoral Students WDS'2001, Prague, Czech Republic, June 2001

Narushima Y., Sakakibara S., Watanabe K., Nishimura K., Yamada H., Nakajima N., Yamazaki K., Cooper A., *"Low-n ideal MHD analysis in limiter plasma on LHD"*, 12th Int. Toki Conference and 3rd General Scientific Assembly of Asia Plasma & Fusion Association,, Ceratopia Toki, Toki City, Japan, December 2001

Nikkola P., Harvey R.W., Sauter O., Coda S., *"Effect of radial particle diffusion on electron cyclotron current drive in the TCV tokamak"*, 9th European Fusion Theory Conference, Helsingor, Denmark, October 2001,

Ongena J. et al, Sauter O., *"Recent progress on JET towards the ITER reference mode of operation at high density"*, (Invited talk) 28th EPS Conference on Controlled Fusion and Plasma Physics, Funchal, Madeira, Portugal, June 2001

Pochelon A., Angioni C., Matsinen M., Gorenlenkov N., McClements K.G., Budny R., de Vries P.C., Howell D.F., Nave M.F.F., Sauter O., Sharapov S., and conributors to the, EFDA-JET workprogramme, *"Sawtooth stabilisation by neutral beam-injected fast ions in JET"*, 28th EPS Conference on Controlled Fusion and Plasma Physics, Funchal, Madeira, Portugal, June 2001, P5.009

Popovich P., Cooper W.A., Villard L., *"Electromagnetic waves propagation in 3D plasma configurations"*, 9th European Fusion Theory Conference, Helsingor, Denmark, October 2001

Redi M.H., Canik J., Dewar R.L., Fredrickson E.D., Cooper W.A., Johnson J.L., Klasky S., *"Localized ballooning modes in compact quasiaxially symmetric stellarators"*, 28th EPS Conference on Controlled 28th EPS Conference on Controlled Fusion and Plasma Physics, Funchal, Madeira, Portugal, June 2001

Rost J.C., Porkolab M., Coda S., Mazurenko A., Nelson-Melby E., "Phase contrast imaging on DIII-D and ALCATOR C-MOD", 10th Int. Symposium on Laser-Aided Plasma Diagnostics, Fukuoka, Japan, 2001

Sauter O., Westerhof E. , Mayoral M.L., Howell D.F., Mantsinen M.J., Alper B., Angioni C., Belo P., Buttery R., and conributors to the EFDA-JET

workprogramme, *"Neoclassical tearing mode seed island control with ICRH in JET"*, 28th EPS Conference on Controlled Fusion and Plasma Physics, Funchal, Madeira, Portugal, June 2001, P5.001

Scavino E., Bakos J.S., Weisen H., Zabolotsky A., *"Impurity transport in shaped TCV plasmas"*, 28th EPS Conference on Controlled Fusion and Plasma Physics, Funchal, Madeira, Portugal, June 2001

Schäublin R., *"TEM imaging of small crystal defects"*, Dreiländertagung für Elektronenmikroskopie - Conference on Modern Microscopical Methods, Innsbruck, Austria, September 2001

Schäublin R., Leguey T., Spätig P., Baluc N., Victoria M., *"Microstructure and mechanical properties of two ODS ferritic/martensitic steels"*, 10th Int. Conference on Fusion Reactor Materials, Baden-Baden, Germany, October 2001

Schäublin R., Gelles D., Victoria M., *"Microstructure of irradiated ferritic/martensitic steels in relation to mechaical properties"*, 10th Int. Conference on Fusion Reactor Materials, Baden-Baden, Germany, October 2001

Schmitt J., Elyaakoubi M., Sansonnens L., *"Glow discharge processing in the liquid crystal display industry"*, 25th ICPIG, 17-22 July 2001, Nagoya, Japan

Spätig P., Schäublin R., Victoria M., *"Relationship between microstructures and constitutive behavior of a series of tempered martensitic steels",* MRS Spring Meeting "Material Instabilities and Patterning in Metals", San Francisco, USA, April 2001

Subbotin A.A., Mikhailov M.I., Nührenberg J., Isaev M.Yu., Cooper W.A., Heyn M.F., Kalyuzhnyi V.M., Kasilov S.V., Kernbichler W., Nemov V.V., Shafranov V.D., *"Optimization of N = 6 Helias-type stellarator"*, 28th EPS Conference on Controlled Fusion and Plasma Physics, Funchal, Madeira, Portugal, June 2001

Suttrop W.A. et al., Sauter O., *"High density performance ELMy H-mode plasmas in JET"*, invited talk at the 43rd APS meeting 2001

Valovic M. et al., Sauter O., *"Long time-scale desity peaking in JET"*, 28th EPS Conference on Controlled Fusion and Plasma Physics, Funchal, Madeira, Portugal, June 2001

Victoria M., *"Participation in, Gordon Research Conferences"*, Materials Processes far from Equilibrium, USA, July 2001

Victoria M., *"Requirements for a fusion irradiation facility"*, 7th General Meeting of the European Spallation Source, Graz, Austria, September 2001

Verhoeven A.G.A., Van Amerongen F.J., Elzendoorn B.S.Q., et al., Alberti S., Fasel D., Henderson M., Marmillod P., Tran M.Q., *"The ECRH system for JET-EP"*, IVEC 2001, 2-4 April 2001, Huis ter Duin, Noordwijk, The Netherlands

Verhoeven A.G.A., Van Amesungen F.J., Elzendoorn B.S.Q. et al., Alberti S., Fasel D., Henderson M., Marmillod P., Tran M.Q., *"The ECRH for JET –EP"*, 26th Int. Conf. On Infrared and Millimeter Waves, September 10-14, 2001 Toulouse, France

Yamazaki K., Tokar M., Funaba H., Peterson B.J., Noda N., Cooper W.A., Narushima Y., Sakakibara S., Watanabe K.Y., Yamada H., Tanaka K., Ida K., Narihara K., LHD Exp. Group, *"Plasma and impurity transport modeling of NBI-heated LHD and helical reactor systems"*, 28th EPS Conference on Controlled Fusion and Plasma Physics, Funchal, Madeira, Portugal, June 2001

Yao T., Schäublin R., Victoria M., *"The microstructure and tensile properties of pure Ni single crystal irradiated with high energy protons"*, 10th Int. Conference on Fusion Reactor Materials, Baden-Baden, Germany, October 2001

B.3 Seminars presented at the CRPP in 2001

Dr. R. Ganesh, Dept. of Electrical Eng. Pohang Univ. of Science & Technology, Pohang, South Korea, *"Statistical mechanics of two dimensional vortices"*

Dr. M. Brunetti, Dipt. Di Fisica, Univ. di Pisa, Italy, *"Long-time evolution of inviscid and Landau damping"*

Dr. P. Mantica, Ist. di Fisica del Plasma, ENEA-CNR, Milano, Italy, *"Heat convection and transport barriers in low magnetic shear Rijnhuizen tokamak project plasmas"*

Dr. J. Graves, School of Mathematical Sciences, Univ. of Nottingham, U.K., *"Kinetic internal kink meodes and sawteeth in JET"*

Dr. V. Andreev, Kurchatov Inst., Moscow, Russia, *"Reconstruction of the power deposition and transport* coefficients after ECRH switch-off (-on) from the solution of the inverse problem"

Dr. A. Fasoli, PSFC/MIT, Cambridge, USA, *"Laboratory observation of fast collisionless magnetic reconnection"*

Dr. A. Karpushov, Budker INP, Novosibirsk, Russia, *"Experimental model of the neutron source based on the gas dynamic trap concept"*

Dr. Ge Zhuang, DRFC-CEA, Cadarache, France, *"Electron beam penning trap and instantaneous spherical electron focus"*

Dr. H.P. Wagner, Inst. Supérieur de Technologie, Luxembourg, *"Coaxical plasma accelerators: From fusion technology and space propulsion to industrial processing"*

Dr. J. Carlsson, ORNL, Oak Ridge, USA, *"A backward Monte-Carlo method for parabolic equations"*

Dr. L. Porte, PSFC, MIT, Cambridge, USA, *"An overview of collective Thomson scattering on TEXTOR tokamak"*

Dr. L. Fattorini, Consorzio RFX, Assoc. EURATOM-ENEA, Padova, Italy, *"Reflectometry in magnetically confined plasmas"*

Prof. D. Larbalestrier, Appl. Superconductivity Center, Dept. of Materials Science and Engineering, Dept. of Physics, univ. of Wisconsin, USA, *" Materials issues in conductor design for power applications of superconductors"*

Dr. S. Zhang, Inst. of Plasma Physics, The Chinese Acad. of Sciences, Hefei, PR of China, *"Application of far-infrared and millimeter wave techniques in plasma diagnostics in the Hefei tokamaks"*

Prof. A. Kritz, DOE & Lehigh Univ., USA, *"The US national transport code collaboration (NTCC)"*

Dr. E. Nelson-Melby, PSFC, MIT, Cambridge, USA, *"Phase contrast imaging of ion Bernstein waves in ALCATOR C-mod"*

Dr. V. Shevchenko, UKAEA Technology, Culham sicnece Center, Abingdon, UK, *"Electron Bernstein wave studies on COMPASS-D and MAST"*

Dr. P. Gohil, General Atomics, San Diego, USA, *"Progress in advanced tokamak scenarios in DIII-D"*

Dr. J. Mlynar, CRPP, EPFL, *"Fast algorithm for tomography reconstruction and plasma position measurements"*

Dr. L. Laveder, Observatoire Côte d'Azur, Nice, France, *"Alfvén-wave filamentation and transverse turbulence in Hall-magnetohydrodynamics"*

Dr. S.M. Ahmed, Inst. For Plasma Research, Bhat, Gandhinagar, India*, "Kinetic energy distribution of h-atoms in e-H2 collisions"*

Dr. N.N. Gorelenkov, PPPL, Princeton, USA, *"Sawtooth stabilisation by beam ions in JET"*

Dr. G.A. Collins, Australian Nuclear Science and Technology Organisation (ANSTO) Australia, *"Engineering surfaces with plasmas"*

Prof. R. Boswell, Research School of Physical Sciences & Engineering, ANU, Canberra, Australia, *"Communication systems and the role of plasma processing"*

Dr. R.A. Pitts, CRPP, EPFL, *"First divertor and SOL physics results from 2001 pure helium campaign on EFDA-JET"*

Prof. G.M. Zaslavsky, Physics and Mathematics Dept., Univ. of New York, USA, *"What is anomalous transport? Why we need it? How to control it?"*

Dr. H. Reimerdes, CRPP, EPFL, *"MHD issues in the TCV tokamak"*

P. Crausaz, Ecole d'Ingénieurs du Canton de Neuchâtel, *"Traitement et caractérisation des surfaces"*

M. Podesta, Politecnico di Milano, Italy, *"Langmuir's probe measurements and modelling in front of the LH grill of the tokamak CASTOR"*

Dr. M-C. Firpo, Univ. degli Studi di Firenze – Facolta di Ing. – Dept. di Energhia "Sergio Stecco", Firenze, Italy, *"Interaction onde-particule et structures cohérentes"*

Dr. G.T. Hoang, DRFC/CEA, Cadarache France*, "Confinement et transport dans TORE SUPRA"*

A. Karpushov, CRPP, EPFL, *"Charge exchange neutral particle analysis (NPA-CX) Status and perspectives (Physical issues)"*

A. Boboc, Consorzio FRX/ENEA, Padova, Italy, *"Overview of polarimetric results at RFX and TCV"*

T. Kruml, DP – IGA/EPFL. *"Fatigue damage mechanisms in stainless steels"*

B. Schaerz, CRPP, EPFL, *"The effect of feedback controller on superconducting tokamak AC losses"*

Dr. V. Krivenski, DRFC-CEA, Cadarache, France, *"Distortion du corps de la fonction de distribution électronique pendant le chauffage cyclotronique électronique"*

Dr. A. Sushkov, RRC Kurchatov Inst. Moscow, Russia, *"Non-local response of the electron transport to ECRH"*

F.M. Poli, EURATOM-ENEA, CR Frascati, Roma, Italy, *"Runaway electrons in the FTU tokamak"*

Dr. D. Testa, MIT, Cambridge, USA, *"Recent results with the JET Alfvén Eigenmode active diagnostic system"*

J.-Y. Favez, CRPP, EPFL, *"Comparing TCV experimental VDE responses with DINA code simulations"*

B.4 Other external presentations in 2001

Appert K., Universität Greifswald, Greifswald, Germany, June 2001, *"Theoretische Fusionsplasmaphysik oder Der Zwiespalt zwischen Grundlagenforschung und Ingenieurwissenschaft"*

Baluc N., CNRS – Campus de Luminy, Marseille, France, June 2001, *"Mechanical behavior of icosahedral Al-Cu-Fe"*

Ballutaud J., Howling A.A., Sansonnens L., Hollenstein Ch., CTI* Monitoring Meeting held at CRPP, EPF-Lausanne, 17 May 2001, *"Investigation of layer uniformity in small gap PECVD reactor. First measurements of aSi:H layer density with ellipsometer and FTIR"*

Ballutaud J., Howling A.A., Sansonnens L., Hollenstein Ch., CTI Monitoring Meeting held at UNAXIS, Truebbach, 13 September 2001, *"Optimisation of intrinsic layer of aSi:H for solar cell, results on the influence of the depositoin rate on layer density. SIMS analysis on p layer-i layer structure to study the boron contamination of the intrinsic layer in single chamber process"*

Bottino A., CRPP Theory Group, Max-Planck-Institut für Plasmaphysik, Garching, Allemagne, June 2001, *"A global approach to the study of microinstabilities in experimental devices"*

*CTI = Commission pour la Technologie et l'Innovation

Cooper W.A., Fischer O., Haberhauer S., Mangili A., "Users' Day 2001", CSCS, Manno, Switzerland, September 2001, "Sphellamak reactor equilibrium, stability and confinement"

Delachaux T., Hollenstein Ch., Lévy F., Verdon C., Dinger R., CTI Monitoring Meeting held at CRPP, EPF-Lausanne, 19 January 2001, *"Développement d'une modélisation chimique de la décharge plasma"*

Delachaux T., Hollenstein Ch., Lévy F., Verdon C., Dinger R., CTI Monitoring Meeting held at CRPP, EPF-Lausanne, 18 April 2001, *"Synthèse des résultats sur la formatin de la couche ZrN et mise en activité du nouveau réacteur de taille industrielle dans nos laboratoires"*

Delachaux T., Hollenstein Ch., Lévy F., Verdon C., Dinger R., CTI Monitoring Meeting held at CRPP, EPF-Lausanne, 20 June 2001, *"Cause permettant la mise en évidence de la diffusion de l'azote dans t-ZrO2 et résultats des expériences effectuées sur le nouveau réacteur"*

Furno I., Los Alamos National Laboratory, Los Alamos, USA, January 2001, *"Sawtooth activity modification in ECH/ECCD experiments on TCV"*

Gindrat M., Dorier J.-L., Hollenstein Ch., CTI Monitoring Meeting held at CRPP, EPF-Lausanne, 21 February 2001, *"First measurements performed on the CRPP plasma torch: optical emission spectroscopy and imaging of an argon plasma jet for different pressures"*

Gindrat M., Dorier J.-L., Hollenstein Ch., CTI Monitoring Meeting held at Sulzer Metco, Wohlen, 26 June 2001, *"Imaging of the plasma jet performed on the CRPP plasma torch: the restrike effect and estimation of the jet velocity. Spectroscopic measurements of the plasma jet at Sulzer Metco for different spraying conditions"*

Gindrat M., Dorier J.-L., Hollenstein Ch., CTI Monitoring Meeting held at CRPP, EPF-Lausanne, 3 December 2001, *"Results of the enthalpy measurements campaign at Sulzer Metco: determination of the free-stream jet parameters (enthalpy, temperature, mach number and velocity) for different gases mixtures and pressures"*

Hollenstein Ch., Charles University, Faculty of Mathematics and Physics, Dep. of Macromolecular Physics, Praha, Czech Republic, May 2001, *"Plasmachemistry with special regard to IR spectroscopy"*

Hollenstein Ch., WE-Heraeus-Stiftung, Hanau, Germany, October 2001, (260. WE-Heraeus-Seminar), *"Dust formation in reative gases"*

Manini A., Max-Planck-Institut für Plasmaphysik, Garching, Germany, January 2001, *"Analysis of ECH sawoothing discharges for power deposition profile measurements on TCV"*

Marinucci C., *"Heating tests peformed on the 11th of September in TOSKA"*, 15th TFMC Test and Analysis Meeting, Cadarache, November 2001

Martin Y., *"Profession: physicien"*, Forum Horizon, Lausanne, Mars 2001

Sansonnens L., *"Modellisation of gas flow and chemistry in KAI type plasma reactor"*, Unaxis Palaiseau, France, January 2001

Sauter O. and TCV Team, Culham Science Center, UKAEA, UK, *"Steady-state fully non-inductive operation with ECCD and current profile control in the TCV tokamak"*

Victoria M., Dept. of Materials, Oxford University, Oxford, U.K., June 2001, *"The mechanisms of radiation hardening in pure metals and alloys"*

Victoria M., Paul-Scherrer-Institut, November 15, 2001, *"Towards radiation resistant materials"*

Wesche R., *"Characterisation of the NbTi Strands for the CONDOPT Experiment in SULTAN"*, From Strand Properties to Conductor Behaviour Meeting, Cadarache, March 2001

B.5 Conferences and meetings organised by the CRPP

ITER Expert Group Meeting on Confinement Database and Modelling, April 2 – 6, 2001, organised on the site of the EPFL. 21 participants attended the meeting. During this meeting participants presented their work done in the range of the activities attributed to the expert group. New contributions for the international LH threshold and H-mode confinement databases, new analyses performed on data from these databases and comparison of results obtained from different transport models were the main topics covered by these presentations. Some time was also left for further studies of the databases and the different models. Finally, a list of 'homeworks' was established.

EFDA-TCS Meeting, April 11, 2001, organised on the site of the EPFL. About 22 members attended the meeting.

ECW-CC Meetings, July 3-4, 2001, Chavannes-de-Bogis (near Geneva)
About 20 participants attended the meeting (12 + 8 from CRPP).
and
November 20-21, 2001 at the same place.
About 30 participants attended the meeting (18 + 12 from CRPP).

Meeting Association EURATOM – Confédération Suisse — CH-Industry, December 5, 2001, organised at the Kultur Casino, Bern. About 35 participtantes attended the meeting (+ 3 Aymar, Andreani, Rager) (+ 4 Tran, Conscience, Fasoli, Lister, Paris).

APPENDIX C External activities of CRPP Staff during 2001

C.1 National and international committees and ad-hoc groups

MEMBERSHIP

K. Appert	EFDA* JET Sub-Committee
A. Fasoli	EFDA* JET Sub-Committee
Ch. Hollenstein	Member of the "Conseil scientifique du Département Science pour l'Ingénieur du CNRS"
J.B. Lister	ITER MHD, Disruption and Control Expert Group
P.J. Paris	Member of the European Network Information Member of the ACP-EFDA board
R. Schäublin	Member of the board of the Swiss Society for optics and microscopy
M.Q. Tran	Electron Cyclotron Wave Task Area Leader Chairman of the Electron cyclotron Wave-Coordinating Committee Consultative Committee for the Euratom Specific Research and Training Programme in the field of Nuclear Energy, Fusion (CCE-FU) CCE-FU Special Working Group on "Possible joint implementation of ITER" CCE-FU Fusion Physics Committee EFDA* Steering Committee EFDA* Technology Sub-Committee Accelerator Driven System Working Group set-up by the Secretary of Science and Research
F. Troyon	Chairman of the JET-Council
G. Vecsey	SOFT Organising Committee International Magnet Technology Conference, Organizing Committee
M. Victoria	Chairman, Executive Committee IEA Fusion Material Agreements Chairman, IEA Modeling and Experimental Validation Collaboration Member, International Advisory Committee fo the Int. Conf. On Fusion Reactor Materials EFDA Task Coordinator on Modelling
L. Villard	CCE-FU Fusion Physics Committee Member of the "Conseil Scientifique du Département de Recherche sur la Fusion Contrôlée" – CEA - France
H. Weisen	Member of the International Advisory Board of the IPP Prague, Czech Republic

PARTICIPATION

R. Behn	Working group on Thomson Scattering, EFDA-JET

* EFDA: European Fusion Development Agreement

B. Duval	Remote Participation Users Group, EFDA-JET
J.B. Lister	EU Domestic Assessment ad hoc group of ITER-FEAT Ad hoc group for FTU-D
Y.R. Martin	ITER Confinement Database and Modelling Expert Group
O. Sauter	ITER Physics Expert Group on MHD, Disruption and Control
M. Q. Tran	Selection Committee of the IAEA 3rd TCM on Steady State Operation of magnetic fusion devices
H. Weisen	Edge and Pedestal Physics Expert Group
C. Marinucci	ITER TFMC Test and Analysis Group

C.2 Editorial and society boards

S. Alberti	Member of the Committee of the SSP (Swiss Physical Society) Responsible for Applied Physics
Ch. Hollenstein	Vice President of the Swiss Vacuum Society Member of the Committee URSI (Union Radio-Scientifique Internationale) Member of the Editorial Board of Plasma Chemistry and Plasma Processing
J.B. Lister	Member of the Editorial Board of Plasma Physics and Controlled Fusion Vice President of the European Physical Society Plasma Physics Division Board and representative of this board at the APS
C. Marinucci	Guest Editor of Proceedings of CHATS-Y2K Workshop
Y.R. Martin	Chairman of the AVCP (Association Vaudoise des Chercheurs en Physique)
P.J. Paris	Project Manager : Interactive Model of ITER and start of Fusion Power Plant Virtual Reality Member of the Fusion Expo Consortium Committee Chairman of IASEN (Int. Association of Specialists on Energy) Member of the FRE Committee (Fédération Romande de l'Energie)
M.Q. Tran	Member of the Board of Editors of Nuclear Fusion
M. Victoria	Invited Editor, J. Nucl. Materials

C.3 EPFL committees and commissions

K. Appert	Commission d'Informatique, EPFL
Ch. Hollenstein	Commission de Recherche du Département de Physique, EPFL
X. Llobet	Commission Technique d'Informatique , EPFL
L. Villard	Commission d'Enseignement du Département de Physique, EPFL
H. Weisen	Commission de Recherche du Département de Physique, EPFL

APPENDIX D

D.1 Lausanne Reports (LRP)

Alberti S., Goodman T.P., Henderson M.A., Manini A., Moret J.-M., Gomez P., Blanchard P., Coda S., Sauter O., and the TCV Team, *"Full absorption of 3rd harmonic ECH in TCV target plasmas produced by 2nd harmonic ECH and ECCD"*
LRP 691/01

Angioni C., *"Modelling of electron transport and of sawtooth activity in tokamaks"*, (thèse EPFL No. 2669(2001))
LRP 709/01

Angioni C., Pochelon A., Gorelenkov N.N., McClements K.G, Sauter O., Budny R.V., de Vries P.C., Howell D.F., Mantsinen M., Nave M.F.F., Sharapov S.E., & contributors to the EFDA-JET workprogramme, *"Neutral beam stabilization of sawtooth oscillations in JET"*
LRP 705/01

Bruzzone P., Editor, *"Segregated Copper Ratio Experiment on Transient Stability (SeCRETS) - EU Task M29 / ITER Task N11TT03, Final Report"*
LRP 689/01

Cooper W.A., Okamura S., Yamazaki K., *"Effect of toroidal current and profile on ballooning instability mechanisms in a quasiaxisymmetric stellarator"*
LRP 696/01

Degeling A., Martin Y.R., Bak P.E., Lister J.B., Llobet X., "*Dynamics of edge localised modes in the TCV"*
LRP 699/01

Dorier J.-L., Gindrat M., Hollenstein Ch., Loch M., Refke A., Salito A., Barbezat G., *"Plasma Jet properties in a new spraying process at low pressure for large area thin film deposition"*, Presented at the ITSC 2001, International Thermal Spray Conference, Singapore, 28-30 May 2001
LRP 690/01

EPS Participants, Papers presented at the 28th EPS Conference on Controlled Fusion and Plasma Physics, Funchal, Madeira, Portugal, June 2001
LRP 698/01

Favez J.-Y., Khayrutdinov R.R., Lister J.B., Lukash V.E., *"Comparing TCV experimental VDE responses with DINA code simulations"*
LRP 707/01

Fischer O., *"The behaviour of magnetic field lines and drifts in 3D configurations"*, (Thèse EPFL No. 2380(2001))
LRP 693/01

Fischer O., Cooper W.A., Isaev M.Yu, Villard L., *"Neoclassical transport and alpha-particle confinement in novel 3D reactor systems"*
LRP 694/01

Furno I., *"Fast transient transport phenomena measured by soft X-ray emission in TCV tokamak plasmas"* (thèse EPFL 2434 (2001)
LRP 703/01

Gindrat M., Dorier J.-L., Hollenstein Ch., Loch M., Refke A., Salito A., Barbezat G., *"Effect of specific operating conditions on the properties of LPPS plasma jets expanding at low pressure"*
LRP 712/01

Hofmann F., Furno I., Gersasimov S., Martin Y., Milani F., Nave M.F.F., Reimerdes H., Sartori F., Sauter O., *"Effect of ELMs on the measurement of vertical plasma position in TCV and JET*"
LRP 702/01

Jodoin B., Gindrat M., Dorier J.-L., Hollenstein Ch., Loch M., Barbezat G., *"Modelling and diagnostics of a supersonic DC plasma jet expanding at low pressure"*
LRP 713/01

Klinger L., Vos J.B., Appert K., *"Gradient evaluation on general structured hexahedral meshes using isoparametric transforms"*
LRP 704/01

Lister J.B., Sharma A., Limebeer D.J.N., Nakamura Y., Wainwright J.P., Yoshino R., *"Plasma equilibrium response modelling and validation on JT-60U"*
LRP 680/00

Magni D., *"Etude des plasmas organosiliciés dilués en oxygène utilisés pour la déposition d'oxyde de Silicium"*, (Thèse EPFL 2461(2001))
LRP 706/01

Manini A., Moret J.-M., Alberti S., Goodman T.P., Henderson M.A., "Modulated ECH power absorption measurements using a diamagnetic loop in the TCV tokamak"
LRP 708/01

Marmy P, Leguey T., Belianov I., Sauder M., Brütsch R., *"ITER TASK BL 14.2: Titanium Alloys Irradiation Testing., Final Report on "The tensile and fatigue behavior of the titanium alloys Ti6Al4V and Ti5A12.4Sn before and after irradiation with protons to doses up to 0.3 dpa"*
LRP 695/01

Mlynar J., *"TCV DNBI profile and attenuation studies with Code Manual"*
LRP 692/01

Mlynar J., Shukaev A.N., Bosshard P., Duval B.P., Ivanov A.A., Kollegov M., Kolmogorov V.V., Llobet X., Pitts R.A., Weisen H., *"Diagnostics Neutral Beam Injector at the TCV tokamak"*
LRP 710/01

Pochelon A., Hofmann F., Reimerdes H., Angioni C., Behn R., Duquerroy R., Furno I., Goodman T.P., Gomez P.,Henderson M.A., Martynov A., Nikkola P., Sauter O., Sushkov A., *"Plasma shape effects on sawtooth/internal kink stability and plasma shaping using EC wave current profile tailoring in TCV, 18th IAEA Fusion Energy Conference, Sorrento, Italy, October 2000"*
LRP 697/01

Reimerdes H., *"MHD stability limits in the TCV tokamak"*, (Thèse EPFL: 2399(01))
LRP 700/01

Reimerdes H., Sauter O., Goodman T., Pochelon A., *"From current driven to neoclassically driven tearing modes"*
LRP 716/01

Schärz B., Bruzzone P., Favez J.-Y., Lister J.B., Zapretilina E., *"The effect of the feedback controller on superconducting tokamak AC losses, + AC-CRPP user manual"*
LRP 714/01

Sharma A.S., Limebeer D.J.N., Jaimoukha I.M., Lister J.B., *"Modelling and control of TCV"*
LRP 715/01

Villard L., Bottino A., Vaclavik J., *"Radial electric fields and global electrostatic microinstabilities in tokamaks and stellarators"*
LRP 711/01

Weisen H., Furno I., Alberti S. and the TCV Team, *"Shape dependence of Sawtooth inversion radii and profile peaking factors in TCV L-mode plasmas"*
LRP 701/01

D.2 Internal Reports (INT)

Bosshard P., *"Présentation et étude des performances du diagnostic CXRS sur TCV"*
INT 201/01

Hofmann F., Isoz P.-F., Moret J.-M., *"Hard-wired coil protection in TCV"*
INT 202/01

Howling A.A., *"Interference, reflectance & transmittance for thin films"*
INT 203/01

APPENDIX E The basis of controlled fusion

E.1 Fusion as a sustainable energy source

Research into controlled fusion aims to demonstrate that it is a valid option for generating power in the long term future in an environmentally, politically and economically acceptable way. Controlled fusion is a process in which light nuclei fuse together to form heavier ones: during this process a very large amount of energy is released. For a fusion reactor it is planned to use the two isotopes of hydrogen: deuterium (D) and tritium (T), which fuse together much more readily than any other combination of light nuclei according to the following reaction:

$$D^2 + T^3 \rightarrow He^4 + n + 17.6MeV$$

The end products are helium and neutrons (n). The total energy liberated by fusing one gram of a 50:50% mixture of deuterium and tritium is 94000kWh, which is 10 million times more than from the same mass of oil. 80% of this energy is carried by the neutrons with an energy of 14MeV while the remaining 20% is carried by the helium nucleus. All this energy eventually becomes heat to be stored or converted by conventional means into electricity.

The temperature at which fusion reactions start to become significant are above a few tens of millions of degrees. For the D-T reaction, the optimal temperature is of the order of 70-200 million degrees. At such temperatures the D-T fuel is in the plasma state.

Deuterium is very abundant on the earth and can be extracted from water (0.034g/l). Tritium does not occur naturally, since its half-life is only 12.3 years, but it can be regenerated from lithium using the neutrons produced by the D-T fusion reactions. The two isotopes of natural lithium contribute to this breeding of tritium according to the reactions:

$$Li^6 + n \rightarrow He^4 + T^3 + 4.8MeV$$

$$Li^7 + n \rightarrow He^4 + T^3 + n - 2.5MeV$$

The relative abundance of the two lithium isotopes Li^6 and Li^7 are 7.4% and 92.6%, respectively. The known geological resources of lithium both in the earth and in the sea water are large enough to provide energy in an unlimited time.

E.2 Attractiveness of fusion as an energy source

The inherent advantages of fusion as an energy source are:

- The fuels are plentiful and their costs are negligible because of the enormous energy yield of the reaction;
- The end product of the reaction is helium, an inert gas;
- No chain reaction is possible; at any time only a very small amount of fuel is in the reacting chamber and any malfunction would cause an immediate drop of temperature and the reaction would stop;
- No after-heat problem can lead to thermal runaway;

- None of the materials required by a fusion power plant are subject to the provisions of the non-proliferation treaties.

Its further potential advantages are:

- Radioactivity of the reactor structure, caused by neutrons, can be minimised by careful selection of low-activation materials resulting in a manageable quantity of long lived radioactive waste;
- The release of tritium in normal operation can be kept to a very low level. The inventory of tritium in the breeding section of the reactor and on the site can be sufficiently small so that the worst possible accident could not lead to a harmful release to the environment requiring evacuation of the nearby population.

APPENDIX F Glossary

The following is a general purpose glossary for the field of controlled fusion and plasma physics.

Additional heating: Usually with reference to a plasma which is initially heated by a toroidal current induced in the plasma (ohmic heating), additional heating designates other means of heating a plasma (absorption of electromagnetic waves or of injected fast neutral particles).

Advanced Tokamak Scenarios: Tokamaks normally generate natural profiles of plasma current and plasma pressure. Using external non-inductive current drive and local control of the current and pressure profiles can allow access to enhanced regimes and even steady state operation, generally referred to as Advanced Tokamak Scenarios.

ALCATOR C-MOD: High field, high density tokamak at MIT (USA) with an elongated, diverted plasma.

Alfvén gap modes: The toroidal nature of tokamak plasmas produces gaps in the otherwise continuous spectrum of Alfvén waves, populated by discrete, weakly damped Alfvén gap modes. Under certain conditions these modes can be destabilised by resonant energy transfer from energetic particles, e.g. α-particles from fusion reactions.

Alfvén waves: A fundamental plasma wave, which is primarily magneto-hydrodynamic in character with an oscillation of the magnetic field and, in some cases, plasma pressure. In tokamaks, these waves are typically strongly damped. See also fast Alfvén wave.

Alfvén velocity: The velocity of propagation of Alfvén waves in the direction of the magnetic field; it is proportional to the magnetic field strength, and inversely proportional to the square root of the mass density.

alpha particle, or α-particle He^4: The nucleus of the helium atom, composed of two protons and two neutrons, is one of the two products of the DT fusion reaction (the other one is a neutron). The α-particles, being electrically charged, are trapped by the magnetic confinement field and therefore can release their energy to the plasma contrary to the neutrons which escape from the plasma and transfer their energy in the blanket surrounding the plasma core. The plasma heating which is provided by these α-particles as they slow down due to collisions is essential for achieving ignition.

Alternative lines: Magnetic confinement development other than the tokamak.

Analytic/Computational modelling: Analytic: algebraic solution of basic equations. Computational: numerical solution of basic equations.

Anomalous transport: Measured heat and particle loss is anomalously large compared with collisional theory of heat transport in toroidal plasmas.

ASDEX-Upgrade: Medium-sized Tokamak at Garching (Association Euratom-IPP, Germany) with an elongated, diverted plasma.

Aspect ratio: The ratio between the large radius and the small radius of a torus.

Auxiliary heating: See additional heating.

Ballooning instability: A local instability which can develop in the tokamak when the plasma pressure exceeds a critical value; it therefore constrains the maximum β that can be achieved. It is analogous to the unstable bulge which develops on an over-inflated tyre.

Beta (β): Ratio of plasma pressure to magnetic field pressure. One of the figures of merit for magnetic confinement: the magnitude of the magnetic field pressure determine the cost of the field coil that generates it; since fusion reactivity increases with the square of the plasma pressure, a high value of ß indicates good performance. The highest values achieved in tokamaks reach 40% (START).

Beta-normalised (β_N): The ratio of plasma current (in MA) to the product of minor radius (in m) and magnetic field (in T) characterises the limit to the achievable β imposed by ideal MHD. Beta-normalised is the ratio of β (as a percentage) to the above

ideal MHD parameter. Generally β_N ~3 should be achievable, but techniques for obtaining higher values have been observed experimentally.

Blanket: A structure containing lithium or lithium compounds surrounding the plasma core of a fusion reactor. Its functions are to breed tritium, via lithium-neutron reactions, and to absorb most of the fusion energy to be used for electricity generation.

Bootstrap current: Theory developed in 1970 predicted that a toroidal electric current will flow in a tokamak which is fuelled by energy and particle sources that replace diffusive losses. This diffusion driven "Bootstrap current", which is proportional to β and flows even in the absence of an applied voltage, could be used to provide the poloidal magnetic field: hence the concept of a Bootstrap tokamak, which has no toroidal voltage. A Bootstrap current consistent with theory was observed many years later on JET and TFTR; it now plays a role in optimising advanced tokamaks.

Breakeven: The fusion performance of a power plant is denoted by Q, which is the ratio of the power released by fusion reactions to that used to heat the plasma. As a convention, scientific breakeven corresponds to Q=1 and ignition to Q=infinity. A fusion power plant would operate at Q~50.

Breeding ratio: The number of tritium atoms produced in the blanket of a fusion power station per tritium nucleus burned in the fusion plasma.

Burn: The fusion process of consuming DT fuel in a reactor, releasing energy.

CCE-FU: The Consultative Committee for the Euratom Specific Research and Training Programme in the field of Nuclear Energy, Fusion. Formerly the CCFP.

CEA: Commissariat à l'Energie Atomique, France. Partner in the Association EURATOM-CEA which operates the TORE SUPRA tokamak.

CFI: Committee on Fusion-Industry.

Charge exchange measurement: Measures the plasma ion temperature. Neutral atoms in the plasma (for example from a neutral beam) donate electrons to hot plasma ions, which are thereby neutralised. These hot atoms are no longer confined by the magnetic field and leave the plasma. Their energy is measured by a neutral particle analyser.

CIEMAT: Centro de Investigaciones Energéticas Medioambientales y Tecnológicas, Spain. Partner in the Association EURATOM-CIEMAT. Operates the flexible heliac stellarator TJ-II.

Classical transport: Collisions between the individual particles of a plasma allow them to move across the magnetic field. Theories which describe this mechanism are called "classical" (or "neo-classical" when additional effects due to the toroidal geometry are included). The measured heat and particle transport is usually higher than predicted by these theories.

Collisionality: Non-dimensional parameter, which is the inverse ratio of the mean free path of plasma particles between collisions to a characteristic length of the magnetic field configuration.

Compact torus: Class of closed magnetic configurations in which no material elements (coils, conductors or walls) need to link through the bore of the plasma torus. Thus the vessel of compact tori can be spherical or cylindrical.

COMPASS: COMPact ASSembly, a tokamak for studies of plasma stability, at Culham, UK (Association EURATOM-UKAEA). Originally with circular vessel (COMPASS-C), now with D-shaped vessel (COMPASS-D).

Confinement time: In a fusion plasma neither particles nor energy are perfectly confined. Particle confinement time is the time during which the particles, on average, stay confined. The energy confinement time, which is usually shorter than the particle confinement time, is defined in steady state as the ratio of the plasma energy content to the total power input to the plasma and is a measure of how fast a plasma would cool if there were no heating.

CRPP: Centre de Recherches en Physique des Plasmas. Fusion laboratories of the Association EURATOM-Swiss Confederation at the Ecole Polytechnique Fédérale de Lausanne and the Paul-Scherrer Institute, Villigen (CRPP-Fusion Technology).

Current drive (non-inductive): In a tokamak, plasma current can be driven inductively, with the toroidal plasma acting as a secondary winding of a transformer whose primary coil is at the central column of the device. Continuous current cannot be driven by transformer action. 'Non-inductive' current drive methods are applied either by injecting particles with directed momentum into the plasma or by accelerating electrons by electromagnetic waves so that they carry the current. Also being applied to control instabilities and to optimise confinement by modifying the current profile. The bootstrap effect also drives current.

Current profile (current distribution): The distribution of current density across the minor radius of the plasma.

Current ramp-up (down): The increase (decrease) of plasma current either at the start of operation or during operation.

Cyclotron frequency: Charged particles in a magnetic field have a natural frequency of gyration in the plane perpendicular to the magnetic field - the cyclotron frequency. For electrons in a tokamak, the cyclotron frequency is typically a few tens of GHz (28 GHz per Tesla), and for ions, a few tens of MHz (7.5 MHz per Tesla for deuterium).

Cylindrical approximation: An approximation to the true tokamak geometry in which the torus is straightened, so that the toroidal direction becomes the cylinder axis. There are two directions of symmetry: along the axis (the 'toroidal' direction) and about the axis (the 'poloidal' direction).

DCU: Dublin City University, Ireland. Partner in the Association EURATOM-DCU.

DEMO: Demonstration Reactor (the first device in the European fusion strategy intended to produce significant amounts of electricity).

Deuterium: A stable isotope of hydrogen, whose nucleus contains one proton and one neutron. In heavy water, normal hydrogen is replaced by deuterium. Sea water contains, on average, 34g deuterium per m^3. Deuterium plasmas are used routinely in present-day experiments; in a fusion power plant the plasma will consist of a mixture of deuterium and tritium which fuse more readily then two deuterium nuclei.

DG Research (DG RTD): The Directorate-General of the European Commission, Brussels, responsible for Research and Development**.** Formerly DG XII.

Diagnostic: Apparatus used for measuring one or more plasma quantities (temperature, density, current, etc.).

Diffusion, thermal (or particle): The random flow of heat (or particles) in the presence of a thermal (or density) gradient.

DIII-D: The largest operating US tokamak, run by General Atomics, San Diego. It has a flexible configuration and studies core and divertor physics with intense additional heating.

D-He^3: Deuterium-^{3}Helium: A potential fuel for fusion with low release of neutrons, but which would require a much higher fusion triple product ($nT\tau$) than DT to reach ignition. ^{3}Helium is an isotope of helium which is not available in appreciable quantities on Earth.

Disruption, Disruptive instability: A complex phenomenon involving MHD instability which results in a rapid release of energy to the wall and strong electromechanical forces in a tokamak. Plasma control may be lost, triggering a VDE (q.v.). This phenomenon places a limit on the maximum density, pressure and current in a tokamak.

Distribution function: Describes both the space and velocity distribution of plasma particles.

Divertor: A magnetic field configuration with a separatrix, affecting the edge of the confinement region, designed to remove heat and particles from the plasma, i.e. divert impurities and helium ash to divertor plates in a target chamber. Alternative to using a limiter to define the plasma edge.

Double null: See Single/double null divertors.

Drift kinetic theory: Kinetic theory which describes plasma processes which have spatial scales much greater than the particle Larmor radii.

Drift orbits: Particle motion is tied to straight magnetic field lines. However, electric fields and gradients of the magnetic field give an additional drift perpendicular

to the magnetic field creating drift surfaces displaced from the magnetic surfaces.

Driven current: Plasma current produced by a means external to the plasma, inductively or non-inductively.

Driver: In inertial confinement fusion, the laser or particle beam system used to compress a target pellet.

DTE: The deuterium-tritium experiment at JET which in 1997 set new records for fusion power production. Followed the Preliminary Tritium Experiment of 1991.

ECCD: Electron Cyclotron Current Drive. Non-inductive current drive technique using directed electron cyclotron resonance waves.

ECE: Electron Cyclotron Emission. Radiation emitted by electrons as a result of their cyclotron motion around magnetic field lines. Used to measure electron temperature.

ECH: Electron-Cyclotron Heating. Radio wave heating near the resonance frequency (or its multiple) of the electron gyration in a magnetic field. In present and future machines ECH is at typically 60-170 GHz, depending on the magnetic field strength in a machine.

EFDA: European Fusion Development Agreement. The new organisational framework of the EU fusion activities on the exploitation of the JET Facilities, international collaboration (including ITER) and supporting technology. EFDA replaces the NET agreement.

EFET: European Fusion Engineering & Technology: a fusion technology oriented European Economic Interest Grouping.

Electron temperature: A measure of electron thermal energy in units of degrees or electron volts (1 eV ~ 10^4 degrees Kelvin).

ELM: Edge localised mode. An instability which occurs in short periodic bursts during the H-mode in divertor tokamaks. It modulates and enhances the energy and particle transport at the plasma edge. These transient heat and particle losses could be damaging in a reactor.

ENEA: Ente per le Nuove Tecnologie, l'Energia e l'Ambiente, Italy. Partner in the Association EURATOM-ENEA.

Energetic particle: In terms of energy, the particles in a plasma can be divided into two classes. The more numerous thermal particles are characterised by a temperature typically in the range 1-30 keV for modern tokamaks. The less numerous class of energetic particles has significantly higher energy up to several MeV. Energetic particles can be created by electric fields, fusion reactions, neutral beam injection or RF heating.

Error fields: The magnetic coils of a tokamak are designed to give the desired magnetic field configuration. The finite number of coils and imperfections in their construction lead to unwanted deviations from this configuration known as error fields. These could lead to disruptions and are of particular concern for larger tokamaks.

EXTRAP T-II: External Trap II, a medium-sized reversed field pinch (RFP) at the Royal Institute of Technology, Stockholm (Association EURATOM-NFR), built for RFP transport and shell stabilisation studies in support of RFX.

EURATOM: European Atomic Energy Community.

Faraday rotation: The rotation of the plane of polarisation of light passing through a magnetised plasma.

Fast Alfvén wave: The fast Alfvén wave exists over a broad frequency spectrum, from the ion cyclotron range of frequencies (ICRF) where its character is electromagnetic, down to magnetohydrodynamic frequencies. Its velocity is comparable to the Alfvén velocity. The fast Alfvén wave is used routinely for high-power (~20MW) ICRF heating on JET, as it is efficiently absorbed in the plasma by the mechanism of ion cyclotron resonance. Although usually stable in tokamaks, the wave can be excited by energetic ion populations.

Fast wave current drive: Current drive produced by a fast wave. The wave can penetrate the plasma more easily than a lower hybrid wave.

Feedback: Use of measurements of plasma parameters to control the parameters, shape or profiles of the plasma to obtain desired conditions.

Field lines, Flux surfaces: Imaginary lines marking the direction of a force field. In a

tokamak these define a set of nested toroidal surfaces, to which particles are approximately constrained, known as flux surfaces.

Field reversed configuration: A compact torus with a strongly elongated plasma. The plasma is contained in a cylindrical vessel inside a straight solenoid. The confining magnetic field usually has only a poloidal component. Not to be confused with reversed field pinch.

FIR: Far infra-red (e.g. wavelength ~ 0.2 to 1mm). FIR lasers are used to measure the magnetic field and plasma density.

"**Fishbones**": Rapid bursts of MHD activity sometimes observed when neutral beam heating is used in tokamaks (fishbone refers to the shape of the bursts in oscillating magnetic field when plotted as a function of time).

First wall: The first material boundary that surrounds the plasma. Today, the first wall in all machines is protected by low-Z materials (such as carbon tiles, boron or beryllium coating).

Flat-top current: Constant current during quasi-stationary operating conditions.

Fokker-Planck Code: A computer code to calculate the velocity distribution of plasma particles allowing for collisional relaxation and plasma heating. Calculates distribution functions (q.v.).

FOM: Stichting voor Fundamenteel Onderzoek der Materie (Foundation for basic investigations of matter), The Netherlands. Partner in the Association EURATOM-FOM.

FPC: The Fusion Physics Committee, a sub-committee of the CCE-FU which reports to it principally on the physics aspects of the programme. Formerly the Programme Committee (PC).

FTC: The Fusion Technology Committee, a sub-committee of the CCE-FU which reports to it principally on strategic issues.

FTU: Frascati Tokamak Upgrade, a high density, high current tokamak at Frascati, Italy (Association EURATOM-ENEA).

Fusion triple product: Product of (ion) density, (ion) temperature and energy confinement time. A measure of the proximity to break-even and ignition.

Fusion product: The product of a fusion reaction, for example an α-particle or neutron in a deuterium-tritium plasma.

Fusion reactivity: Fusion reaction rate. For present typical tokamak conditions, it increases with the square of the density and the ion temperature of the plasma.

Full wave theory: Wave theory which includes complete accounting of wave energy (transmitted, reflected and absorbed, including energy transferred to other waves) for studying RF heating.

FZK: Forschungszentrum Karlsruhe, Germany. Partner in the Association EURATOM-FZK, active in fusion technology and, with the development of gyrotrons, in plasma engineering.

FZJ: Forschungszentrum Jülich GmbH, Germany. Partner in the Association EURATOM-FZJ, operating the tokamak TEXTOR.

GSI: Gesellschaft für Schwerionenforschung, Darmstadt, Germany. Studying heavy-ion physics, and driver physics with possible application for inertial confinement fusion.

Gyro-kinetic theory: Version of kinetic theory in which the Larmor radius is not assumed to be small. An essential theory for investigating fine-scale instabilities which might be responsible for driving turbulence, which may in turn be responsible for anomalous transport.

Gyrotron: Device used for generating high power microwaves in the electron cyclotron range of frequencies (50 - 200 GHz). This UHF wave is mostly used to heat the plasma at the electron cyclotron resonance frequency. It also could be used to diagnose the plasma.

Heliac: Stellarator configuration with a central toroidal coil around which the plasma column is wound helically. Because of its high capability of investigating a wide range of stellarator configurations, it is used for TJ-II.

Helias: Optimised stellarator configuration, used with modular coils for Wendelstein VII-X (Germany) and SHEILA (Australia).

H-mode: A High confinement regime that has been observed in tokamak plasmas. It

develops when a tokamak plasma is heated above a characteristic power threshold, which increases with density, magnetic field and machine size. It is characterised by a sharp temperature gradient near the edge (resulting in an edge "temperature pedestal"), ELMs and typically a doubling of the energy confinement time compared to the normal "L" regime. Today, a variety of high confinement modes have been identified in divertor and in limiter configurations (e.g. the I-mode), which, in part, have been obtained by special tailoring of the radial plasma current profile.

H-transition (or L-to-H transition): Transition into the H-regime from the L-regime, usually quite sudden, at a certain threshold power of additional heating and specific plasma parameters.

Halo currents: See Vertical Displacement Event.

Helicity injection: The helicity of a toroidal plasma is related to a linkage of toroidal and poloidal magnetic fluxes, and is approximately conserved throughout a discharge. If additional helicity can be injected, the plasma current could be sustained or even increased.

Helium ash: Fusion reactions in a deuterium-tritium plasma produce energetic α-particles (helium nuclei), which heat the plasma as they slow down. Once this has happened, the α-particles have no further use: they constitute helium ash, which dilutes the fuel and must be removed to maintain a burning plasma.

High beta (β): Condition in which the plasma energy is a significant fraction of the energy in the magnetic field. An alternative measure is the ratio between the plasma energy and the energy in the poloidal magnetic field, the poloidal β.

High field ECH launch: Electron cyclotron waves can be launched from the inside of the plasma torus. This allows higher density plasma to be heated.

Hydrogen: The lightest element; the nucleus consists of only one proton, the atomic shell of one electron. Isotopes of hydrogen, with one or two additional neutrons in the nucleus, are deuterium and tritium respectively.

IAEA: International Atomic Energy Agency (of the United Nations), Vienna, Austria. The ITER-EDA is undertaken under the auspices of the IAEA.

ICE: Ion Cyclotron Emission. Observed in JET and TFTR as a suprathermal signal, apparently driven by collective instability of energetic ion populations such as fusion products and injected beam ions.

ICF: Inertial Confinement Fusion. Intense beams of laser light or light or heavy ion beams are used to compress very rapidly and heat tiny target pellets of fusion fuel to initiate fusion burn in the centre. Sufficient fusion reactions must occur in the very short time before the fuel expands under its own pressure. The inertia of the pellet's own mass determines the time scale during which fusion reactions occur, hence the name inertial confinement.

ICRH: Ion Cyclotron Resonance Heating by launching waves into the plasma in the range of the ion cyclotron frequency (radio frequency, typically at several tens of MHz).

ICRF: Ion Cyclotron Resonance Frequencies.

Ideal: In the context of MHD, 'ideal' implies that the magnetic field and the plasma always move together. For this to occur, the electrical resistivity of the plasma must be negligible.

Ideal internal kink modes: An MHD instability of the central region of a tokamak. This, or its close relative the resistive internal kink mode, may be involved in the Sawtooth disruptions which occur in most Tokamaks.

IEA: International Energy Agency (of the OECD), Paris, France. Implementing agreements for international collaboration on specific topics in fusion have been set up in the frame of the IEA.

Ignition condition: Condition for self-sustaining fusion reactions: heat provided by fusion α-particles replaces the total heat losses. External sources of plasma heating are no longer necessary and the fusion reaction is self-sustaining. Ignition is not required for energy gain in a power station. Retaining a level of external heating or current drive will be required to control the plasma pressure and current profiles, to optimise the performance, leading to a so-called "driven burn".

Impurities: Ions, other than the basic plasma ion species, which are unwanted as they lose energy by radiation and dilute the plasma.

Impurity screening: The prevention of impurities from entering the plasma.

Internal kink: A type of MHD instability that can occur within the central region of the plasma (where q < 1) reducing the peak temperature and density.

Internal Reconnection Event (IRE): An instability which breaks magnetic field lines and reconnects them with a different topology to reduce the system to a lower energy state - associated with the operating limits of spherical tokamaks.

Ion Bernstein wave: A wave which only exists in a hot plasma and is supported by the ions. It propagates at right angles to the magnetic field, when it is undamped, at harmonics of the ion cyclotron frequency. There is also an electron Bernstein wave which propagates at harmonics of the electron cyclotron frequency.

Ion Cyclotron Current Drive (ICCD): Non-inductive current drive using ICRH.

Ion Cyclotron Resonance Heating (ICRH) / Ion Cyclotron Resonance Frequencies (ICRF): Additional heating method using RF waves at frequencies (~ 20-50 MHz) matching the frequency at which ions gyrate around the magnetic field lines.

IPP: Max-Planck-Institut für Plasmaphysik, Garching, Germany. Partner in the Association EURATOM-IPP, operating the tokamak ASDEX-Upgrade and the stellarator Wendelstein VII-AS. Also has sites in Berlin and in Greifswald, where the construction of the large superconducting stellarator Wendelstein VII-X is in progress.

IR: Infra Red part of the electromagnetic spectrum.

IRE: Internal Reconnection Event.

IST: Instituto Superior Técnico, Portugal. Partner in the Association EURATOM-IST.

ISTTOK: Tokamak, for study of non-inductive current drive, at the Instituto Superior Técnico (IST), Lisbon, Portugal.

ITER: International Thermonuclear Experimental Reactor (the next step as a collaboration between EURATOM, Japan, the Russian Federation and originally the USA, under the auspices of the IAEA). After a conceptual design phase - CDA (1988-1990), and engineering design activities (ITER-EDA, 1992-2001), now under the Coordinated Technical Activities (CTA). TAC, Technical Advisory Committee. See also Next Step.

JAEC: Japan Atomic Energy Commission, Tokyo, Japan.

JAERI: Japan Atomic Energy Research Institute. Headquarters in Tokyo, Japan.

JET: Joint European Torus. The largest tokamak in the world, sited at Abingdon, UK. Operated as a Joint Undertaking (JET Joint Undertaking), until the end of 1999. The scientific exploitation of the JET facilities is now guaranteed by the Euratom fusion Associations within the EFDA framework. The operation of the facility is the responsibility of the Association Euratom-UKAEA.

JT-60U: Japanese tokamak at Naka. The largest Japanese tokamak and second largest operating experiment after JET, but not designed for use with D-T fuel.

keV: Kilo-electronvolt. Energy which an electron acquires passing a voltage difference of 1000 volts. Also used to measure the temperature of a plasma (1 keV corresponds to 11.8 million degrees Kelvin).

Kinetic instability: Oscillation which is unstable as a result of the energy distribution of ions or electrons.

Kinetic theory: A detailed mathematical model of a plasma in which trajectories of electrons and ions are described. More complex than fluid and two-fluid theories, it is necessary in the study of RF heating and some instabilities, particularly when energetic particles are involved.

L-H transition: Change from L regime to H regime (usually quite sudden).

L-mode: As opposed to the H mode. Regime with degradation of confinement, in additionally heated plasmas, with respect to plasmas heated ohmically by the plasma current.

Langmuir probe: Electrical probe inserted into the edge of a plasma for measurements of density, temperature and electric potential.

Larmor radius: Radius of the gyratory motion of particles around magnetic field lines.

Large scale ideal modes: A large scale mode has a wavelength which is a significant fraction of the plasma dimensions and assumes ideal MHD.

Laser ablation: Use of lasers to produce a sudden influx of impurities into the plasma from a solid surface.

Last closed flux surface: The boundary separating those magnetic field lines that intersect the wall (open lines) from the magnetic field lines that never intersect the wall (closed lines).

Lawson criterion: The value of the confinement time multiplied by the ion density (at the required temperature) which must be exceeded in a fusion reactor to reach ignition.

Limiter: A material surface within the tokamak vessel which defines the edge of the plasma and thus avoids contact between the plasma and the vessel. A pumped limiter can also be used to remove heat and particles and is an alternative exhaust system to the divertor.

LLNL: Lawrence Livermore National Laboratory, Livermore, USA.

Locked modes: MHD modes that cease rotating (though they can still grow).

Low-activation materials: Materials which do not develop high, long-lived radioactivity under neutron irradiation.

Low aspect ratio: Low ratio of major to minor radius of the torus.

Lower hybrid current drive (LHCD): Non-inductive current drive using lower hybrid waves.

Lower hybrid heating (LHRH): Plasma heating by radio frequency waves at the "lower hybrid" resonance frequency in the plasma. Typical frequencies are a few GHz.

Lower hybrid (LH) wave: A plasma wave of frequency between the ion and electron cyclotron frequencies. It has a component of electric field parallel to the magnetic field, so it can accelerate electrons moving along the field lines.

Magnetic axis: The magnetic surfaces of a tokamak form a series of nested tori. The central 'torus' defines the magnetic axis.

Magnetic Confinement Fusion (MCF): Confinement and thermal insulation of a plasma within the reactor core volume by the action of magnetic fields. In toroidal magnetic confinement, usually both toroidal and poloidal components of the magnetic field are needed (the field lines are threaded like the filaments of a cable which is bent into a ring).

Magnetic islands: Islands in the magnetic field structure caused either by externally applied fields or internally by unstable current or pressure gradients. See tearing magnetic islands.

Magnetic surfaces (flux surfaces): In toroidal magnetic confinement, the magnetic field lines lie on nested toroidal surfaces. The plasma pressure, but not the amplitude of the magnetic field, is a constant on each magnetic surface.

Magneto-acoustic cyclotron instability: This instability results from an exchange of energy between the fast Alfvén wave (or magneto-acoustic wave) and an ion Bernstein wave which has a source of free energy through the presence of a population of energetic (non-thermal) ions, e.g. fusion products. The instability occurs for propagation perpendicular to the equilibrium magnetic field.

Major radius: The distance from the tokamak symmetry axis to the plasma centre.

Marfe: A localised and radiating thermal instability sometimes observed near the edge of tokamak plasmas.

Marginal Stability: Close to the transition from stability to instability.

MAST: Mega Amp Spherical Tokamak at Culham (Association EURATOM-UKAEA), twice as big as START. Began operation in 1999.

MeV: Mega-electronvolt, unit for nuclear energies. Energy which an electron acquires passing a voltage difference of 1 million volts.

MHD (Magnetohydrodynamics): A mathematical description of the plasma and magnetic field, which treats the plasma as an electrically conducting fluid. Often used to describe the bulk, relatively large-scale, properties of a plasma.

MHD instabilities: Unstable distortions of the shape of the plasma/magnetic field system.

Microinstabilities: Instabilities with characteristic wave-lengths similar to the ion Larmor radii, rather than to the tokamak dimensions. These are thought to be responsible for the fine scale turbulence in tokamaks, and hence anomalous transport.

Minor radius: Half the small diameter of the tyre-shaped toroid.

Mirnov coils: Pick-up coils at the edge of the plasma for measuring the time variation of magnetic fields arising from instabilities.

Mirror: A linear magnetic confinement concept with a weaker magnetic field in a central region and with strong fields at both ends which reflect contained particles by the mirror effect. Some variants exist to increase the magnetic field in all directions from the centre or to improve the closure of the bottlenecks. The Tandem Mirror confinement concept also involves electrostatic fields.

MIT: Massachusetts Institute of Technology, Boston, USA. Operates the high-field divertor tokamak ALCATOR C-MOD.

Mode: A resonant wave or oscillation in a plasma. Also used as a synonym for an operating regime.

Mode number: Characterises the wavelength of a mode.

Monte Carlo code: A statistical technique used in numerical calculations where events may occur many times, each with a certain probability.

Motional Start Effect (MSE): The measurement of shifts and splitting of spectral lines emitted from particles moving in a local electric field. This can be interpreted to give the local magnetic field inside the tokamak if the particle velocity is known, and is a major diagnostic on some tokamaks to deduce the current profile.

MPQ: Max-Planck-Institut für Quantenoptik, Garching, Germany. Active, within its programme, in ICF (laser fusion) related physics. Partially supported by Euratom, for a “keep in touch activity” in ICF.

Negative ion beam: To produce neutral beams, negative ions (obtained by the addition of electrons to neutral atoms) are accelerated and then neutralised before entering the plasma. The efficiency of creating neutral beams from positive ions is too low at the beam energy required for a fusion power station, of the order of 1 MeV.

Neo-classical theory: Classical collisional plasma transport theory, corrected for toroidal effects. The neoclassical theory predicts the existence of the bootstrap current.

Neo-classical tearing mode: The magnetic island produced by a tearing mode perturbs the bootstrap current which further amplifies the island and degrades confinement or leads to a disruption.

NET: Next European Torus, a design for the Next Step which had been prepared by the NET team (located at the Association EURATOM- IPP in Garching) and which has largely influenced the ITER design. The European ITER contributions in physics and technology were organised by the NET team, until its replacement by EFDA in 1999.

Neural network: A computer algorithm that uses incoming data to derive plasma parameters, having previously been "trained" on a series of examples of a non-linear input-output mapping.

Neutrons: Neutral particles in the nucleus. Products of Deuterium-Tritium and other fusion reactions.

Neutral beams: Since charged particles cannot easily penetrate the magnetic confinement fields of the plasma, high energy beams of neutral atoms are injected into the plasma for fuelling, heating and current drive. Within the plasma, the atoms of the beam are ionized and are then confined.

Neutron multiplier: The fusion of deuterium and tritium consumes one tritium nucleus per reaction, producing one neutron. Since in the blanket of a power station not every neutron reacts with lithium to produce a new tritium atom, a neutron multiplying element may be used in the blanket to enhance the tritium production so as to make the power station self-sufficient in tritium supply.

Next Step: The next experimental device in the strategy of the European Fusion

Programme. Presently pursued via the ITER EDA, with a European activity as a fall-back option. The generic name for an experimental reactor with a long pulse burning plasma at high fusion gain.

NFR: Naturvetenskapliga Forskningsrädet (Natural Science Council), Sweden. Partner in the Association EURATOM-NFR.

NIFS: National Institute for Fusion Science, Nagoya, Japan.

NRIM: National Research Institute for Metals, Sakura-mura, Japan.

Non-inductive heating and current drive: See additional heating and current drive.

NSTX: Spherical tokamak at Princeton, USA. A similar size to MAST, but of different design. Started operation in 1999.

Ohmic heating (OH): The resistive heating resulting from a current flowing within the plasma corresponding to the heating of a wire by a current flowing through it. Ohmic heating in a tokamak is insufficient to reach thermonuclear temperatures since, contrary to a wire, the resistance of a plasma decreases strongly with increasing temperature, thus making Ohmic heating weak at high temperatures.

ORNL: Oak Ridge National Laboratory, USA.

Operating limits: See tokamak operating boundaries.

Optimised shear: Adjusting the current profile to optimise tokamak.

PbLi: Eutectic lithium-lead alloy considered for use as blanket breeding material.

Peeling mode: An edge MHD instability which exists when the current density at the plasma edge is non-zero. It may be associated with ELMs.

Pellet: In inertial confinement concepts, the fuel is contained in tiny spheres, called pellets, which are compressed by laser or particle beams. In magnetic fusion, pellets of frozen hydrogen, deuterium, tritium, accelerated up to several kilometres per second, are used to refuel the plasma and to obtain very high densities.

PIREX: Proton Irradiation Experiment, material test facility (Association Euratom-Switzerland, CRPP-FT, PSI, Villigen, CH).

Plasma: State of matter above a few thousand degrees where atoms are broken into their constituents, ions and electrons, thereby creating an electrically conducting medium. Plasmas can therefore interact strongly with electric and magnetic fields.

Plasma confinement: Retention of plasma energy or particles within a given region, including the heat and particle losses from the plasma.

Plasma parameters: Physical quantities which characterise the plasma and which must be measured experimentally, such as current, density, temperature, confinement time, beta.

Plasma pressure: Proportional to the product of plasma density and temperature. There is an electron and an ion pressure and the plasma pressure is the sum of the two. In magnetic confinement devices, this pressure is counterbalanced by magnetic pressure.

Plasma shape: Describes the plasma vertical cross-section, circular, elongated, D-shape, diverted, single null, double null.

Polarimetry: Measurement of the rotation of the plane of polarisation of light passing through a magnetically confined plasma; used to measure the local magnetic field and thus the safety factor (see Faraday rotation).

Poloidal field: Component of the magnetic field perpendicular to the toroidal direction and the major radius. The poloidal field is essential for confinement and is generated in a tokamak by the plasma current and the external coils.

Power threshold: The L-H transition and improved performance regimes related to reversed shear occur when the power exceeds a certain threshold value - the power threshold.

PPPL: Princeton Plasma Physics Laboratory, New Jersey, USA.

Preliminary Tritium Experiment (PTE): Three plasma discharges on JET, November 1991, into which a significant amount of tritium was injected for the first time in a tokamak. The power liberated from fusion reactions (~ 2MW for ~ 2 seconds) was in

accordance with expectations. Followed by the more ambitious DTE in 1997.

Profile: Variation of plasma parameters with minor radius.

Profile control: Controlling the profiles of pressure, density or current, in order to control instabilities.

PSI: Paul-Scherrer-Institut, Villigen, Switzerland, active, in muon physics among others fields. The Association EURATOM-Swiss Confederation has their fusion technology activities working in superconductor and materials technology located at Villigen.

Pumped divertor: Divertor field lines directed into a pumped chamber surrounding the target plate.

q, q_{95}: See Safety factor.

Q: Ratio of fusion power to total additional heating power. At Q=∞, no external power is required and the plasma is said to be ignited. A power station should operate with Q~50 to be economical.

Radial electric field: Arises when there is a charge imbalance in the plasma.

Radio frequency (RF) heating: Heating with waves in the radiofrequency range at resonance frequencies of the plasma (see ECH, ICRH, LHH).

Reflectometry: Use of reflected microwaves to measure plasma density.

Relaxation: The evolution of a plasma to a lower energy state.

Resistive ballooning modes: A class of ballooning mode which would be stable in the absence of resistivity, but can be unstable in its presence. Related to tearing modes, but topologically different.

Resistive instability: Instability due to diffusion and rearrangement of magnetic field lines. When the plasma resistivity is small, these instabilities have a slow growth rate.

Resistivity: The tendency to resist the flow of electric current, thereby dissipating energy. Plasmas are very good conductors of electric current, so that their resistivity can often be neglected. In this case, 'ideal' magnetohydrodynamics may be applied.

Resonant ions/electrons: Resonance occurs when one of the characteristic frequencies of particle motion in the plasma (for example, the cyclotron frequency) matches the frequency of some applied perturbation (for example, an RF wave).

Resonant magnetic perturbation (RMP): An externally applied magnetic perturbation matched to the spatial structure and optionally the frequency and phase of an instability.

Reverse Field Pinch (RFP): A toroidal magnetic confinement device, similar to a tokamak, in which the poloidal and toroidal fields are of comparable magnitude. Capable of higher plasma current and pressure for a given external magnetic field. They require a conducting shell close to the plasma for stabilisation.

Reverse (magnetic) shear: In a tokamak the current density is usually greatest at the magnetic axis, in which case the safety factor increases from the centre to the edge of the plasma. Using non-inductive current drive and/or the bootstrap current the current density can be made to increase away from the centre. In this "reverse shear" case, the safety factor has a minimum away from the plasma centre. Using reverse or low shear ("optimised shear") some tokamaks, notably DIII-D and TFTR in the US and more recently JT-60U in Japan and JET, have shown greatly improved plasma performance. Reverse shear is an attractive option for advanced tokamak scenarios.

RF: Radio-Frequency.

RFX: Reversed Field pinch Experiment at CNR-Padova, Italy (Association EURATOM-ENEA).

RISØ: Forskningscenter Risø, Denmark. Partner in the Association EURATOM-RISØ.

Rotational transform: Measure of the ratio of poloidal to toroidal flux defining the pitch of the helical field lines. The q-value of the tokamak is proportional to the reciprocal of the rotational transform.

RTP: Rijnhuizen Tokamak PETULA, for study of transport in a plasma, at Nieuwegein (Rijnhuizen), the Netherlands (Association EURATOM-FOM). Ceased operation in 1998, the activities of the Association being transferred to TEXTOR, as part of the Tri-lateral Euregio Cluster.

Runaway electron: An electron with a very high energy has a decreasing probability of colliding with another charged particle and of losing its energy. Such a particle then gains more and more energy in the electric field of a tokamak, reaching 10's of MeV.

Safety factor: Number of turns the helical magnetic field lines in a tokamak make round the major circumference for each turn round the minor circumference, denoted q. Has no connection with the ordinary sense of "safety" other than q=1 surfaces are ideally unstable. For diverted plasmas q goes to infinity at the separatrix, so instead q_{95} is used to describe the safety factor near the edge, which is the safety factor of the plasma surface which contains 95% of the poloidal flux.

Sawtooth: A cyclically recurring instability which causes an energy loss from the central region of tokamak discharges. The temperature periodically falls abruptly, then slowly recovers. The jagged trace produced by plotting temperature against time gives the instability its name.

Sawtooth crash: The rapid collapse of the central temperature in a tokamak during a sawtooth cycle.

Scaling laws: Empirical or theoretical expressions for how various plasma phenomena (eg confinement, power threshold, etc) vary with tokamak parameters. They are particularly used for predicting the performance of future tokamaks.

Scrape-off-layer (SOL): The residual plasma between the "edge" of the plasma (defined by the limiter radius or the separatrix) and the tokamak vessel wall.

Semi-empirical: A theoretical approach in which the behaviour of some key quantities is deduced from experiment, rather than a priori.

SEAFP: The Safety and Environmental Assessment of Fusion Power is an extensive study conducted by several teams in the associated laboratories, NET, industry and the JRC, published in June 1995.

SEAL: The Safety and Environmental Assessment of Fusion Power Long-term is a programme, launched in 1995, being undertaken for the European Commission in the framework of the Fusion Programme.

Separatrix: Magnetic surface at which the rotational transform vanishes and the safety factor becomes infinite.

Shear: The safety factor usually varies from magnetic surface to magnetic surface across the plasma cross-section; this variation is measured by the non-dimensional quantity called "shear". Also refers to the variation of plasma flow (flow shear). If the type of shear is not specified, it usually means magnetic shear.

Single/double null: Points of zero poloidal magnetic field where the separatrix crosses itself are the X-points or nulls. Usually sited above and/or below the plasma. Tokamak divertor configurations have either one or two nulls.

Single fluid model: The set of equations which represent a plasma as a magnetised, electrically conducting fluid with the usual fluid properties of viscosity, thermal conductivity, etc. The possibility of distinct behaviour of electrons and ions (i.e. 2 "fluids") is excluded.

Small aspect ratio: Same as Low aspect ratio.

Spectroscopy: The detection and analysis of the spectrum of radiation emitted by a plasma. This can yield information about temperatures, impurities, rotation, using different parts of the electromagnetic spectrum (IR, visible, VUV, XUV, etc.)

Spherical tokamak (ST): A very low aspect ratio tokamak - it appears almost spherical, though topologically it remains a torus with a centre column. The spherical tokamak is being further investigated, with a larger experiment, MAST.

Spheromak: A spherical plasma in which comparable toroidal and poloidal currents flow. The toroidal current is not driven by transformer action.

Stability theory: The theory of how small perturbations to a system evolve in time. Spontaneous growth is due to instability. Instabilities can saturate at some small amplitude, in which case they may degrade confinement, or grow uncontrollably, in which case the equilibrium is lost leading to a disruption.

START: Small Tight Aspect Ratio Tokamak, a "spherical" tokamak with a very small

aspect ratio at the Association EURATOM-UKAEA (Culham). This very fat ring-shaped configuration showed experimentally a lesser tendency to disruptions and is efficient in its use of magnetic energy. Ceased operation in 1998, replaced by MAST.

Start-up assist: Assisting plasma formation to cross a range of plasma temperature at which impurities radiate strongly, with the aim of minimising the start-up delay and transformer requirements, usually using ECH.

STC: Scientific and Technical Committee, advisory committee set up by the EURATOM Treaty, competent for nuclear programmes.

Steady state power plant: A continuously (as opposed to cyclically) operated power plant.

Stellarator: Closed configuration having the shape of a three-dimensionally distorted ring in which the plasma is confined principally by an externally generated magnetic field (produced by non-planar coils outside the plasma vessel). The coils can be arranged in a modular fashion. Stellarators do not need a transformer; they need an additional heating system for the plasma start-up. Due to the fact that no toroidal plasma current is needed to maintain the confinement configuration, they naturally provide steady state operation.

SULTAN: Supra Leiter Test ANlage. Large Superconductor Test Facility, CRPP at PSI Villigen, Switzerland (Association EURATOM-Swiss Confederation).

Super Alfvénic velocity: A velocity greater than the Alfvén velocity. In a tokamak, only energetic particles have super Alfvénic velocities; because they satisfy this condition, they may resonantly transfer their energy to magnetohydrodynamic modes, which may grow as a result (eg TAE modes).

Superthermal radiation: Electromagnetic radiation produced by energetic particles, as opposed to thermal particles.

Survey spectrometer: An instrument which gives information concerning the radiated spectrum over a large range of frequencies.

TAE modes: Toroidal Alfvén Eigenmodes. One class of Alfvén gap modes.

Target plates: See Divertor.

TCV: "Tokamak à Configuration Variable", for study of elongated and strongly shaped plasmas, at Lausanne, Switzerland (Association EURATOM-Swiss Confédération).

TEKES: Technology Centre Finland. Partner in the Association EURATOM-TEKES.

Tearing magnetic islands: The disturbance caused by a tearing mode which alters the topology of the confining magnetic field and causes transfer of heat across the affected region.

Tearing mode: A class of resistive MHD instability which has been predicted theoretically in tokamaks and positively identified in experiments.

Temperature pedestal: In an H-mode discharge there is a region of steep temperature gradient at the plasma edge. The temperature at the top of this steep gradient region is the temperature pedestal.

Tesla: Unit of magnetic field strength (more exactly the magnetic induction). $1T = 1Vs/m^2 = 10{,}000Gauss$.

TEXTOR: Torus Experiment for Technology Oriented Research. Tokamak at Jülich, Germany (Association EURATOM-FZJ). Refurbished and upgraded, in 1994, as TEXTOR-94.

TFTR: "Tokamak Fusion Test Reactor" at Princeton, the largest US device with a major campaign using deuterium-tritium fuel from 1993 - 1997. Ceased operation in March 1997.

Thermal cycling: Successive heating and cooling of materials can lead to cracks or rupture, particularly at boundaries between materials that expand at different rates.

Thermal particles: As a result of collisional energy exchange, the energy of most plasma particles falls within a Maxwellian distribution which is described by a single temperature (typically 1-30keV for tokamaks). These are the thermal particles, as distinct from energetic particles which lie outside the thermal distribution.

Thomson scattering diagnostic: Diagnostic to measure temperature and

density by detecting laser light scattered and Doppler shifted by the thermal plasma electrons.

Tight aspect ratio: Same as Low aspect ratio.

TJ-II: A heliac stellarator at Madrid, Spain (Association EURATOM-CIEMAT). (TJ-IU was a torsatron at CIEMAT, built and operated in preparation for TJ-II).

Tokamak: Magnetic configuration with the shape of a torus. The plasma is stabilised by a strong toroidal magnetic field. The poloidal component of the magnetic field is produced by an electrical current flowing toroidally in the plasma. This current is induced via transformer action and, for steady state, must be maintained by non-inductive current drive and by self-generation of bootstrap current inside the plasma.

Tokamak operating boundaries: The set of plasma parameters, beyond which it is impossible to operate a tokamak. Careful choice of plasma cross-sectional shapes and current and pressure profiles can increase the operating regime.

TORE SUPRA: Large tokamak with superconducting toroidal magnetic field coils and a circular plasma cross-section at the Association EURATOM-CEA in Cadarache, France.

Toroidal Alfvén Eigenmodes: See TAE modes.

Toroidal field: The component of the magnetic field along the major circumference of the torus. The largest magnetic field component in a tokamak.

Toroidal stability: Stability analysis taking account of effects due to the toroidal geometry. These are sometimes neglected to identify possible instabilities, but must usually be included for accurate predictions of stability boundaries.

Toroidal turbulence code: A turbulence code which includes effects due to the toroidal geometry.

TOSKA: Large facility testing for superconductors (Association EURATOM-FZK, Karlsruhe, Germany).

Transformer drive: The use of a transformer action to produce plasma current.

Transport: The processes by which particles and energy move across magnetic surfaces.

Transport barrier: In certain operational scenarios (e.g. the H-mode or ITB-mode) a region of low transport exists giving rise to a steep local pressure gradient. Such a region is referred to as a transport barrier.

Transport scaling: The magnitude of heat transport may be expressed, empirically or theoretically, in terms of a simple functional dependence on a few plasma parameters. This allows us to model how the heat transport varies (scales) in response to changes in the value of these parameters.

Trapped particles: The outside (large major radius) of a tokamak plasma has a lower magnetic field than the inside. Particles with low velocity parallel to the magnetic field compared with the velocity perpendicular to the magnetic field may not enter the higher field (inside) region and become trapped on the outside. They are not free to circulate toroidally but instead bounce back and forth, performing so-called banana orbits.

Tri-lateral Euregio Cluster (TEC): A collaboration between the Associations Euratom-FZJ, -FOM and –Etat Belge, to exploit the TEXTOR tokamak at FZJ, Julich, Germany.

Tritium: An isotope of hydrogen, whose nucleus consists of one proton and two neutrons. Tritium does not occur naturally, because it is unstable to radioactive decay with a half-life of 12.3 years. Due to its rapid decay, tritium is almost absent on earth. For a fusion reactor, tritium will be produced in the breeding blanket surrounding the core of a fusion power station. Special tritium-handling technology is required whenever the use of deuterium-tritium plasmas is contemplated and has been developed on TFTR and JET.

Tritium inventory: The amount of tritium contained in a fusion power station or in a specified part of it.

Turbulence: Randomly fluctuating, as opposed to coherent, wave action. For example, the turbulent water beneath a waterfall can only be described in terms of its averaged properties, such as the scale and duration of fluctuations; whereas a

more systematic description can be given to waves on the surface of a still pond.

Turbulent transport: Anomalous heat transport associated with plasma turbulence.

Two-fluid model and multi-fluid model: The extended set of equations which represent a plasma as interpenetrating and interacting fluids of electrons and ions, impurity ions etc.

UKAEA: United Kingdom Atomic Energy Authority. Partner in the Association EURATOM-UKAEA which operates the tokamak COMPASS-D and the spherical tokamak MAST. Also charged with the operation of the JET facilities under EFDA.

Vertical Displacement Event (VDE): An event which arises when control of the plasma is lost and the plasma moves vertically. It can lead to a "halo current" in components which surround the plasma resulting in large, potentially damaging, forces on these components. The forces are much larger in larger tokamaks and are therefore a particular concern for JET and ITER.

VUV: The "Vacuum Ultra Violet" range of the electromagnetic spectrum.

Warm plasma refuelling: Fuelling of plasma using medium energy particles or particle clusters.

WEC: World Energy Council.

WENDELSTEIN VII-AS: Advanced stellarator, in operation at Garching, Germany (Association EURATOM-IPP).

WENDELSTEIN VII-X: Large advanced superconducting stellarator, optimised to produce a reactor-relevant plasma configuration, designed at Garching. Construction in progress at Greifswald, Germany (Association EURATOM-IPP) with first operation scheduled for 2006.

X-point: See single/double null.

XUV: The "Extreme Ultra Violet" range of the electromagnetic spectrum. Shorter wavelengths than VUV.

Acknowledgement: This glossary was adapted from the "Glossary of fusion terms" by UKAEA Culham, UK, and from the glossary of "Fusion programme evaluation", 1996, EUR 17521, European Commission.

APPENDIX G Sources of Financial Support

The work carried out at the CRPP and presented in this annual report was financed from several sources. The major long-term financial support is derived from the Ecole Polytechnique Fédérale de Lausanne (EPFL), EURATOM, the Paul Scherrer Institute (PSI) and the Swiss National Science Foundation. Other public and private organisations which contributed funding for our research in 2001 include, in alphabetical order: ASULAB, Balzers, Balzers Tribology and Balzers Process Systems, the Swiss Commission pour la Technologie et l'innovation (CTI), the Conseil des Ecoles Polytechniques Fédérales (CEPF), the Office Fédéral de l'Energie (OFEN), the Office Fédéral de l'Education et de la Science (OFES), Dow Corning, Rolex, Sulzer Metco AG, Tetra Pak SA and Unaxis.